Studying the effects of DNA replication stress on genome integrity and cell viability

Thesis submitted for the degree of

Doctor of Philosophy

at the University of Leicester

by

Kheloud Mohammed Alhamoudi

BSc (Biochemistry), MSc (Molecular Genetics)

Department of Genetics and Genome Biology

University of Leicester

Supervisor

Dr. Steven S. Foster

2018

Abstract

Studying the effects of DNA replication stress on genome integrity and cell viability

Kheloud Mohammed Alhamoudi

Accurate replication of the genome during cell division is essential for maintaining genome integrity and suppressing diseases such as cancer. DNA replication forks can stall, collapse and/or break when they encounter obstacles present in DNA. This causes DNA replication stress, which is a major source of genome instability and mutations during carcinogenesis and cancer evolution. A number of studies have investigated how cells respond to replication stress by using various genotoxic agents such as radiation or therapeutic agents. However, these agents cause genome-wide damage; thereby, preventing control over where replication forks collapse or break, and preventing replication stress-associated molecular events from being studied directly. Here, we aimed to overcome these current methodological limitations by developing an innovative FLP-FRT system. The FLP-FRT system is designed to induce the generation of broken DNA replication forks at specific loci in mammalian cells. The system utilises a mutant FLP recombinase that binds to an integrated FLP recognition target site (FRT) marked with a florescent locus labelling system and generates an irreversible protein adduct and DNA single-strand break. Upon DNA replication, the fork encounters the gap leading to fork breakage and the formation of a single-ended DNA double-strand break. Using the ANCHOR labelling tool, the ANCH3-ANCH4 sites flanking the FRT sequence were simultaneously visualized. Our findings suggest that cells with a broken fork display a notable reduction in cell viability when compared to a direct DSB, suggesting they are more cytotoxic, as hypothesized. In conclusion, our study shows that the features of FRT-FLP system offers a widely applicable and powerful tool to directly study replication stress at a very high resolution at the damage site within single cells in *vivo*. This novel tool permits genetic, biological and microscopic analyses of broken replication fork resolution in mammalian cells, which can shed light on important aspects of cancer cell biology and the development of new therapeutic clinical strategies.

Acknowledgments

I would first like to express my sincere thanks and gratitude to my supervisor, Dr. Steven Foster, for his guidance and for providing me with the opportunity to work on an exciting novel project in his laboratory, and for all his guidance throughout the project.

I also wish to express my gratitude to Dr. Nicola Royle for her valuable advice throughout my research project. I am also grateful to Dr. Kees Straatman for his guidance and co-operation in the microscopy work required in this project, besides his excellent support, ideas, throughout the four years-it was appreciated. I would like to thank Dr. Jennifer Higgins for helping in the FACS analysis.

I wish to thank Nicky Butler, Dr. Victoria Cotton and Rob Mason for their invaluable and outstanding technical assistance during the period of my project work,

I also want to express my acknowledge to everyone in labs G19 and G18 in the Department of Genetics for making the past four years very pleasant and enjoyable journey. I have spent wonderful years working with each and every one of them. A special thanks to my fellow PhD student Ahmed Alhendi for being ready to help me whenever required. I am grateful to all my friends Ibtihal Al-shamarti, Carmen Garrido, Shurooq Aljebur, Danae Georghiou, Salwa Almayouf, Noor bafana, Warda Alharbi for good times and memories in the past few years.
I am most thankful for my best friend Marwa Aldriwesh, whom I met here in Leicester for all her continuous support and love during this challenging years.

No words can express my thanks and love to my children Yara and Mansour for their love, patience throughout my PhD study.

Last but not least, I wish to offer my appreciation to my lovely parents Mohammed and Afaf Alhamoudi their continuous, unconditional support and encouragement. And all my wonderful sisters; Shoroug, Ashwag, Abrar and Aisha for always cheering me on.

With love,

Kheloud

Table of contents

List of figures

List of tables

List of abbreviations

A-NHEJ	Alternative end joining
ATM	Ataxia-telangiectasia mutated
ATR	AMT and Rad3 related
BER	Base excision repair
BIR	Break-induced replication mechanism
BRCA1	Breast cancer substrate protein1
BRCA2	Breast cancer substrate protein2
Cdc6	Cell division cycle 6 protein
Cdc45	Cell division cycle 45
CDK	Cyclin-dependent kinase
CdtI	DNA replication complex
CGR	Complex genomic rearrangements
CHK	Checkpoint kinases
CIN	Chromosome instability
C-NHEJ	Classical or canonical
CNVs	Copy number variants
CPT	Camptothecin
DDK	DdF4-dependent kinase
DDR	DNA damage response
DDT	DNA damage tolerance
DNA PKcs	DNA-dependent protein kinase
dNTPs	Deoxyribonucleoside triphosphates
DSBR	Classical double Holliday junction
DSBs	Double strand breaks
dsDNA	Double-stranded DNA
FRT	FLP recognition target sites
G1-phase	Gap1 phase
G2-phase	Gap2 phase
GCR	Gross chromosomal rearrangement

GIN	Genomic instability
GINS	Go-ichi-ni-san
HJ	Holliday junction
HR	Homologous recombination
HU	Hydroxyurea
IR	Ionizing radiation
LOH	loss of heterozygosity
M-phase	Nuclear division phase
MCM2-7	Minichromosome maintenance protein complex
MIN	Mini- or microsatellite instability
MMBIR	Microhomology-mediated BIR
MMR	Mismatch repair
MMS	Methyl-methane sulfonate
MRN	MRE11meiotic recombination 11/RAD50/NBS1
NBS1	Nijmegen breakage syndrome 1
NER	Nucleotide excision repair
NHEJ	Non-homologous end-joining
ORC	Origin recognition complex
PARP	Poly (ADP) ribose polymerase
PIK	Phosphoinositide kinase-related proteins
Pol ε	DNA polymerase epsilon
Pol δ	Replicative polymerase delta
Pol α	Polymerase alpha primase
Pre-RC	Pre-replication complex
RF	Replication fork
ROS	Reactive oxygen species
RPA	Replication protein A
RS	Replication stress
S-phase	DNA synthesis phase
SCE	Sister chromatid exchange
SDSA	Synthesis-dependent strand annealing
Se-DSBs	Single-ended double strand breaks
SMC1	Structural maintenance of chromosomes 1

SSA	Single strand annealing
SSBs	Single strand breaks
ssDNA	Single-strand DNA
TLS	Error-prone translesion synthesis
TOP1	Topoisomerase I DNA cleavage complex
UV	Ultraviolet

Chapter 1: Introduction

1.1 Genomic instability

Maintaining genome integrity and preventing genomic instability (GIN) ensures the faithful and accurate propagation of genomic information for subsequent generations, and is essential to the suppression of human diseases (Abbas et al., 2013). GIN can occur during any phase of the cell cycle (Draviam et al., 2004). GIN is a broad term, encompassing a set of processes prone to genomic change, which can result in a range of unscheduled genetic alterations ranging from mutations to large-scale chromosomal readjustments. Mutations might include nucleotide base pair substitutions, micro-insertions, deletions or inversions (Lengauer et al., 1998). While, large-scale chromosomal rearrangements involve segmental duplications, whole chromosome deletions, translocations or aneuploidy (Savage, 1976). These rearrangements can alter cell function and viability, and have been associated with a large number of human pathological disorders, which include premature aging (McMurray and Gottschling, 2003), inherited diseases (e.g., the neurological disease amyotropic lateral sclerosis, and the neuromuscular disease myotonic dystrophy) (Jeppesen et al., 2011; Mefford and Eichler, 2009) and various types of cancer (Negrini et al., 2010; Shen, 2011). GIN can be naturally generated, playing important roles in initiating important scheduled biological recombination processes, such as meiotic recombination (Neale and Keeney, 2006), mating-type switching in budding yeast, and mammalian immunoglobulin V(D)J joining (Aylon and Kupiec, 2004; Bassing and Alt, 2004; Gellert et al., 1999). The key role of GIN in tumorigenesis and a number of rare cancer-prone genetic diseases has positioned it at the center of cancer biology and biomedical research (Abbas et al*.,* 2013). Mutation events also contribute to driving polymorphic variation in populations and human genome evolution (Aguilera and Garcia-Musa, 2013).

1.2 Sources of DNA damage and genomic instability

Genomes suffer thousands of DNA lesions every day (Lindahl, 1993). GIN can be induced in a variety of ways, either by exposure to multiple known exogenous genotoxic sources (i.e., environmental agents), by endogenous cellular sources and/or interactions between these sources (Figure 1.1).

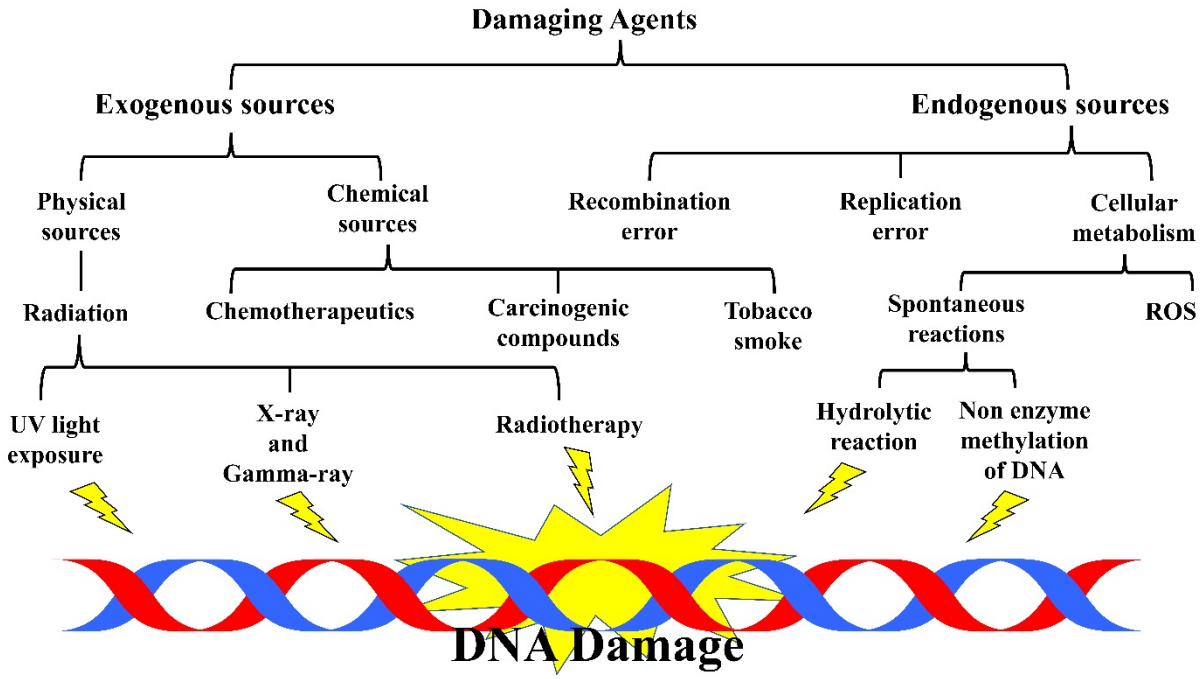

Figure 1.1 Classification of exogenous and endogenous sources of DNA damage. DNA damage can be induced by variety of sources either by exposure to multiple exogenous genotoxic sources such as radiation, chemotherapeutics and tobacco smoke. It can also induce by endogenous cellular sources such as normal cellular metabolism, recombination or replication errors.

Many studies have focused on documenting and identifying the numerous environmental risk factors contributing to DNA lesions; these include physical and chemical sources (Doll and Peto, 1981).

Physical DNA damage can arise upon exposure to environmental ionizing radiation (IR). IR sources are various, including radioactive decay, exposure to X-rays during cancer radiotherapy, and ultraviolet (UV) radiation from sunlight (Ward, 1988). Residual UV-A and UV-B can induce up to 10^5 DNA lesions per exposed cell every day (Hoeijmakers, 2009). Chemical sources, such as agents used in cancer chemotherapy treatments, such as compounds listed in Table 1.1 (e.g., topoisomerase I or II inhibitor agents, such as Camptothecin (CPT) and etoposide, respectively) induce the formation of a variety of DNA lesions by trapping topoisomerase-DNA and covalent complexes (Wogan et al., 2004). Additionally, alkylating agents such as methyl-methane sulfonate (MMS), induce the formation of DNA lesions by attaching alkyl groups to DNA bases (Hanway et al., 2002).

Table 1.1 Examples of some of the most common replication stress inducing compounds.

Compounds	Effect	Reference
Cisplatin (cis)	Act on replication by direct interaction with DNA causing DNA crosslinks and bulky lesions.	Harder and Rosenberg, 1970
Hydroxyurea (HU)	Chemical interference with the metabolism of deoxyribonucleotide triphosphates (dNTPs) for DNA polymerase at replication forks. Leading to stalled DNA replication forks, subsequently collapse into DSBs.	Petermann et al., 2010; Branzei and Foiani, 2010; Zegerman and Diffley, 2010
Aphidicolin (APH)	Direct interferes with DNA replication in S-phase via inhibition of the activity of replicative polymerases α, ε and δ.	Cheng and Kuchta, 1993
Camptothecin (CPT)	Interference with topoisomerase I (TopoI), a nuclear enzyme that reduces the torsional stress of supercoiled DNA. Causing SSB and subsequently se-DSB.	Hsiang et al., 1989; Wogan et al., 2004; Koster et al., 2007
Etoposide	Interference with topoisomerase II (TopoII). Prevent DNA unwinding and halt relaxation of torsional stress, causing DSB.	Deweese and Osheroff, 2009

GIN can also arise from the endogenous risk factors during normal cellular metabolic processes. For example, routine errors introduced during DNA replication, such as DNA mismatches, deoxyribonucleoside triphosphates (dNTP) misincorporation and DNA strand breaks can lead to mutations and GIN (Froelich-Ammon and Osheroff, 1995). In addition, DNA breaks can be generated by free reactive oxygen species (ROS), and nitrogen compounds produced during normal cellular metabolism (Hoeijmakers, 2009). For example, macrophages and neutrophils, which produce during inflammation and infection, and can generate oxidized DNA bases and break the phosphodiester bonds in the backbone of the DNA helix (Jena, 2012; Cadet and Wagner, 2013). These normal metabolic processes trigger various modifications to DNA, interconversion between DNA bases caused by deamination, modification of DNA bases through alkylation and DNA depurination. Thereby, leading to spontaneous loss of DNA bases (Kawanishi et al*.,* 2006; Lindahl and Barnes, 2000).

1.3 Types of DNA damage and genomic rearrangements

The agents discussed in Section 1.2 can cause a range of DNA damage types as illustrated in Figure 1.2. DNA damage can be broadly categorized into base pair damage or DNA phosphodiester backbone breakage. Base pair damage involves the substitution of a single nucleotide, loss of the DNA base(s), inter- or intra-strand crosslinks, and the formation of pyrimidine dimers when covalent cross linkage occurs between the cytosine and thymine residues (Jackson and Bartek, 2009).

DNA backbone damage includes DNA single strand breaks (SSBs) and DNA double strand breaks (DSBs). SSBs are the most frequent steady-state DNA breakages, they can arise spontaneously due to errors in DNA metabolism. Alternatively, DSBs can be formed when two SSBs arise in close proximity to each other on the opposite DNA strands, or when the DNA-replication apparatus encounters an SSB. Although DSBs do not occur as frequently as the other DNA lesions listed above, they are considered difficult to repair, and are extremely genotoxic and mutagenic DNA lesions (Khanna and Jackson, 2001). This is because they cause a major disruption in genetic integrity with the potential to affect the expression of multiple genes (Bartek et al., 2007).

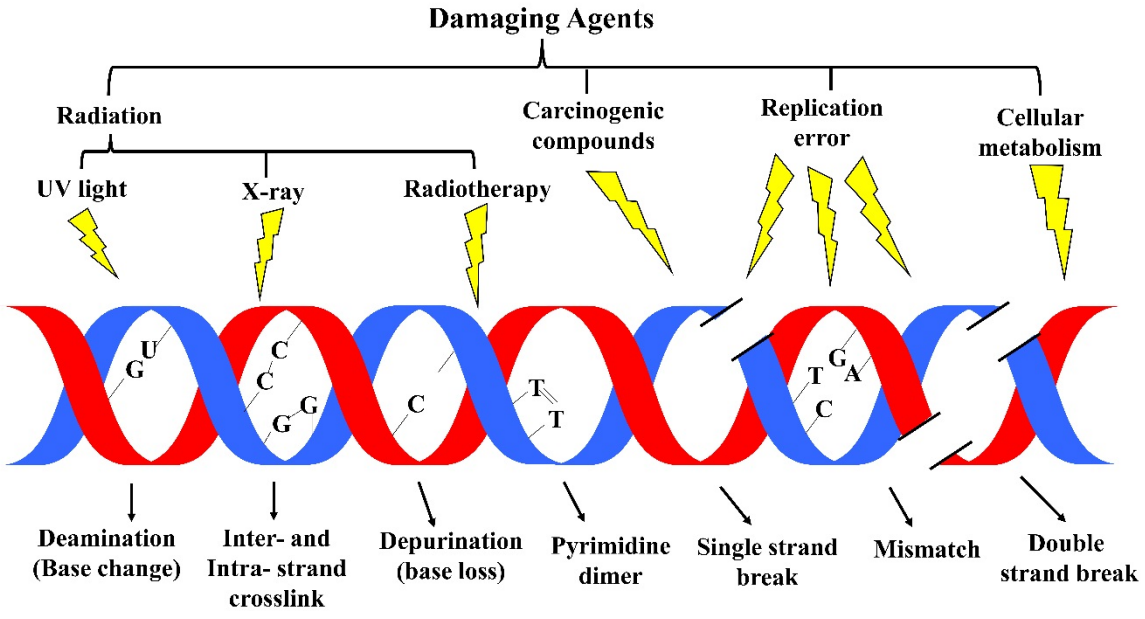

Figure 1.2 Summary of sources of DNA damage and associated lesion generated. Endogenous and environmental sources of DNA damage subsequently generate different type of DNA lesions ranging from modified bases to DNA phosphodiester backbone breakage, such as the substitution of a single nucleotide, loss of the DNA base(s), inter- or intra-strand crosslinks, and the formation of pyrimidine dimers, single strand breaks or double strand breaks.

Repair of DSBs is critical for cell survival and viability, yet the cell faces a particular challenge when repairing DSBs. The presence of an unrepaired DSB poses a hazard to genomic integrity and can trigger the DNA-damage response system, thus resulting in cell cycle arrest, cell death or hereditary changes. Additionally, if not repaired correctly, such lesions may lead to the loss of genetic information or to the accumulation of point mutations or pose a serious threat of chromosomal translocations. Subsequently, when a cell continues to divide, the broken chromosome fragments will missegregate, leading to aneuploidy.

Defective DNA structures, along with the lost functionality resulting from these types of DNA breakages have the potential to subsequently cause mutagenicity, cellular changes or cellular death (Ciccia and Elledge, 2010).

The difficulty in repairing a DSB means that the breakages can cause several types of instability events leading to rearrangements (Figure 1.3). These instabilities can result in micro mutations, chromosome instability (CIN) and/or complex genomic rearrangements (CGR).

CIN refers to variations in chromosome number, leading to continuous losses or gain from the whole, or part of, the chromosome, and is associated with failures affecting chromosomal segregation apparatus or spindle mitotic checkpoints (Savage, 1976). Chromosomal rearrangements have a simple aetiology requiring the generation of one or more DNA ends, from a range of DNA structures, including DSBs (Lemoine et al., 2005; Mimitou and Symington, 2008; Putnam et al., 2009). Therefore, it has been recognised that DSBs function as both initiators and intermediates of a wide range of chromosomal rearrangements (Burrell et al., 2013). Lengauer et al. has demonstrated that alterations in chromosome number have the ability to cause aneuploidy and gene amplification (1998). Such changes affecting growth-controlling genes have been found in neoplastic cells of nearly all major human tumour types, providing persuasive evidence for the genetic basis of human cancer (Lengauer et al.,1998).

CGR is a term used to refer to instability events that involve complex genetic alteration patterns consisting of two or more breakpoint junctions, and leading to more than one simple rearrangement. CGRs are thus recognized as a major component of tumour formation or progression, the associated rearrangements include unequal sister chromatid exchange (SCE), copy number variants (CNVs), hyper-recombination, loss of heterozygosity (LOH) and/or gross chromosomal rearrangement (GCR) (Liu et al., 2012).

Recent work suggests that such genetic alterations are in most cases generated by single-strand DNA (ssDNA) gaps or DSBs that have been generated as a consequence of replication stress (RS) and cover events mediated by homologous recombination (HR) and non-homologous end-joining (NHEJ) mechanisms.

Several studies have indicated that low fidelity replication mechanisms and events mediated by HR and NHEJ repair mechanisms contribute to a wide range of complex human genomic rearrangements. SCE occurs due to changes in the genetic linkage or because of fusion or breakage affecting two DNA fragments. By contrast, GCR are induced by translocations, deletions, or insertions of genetic information, as initiated primarily by NHEJ of DNA fragments (Charames and Bapat, 2003). In summary, many sources and types of damage occur, and this can set in motion the generation of various classes of mutations depending on context.

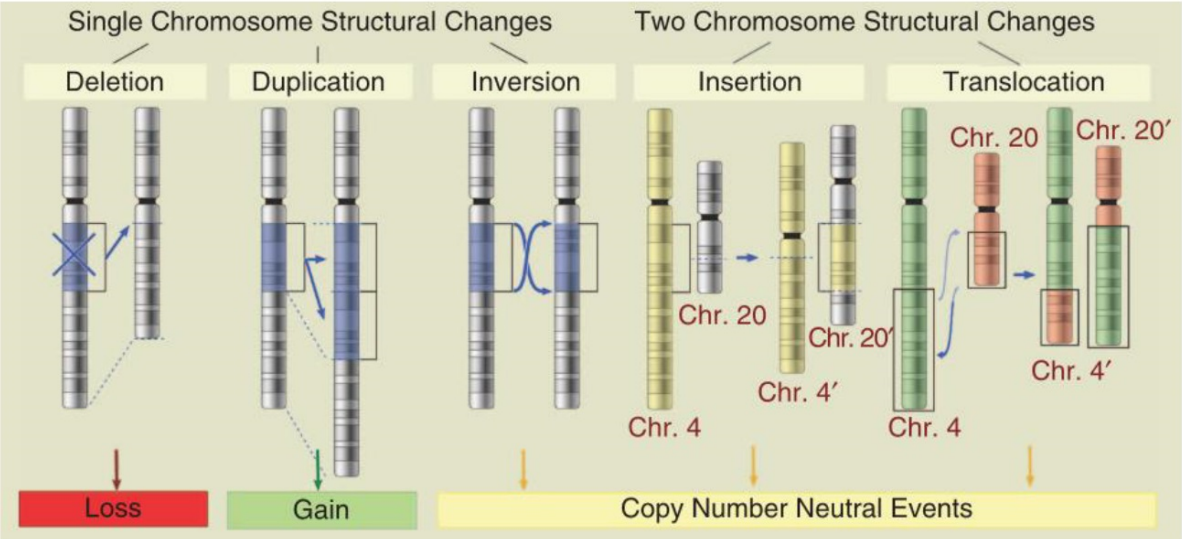

Figure 1.3 Schematic representation of instability events leading to rearrangements. These instabilities can result in chromosome instability (single chromosome structural change) leading to continuous losses or gain from the whole, or part of, the chromosome. It can also result in complex genomic rearrangements (two chromosomes structural change) that involve complex genetic alteration patterns consisting of two or more chromosomes, leading to unequal sister chromatid exchange, copy number variants, hyper-recombination, loss of heterozygosity or gross chromosomal rearrangement. (This figure is taken from Alqallaf et al., 2013).

1.4 Eukaryotic DNA replication

Accurate replication of the genome by cell division, and faithful transmission and propagation of intact genetic information from one cell to its offspring, is a prerequisite to maintain genome integrity (Masai et al., 2010).

Cells accomplish this by undergoing continuous cycles of DNA replication, division of the nucleus and finally partitioning of the cytoplasm. This sequential cycle is termed the cell cycle (Bell and Dutta, 2002). It is a cell division cycle composed of four phases: the nuclear division (M) phase, the gap1 (G1) phase, the DNA synthesis (S) phase, and the gap2 (G2) phase (Massague, 2004).

DNA replication is carried out by the replisome, and is defined as the process whereby the DNA replicative polymerases utilizes the template strand to permit the synthesis of a complementary strand (Leman and Noguchi, 2013). Eukaryotic chromosomal DNA replication can occur simultaneously in hundreds of thousands of licensed loci within the genome; which are known as origins of replication (Bielinsky and Gerbi, 2001). Origins of replication establish bidirectional replication fork (RF) machinery (Nishitani and Lygerou, 2002).

The RF is a complex structure, in which DNA synthesis requires various replicative enzymes (Waga and Stillman, 1998). Once DNA replication commences, origins fire and time-regulated replication origin licensing occurs. Replication origins have been identified in budding yeast, and can be divided into early-replicating, late-replicating, and dormant origins (Raghuraman et al., 2001). Licensed dormant origins do not fire in an unperturbed S-phase, however they can be activated following replication stress (RS), to ensure completion of DNA replication (Wu et al., 2014). DNA replication occurs in three principal stages: (1) initiation of the unwinding of the DNA double helix by the replicative helicase, (2) elongation of the newly synthesized strand by DNA polymerases, and (3) termination (Johnson and O'Donnell, 2005). At each stage, cells must balance accuracy, thus facilitating DNA synthesis if they are to successfully complete replication (Leman and Noguchi, 2013).

1.4.1 Replication initiation

Replication initiation occurs with the generation of the pre-replication complex (Pre-RC) (Bielinsky and Gerbi, 2001). The formation of this complex occurs during the early stages of the G1 phase of the cell cycle, and involves several cooperative initiator proteins (Bell and Stillman, 1992).

These proteins include the origin recognition complex (ORC), chromatin licensing and DNA replication complex (CdtI), cell division cycle 6 protein (Cdc6), and minichromosome maintenance protein complex (MCM2-7) (Zou and Stillman, 2000; Nishitani et al., 2000). These initiation factors are highly regulated, and restricted to the G1 phase to prevent multiple random replications during a single cell cycle (Saxena and Dutta, 2005). The ORC complex recognizes replication origin sites and binds to the DNA throughout the genome. This association then acts as a platform, recruiting CdtI and Cdc6 to the previously bound ORC (Hofmann and Beach, 1994). The resultant combined activities cause a double hexamer of the MCM2-7 complex to assemble at the replication origins (Blow and Dutta, 2005).

At the transition of G1 to the onset S-phase, the pre-RC will transform into an active RF. This accomplished via two S-phase kinases; cyclin-dependent kinase (CDK) and DdF4-dependent kinase (DDK) (Zou and Stillman, 2000). Cell division cycle 45 (Cdc45) and go-ichi-ni-san (GINS) target the phosphorylated MCM complex and bind to it, producing an active replicative helicase, termed the CMG complex (Moyer et al., 2006).

Due to the licensing of the replication origins through the S-phase, through a combination of replication proteins, the parental DNA duplex helix is unwound via the MCM2–7 DNA helicase complex, to prepare the chromatin for replication (Pacek and Walter, 2004). At this point, as illustrated in Figure 1.4, a Y-like structure is formed, becoming a specialized apparatus for carrying out DNA synthesis (Waga and Stillman, 1998; Jossen and Bermejo, 2013). The topoisomerase I DNA cleavage complex (TOP1) will then relieve topological stress and remove the supercoils caused by the unwound, double-stranded helical DNA structure ahead from the RF during DNA replication (Wang, 2002). RF can be established, producing an ssDNA template to enable the replicative polymerase (primase that synthesizes RNA primers) to commence DNA synthesis (Waga and Stillman, 1998; Araki, 2011). Replication protein A (RPA) plays an important role in stabilizing ssDNA tracks, thus preventing the engagement of recombination factors (Iftode et al., 1999).

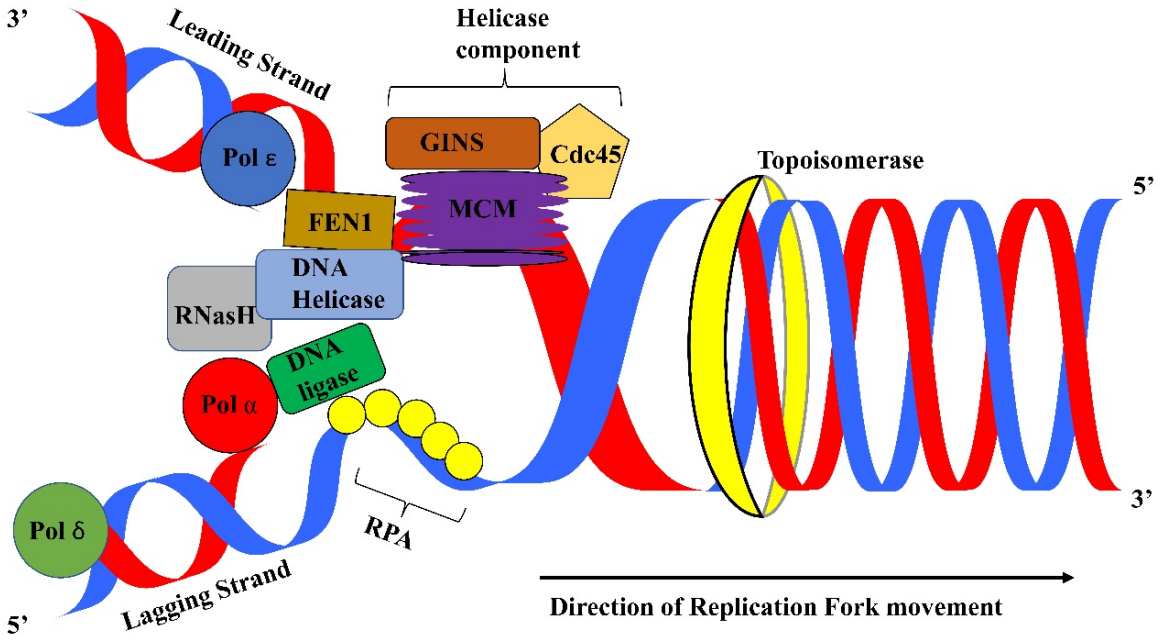

Figure 1.4 The mechanism of eukaryotic DNA replication. This diagram depicts the simultaneous synthesis of both leading and lagging strands and the major replication enzymes involved.

1.4.2 Replication elongation

Elongation of the RF and DNA synthesis requires the recruitment of DNA polymerases (Pol α, Pol δ, Pol ε), RPA, and primase (Walter and Newport, 2000). Studies report that Cdc45 plays a critical role in loading DNA polymerase to the ssDNA in the RF apparatus (Pacek and Walter, 2004; Labib et al., 2000).

The primase first synthesizes RNA primers that are complementary to the parental ssDNA template (Aguilera and Garcia-Musa, 2013), providing a starting point for DNA synthesis for both continuously and discontinuously on the leading and lagging strands, respectively (Araki, 2011). The ssDNA acts as a template for replicative DNA polymerase epsilon (pol ε), making it possible to synthesize the leading strand and move toward the RF in a constant direction (Pursell et al., 2007; Burgers, 2009). Progressive elongation of the lagging synthesized strands is catalyzed by the replicative polymerase delta (pol δ) and polymerase alpha primase (pol α) (Walter and Newport, 2000). These enzymes synthesize DNA creating an opposite orientation to RF. However, synthesis of the lagging strand is more complex and requires both pol δ and pol α to synthesize discontinuous fragments, which are called Okazaki fragments (Burgers, 2009).

1.4.3 Replication termination

As DNA synthesis proceeds further, a number of additional factors assist the process of RF termination. Lagging strand maturation occurs when primer RNA displacement creates a flap structure cleaved by FEN1, which is then replaced with nucleotide bases (Waga and Stillman, 1998). The gaps between the Okazaki fragments of the lagging strand are sealed with DNA ligase (Lindhal and Barnes, 1992). The resulting intermediate is then processed by the DNA2 helicase and RNaseH to ensure replisome stabilization, and coordination between the replication and establishment of two-sister chromatid cohesion that continues together until anaphase (Leman and Noguchi, 2013; Wu et al., 2014). Defects in the replication process can become a major source of DNA breaks and RS.

1.5 Replication stress

To preserve cell viability and prevent disease it is vital to maintain RF stability in dividing cells. *In vivo* studies have demonstrated that various processes hinder RF progression which can cause RS (Pacek and Walter, 2004; Carr et al., 2011; Mirkin and Mirkin, 2007; Labib and Hodgson, 2007). RS is complex and can be defined as "an aberrant progression of the DNA RF, resulting in impaired DNA synthesis and functionality", with grave implications for cell survival and human diseases (Bartek et al., 2007). Furthermore, RS is a common hallmark of cancer cells and is a major source of transformation of pre-malignant into malignant cells (Hanahan and Weinberg, 2011).

RS can occur prior to, or as a consequence of, DNA damage. RS is related to spontaneous GIN, and is one of the major sources of chromosomal re-arrangements and unscheduled recombination events (Zeman and Cimprich, 2014).

During S-phase, RF can be altered by encountering certain unrepaired DNA damage, or a variety of physical obstacles of both intracellular and extracellular origin (Ciccia and Elledge 2010). These obstacles include the replication barrier factors present in chromatin DNA, such as DNA binding proteins, unusual secondary structures, and transcription complexes. These obstacles are known as natural impediments to DNA replication, because they interfere with RF progression. Consequently, this causes stalling, collapsing, and breaking of RF (Carr et al., 2011). It thereby primes genomic rearrangements, threatening genomic integrity (Mirkin and Mirkin, 2007; Labib and Hodgson, 2007).

1.5.1 Replication fork stalling

RF stalling is a stochastic event in eukaryotes, and one that has been thoroughly studied. RF stalling functionally implies the fork complex temporarily pauses or experiences a short delay, and that replisome movement is compromised until either the repair mechanism takes effect or the obstacle is removed without replisome disassembling (Deshpande and Newlon, 1996; Calzada et al., 2005). DNA is most vulnerable during S-phase as the replisome must overcome a wide range of intrinsically challenging obstacles or difficulties. This includes unusual DNA sequences, such as repetitive DNA elements, including triplet and telomeric repeats, and secondary DNA structures; for example, palindromic sequences that form hairpins and topological constraints (McMurray, 2010; Kim and Mirkin, 2013). Additionally, fork stalling might arise at sites occupied by tightly bound protein-DNA complexes (Aguilera and Garcia-Musa, 2013) (Figure 1.5). Stalled forks typically result in the formation of stretches of ssDNA. This ssDNA frequently forms when replicative helicase continues to unwind parental DNA after polymerase stalling (Byun et al., 2005).

A vast number of experimental observations have indicated that stalled forks require activation and regulation of the S-phase checkpoint for their stabilization, including protein kinase ATR and Chk1 (Lopes et al., 2001; Byun et al., 2005; Labib and Piccoli, 2011), which have been demonstrated to play an important role in preventing fork collapse and maintaining genome stability (Lambert and Carr, 2013; Aguilera and Garcia-Musa, 2013).

Temporarily stalled forks do not pose any danger to the genome integrity because different repair and restart replication mechanisms (see Section 1.8.1 for further details) are able to rescue the stalled fork to ensure the duplication of the genome, completion of cell cycle, and to minimize the possibility of further fork collapse (Weinert et al., 2009; Heller and Marians, 2006). Despite the complex response initiated by the cell to stabilize and restart a stalled fork as described in subsequent sections. the failure to restart stalled forks can lead to subsequent collapse, particularly due to defective RS-response (Ragland et al., 2013; Tercero and Diffley, 2001).

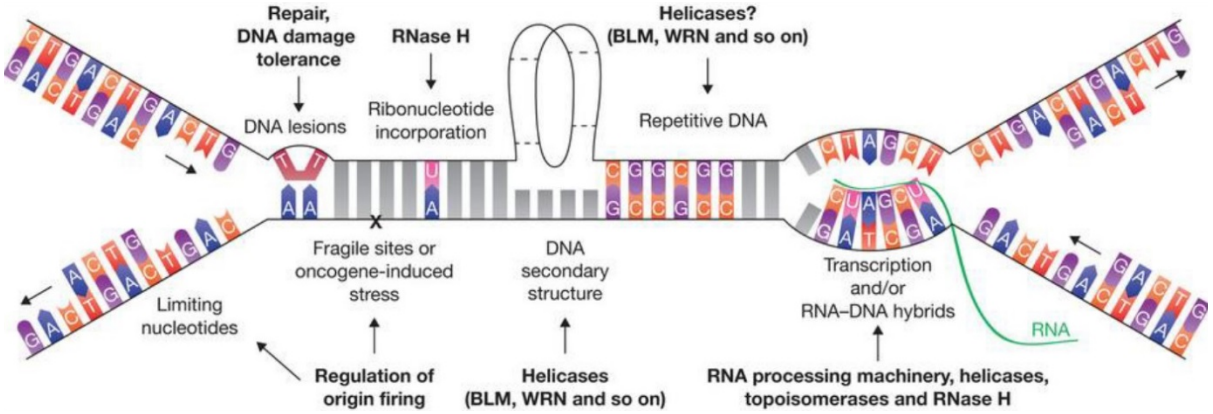

Figure 1.5 Overview of the different causes of replication stress. This figure shows the number of causes and obstacles with the ability to stall, collapse or break the DNA replication fork. This figure is taken from Zeman and Cimprich (2014).

1.5.2 Replication fork collapse

RF collapse generally refers to a process that arises after the disassociation of replisome factors. This includes DNA polymerase and other RF factors from the site of synthesis (Cobb et al., 2003). It occurs when a large number of replication barriers are present on the chromatin DNA (Sabatinos, 2010). The defects caused by replisome disassembly induce the formation of stretched SSBs, causing DNA breakages with potential to be a source of GIN (Aguilera and Gomez-Gonzalez, 2008).

During S-phase, replication machinery can interfere with other DNA mechanisms, such as the transcriptional apparatus present in replication templates (Helmrich et al., 2013), wherein the replicative helicase and transcriptional RNA polymerases compete to operate on the same DNA template, causing collisions and clashes (Bermejo et al., 2012). This process is now understood to be a major cause of fork collapse, and as such has received renewed attention as a source of RS, although it is not fully understood.

In addition, replication that interferes with the higher order chromatin structures established by co-transcriptional processes is believed to also be responsible for collapsing RF progression. Moreover, evidence has demonstrated that fork collapse may be generated by uncoupling between DNA unwinding helicases and the progression of DNA polymerases (Sogo et al., 2002; Byun et al., 2005). In addition, fork collapse can occur when uncoupling occurs between leading and lagging strand polymerases (Pages and Fuchs, 2003) in the presence of damaged DNA generated by endogenous or exogenous sources (Branzei and Foiani, 2009).

Collapsed RFs might also arise from S-phase checkpoint inactivation (Ragland et al., 2013). Additionally, under RS, collapse might be induced by inter-strand DNA crosslinks, or replication inhibitor agents generating bulky DNA adducts, and DNA topological adducts generated by chemical agents, such as DNA topoisomerase adducts, which can block and inhibit replicative helicase activity (Zeman and Cimprich, 2014). Furthermore, collapse might be induced by base-adducts, chemical agents that are generated by MMS, or by direct inhibition of DNA synthesis resulting from the depletion of dNTPs induced by the addition of HU (Petermann et al., 2010; Branzei and Foiani, 2010; Zegerman and Diffley, 2010; Ray Chaudhuri et al., 2012).

A number of studies have demonstrated that the absence or inactivation of the S-phase checkpoint, resulting in incomplete DNA replication, will lead to the accumulation of DNA breaks and thus increase risk of RF breakage, and consequently causing chromosomal rearrangements (Liu et al., 2012).

1.5.3 Replication fork breakage

Replication-associated DSBs may be generated directly due to the presence of SSBs owing to the endogenous or exogenous factors mentioned previously. In addition, fork breakage may induced indirectly in several ways, when RF machinery encounters persistent SSBs and stretched ssDNA (which can be found at the stalled fork), and/or exposed nicks/gaps left behind by the collapsed fork. Under prolonged failure conditions these structures can lead to the discontinuation of DNA synthesis in the nascent strand, thus could involve generation of fork breakage.

Under RS and as illustrated in Figure 1.6, ssDNA nicks will passively convert to DSB particularly associated with the formation of single-ended double strand breaks (se-DSBs)/ broken fork (BF), although very little is understood concerning the physical structure of broken forks. (Cortes-Ledesma and Aguilera, 2006).

DSBs are hazardous to the genome and represent the greatest challenge during DNA replication (Pacek and Walter, 2004; Carr et al., 2011). se-DSBs are a fundamentally different structure to direct DSB, lacking a second DSB-end, potentially posing resolution problems, meaning they may be susceptible to events such as the aberrant end joining of two distinct se-DSBs.

Thus, it was hypothesised that se-DSBs are potentially highly genotoxic, and, if not correctly processed, threaten genome stability. This is because it could anneal to another sequence in the genome, leading to unscheduled genomic rearrangement events and potentially cell death (Cobb et al., 2005). Replication of induced DSB can cause two broken chromosomes, termed double fork breakage. The failure to repair these types of RS can result in tumorigenic translocations and other types of mutations.

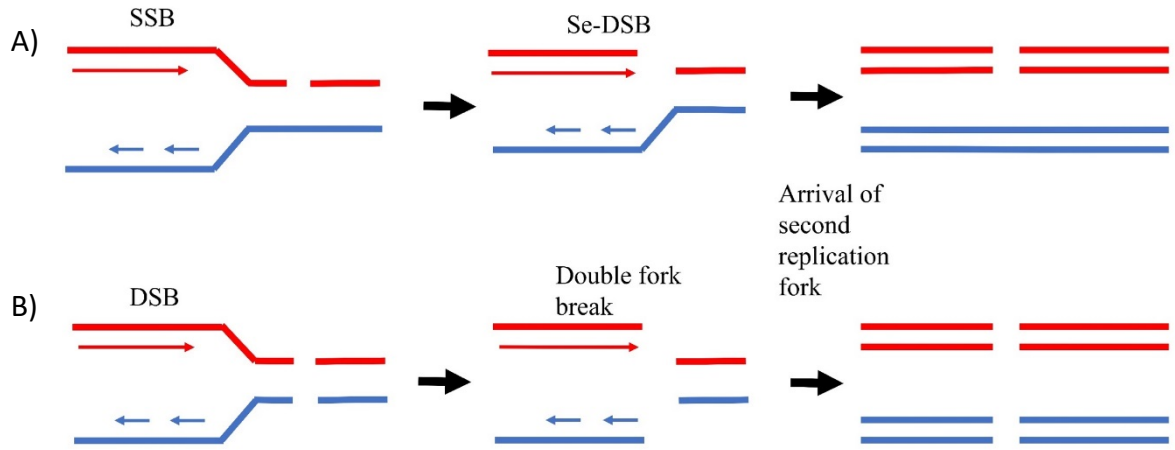

Figure 1.6 Mechanistic model of causes of replication fork breakage. This figure shows different causes that can alter the replication fork progression and breakage. **A)** Replication fork encountering a single strand break or a gap will directly lead to fork breakage and single-ended double strand break (se-DSB). Therefore, a single ended double strand break (se-DSB) might form if the replication fork does not properly proceed. **B)** Replication fork encountering a double strand break (DSB) will directly lead to replication fork breakage and promote the formation of direct DSB.

1.6 The DNA damage response

Cells must counteract the threat of DNA damage and constant assaults on DNA if they are to duplicate and deliver genetic material to the next generation intact and unchanged. To respond to these threats, eukaryotic cells have evolved a variety of surveillance mechanisms, collectively known as DNA damage response (DDR) (Harper and Elledge, 2007; Jackson and Bartek, 2009; Jossen and Bermejo, 2013). As illustrated in Figure 1.7, the DDR comprises of a complex, interlinked network of pathways that include signal transduction cascades that detects DNA damage and signals its presence. The DDR response pathway is driven by several modification events such as phosphorylation, ubiquitylation, sumoylation or acetylation (Elledge, 1996; Zhou and Elledge, 2000; Sirbu and Cortez, 2013).

They then execute a choreographed response and transduce the information to downstream proteins acting to mitigate DSBs and RS, maintain genome integrity and suppress the proliferation of unstable cells by regulating checkpoints, along with DNA repair, senescence and apoptosis (programmed cell death mechanisms) (Zhou and Elledge, 2000; Rouse and Jackson, 2002). These cell growth inhibitors are mainly evolutionarily conserved among eukaryotes, and serve as a potential anticancer barrier by responding to RF stalling and breakdown (Jackson and Bartek, 2009). As discussed in section 1.10, inherited defects in these genome protection mechanisms are responsible for a number of human diseases, including cancer (Lengaure et al., 1998).

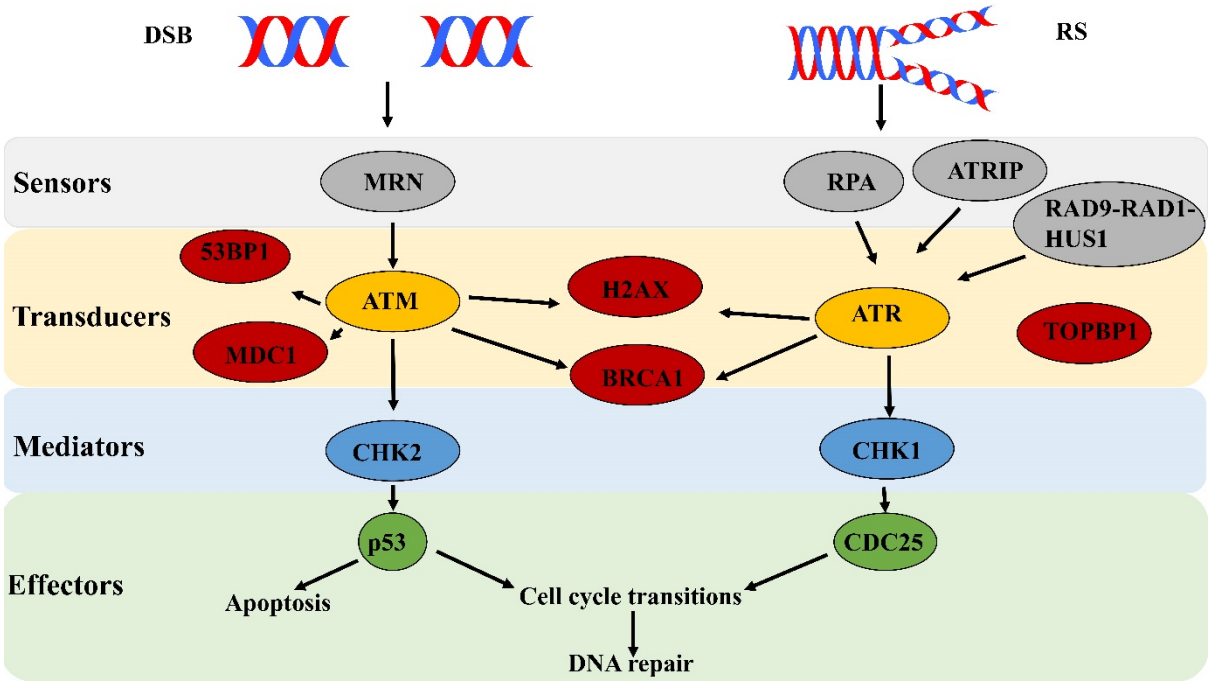

Figure 1.7 General overview of DNA damage response pathways. This figure depicts a linear outline of the different interlinked networks involving signalling, sensing, transducing and effecting DNA damage or replication stress.

1.6.1 DNA damage sensing

Some proteins sense DNA damage, aberrant DNA structures and/or replication interference processes, and initiate the generation of a downstream checkpoint signalling response. However, a DNA damaging agent typically generates several types of damage; thus, detection is complicated as several sensors might be activated (Helt et al., 2005).

DDR-signalling regulators composed of conserved phosphoinositide kinase (PIK)-related proteins, including ataxia-telangiectasia mutated (ATM), the AMT and Rad3 related (ATR), and DNA-dependent protein kinase, catalytic subunit (DNA PKcs) protein kinases, and by members of the poly (ADP) ribose polymerase (PARP) family (Lovejoy and Cortez, 2009). DNA damage sensing is considered the first step in triggering DDR pathways and activating checkpoint pathways leading to cell cycle arrest or delay (Kastan and Bartek, 2004). Although, structurally speaking, both proteins belong to the phosphatidylinositol 3-kinase-related kinase (PIKK) family of protein kinases, they participate in different cellular responses (Keith and Schreiber, 1995).

ATM and DNA-PKcs are primarily activated by DNA damaging agents that create DSBs or stress, which then affects chromatin structure (Canman et al., 1998; Meek et al., 2008). However, DNA-PKcs does not appear to play a major role in cell-cycle checkpoint signalling (Burma et a., 1999). Nevertheless, it is an important enzyme that primarily regulates the smaller group of proteins involved in the NHEJ DSB repair pathway (Lieber, 2010). In unstressed cells, ATM is present in a close dimeric conformation (homodimer), wherein the kinase domain is physically blocked (Bakkenist and Kastan, 2003). Research suggests, the introduction of a single DSB, ATM senses and responds to changes in chromatin structures, leading to conformational change in the intermolecular ATM protein, which then induces extremely rapid and extensive auto-phosphorylation, causing dissociation of the inactive homodimer, converting it into an active monomer (Bakkenist and Kastan, 2003). The activated ATM monomer is recruited to the DSB sites. Several in vitro studies have demonstrated that recruitment to the damaged site occurs via a multiprotein complex, MRE11 (meiotic recombination 11)/RAD50/NBS1, collectively known as the MRN complex (Carson et al., 2003; Lee and Paull, 2004). In human cells, MRN is essential for damage-induced chromatin association of ATM (Andegeko et al., 2001; Lee and Paull, 2004) and for efficient ATM auto-phosphorylation following damage (Uziel et al., 2003).

Meanwhile, the ATR kinase is activated by stalled RFs (Shechter et al., 2004; Cimprich and Cortez, 2008). The activated ATR is recruited due to cellular stress that affects the DNA RF progression and leads to the accumulation of RPA-binding protein coating an abnormal stretch of ssDNA, generated at the stalled DNA replication forks, which responds broadly due to exposure to stresses (Wold, 1997). Thus, this stimulates the binding of ATR-interacting protein (ATRIP) and leads to the recruitment and in vitro subcellular localization of its heterodimeric partner, ATR, to the site of RF (Cortez et al., 2001).

Whereas cells tolerate the absence of ATM (Shiloh and Kastan, 2001), it has been observed that depletion of RPA prevents DNA replication and the binding of ATR to chromatin, thereby reducing cell viability (Brown and Baltimore, 2003). This suggests ATR is required for normal progression in the cell cycle, which is consistent with the observation that ATR plays a critical role in the normal progression of DNA RFs (Shechter et al., 2004).

1.6.2 Signal transduction

Recognition of DNA lesions by sensor proteins, and the localization of phosphorylated ATM and ATR proteins to the DNA damage site generates docking sites that facilitate the recruitment of checkpoint mediator proteins.

Once recruited to the DNA break, the activated ATM is able to phosphorylate other critical downstream targets, such as p53, nucleoplasmic substrates including Nijmegen breakage syndrome 1 (NBS1), breast cancer 1 (BRCA1) and structural maintenance of chromosomes 1 (SMC1), which accumulate and localize at the DNA damage sites (Kitagawa et al., 2004; Mochan et al., 2004; Matsuoka et al., 2000; Xu et al., 2001). These have been demonstrated as critical mediators in checkpoint signalling for the efficient phosphorylation of multiple specific ATM substrates in response to specific types of DNA damage or replication interference (Wang et al., 2002; Kastan and Lim, 2000). Although MRN might function upstream of ATM in signalling, Nbs1 itself is a substrate of ATM, and phosphorylation of Nbs1 generates a downstream signalling role affecting ATM activation (You et al., 2005; Lim et al., 2000).

ATR once activated is localized to ssDNA regions, it stimulates recruitment of several other proteins and protein complexes to the ssDNA site (Zou and Elledge, 2003). These include the clamp-loading RSR complex, which contains RAD17, and participates in the loading of RAD9–RAD1–HUS1 (9–1–1) (Zou et al., 2003). The 9-1-1 complex structurally resembles the trimeric, proliferating cell nuclear antigen (PCNA) clamp, which functions in DNA replication and repair (Venclovas and Thelen, 2000). While the RAD17 protein is structurally similar to various subunits of the replication factor C (RFC) and forms an RFC-like complex (Griffiths et al., 1995). This complex acts as a DNA damage-activated loader of the 9-1-1 sliding clamp onto chromatin (Ellison and Stillman, 2003; Bao et al., 2004). Loss of RAD17 or RAD1 has a major impact on ATR-dependent checkpoint signalling (Wang et al., 2003; Zou et al., 2003). Several additional proteins, including Claspin, TopBP1, and MDC1 are required for ATR-dependent phosphorylation of Chk1 and Brca1 (Chini and Chen, 2003).

Moreover, it has been observed that they bind to chromatin structures and physically interact with ATR, Brca1, and Chk1 during DNA damage and RS (Chini and Chen, 2004; Lin et al., 2004). The interaction between ATR-ATRIP, RAD17, and RAD9 complexes is critical for phosphorylation of cell-cycle checkpoint signals in response to DNA damage and replication disruption, revealing a direct connection between ssDNA and checkpoint signal activation (Zou and Elledge, 2003), which helps cells complete DNA replication under stress (Brown and Baltimore, 2003).

These mediators help transmit checkpoint signals to the signal transducer protein kinase, which comprises two families of checkpoint kinases (CHK), the Chk1 and Chk2 kinases (Bartek and Lukas, 2003). The Chk1 kinase is highly conserved among eukaryotes. Activation of Chk1 is predominantly ATR-dependent (Liu et al., 2000). Studies have reported that the loss of Chk1 results in viable but proliferation-retarded cells (Brown and Baltimore, 2003; Liu et al., 2000), whilst the Chk2 kinase is the main target of ATM, responding primarily to the formation of DSBs (Matsuoka et al., 2000). Takai et al. (2002) suggested that CHK2 plays a role in regulating apoptosis.

1.6.3 Signal effectors

Downstream of the CHK1/CHK2 activation, the effector proteins for both PIK and CHK kinases, such as Cdc25C, p53, BRCA1, NBS1, and SMC1 (Bakkenist and Kastan, 2003). Effector proteins are targeted and phosphorylated directly by ATM/ATR or CHK2/CHK1 respectively (Harper and Elledge, 2007). These activated effectors proteins will contribute to execute the functions of DDR. The signal is maintained by an interface of coordinated actions between different cellular pathways, including DNA repair, transcription regulation, chromatin remodelling, apoptosis, and cell cycle checkpoints as illustrated in Figure 1.8 (Rouse and Jackson, 2002).

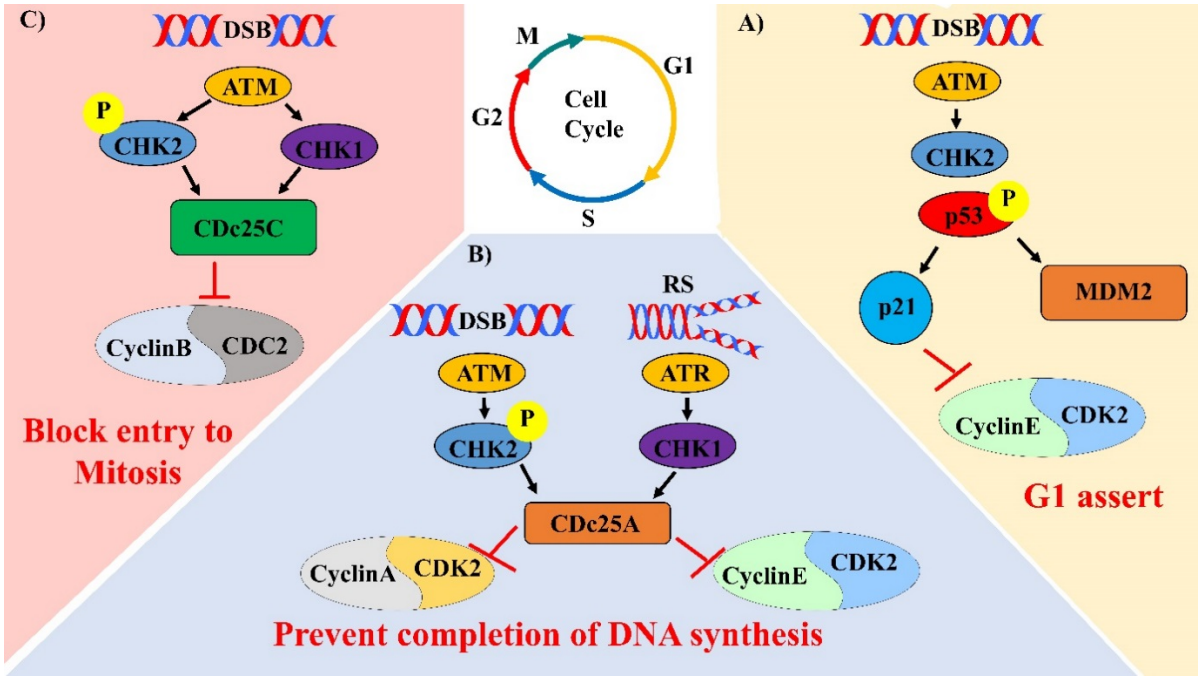

Figure 1.8 Overview of cell cycle checkpoints control and activation in response to replication stress.

ATM/CHK2 and ATR/CHK1 are essential mechanisms for controlling the DNA replication process and monitoring cell cycle progression during S-phase. They inactivate and degrade cyclin-dependent kinases (CDKs) by transcription factor p53 (DiTullio et al., 2002; Ward et al., 2003), by interfering with and contributing to the different mechanisms involved in cell cycle control by reducing the CDKs' function in different cellular processes (Jossen and Bermejo, 2013). It slows down and arrest the cell cycle by activating and accumulating the CDK cyclin-dependent inhibitor (p21) (Kastan et al., 1991). Depending on the nature of the DNA lesion and the cell cycle phase, inhibition of CDKs arrests cell cycle progression at the G1-S transition, intra S-phase, and G2-M transition.

The G1-S transition checkpoints provide repair mechanisms over an extended time frame for the completion of DNA lesion removal; thereby, allowing disrupted RFs to recover prior to replication or mitosis (Figure 1.8.A). Unrepaired DNA lesions have the potential to be converted into inheritable mutations through DNA synthesis. These checkpoints are specialized signal transduction mechanisms thought to maintain genetic integrity (Kinzler and Vogelstein, 1997). ATM and Chk2 phosphorylate and stabilize p53, limiting the interaction between p53 and MCM2 (Maya et al., 2001). The p53 tumour suppressor has a significant impact on the DNA damage induced G1/S checkpoint.

A major consequence of p53 activation is an increased accumulation and expression in cyclin-dependent kinase (CDK) inhibitor, p21 (Harper et al., 1995). This suppresses the function of cyclin E/CHK2 kinase, resulting in inhibition of G1-S transition and preventing the replication of damaged DNA (Massague, 2004). When CDK activity is required, a group of tyrosine phosphatases, such as Cdc25A, Cdc25B, and Cdc25C are capable of removing inhibitory tyrosine phosphorylation from both Cdk1 and Cdk2 kinases; this then promotes entry into and progression through S-phase and mitosis (Jin et al., 2003).

Intra-S checkpoints respond to aberrant RF and spontaneous intra-S-phase damage, monitoring cell cycle progression through a number of different processes. Both ATM/CHK2 and ATR/CHK1 participate in controlling replication processes during this phase by triggering degradation and inactivating CDC25 phosphatase. This in turn inactivates Cyclin E/CDK2 and Cyclin A/CDK2, thereby preventing the completion of DNA synthesis (Figure 1.8.B) (Lukas et al., 2004).

The G2-M checkpoint controls and allows cell cycle arrest prior to chromosome segregation. When cells enter the G2 phase with unrepaired, persistent DNA damage, or experience damage in G2, ATM/CHK2 targets and blocks CDC25 activation, causing the activation of cyclin B/CDC2 and blocking entry to mitosis (Figure 1.8.C) (Bakkenist and Kastan, 2003).

In addition to controlling cell-cycle arrest, DDR pathways regulate a variety of physiological processes, determining whether to stimulate activation of DNA repair pathways and RF recovery. This can be accomplished in a number of ways; either by inducing DNA repair proteins, by modulating phosphorylation, or by recruiting DNA repair proteins to the sites of DNA damage. If the above events enable effective DNA repair, DDR inactivation allows resumption of normal cell function.

In contrast, unsuccessful repair triggers persistent DDR signalling, may induce senescence, or cell death by apoptosis. Thus, the checkpoint comprises a subroutine integrated into the larger DNA damage response pathway, which regulates a multifaceted response (Figure. 1.8) (Gasser and Raulet, 2006).

1.7 DNA repair mechanisms

Repair of DSBs is critical for cell survival and viability; this represents a particular challenge for cells. Various types of DNA repair mechanism exist and act to maintain genome stability. Differing types of DNA damage require a unique set of cellular repair responses. There are two principal mechanisms informing the repair of DNA DSBs: NHEJ and HR (Rothkamm et al., 2003).

1.7.1 Non-homologous end joining

NHEJ is the predominant DSB repair mechanism in mammalian cells and can operate in any phase of the cell cycle (Weterings and Van Gent, 2004). It is an error-prone process, which mediates the direct rejoining of two broken DSB DNA terminals independently of the sequence.

NHEJ also has a role in rejoining physiological breaks in variable diverse joining (V(D)J) recombination in the antibody chain gene (Soulas-Sprauel et al., 2007), and the immunoglobulin class switch recombination CSR (Bothmer et al., 2010).

When DSB is generated, ATM kinase recruits and phosphorylates H2AX at serine 139 (γH2AX) (Celeste et al., 2003), and highly abundant heterodimer Ku70 and Ku86 proteins are recruited to the DSB ends, to initiate the classical or canonical (c-NHEJ) repair pathway (Lieber, 2008). The Ku complex is ring-shaped and binds tightly to the broken DNA ends, forming a stable DSB (Walker et al., 2001). This recruit and activates the DNA-PKcs, which is a catalytic subunit forming a DNA-PK complex (Figure 1.9) (Van Heemst et al., 2004). The DNA-PK complex undergoes auto phosphorylating (Ding et al., 2003), promoting the recruitment of several NHEJ repair proteins to the DSB (Lieber, 2010). The X-ray cross complementing protein (XRCC4) acts as a scaffolding protein, allowing DNA ligase VI to bind to the DNA, ligating the adjacent DSB ends (Nick McElhinny et al., 2000). This attracts the XRCC4-like factor (XLF) and endonuclease ARTEMIS, which plays an important role in enhancing ligase VI function, which is involved in carrying out DNA repair processing (Ahnesorg et al., 2006).

A new sub pathway has been identified, which is known as alternative end joining (A-NHEJ), or microhomology-mediated end joining (MMEJ) (McVey and Lee, 2008). This pathway is considered highly error prone, and can increase incidences of abnormal joining (Han and Yu, 2008). Although the mechanistic details for this pathway are yet to be determined to the same extent as the classical pathway, it is known that this pathway is Ku independent (Weinstock et al., 2007), leading to an increase in illegitimate joining using the 53BP1, MRN complex alongside the exonuclease CtlP (Deriano and Roth, 2013). It also relies on DNA ligase III for end processing, in place of ligase VI (Kasparek and Humphrey, 2011). However, both NHEJ pathways can lead to CIN and subsequently GIN.

Recent studies have demonstrated that A-NHEJ is more deleterious, inducing genome rearrangement, such as chromosomal deletions, insertions or translocation at the breakpoints (McVey and Lee, 2008). Thus, it probably underlies oncogenic transformation.

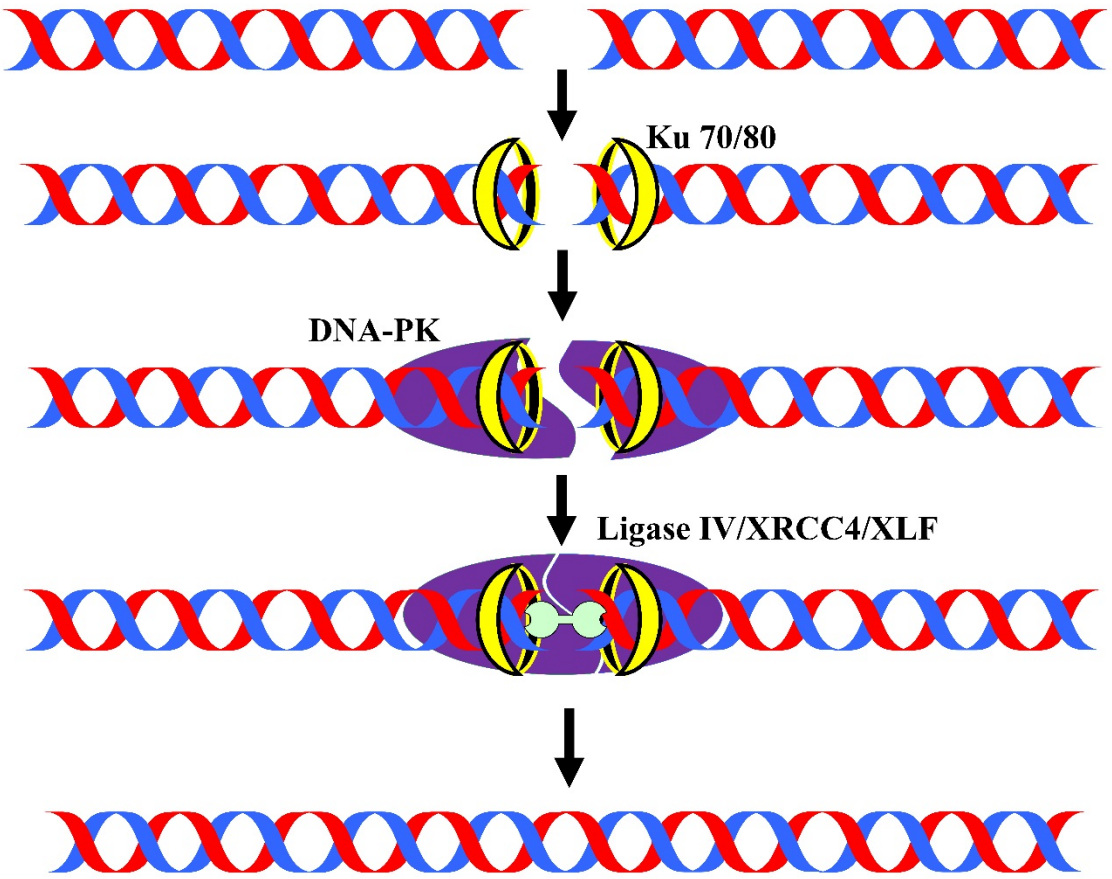

Figure 1.9 Schematic model for classical non-homologous end joining DNA repair pathway involved in the repair of DNA double strand breaks. This figure shows a linear pathway consisting of interactions between several repair proteins. The Ku70/80 protein will first be recruited to DSB and promotes the association of DNA PKcs. The DNA ends are finally sealed by ligase IV/XRCC4/XLF.

1.7.2 Homologous recombination

HR is a less error-prone repair process that occurs in late S and G2 phases of the cell cycle (Ira et al., 2004). It has the ability to accurately repair direct DSBs and se-DSBs using a sister chromatid sequence as a repair template for recombination (Szostak et al., 1983). There are several sub pathways, such as synthesis-dependent strand annealing (SDSA), the classical double Holliday junction (DSBR), and single strand annealing (SSA); all of which contribute to DSB repair. As illustrated in Figure 1.10, these HR sub pathways share common processes and factors, including initiating, end processing, and annealing (San Filippo et al., 2008).

HR is always initiated with a 5'-3' resection of broken DSB ends, promoted by cyclin dependent kinase 1 (CDK1) and mediated by the MRN complex. This complex recruits CtIP protein to trim the 5' end of the break, and, along with other nucleases such as Exo1, created a ssDNA 3' overhang (Ira et al., 2004; Sartori et al., 2007). The exposed 3' overhang is coated first by RPA, and then it replaced RAD51, facilitated by several associated proteins, such as BRCA1 and BRCA2 (Zhong et al., 1998). RAD51 plays a key role in the formation of a nucleoprotein filament, which is capable of a homology search and thus maintaining genome integrity (Baumann et al., 1996). This is consistent with the observation that cells lacking RAD51 accumulate chromosomal aberrations (Sonoda, 1998). The generation of the ssDNA 3' overhang is followed by invasion of the undamaged sister chromatid or homologous chromosome, and formation of heteroduplex DNA, which displaces the DNA strand and forms a D-loop (Ferguson and Holloman, 1996). DNA repair synthesis is carried out beyond the break site, by utilizing one of the HR sub pathways such as those below (Symington and Gautier, 2011).

1.7.2.1 Classical double holliday junction

As illustrated in Figure 1.10.1, in the DSBR pathway, both resected ends of the DSB invade the homologous duplex. One of the free 3' overhangs then extend to create a D-loops and allowing the formation of an initial HJ. Then, a second branch migration from the opposite DNA leads to the formation of a second HJ (Helleday et al., 2007). Finally, these HJs can be resolved in a horizontal or vertical manner, leading to a crossover or non-crossover respectively (Kasparek and Humphrey, 2011).

1.7.2.2 Synthesis-dependent strand annealing

In the SDSA pathway, the 3' end in the D-loop can be extended by the DNA polymerase (eta) to restore missing sequences (McIlwraith et al., 2005), leading to the formation of an X-shaped structure known as the HJ (Figure 1.10.2) (Helleday et al., 2007). Once the repair is complete, sliding the HJ towards the 3'end releases the newly synthesized end. Several proteins, such as RAD54, BLM and WRN, participate in releasing the invading strand, in a process termed 'branch migration' (Nimonkar et al., 2003).

The released strand can then anneal to the other side of the DSB by RAD51 (Forget and Kowalczykowski, 2010). A final process is then carried out to remove flaps, and refill gaps, using DNA ligase I to seal the remaining nicks. This pathway is associated with an exchange of sequential genetic information, resulting in gene conversion, whereby the information is transferred from the unbroken homologous chromosome to the break point. Whereas, if sister chromatid used, no gene conversion event occurs (Kasparek and Humphrey, 2011).

1.7.2.3 Single strand annealing

The SSA is created if the DSB occurs between or adjacent to two repeated sequences. This pathway is mechanistically distinct from the previous HR sub pathway, as no strand invasion stage is required. Nevertheless, the final process in the completion of this sub pathway is similar to that found in other pathways, which informs the removal of remaining flaps filling in single strand gaps (Helleday et al., 2007). When SSA occurs, the 3' overhang ends find homology with each other in a RAD51-independent manner; they then anneal by utilizing RPA and RAD52. However, this mechanism is always error-prone, because it leads to the permanent deletion of varying sizes of sequences in the chromosome, and inevitable loss of information in the two repeats; this arises when the two-sequence homology arises from different adjacent chromosomes (Figure 1.10.3) (Kasparek and Humphrey, 2011).

Moreover, inefficient HR, which involves SSA and/or crossovers, has always been strongly associated with chromosomal rearrangements, such as deletions and translocations. Studies have demonstrated that the repetitive-DNA expansions caused by erroneous or error-prone DNA replication can occur when HR is impaired.

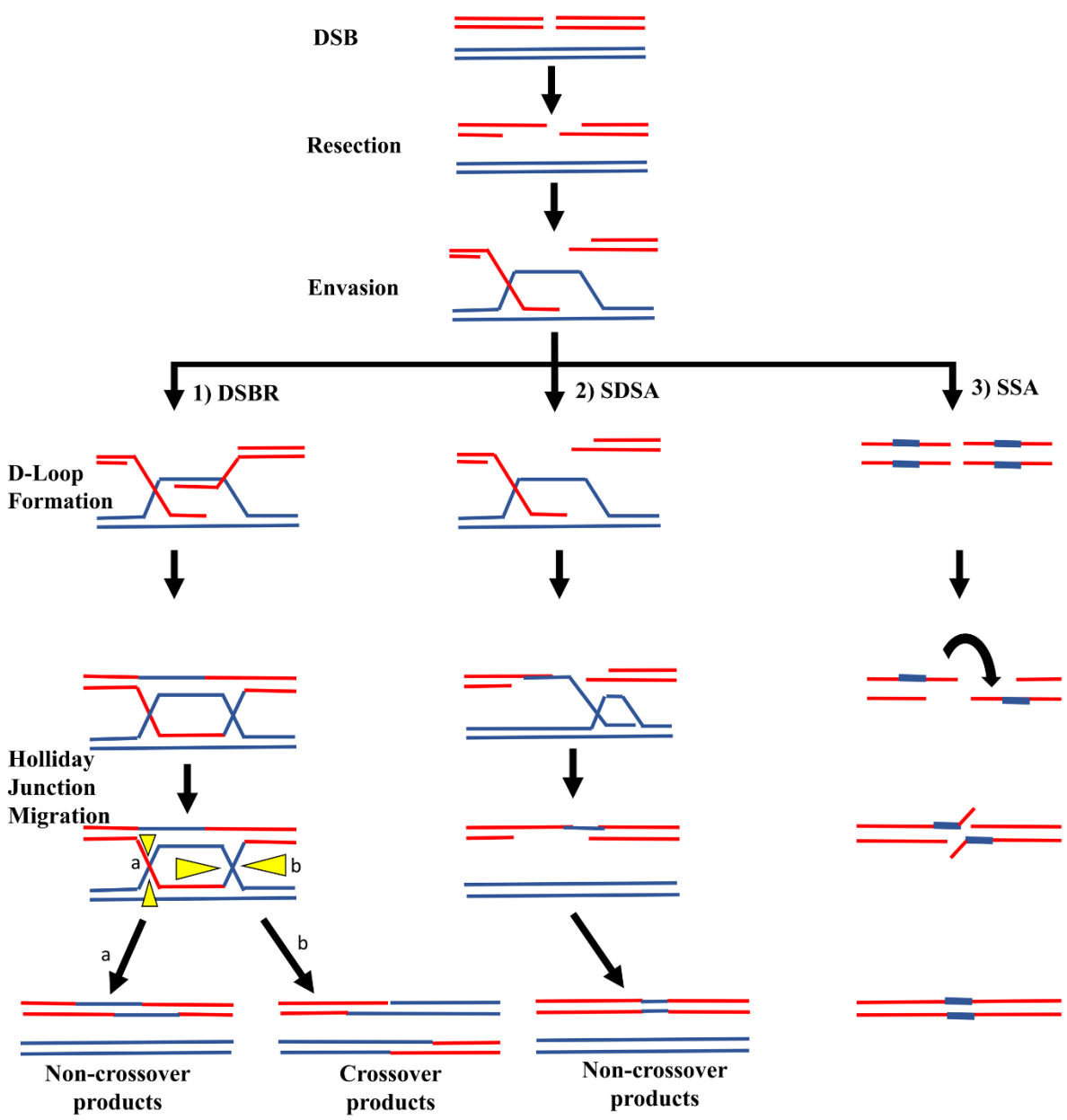

Figure 1.10 Schematic model for homologous recombination repair pathways involved in repairing both DNA double strand breaks and DNA single strand breaks. This figure illustrates three different sub pathways: the classical double Holliday junction (DSBR), synthesis-dependent strand annealing (SDSA), and single strand annealing (SSA). The pathway for these mechanisms starts with the resection of DSB ends, invasion of, and formation of, the D-loop. **(1)** DSBR occurs and forms double Holliday junctions, leading to the formation of crossovers or non-crossover products. **(2)** SDSA occurs via forming a single Holliday junction and leads to the formation of non-crossover product. **(3)** SSA is a distinct mechanism that occurs after resection of DSB ends and annealing of the two single stranded ends, without invasion of a sister chromatid.

1.8 Repair of aberrant replication fork

In addition to the previously described mechanisms of HR sub pathways during direct DSB repair, research has indicated that HR plays a crucial role in repairing and restarting the synthesis of broken DNA RFs during the S-phase by using the sister chromatid sequence to allow RF restart (Michel et al., 2001).

1.8.1 Repair of stalled forks

When a stalled RF remains associated with the functional replisome, DNA synthesis can recover without fork remodelling (Zeman and Cimprich, 2014). Current understanding of the fate of stalled RFs in eukaryotic and prokaryotic cells has been derived largely from in vivo studies (further details will be found in Section 1.12), which suggest stalled forks remain intact and that DNA synthesis can either resume immediately following removal of the original obstacle, or after a short delay once the repair mechanism has occurred; this then allows the coordination of fork-processing (Deshpande and Newlon, 1996; Calzada et al., 2005; Breier et al., 2005). Indeed, it is thought that stalled forks are usually rescued, and the damage repaired by regulatory and error-free repair mechanisms, to prevent fork collapse and breakage (Heller and Marians, 2006; Atkinson and McGlynn, 2009).

As mentioned in previous sections, generation of aberrant RF structures, and the extended persistence of ssDNA adjacent to stalled, newly replicated dsDNA is the principal signal triggering replication checkpoint activation (Branzei and Foiani, 2009).

A vast number of experimental observations have demonstrated that ATR is crucial for stalled RFs, the accumulation of ssDNA, and when triggering the S-phase checkpoint response (Cimprich and Cortez, 2008; Helt et al., 2005; Zhou and Elledge, 2003; Friedel at al., 2009). Once ATR is activated due to ssDNA at stalled forks, it inhibits cell-cycle progression and suppresses the firing of late replication origins, thereby providing additional time for the resolution of stress (Shechter et al., 2004). Thereby, allowing the cell to preserve resources in order to complete DNA synthesis in the vicinity of stalled RFs before mitosis occurs, therefore avoiding generating DNA damage and GIN (Shechter et al., 2004; Cimprich and Cortez, 2008). In addition, ATR helps stabilize and restart stalled RFs, to prevent unscheduled recombination (Brown and Baltimore, 2003).

Upon recruitment to RF, ATR phosphorylates several downstream effector factors, including CHK1, helping the cell to survive and complete DNA replication under stress (Liu et al., 2000). In this sequence, MCM is phosphorylated, contributing to its association with active forks and preventing replisome disassembly and collapse (Branzei and Foiani, 2010).

Intact S-phase checkpoints, arising in response to RS, are essential to the maintenance of functional forks by preventing their collapse. This was deduced based on the observation that checkpoint mutations and mutations in ATR kinase targets contribute to fork collapse when replication inhibitors and accumulated HJ structures are present. Thus, they are responsible for genetic disorders correlated with chromosomal loss, increase rates of translocation, and cause premature ageing or cancer.

1.8.2 Repair of collapsed forks

Once a fork collapses as a result of a lesion or any other factor discussed in Section 1.5.2, it prevents further DNA polymerization (Cobb et al., 2003; Yao and O'Donnell, 2010). Attempts to restart a collapsed fork are likely to prove susceptible to the actions of a variety of specific enzymes, including exonucleases, endonucleases, DNA helicases, and/or recombination proteins, in an effort to restart synthesis and process newly replicated strands with suitable configurations (Cotta-Ramusino et al., 2005). Studies of collapsed RFs in eukaryotic and prokaryotic cells proposed that collapsed RF may repair and restart replication via template switch pathways by utilizing a sister-strand as a template and subsequently can form several structures (Figure 1.11).

Collapsed replication machinery could be reprimed via pathways that permit the cell to bypass the DNA lesion using specialized polymerases. Lesion bypass, or 'tolerance', can arise through a switch from high-fidelity replicative polymerase to translesion polymerase (Heller and Marians, 2006). Lesions that block leading-strand or lagging-strand synthesis, without impeding fork progression, can be bypassed by the RF, forming topological intertwining between the two strands, a structure named as hemicatenane (Ahmed and Podemski, 1998). The hemicatenane is then resolved, most likely by the action of the helicase and topoisomerase. Collapsed replication forks can be repaired by fork reversal, leading to the formation of the so-called 'chicken foot' structure (Zou and Rothstein, 1997; Sogo et al., 2002).

Recent evidence has also suggested that regressed RF structure may resolve with more complicated mechanisms, involving replication and/or strand invasion, or possibly by following HJ-cleavage, which seems particularly susceptible to nuclease digestion and therefore potentially forms a DSB in the absence of ATR signalling (Michel et al., 2001). The regressed RF can restart a fork after a lesion has been bypassed, generating a ssDNA gap behind the fork, or creating ssDNA gaps between two flanking Okazaki fragments (Pomerantz and O'Donnell, 2010). In both cases, ssDNA gaps are then repaired with error-prone translesion synthesis (TLS), or filled using specialized lesion bypass pathways, referred to as DNA damage tolerance (DDT) (Lehmann et al., 2007). However, the physiological role of these structures remains unclear.

Together, these replication fork mechanisms support complete replication, preventing prolonged fork blockage. However, a number of studies have suggested template switching mechanisms serve to induce GIN (Putnam et al., 2010).

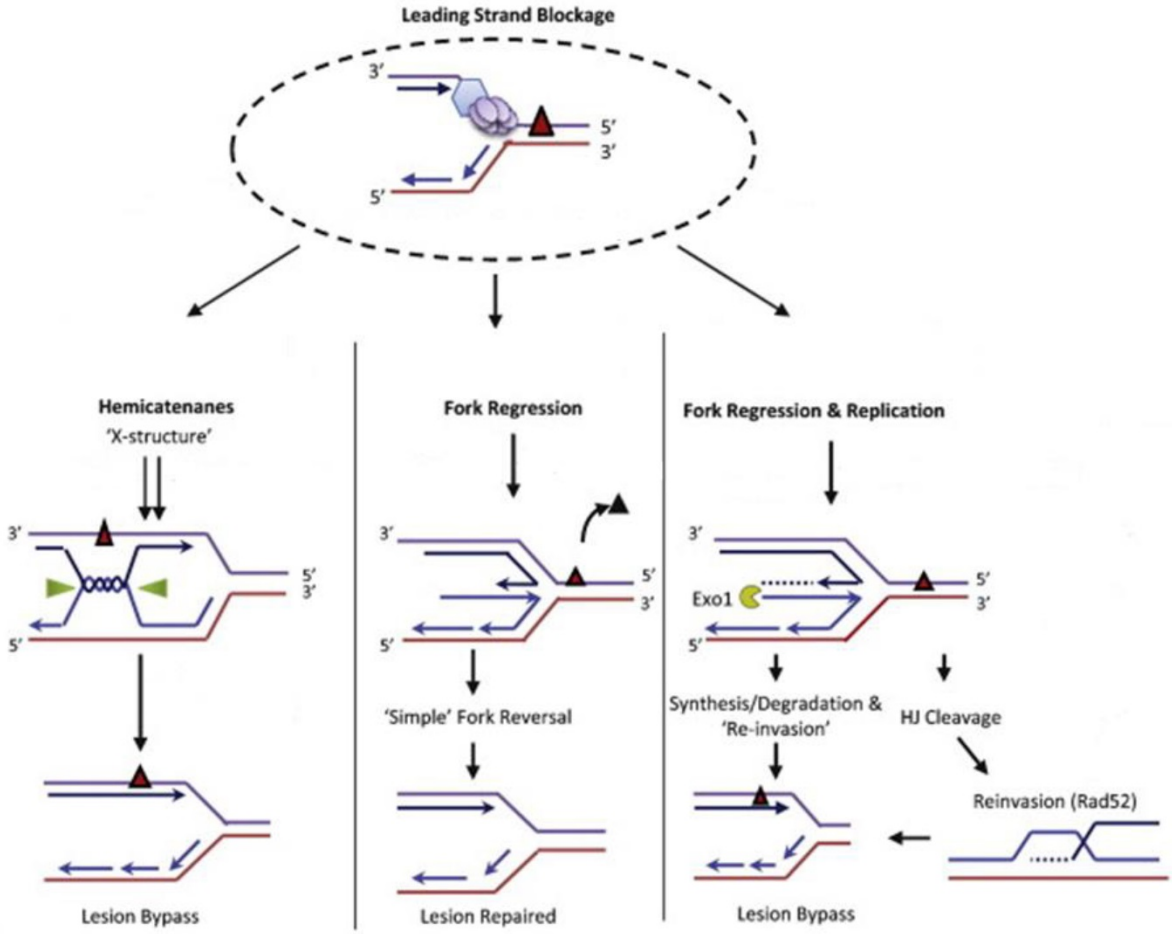

Figure 1.11 Schematic models for repairing and restarting collapsed replication fork. (Left panel): Lesions that block leading- or lagging-strand synthesis, without impeding fork progression, can be repaired by template switching pathway by utilizing a sister-strand as a template. Lesion bypassed by the RF, forming hemicatenane. **(Middle panel)**: Collapsed replication forks can be repaired by simple fork reversal, leading to the formation of the so-called 'chicken foot' structure that allow lesion repair. (**Right panel**): Regressed fork can be combined with lesion bypass. Adapted from (Weinert et al., 2009).

1.8.3 Repair of broken fork

HR can mend se-DSBs that arise during aberrant DNA replication fork progression, including following collision with a SSB, via break-induced replication mechanism (BIR) this may require HR proteins to facilitate correct pairing (Kraus et al., 2001; Michel et al., 2001), or recombination dependent replication (Llorente et al., 2008).

In mammalian cell lines, the precise molecular mechanisms underlying the BIR pathway remain obscure and speculative because of technical and methodological limitations. However, recent studies of the yeast *Saccharomyces cerevisiae* reveal BIR shares initial steps with HR (Sakofsky et al., 2012).

BIR events begin with 5' and 3' resections of a broken se-DSB, creating a 3' overhang ssDNA that can locate intact homologous chromosomes and conduct invasion of sister chromatids to permit RF restart (Llorente et al., 2008). According to existing yeast models, BIR can employ three proposed mechanisms, all of which share a similar round of strand invasions as an initial step, but differ in how they model the migration of the D-loop in the later phases of recombination (Figure 1.12) (Kraus et al., 2001). Strand invasion precedes either RAD51-dependent or RAD51-independent pathways (Davis and Symington, 2004; Malkova et al., 1996). The latter pathway is known as microhomology-mediated BIR (MMBIR) (Zhang et al., 2009); which requires certain replication factors such as DNA helicase, Cdc45, MCM, and GINS (Szostak et al., 1983).

In addition, BIR is associated with template switching of the damaged replicating strand with the undamaged sister chromatid, in order to attain DNA synthesis (Smith et al., 2007). Thus, template-switching BIR can be highly mutagenic, meaning the process could be important for genome rearrangements, evolution, and the understanding of disease development in humans (Deem et al., 2011; Burrell et al., 2013).

Studies into mammalian cells indicate that inefficient HR is a dangerous source of GIN (Zhang et al., 2009) and can lead to LOH, as implicated in genetic diseases such as cancer (Burrell et al., 2013; Peto, 2001). Indeed, MMBIR has been associated with chromosome rearrangements, such as CNV (Sakofsky et al., 2012).

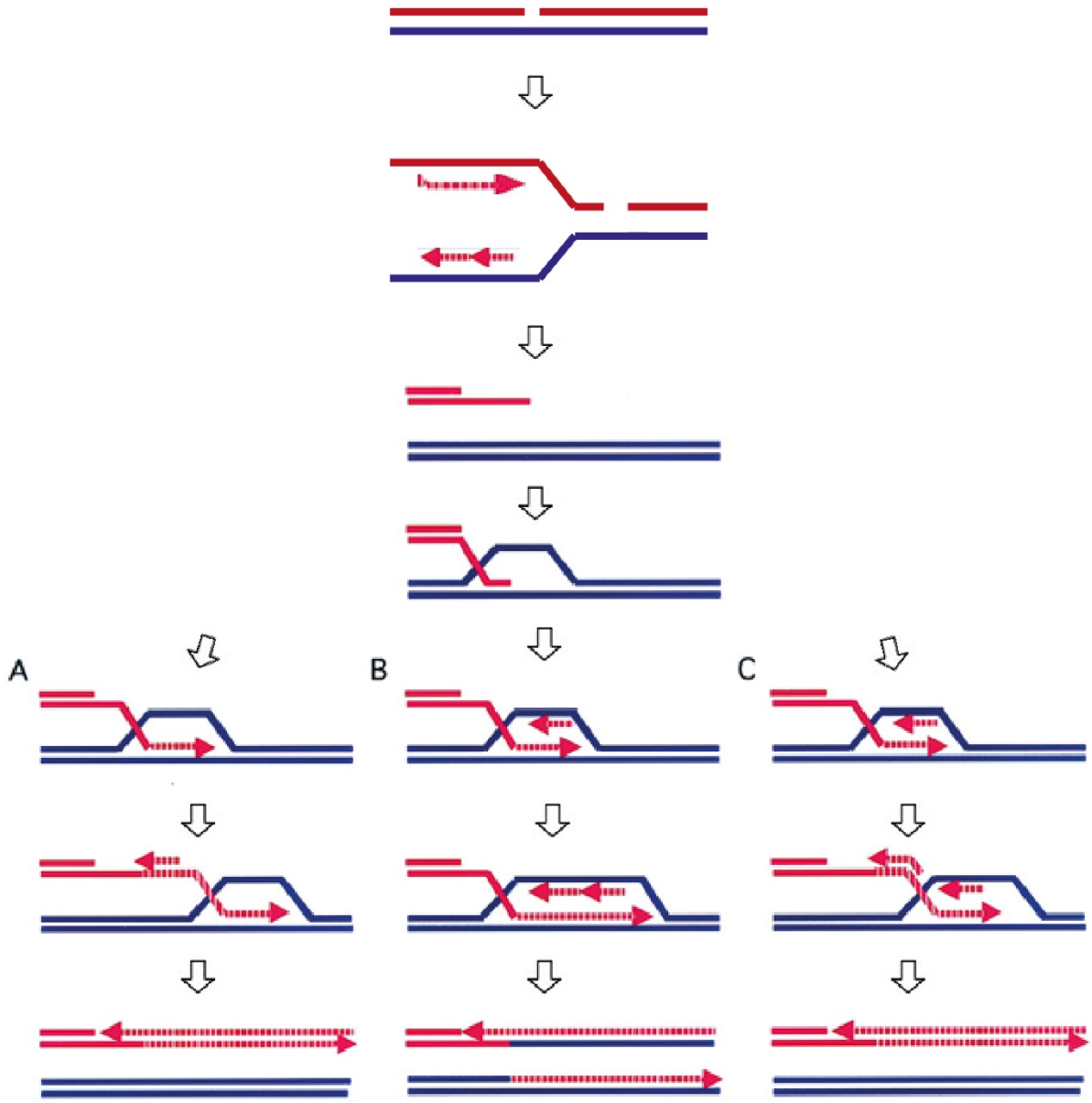

Figure 1.12 Schematic mechanisms for break induced repair and the proposed sub pathways involved in the repair of single ended DSB. **(A)** 3′ end of the invading strand creates a D-loop that migrates the template and initiates DNA replication. The newly synthesized DNA strand can then be double-stranded. **(B)** Strand invasion sets up a D-loop that could be transformed into a complete unidirectional replication fork, and a single Holliday junction is formed that must be resolved by cleaving the DNA strands. After cleavage of the Holliday junction, remaining nicks can be ligated and replication can proceed normally. **(C)** Strand invasion establishes a replication fork, in which branch migration enzymes displace both newly synthesized DNA strands as the replication structure migrates down the template. This figure is adapted from (Kraus et al., 2001).

1.9 Replication stress and cancer

An association has been established between a number of genetic diseases and inhirited or sporadic defects in: (1) DNA replication machinery; (2) damage signalling; (3) replication stress response; and (4) repair pathways (Kastan, 2007; Jackson and Bartek, 2009). As listed below in Table 1.2, the partial loss (i.e. hypomorphic mutation) of these proteins might be expected to contribute to multiple genetic human pathologies, including: neurodevelopmental/neurodegenerative (Kulkarni and Wilson, 2008), premature aging (Schumacher et al., 2008), and a predisposition to cancer (Gorgoulis et al., 2005).

Cancer is a genetic disease that arises from aberrant cell cycle regulation, and results in uncontrolled cell proliferation. This aberrant proliferation is ultimately caused by accumulation of DNA mutations from DNA-RS and/or DNA-damage formation. These mutations lead to either oncogenes activation, or the inactivation of tumour suppressors (Peto, 2001). A fundamental feature of the majority of cancers is their display of GIN, which is considered a hallmark of many tumours, providing a source of genetic alteration (Negrini et al., 2010).

The majority of the early stages of neoplastic lesions contain elevated levels of DDR, which protect against malignancy through the introduction of cellular senescence or apoptosis (Bartek et al., 2007). It has recently been demonstrated that pre-cancerous cells have the ability to evolve tolerance against DNA damage, continuing to proliferate whilst under RS. This ability is achieved based on several mechanisms, including bypass DDR-mediated cell growth inhibitors or mutations in the DDR mechanism (DNA repair and DDR signalling), resulting in a defective DDR and elevated GIN (Foster et al., 2012).

Cell growth inhibitors are well conserved among eukaryotes, and serve as a potential cancer barrier, by responding to RF stalling and breakdown (Jackson and Bartek, 2000). Multiple mutations (or epigenetic inactivation) in these DDR genes during cell division co-operate to promote GIN, and subsequently the immortalization and transformation of cells during tumour development, thereby allowing malignant progression. This facilitates senescence, apoptosis bypass, and tumour-cell survival and proliferation, despite the accumulation of DNA damage, along with enhanced mutation rates and GIN (Luo et al., 2009).

In cancer cells harboring an ineffective damage response, continuous RS will cause defective cell cycle arrest and various mutations, not only contributing to the initiation of the disease, but also influencing both the progression of the disease's chromosomal instability and tumour heterogeneity (Burrell et al., 2013), which in turn drives tumour evolution.

It has been demonstrated recently that RS contributes to both cell transformation and predisposition to cancer (Tomasetti and Vogelstein, 2015), although the relationship between RS and tumorigenesis has yet to be elucidated, and RF recovery failure might prove an important feature of the oncogenic process. Studies report that abnormal DNA replication in cancer cells is linked to wide-scale genome aberrations, i.e. CIN (Burrell et al., 2013). It has also been confirmed that CIN is present in the majority of sporadic solid tumours (i.e. colorectal cancers), thus suggesting a causative link between RS and cancer (Vogelstein and Kinzler, 2004; Armaghany et al., 2012).

Mutations in replication machinery, or dysregulation of replication timing (i.e. mutations in genes involved in replication origin licensing), result in a reduction in the number of licensed origins, leading to the persistence of stalled RF; they have thus been found to play an important role in increasing GIN (Kawabata et al., 2011).

Furthermore, additional forms of GIN include GCRs, including translocations and CNV, which result in aberrant expression of oncogenes (Kasparek and Humphrey, 2011). GCRs are strongly stimulated by a mutation that effects S-phase checkpoint proteins, thus causing premature S-phase entry and breaks that accumulate due to collapsing and/or breaking RF, i.e. a mouse cell line with defective MCM4 is associated with a higher level of chromosome breaks (Nussenzweig and Nussenzweig, 2010).

A considerable number of additional inherited human diseases have been linked to defects in the DNA repair processes. Research reveals that both fork instability and defective DSB DNA repair relate to both predisposition to cancer and aging. Mutations in the HR or NHEJ repair gene (i.e. Rad51 or KU70/80, respectively) slightly increase GCRs, and have been associated with an increased risk of cancer (Fattah et al., 2008). Such rearrangements imply these repair pathways potentially play a role in GCR suppression. In vitro studies have demonstrated that mutations in NHEJ repair frequently correspond to increased levels of chromosomal translocation, resulting in a predisposition to lymphoid malignancies (Nussenzweig and Nussenzweig, 2010).

Similarly, deregulated HR key proteins have also been identified as contributors to cancer, while ATM deficiency has been found to generate translocations and promote tumorigenesis (Nussenzweig and Nussenzweig, 2010).

BRCA1 and BRCA2 genes in the HR repair pathway accumulates chromosome aberration and confers susceptibility to breast and ovarian cancers (Fackenthal and Olopade, 2007),

Table 1.2 A selection of DDR genes with their association in human diseases.

Gene	Disease	Reference
RNase H2	Aicardi–Goutieres syndrome	Crow et al., 2006;
ORC complex	Meier–Gorlin syndrome	Hossain and Stillman, 2012; Kerzendorfer et al., 2013; Bicknell et al., 2011
ATM	Ataxia-telangiectasia (A-T) Cancer predisposition: breast cancer Hematological neoplasia Lymphomas and leukemias	Gennery, 2006
ATR	Develop Seckel syndrome	O'Driscoll et al., 2003
P53, CHK2	Li-Fraumeni syndrome Cancer predisposition: breast cancer	Li et al., 1988
ATRIP	Develop Seckel syndrome	Ogi et al., 2012
MRN complex	Microcephaly and mental retardation	Demuth and Digweed, 2007
Rad51	FA-like disorder Familiar breast cancer	Levy-Lahad, 2010;
MRE11	Ataxia-Telangiectasia-like disorder (A-TLD)	Schiller et al., 2012
NBS1	Nijmegen breakage syndrome Cancer predisposition: breast cancer B-cell lymphomas	Varon et al., 1998; Spry et al., 2007
BRCA2	Fanconi's anaemia (FA)	Moldovan and D'Andrea, 2009;

	Myelodisplasia (pre-leukemic syndrome) Acute myeloid leukemia (AML)	Fanconi, 1967
BLM	Bloom syndrome Cancer predisposition	Ellis, N. A., German, 1996
WRN	Werner syndrome Cancer predisposition	Oshima et al., 1996
TLS polymerase Pol η	Xeroderma pigmentosum	Broughton et al., 2002
Artemis	Thymic lymphomas	Jacobs et al., 2011
RecQ4L	Rothmund-Thomson (RTS) syndromes, RAPADILINO syndrome and Baller-Gelrold syndrome.	Bernstein et al., 2010; Croteau et al., 2014

1.10 DNA damage response defects and cancer therapy

Cancer therapies largely comprise of DNA damaging radiotherapy and chemotherapies. Such therapies rely on the induction of DNA damage that is lethal for the highly proliferative cells, but without causing excessive damage to the surrounding normal cells that are proficient in DNA damage response (Woods and Turchi, 2013). However, the majority of cancer cells are able to resist this radio- and chemo- therapy lethality by deregulation or overexpression of DDR proteins (Karnitz et al., 2005; Myers et al., 2009; Hills and Diffley, 2014).

This has led to the speculation that, in order to develop more effective cancer therapeutic approaches, a concept needs to be proposed to target and exploit resistance pathways as a means of cancer therapy (Martin et al., 2008). In principle, the inhibition of a pathway on which a cancer cell is dependent (along with reduction in, or absence of, DDR) could enhance the effectiveness of a therapy. Therefore, knowledge of DDR could be used to identify drug targets for cancer, thereby providing a rationale for exploiting DDR mediated proteins, which act to suppress proliferation of aberrant cancerous cells, and so correlate positively with therapeutic outcomes when developing anticancer drugs.

The delicate balance between RS and cancer is currently being exploited to semi-selectively target and transform cells during cancer treatment.

This has recently also been put into practice in a number of pharmacological studies, which have synthesized chemical structures using several network modelling approaches (along with high throughput cell-based screens from compound libraries), to identify, characterize, and predict DDR inhibitors with potential applications for cancer therapy (Table 1.3).

Methods have been demonstrated using PARP1 inhibitors, which block the repair of SSBs, converting them to DSB breaks (Lord et al., 2008). This type of inhibitor has a non-toxic effect on normal cells, but proves strikingly cytotoxic, resulting in lethality in breast cancer cells that have lost BRCA1/2, and consequently the ability to repair DSBs. The accumulation of unrepaired DNA breaks in the absence of both PARP-dependent SSB and HR has led to the PARP1 inhibitor's successful use as a treatment for breast cancer cells mutated in HR genes, including BRCA1 or BRCA2 (Farmer et al., 2005; Bryant et al., 2005).

Consistent with this approach, a number of recent studies have demonstrated that further inhibitors of the DNA repair pathways have also been tested, employing a similar logic to cancer therapy (Fokas et al., 2013). ATM, DNA-PK and CHK1 inhibitors have preferential toxicity towards cancer cells, after treatment with genotoxic agents (Golding et al., 2012; Zhao et al., 2006; Riesterer et al., 2011).

Table 1.3 List of DNA damage response inhibitors. [a]

Compound	Targets	Description	References
Caffeine	ATM, ATR	First ATM, ATR inhibitor radio-sensitiser for p53 deficient cells	Powell et al., 1995
Wortmannin	ATM, PI3K, DNA-PK	Initially identified to inhibit PI3K family, radiosensities cells	Price and Youmell, 1996
CP466722	ATM	Reversible, rapid, highly specific ATM inhibitor	Rainey et al., 2008
KU-55933	ATM	First potent and selective ATM inhibitor Confers marked sensitisation to IR and DNA DSB inducing chemotherapeutics.	Hickson et al., 2004
KU-60019	ATM	Similar to KU-55933, yet improved sensitivity	Golding et al., 2012
KU-559403	ATM	Improved potency over KU-55933 and bio viability	Batey et al., 2013
Schisandrin	ATR	First ATR selective inhibitor, weak activity	Nishida et al., 2009
NU-6027	ATR	NU6027 was originally developed as CDK2 inhibitor, but also potently inhibits ATR activity. Has been demonstrated to chemo- and radiosensitise several breast and ovarian cancer cell lines	Peasland et al., 2011
NVP-BE2234	ATR	Dual inhibitor for PI3K and MTOR	Maira et al., 2008
ETP-46464	ATR	Non-selective ATR inhibitor	Liu et al., 2011

Torinz	ATR	Non-selective ATR inhibitor	Toledo et al., 2011
VE-821	ATR	ATR phosphorylation inhibitor with reduced activity on PIKKs	Charrier et al., 2011
VE-882	ATR	Also known as VX-970, analogue of VE-821, yet greater ATR sensitivity and potency. First inhibitor for clinical development.	Fokas et al., 2012
AZ20	ATR	Selective ATR inhibitor	Jacq et al., 2012
AZD6738	ATR	Analogue of AZ20 with improved solubility and bio viability	Foote et al., 2013
RAD51 B02	Rad51	B02 is a specific inhibitor of RAD51 recombinase. Rad51 is often overexpressed in cancer cells where it helps to cause resistance. RAD51 inhibitors are being sought to aid in cancer treatment It disrupts RAD51 binding to DNA, increasing cell sensitivity to DNA damage	Huang and Mazin, 2014
Mirin	MRE11	Mirin inhibits MRN complex in mammalian cells, thus inhibit ATM activiation	Dupre et al., 2008
NU7441	DNA-PK	Specific inhibitor	Zhao et al., 2006
LY294002	DNA-PK	Inhibits different PIKK family	Vlahos et al., 1994
CC-115	DNA-PK	Inhibits both DNA-PK and TOR kinase	Postel-Vinay et al., 2012
NU-7026 *	DNA-PK	Novel, specific, reversible DNA-dependent protein kinase (DNA-PK) inhibitor. Increases G_2/M arrest and inhibits double-strand break repair. Inactive for ATM, ATR.	Veuger et al., 2003

[a] The DDR inhibitors used in this study are highlighted. The highlighted rows indicate inhibitors been used in this study.

1.11 Studies of replication stress response in eukaryotes

Despite the clinical relevance and biological significance of RS; associated molecular events remain unclear. A number of studies have investigated how cells respond to the forms of DNA damage and RS by using various DNA genotoxic chemical agents that target replication, inducing fork blocks, such as compounds listed in Table 1.1 (Kobayashi et al., 2003; Ahn et al., 2011;-Cobb et al., 2005). Although these RS inducers and their initial effects vary ranging from fork stalling and uncoupling, reversal or "run-off", all can ultimately result is chromosome breakage (Zeman and Cimprich, 2014). Collectively, these studies suggest DNA damage induces fork aberration and subsequent impact genome stability and cell viability. Even though studies of RS induced by genotoxic agents have been very successful previously, yet they are technically limited. These agents cause genome-wide damage, and where forks collapse or break cannot be precisely controlled, preventing events associated with RS from being studied directly. This includes elucidation of the precise molecular mechanisms that underlie the processing of broken DNA RFs (se-DSBs), either during re-initiation and restart of replication forks, or mutation-causing misrepair.

Current understanding of fork behavior, and the fate of stalled replication forks and repair in eukaryotes derive from in vivo studies. The majority of developed systems involved inducible stalling by sites occupied by blocks to DNA replication, such as specific DNA sequences, or protein–DNA complexes usually possessing RF progression. Kobayashi et al. (2003) developed a Fob/RFB system in budding yeast. In this system, a protein called Fob1 binds to a specific replication fork barrier (RFB) site, which is a 100-bp DNA sequence located near the nontranscribed spacer 3' end of the rRNA genes, blocking DNA replication fork in one direction within the ribosomal DNA (rDNA) transcription. However, the high frequency of Fob1-stalled forks does not necessarily alter DNA structures or form unusual chromosome structures (Kobayashi et al., 2003). Similarly, the Rtf1-RTs1 system was developed in fission yeast, blocking DNA replication by generating a stalled fork (Ahn et al., 2011). In this system, the Rtf1 protein typically binds to a specific single RTS1 DNA sequence, and Rtf1 expression blocks DNA replication at sites close to a mating type locus. These systems allow monitoring of fork behavior, showing forks stall briefly prior to resuming replication. However, details regarding the process by which replication resumes are not described. Nevertheless, the Rtf1–RTS system was manipulated to achieve more efficient fork stalling by inserting two inverted RTS1 sequence sites.

Subsequently the expression of the Rtf1 protein caused the stalling of two replication forks; this frequently leads to fork breakage suggesting instability due to rearrangement of chromosomes (Lambert et al*.,* 2005).

Recently, a significant number of experimental systems have suggested a direct association between stalled RF and genome instability. Sundararajan and Freudenreich (2011) directly demonstrated that stalling caused by triplet repeats causes DSB, threatening genome stability. These studies promise huge advances in knowledge regarding how eukaryotic cells respond to aberrant forks, and provide some key insights into the repair and restart mechanisms of stalled forks. However, speculation remains that there is a precise understanding of exactly how replication fork defects are converted into genetic instability and mutations. However, there are very few inducible RS systems, particularly for studying BF. Recently, a site specific *in vivo* system in budding yeast, known as the FLP-nick system, was developed by Nielsen et al. (2009; 2012).

The FLP1 recombination system is a successful *in vivo* technique, originating from the 2 μM plasmid of *Saccharomyces cerevisiae* (budding yeast), used for site-directed recombination for the purpose of manipulating cellular genomes (Kolb, 2002). The process applied here shares similarities with the Cre-lox recombination of bacteriophage p1 (Jones *et al*., 2005), which involves DNA strand exchange between two DNA segments. FLP1 recombination comprises recognition and binding of wild type (WT) FLP recombinase to short DNA sequences at FLP recognition target sites (FRT) (Kolb, 2002).

The normal FLP recombination reaction, catalyzed by WT-FLP recombinase, requires two DNA substrates, and four FLP recombinase monomers (Lee and Jayaram, 1997). Recombination is initiated when 2 FLP monomers recognize and bind to the FRT sites. Strand cutting then follows through nucleophilic attack by the active tyrosine (Tyr343) on a single phosphodiester bond in each substrate. This cleavage is trans-horizontal, with the result that only a single strand break occurs (Chen *et al*., 1992). The cleavage step is followed by a strand exchange step, which forms a transient covalent phosphotyrosine bond with a 3'end DNA backbone phosphate and an adjacent free 5' deoxyribose hydroxyl group (Lee *et al*., 1999). Rapid ligation steps typically reverse this process; for example, a free 5'hydroxl group might attack the partner strand, forming an HJ at opposite end of the strands. This junction then resolves to produce two recombinant DNA products (Lee *et al*., 1999).

As illustrated in Figure 1.13, step arrest mutants of FLP recombinase, such as FlPH305L, generate aberrant long-lived protein DNA complexes (Parsons *et al.,* 1988). Nielson *et al*. (2009) provided a site-specific system, termed the FLP-nick system, which was used to study fork breakage and cellular responses in budding yeast.

The FLP-nick system is based on mutant FlPH305L recombinase, which, when nuclear-localized, attacks the phosphodiester bond of the DNA backbone at the integrated FRT loci (Parsons *et al*., 1988). However, the presence of a covalent bond at the 3'end of the initiated nick is irreversible. The long-lived protein-DNA complexes prevent the subsequent strand exchange and re-ligation steps (Parsons *et al*., 1988). Upon DNA replication, RF encounters the generated SSB, which causes DNA RF breakage at the loci due to fork "run off", generating a se-DSB at a defined genomic site. This testable system enabled the study of cellular responses to single broken RF, leading to genome rearrangement in *Saccharomyces cerevisiae* (Nielsen *et al*., 2009; 2012). This action therefore mimics the mechanism of CPT-induced TOP1 inhibition, leading to long-lived TOP1-DNA adducts and ultimately se-DSBs upon replication (Koster *et al*., 2007).

Despite the progress achieved to date, there is a lack of availability of mammalian based methodical systems to use as tools to study RF, including BF responses and understand its biological significance. The lack of data concerning defined and site-specific broken forks has prevented elucidation of the molecular mechanism that determines RF resolution or misrepair.

The development of novel systems to study RS are essential to boost our current understanding of the molecular mechanisms underpinning replication fork biology, and the associated genome instability that underlies the oncogenic process. Molecular studies to increase understanding of how replication fork recovery mechanisms act to resolve aberrant fork behaviour would provide important clues to understanding which replication fork events might drive genome instability. Advances in current understanding regarding the processes of, and response to, replication stress are crucial steps towards helping to identify the most efficient specialized therapies to help develop new treatments for cancer.

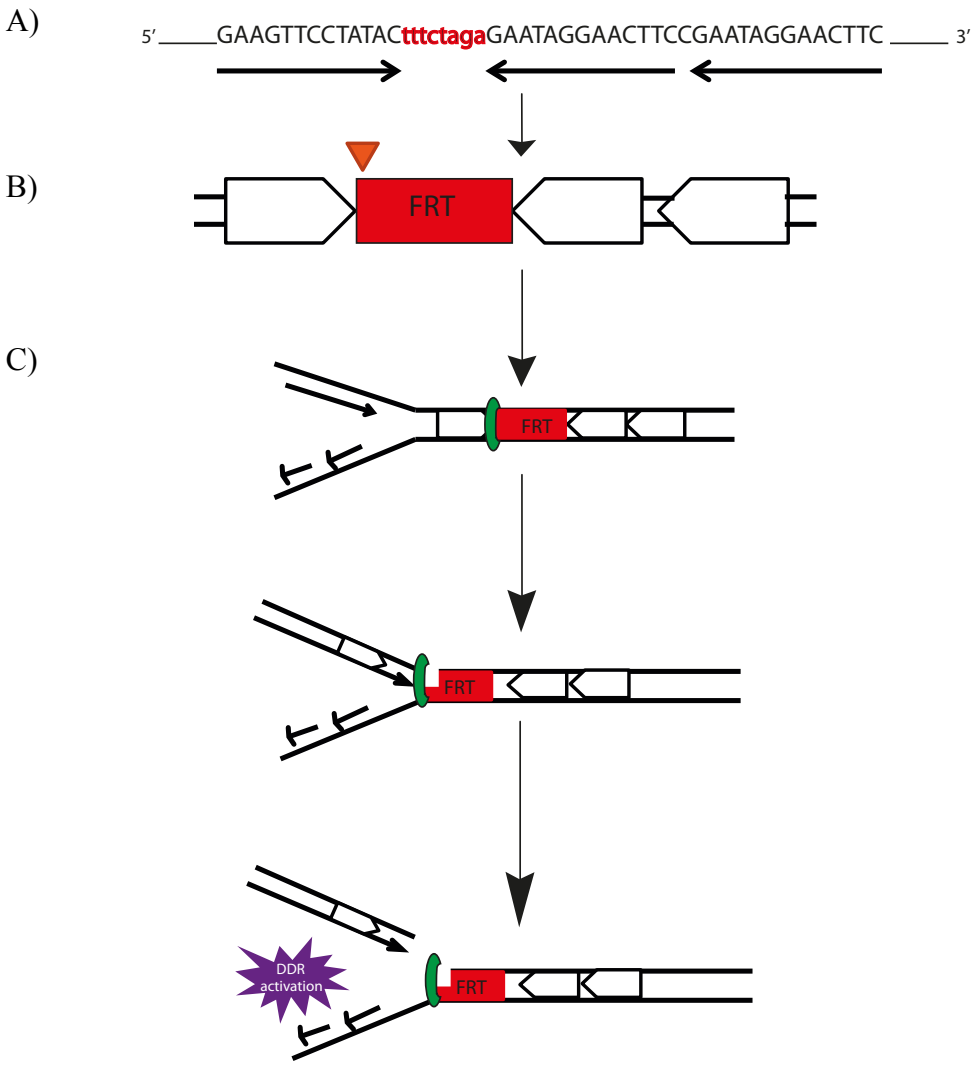

Figure 1.13 Schematic representation of the FLP-nick system. A) The FLP recognition target site (FRT) is 47 nucleotide long, comprising three symmetrical DNA elements (black arrows); each 13 bp long (5' -GAAGTTCCTATTC-3'). Two of these elements were inverted with a reverse orientation, a third element is also present in tandem, upstream from one of the elements. An 8 bp central site-specific recombination spacer (tttctaga) separates the two inverted elements. **B)** FLP recombination comprises recognition and binding of FLP recombinase (Red arrow head) to short DNA sequences at FRT. FlPH305L recombinase, attacks the phosphodiester bond of the DNA backbone at the integrated FRT loci. The presence of a covalent bond at the 3'end of the initiated nick is irreversible. The long-lived protein-DNA complexes prevent the subsequent strand exchange and re-ligation steps. **C)** During DNA replication the single strand break that converted to broken replication fork (se-DSB).

1.12 Study Aim

The overall aim of this project is to clarify the molecular mechanisms of broken DNA replication fork processing and mutagenesis in mammalian cells by developing an inducible FLP-FRT system to generate broken DNA replication forks at specific genomic loci. The research will study the DDR-mediated pathways of BF resolution, which may act to suppress GIN, prevent tumourigenesis, and influence therapeutic resistance, and will determine whether se-DSBs provide a basis for GCRs linked to tumour initiation and heterogeneity.

Objectives

The objectives of this study were:

1. To generate a system to induce broken DNA replication forks (se-DSBs) at specific genomic loci during DNA replication. The development of this system will provide a significant tool with which to study the biological aspects of se-DSB resolution in mammalian cells in *vivo*.
2. To validate the various aspects of the innovative system, including its efficiency as a means of generating replication-dependent se-DSBs in various mammalian cell lines.
3. To analyse the molecular mechanisms of se-DSB processing by conducting various assays, such as viability assays and mutation analyses.

As an independent but interlinked aim of this project, the research investigated the role of NHEJ during S-phase. The laboratory recently uncovered an unexpected role for NHEJ in genome stability maintenance during RS. This project used metaphase spreading and other cellular and molecular techniques to study the evidence of this function as a response to RS.

Chapter 2: Materials and Methods

2.1 Cloning

2.1.1 Solutions

Table 2.1 Solutions used for cloning

Solution	Constituents
EDTA	(ethyldiaminetetra-acetic acid di-sodium salt) was dissolved in dH_2O, and adjusted to pH 8.0 by adding 5 M NaOH.
SDS	Sodium dodecyl sulfate crystals were dissolved in dH_2O at 68°C. The solution was adjusted to pH 7.2 by the addition of concentrated HCl.
dNTPs	Purchased as 100 mM individual stocks (dATP, dTTP, dCTP, dGTP) (Promega#U1330). Working stock of 2 mM was prepared my mixing 2 µl of each dNTP with 92 µl of dH_2O, and stored at -20°C.
5X TBE buffer	5.45 g Trizma base 5 ml 1 M sodium citrate 6 ml 0.5 M EDTA

2.1.2 Primers

Lyophilised primers purchased from SIGMA were prepared by adding nuclease free water (ddH_2O) to a final concentration of 100 µM. 10 µM working primers stocks were prepared by diluting in ddH_2O. All primers were stored at -20°C.

Table 2.2 Oligonucleotides sequences used for amplifications, cloning and sequencing

Oligo name	Oligo sequence (5'>3')
	Cloning Primers
FRT1_ISceI overhangs	CAGGGTAATGAAGTTCCTATACTTTCTAGAGAATAGGAACTTCCGAATAGGAACTTCTAGGGATAA
FRT2_ ISceI overhangs	CCCTAGAAGTTCCTATTCGGAAGTTCCTATTCTCTAGAAAGTATAGGAACTTCATTACCCTGTTAT
FRT1_XholSac_sal_KpnI	GGCTGGCTCGAGCTCAAGAAGTTCCTATACTTTCTAGAGAATAGGAACTTCCGAATAGGAACTTCTGTCGACGGTACCGTGAAC
FRT2_XholISacI_KpnISall	GTTCACGGTACCGTCGACAGAAGTTCCTATTCGGAAGTTCCTATTCTCTAGAAAGTATAGGAACTTCTTGAGCTCGAGCCAGCC
BglII-FRT-EcoNI-primerA	GATCTGAAGTTCCTATACTTTCTAGAGAATAGGAACTTCCGAATAGGAACTTCCCTCC

BglII-FRT-EcoNI-primerB	AGGAGGGAAGTTCCTATTCGGAAGTTCCTATTCTCTAGAAAGTATAGGAACTTCA
EcoNI-FRT-BssHII-primerA	AGACAGCTTTCTAACAACGCCTCCTCCTCTAGGGAAGTTCCTATACTTTCTAGAGAATAGGAACTTCCGAATAGGAACTTCCGCGCGACGGATCGGGAGATCCGTCACT
EcoNI-FRT-BssHII-primerB	AGTGACGGATCTCCCGATCCGTCGCGCGGAAGTTCCTATTCGGAAGTTCCTATTCTCTAGAAAGTAAGGAACTTCCCTAGAGGAGGAGGCGTTGTTAGAAAGCTGTCT
pMK106-EcoRI-dsRed-FP	GGCGCTGGAGCGGGTGCCGATATCGAATTCGACAACACCGAGGACGTCAT
pMK106-ScaI-GR-RP	GTCGCGGCCGCAGTGATCACAGTACTCTAGATCCGGTGGATCCCATTTTT
pMK107-EcoRI-dsRed-FP	ATATGGCCACAACCATGTGCGATATCGAATTCGACAACACCGAGGACGTCAT
pMK107-ScaI-GR-RP	CCAGCGCCTGCACCAGCTCCAGTACTGATCCGGTGGATCCATTTTTGATG
Xho1Sac1.FLP NoATG F.P.	GGCTGGCTCGAGCTCAACCACAATTTGGTATATTATG
Kpn1Sal1.FLP1 NoTAA R.P	GTTCACGGTACCGTCGACATATGCGTCTATTTATGTAGG
XholSacI_FLP1_FP	GGCTGGCTCGAGCTCAAATGCCACAATTTGGTATATT
KpnlSalI_FLP1_RP	GTTCACGGTACCGTCGACATTATATGCGTCTATTTATGT
SacB-ANCH-FP	TGGTGGAATTCTGCAGATATCGCTAGCTTCTCCTCCTGAAA
SacB-ANCH-RP	TGTTATCCCTAGCGTAACTGCGGCCGCAGGAACTTGATATTTTTCA
Site-direct mutagenesis Primers	
Ins-BssHII-ANCH3/4-FP	CTCCCGATCCGTCGCGCGCGACGTCAGGTGGC
Ins-BssHII-ANCH3/4-RP	GCCACCTGACGTCGCGCGCGACGGATCGGGAG
PCR Primers	
ANCH3-4_406-FP	TCTTGGCCTCCATCCTGTCG
ANCH3-4_1081-RP	TGAGAGTAGCATTCAGAATA
ANCH3-4_2977_RP	TTCCAGGGTCAAGGAAGGCA
ANCH3probe_FP	CGTCACTTTGGCAGGATCTTCCA
ANCH3-probe_RP	GCAGAAGACCGAGGGGCTGGGT

Sequencing Primers	
CMV-Forward	GCACCAAAATCAACGGGACTT
IRES-R	ACATATAGACAAACGCACACC
IRES-F	TTGTATGGGATCTGATCTGG
ME-1290-Rv	ATAAGCTGCAATAAACAAGTTAACAACAAC
OsTIR1-seq.FP1	TGACGGGCTAGCCGCCGTCG
OsTIR1-seq.FP2	TCCAGTTGCAAAGACTTGCA
OsTIR1-seq.FP3	TTGCGTCAAAGATGCCGATGC
OsTIR1-seq.FP4	AAGAAGACTTGAACGGATCCA
GR-seq.FP1	TGCTTTGCTCCTGATCTGAT
dsRed -FP	ACATCACCAACCACAACGAGGA
FLP - FP_339bpDS	TCTGATATCACTGATATTGTAA
FLP - FP_889bpDS	CTATAAAAAATGGCCCAAAATC
ANCH3-FP2	GACGACGAAAAGTCTCTTTC
ANCH3-FP3	ATTCGGGATAGCGCCTGCCC
ANCH4_FP2	GCGCATGATGATCGTTCGGG
ANCH4_FP3	GCGAGGAAGTTCAACCAGTT

2.1.3 Polymerase chain reaction (PCR)

PCR reactions were optimized for annealing and extension times in order to obtain maximum product. After defrosting on ice, the following reagents were mixed for a single 50 µl reaction (Table 2.3). After mixing and briefly centrifuging, the reactions were placed in a Veriti Thermal Cycler (Applied Biosystem). A standard cycling programme used was (Table 2.4).

Table 2.3 Recipe used for a 50µl PCR reaction

Reagent	Volume (µl)
Nuclease free water	37.5 µl
10X KAPA Taq Buffer A (contains 1.5 mm magnesium chloride)	5 µl
2 mM dNTPs	5 µl
100 µM F-Primer	0.5 µl
100 µM R-Primer	0.5 µl
DNA sample	1 µl
5 U/µl KAPA Taq Polymerase (KAPA Biosystem)	0.5 µl
TOTAL	**50 µl**

Table 2.4 Overview of the Thermal cycler parameters used

Step	Cycles	Temperature	Time
Denaturation	1X	95ºC	3 min
Annealing	35X	95ºC	1 min
		60ºC	1 min
		68ºC	5 min
Extension	1X	68ºC	5 min
Hold		4ºC	10 min

2.1.4 Annealing of oligonucleotides

100 µM of complementary FRT "oligos" (Table 2.2) were annealed in 10X 1.1 NEB buffer (New BioLabs) by heating at 95°C for 5 minutes; this was performed using water bath and then allow to cool down slowly for approximately 1 hour at RT. Annealed oligos were stored at -20°C.

2.1.5 Determination of DNA concentration

In order to accurately calculate the yield concentration (ng/µl) of DNA in a sample, absorbance in a Nano Drop 1000 spectrophotometer (Thermo Scientific) at 260nm (A260) was determined. The Nano Drop was calibrated using a blank sample containing H20. 1µl of DNA was applied onto the well. The A260/280 ratio was used to determine the DNA purity, where 1.8 to 2.0 is generally accepted as "pure". Lower concentrations might outline the presents of proteins, phenol or contaminants.

2.1.6 Agarose gel electrophoresis

0.8-1% agarose gel (w/v) was prepared (% depended on the size of the DNA fragments), by dissolving 0.8-1 g of powder Seakem LE Agarose (Scientifics laboratory supplies) in 100 ml of 1X TBE buffer (5X TBE diluted in dH2O) and heated in a microwave until fully dissolved. After cooling, ethidium bromide was added in a final concentration of 500 ng/ml to allow visualisation of the presence and size of nucleic acid molecules under UV light. Gels were poured into a gel tray containing a gel comb. After the gel solidify the comb was removed, and gel was submerged in a tank contains 1X TBE buffer. The samples were mixed with 5X blue loading dye (Thermo scientific) in a ratio of 5:1, and then loaded into the bottom of gel wells.

Gene Ruler (1Kb) (Thermo scientific) molecular weight marker was also loaded into the gel wells alongside with the DNA sample. The gel tank was connected to the BioRad electrophoresis power supply, and a voltage of 100V was applied to the gel for 30-40 min.
The agarose gel was analysed and the amplicon bands visualised using Gene-GENIUS Bio imaging system (Syngene); gel images were produced using the Genesnap v6.03 software.

2.1.7 Restriction enzyme digestion of plasmid DNA

All digest reactions were performed using New BioLabs enzymes and appropriate buffers, and incubated at 37ºC for two hours. The digest reactions were run in an agarose gel and desired DNA fragments were extracted from the gel using a scalpel and purified using Zymoclean Gel DNA Recovery kit (Epigenetics) following the manufacturer's instructions. Purified products were stored at -20ºC.

2.1.8 DNA ligation

Ligation was performed by mixing 100 ng of linear vector with insert at a molar ratio of 1:5 (vector: insert) to maximize ligation efficiency, and 1.2 µl of T4 10X ligase buffer and 0.6 µl of T4 DNA ligase (Invitrogen®) and water made up a total reaction volume of 20 µl. The reacted solutions were incubated at room temperature (RT) for 2 hours and then overnight at 4°C. Ligation was confirmed by gel electrophoresis. A vector-only control and an insert-only control were routinely included. For some constructs, ligation was performed through ligation independent cloning (LIC) using the In-Fusion enzyme mix, in the Protein Expression Laboratory (PROTEX) at the University of Leicester.

2.1.9 Site direct mutagenesis

In vitro site direct mutagenesis was conducted using Quick change II kit (Agilent Genomics) following the manufacturer's protocol.

2.1.10 Sequencing

Purified products were sequenced on a 3730 ABI Analyzer (Applied Biosystems) by the Protein Nucleic Acid Chemistry Laboratory (PNACL) at the University of Leicester.

After which, DNA sequences were visualised using the Lasergene software (Finch TV) and analysed using the basic a local alignment search tool, BLASN, hosted by the national centre for biotechnology Information, available at http://blast.ncbi.nlm.nih.gov/Blast.cgi?PROGRAM=blastn&BLAST_PROGRAMS=megaBlast&PAGE_TYPE=BlastSearch. ClustalW, hosted by The European Bioinformatics Institute EMBL-EBI available at http://www.ebi.ac.uk, was used for multiple sequence alignment.

2.2 Microbiology

2.2.1 Solutions

Table 2.5 Solutions used in the microbiology experiments

Solution	Constituents
100 mg/ml Ampicillin	1 g of Ampicillin (D-[-]-aminobenzylpenicillin sodum salt) was dissolved in 10 ml dH_2O, filter sterilised using a 0.2 µm syringe filter, aliquted and stored at -20°C.
50 mg/ml Kanamycin	0.5 g of kanamycin sulfate powder was dissolved in 10 ml dH_2O, filter sterilised using a 0.2 µm syringe filter and aliquted and stored at -20°C.
List of competent cells	ElectroMAX™ DH5α-E™ Competent Cells (Invitrogen™), provided are used for the cloning procedure.
	ElectroMAX™ Stbl4™ Competent Cells (Invitrogen™).

2.2.2 Competent cells preparation

Bacterial growth media stocks (Luria broth, LB) were prepared in dated batches and autoclaved by University of Leicester technical service staff. ElectroMAX™ DH5α-E™ Competent Cells were grown overnight in 500 ml of L-broth to saturation. The culture was then centrifuged at 4000 Xgamx for 15 min at 4°C to collect the cells. The cells were re-suspended in 250 ml of cold milli-Q water for 15 minutes on ice. The cells were centrifuged at 4°C for 15 minutes at 4000 Xgamx. The supernatant was removed, and the cells were re-suspended in 10 ml of 10% glycerol. The competent cells were kept cold at all times and snap frozen and stored at -80°C.

2.2.3 Transformation of competent cells with plasmid DNA

LB agar medium was sterilised by autoclaving. Ampicillin and Kanamycin were added to both the LB medium and the LB agar medium to a final concentration of 100 µg/ml and 50 µg/ml respectively. LB agar plates were prepared by pouring a thin layer of molten LB agar into the Petri dishes (Greiner).

Transformation was performed using frozen DH5α competent cells and ElectroMAX™ Stbl4™ Competent Cells (Invitrogen™). Cells were thawed on ice and then 20 µl were transferred to a pre-chilled 1.5 ml centrifuge tubes containing 2 µl of plasmid DNA and mixed gently by pipetting.

The competent cell/DNA mixture was transferred into a chilled 0.1 cm electroporation cuvette (cell projects). Electroporation transformation was performed using GenePulser II electroporator (BioRad) and adjusting the conditions to: 2.0 kV, 200, 25 µF. 1 ml of SOC medium (Invetrogen) was added and the cells in the cuvette. The solutions were transferred to 15 ml centrifuge tube and were incubated and grown at 37ºC for 60 minutes in a vigorous shaking incubator at 225 rpm. 100 µl of the transformation was then spread into pre-warmed LB agar ampicillin plates; the plates were then inverted and incubated overnight at 37ºC (media-side up). Usually two plates were used for each transformation one spread with 50 µl and 100 µl. Control experiments were performed where the original, undigested vector and untransformed cells are also plated.

2.2.4 Plasmid DNA isolation

Plasmid DNA was isolated using either the plasmid DNA miniprep or maxiprep kits, depending on amount required (OMEGA# D6942-02). Briefly, Following transformation, cells were plated onto selection plates (LB + Ampicillin) and incubated overnight. Using an inoculation loop a single colony was inoculated in a loosely capped falcon tube containing 2 ml or 50 ml of LB broth containing the suitable antibiotic supplementation, and incubated in a shaking incubator overnight. Following over-night incubation, the plasmid extraction was performed using the kit and following the manufacturer's instructions. Except for the final elution step, which was performed by adding 1ml of distilled water to the column instead of the EB buffer. Purified plasmids were stored at -80°C.

2.3 Southern Blot

2.3.1 Solutions

Table 2.6 Solutions used in the Southern Blot experiments

Solution	Constituents
DNA lysis solution	100 mM Tris HCl PH 7.5 100 mM NaCl 10 mM EDTA 1 g Sarkosyl 86 ml dH_2O to make a total volume 100 ml
5 M NaCl	29.22 g NaCl in 100 ml dH_2O
0.5 EDTA	14.6 g EDTA in 100 ml dH_2O PH 8.0
5 M NaOH	20 g NaOH in 100 ml dH_2O
Neutralisation buffer (0.2M Tris-HCl)	24.228 g Trizma base in 1000 ml dH_2O, adjust the PH to 8.0 by adding HCl
2 M sodium Acetate	16.4 NaOAc in 70 ml dH_2O, adjust the PH to 5.6 and bring total volume to 100 ml H2O. store at RT.
Alkalin electrophoresis running buffer	10 ml 5 M NaOH 8 ml 0.5 M EDTA 982 ml dH_2O
Alkalin denaturing loading dye	1 M NaOH 50% glycerol 0.05% bromophenol blue
20X SSC	3 M NaCl 0.3 M Tri-Sodiuom Citrate in 1000 ml dH_2O, adjust the PH to 7.0 by adding HCl
Oligo Stop Solution (OSS)	20 mM NaCl 20 mM Tris-HCl PH 7.5 2 mM EDTA 0.25% SDS
5X Oligo Labelling Buffer (OLB)	Solution A: 1.25 M Tris HCl PH 8.0 0.125 M MgCl2 0.5 mM dATP 0.5 mM dGTP 0.5mM dTTP 257 mM 2-Mercaptoethanol Solution B: 2 M Hepes PH 6.6 Solution C: 100 uM Heamer Primer)
1 M Phosphate (NaHPO4)	97.1 g of Na2HPO4 49.3 g of NaH2PO4.2H2O in 1000 ml dH_2O, adjust the PH 7.2
Modified Church Buffer	400 ml 1M NaHPO4

	65 g SDS in 200 ml dH_2O
Napi wash buffer	1 M NaHPO4 10% SDS make up to 500 ml dH_2O

2.3.2 Genomic DNA isolation

Genomic DNA was extracted and isolated using either the Maxwell 16 cell DNA purification kit (Promega) according to the manufacturer's instructions, or the basic phenol extraction in order to obtain a higher yield of DNA. A pellet of approximate 1 X 10^6 cells was suspended in 0.5 ml 1X SSC and split into two, 2 ml Eppendorf tubes (250 µl/tube). 250 ul of DNA lysis solution and 5 µl of 10 mg/ml RNaseA were added to each tube, mixed gently by inverting the tubes, and incubated for 20 minutes at RT. 2.5 µl of 20 mg/ml Protenase K was added to each tube and incubated at 55ºC for 6 hours. To extract the DNA, the cell lysate was then transferred into a 2 ml phase lock tube (Eppendorf®), followed by adding 0.5 ml of phenol/chloroform/isoamyl alcohol (25:24:1) in the fume hood and mixing thoroughly until a milky colour formed. This mixture was centrifuged at 13,000 rpm for 7 minutes at RT. The aqueous phase was transferred into a fresh 15ml falcon tube, and 100 µl of NaOAc and 2.75 ml of fresh 100% ethanol were added. The samples were mixed and DNA precipitated for 10 minutes at RT. The supernatant was discarded and the DNA pellet was transferred into a clean, 1.5 ml Eppendorf tube and washed with 800 µl of 80% ethanol. Then, the ethanol was removed and the DNA pellet allowed to dry at RT. Finally, the pure DNA was dissolved in 100 µl of dH_2O.

2.3.3 Endonuclease digest of genomic DNA

10 µg of genomic DNA was digested, either with *EcoR*I or *Pst*I in a 2 ml Eppendorf tube. 20 µl of the appropriate buffer and 6 µl of restriction enzyme were added to the DNA samples, bringing the digestion reaction to a total volume of 200 µl with distilled water. The reaction was incubated at 37°C overnight to allow for a complete digestion. Digested DNA was precipitated using 0.3 M of sodium acetate and twice this volume of 100% ethanol, and the reaction was mixed and placed in -20°C for at least 1 hour, followed by centrifugation at 13,000 rpm for 20 minutes at 4°C. Then the pellet was washed with 70% ethanol, and allowed to air dry. The purified DNA was dissolved with 20 µl dH_2O and run on either alkaline gel or native-agarose gel.

2.3.4 Electrophoresis for native gel

Approximately 10 µg of digested DNA was run on the 0.8% agarose gel with ethidium bromide, in a tank containing 0.5X TBE buffer, for 16 hours at 40V. 10 µl of the 1Kb DNA ladder was used alongside in order to assess the product size.

2.3.5 Electrophoresis for alkaline gel

Approximately 10 µg of digested DNA was run on the 1% agarose gel in 50 mM NaCl and 1 mM EDTA. The gel was soaked overnight, in a tank containing 1X alkaline electrophoresis running buffer (50 mM NaOH, 4 mM EDTA). The digested DNA was mixed with denature loading buffer and incubated at RT for 20 minutes to maintaine in a single-stranded state prior to loading into the wells. The gel was run for 16 hours at 40V in a cold room. 10 µl 1Kb DNA ladder was used in combination with the high molecular weight ladder to assess the product size.

2.3.6 Capillary transfer

Gels containing digested DNA were initially submerged in a depurination solution (0.25 M HCL), twice for 20 minutes on a shaker. They were then rinsed briefly with water and placed in denaturation solution (0.5 M NaOH, 1M NaCL), twice for 20 minutes. Gels were rinsed with water and neutralized once by submerging in a neutralization solution (0.5 M Tris, 3 M NaCl PH7.0) for 30 minutes. Blotting apparatus was assembled by filling a tray with 20X SSC, soaking a 3 mm Whatman filter paper in 20X SSC and mounting it into a glass plate placed on top of the tray, and then hanging the two ends of the paper into the bottom of the tray. DNA was transferred into a Hybond-XL transfer membrane (GE Healthcare) by laying the gel on top of a 20X SSC wetted 3mm Whatman filter paper that was in contact with a tray. The nylon membrane was soaked in 2X SSC then placed on top of the gel. Any bubbles caught between the membrane and the gel were rolled out with a glass pipette, then two sheets of Whatman paper the same size as the gel were soaked with 2X SSC and placed on top of the nylon membrane. The blotting apparatus was topped with a 10 cm thick stack of paper towels, a glass plate and a heavy weight and left to set overnight to allow the DNA to be dragged through by capillary action. The next day, the membrane was immersed in 2X SSC and dried for 10 minutes at 80ºC. The transferred DNA was then cross-linked onto the membrane by exposure to UV (short wavelength 700Kj/cm2) using the CL-1000UV crosslinker (UVP).

2.3.7 FLP-ANCH probe

The entire FLP-ANCH3-ANCH4 fragment was amplified and used as a probe. A PCR reaction was set up in a 50 µl reaction consisting of 5 µl of 2mm dNTP mix, 5 µl of Kapa bufferA, 2.5 µl of ANCH3-4_406-FP forward primer, 2.5 µl of ANCH3-4_2977-RP reverse primer, 1 µl of the DNA template (20 ng), 1 µl of Kapa Taq polymerase and 37.5 µl of nuclease free water. The probe amplicon was run on a gel and the band was excised and purified as described previously. Finally, the probe was sequence verified before use.

2.3.8 DNA radio labelling

In a screw led tube, 6 µl 5X OLB, 1.2 µl of bovine serum albumin (BSA) and 2 µl of DNA polymerase Klenow fragment (7.5U) (Invitrogen) were added and mixed gently. 10 ng of PCR product or DNA ladder was denatured by boiling for 3 minutes followed by rapid centrifugation.

The denatured DNA and 1.5 µl ^{32}P œ-dCTP (0.555 MBq) were added to the tube and the reaction was incubated overnight in a water bath at 37ºC to insure the incorporation of radioactive ^{32}P -dCTP. The next day, 30 µl of (30 mg/ml) salmon sperm DNA, and 25 µl 2M Sodium acetate were mixed in a siliconized glass tube. Oligo stop solution was added directly to the DNA probe and then transferred to the siliconized glass tube. The probe was precipitated in 470 µl 100% ethanol, and the pellet was then washed with 500 µl 80% ethanol. The precipitated DNA probe was dissolved in 500 µl H2O, and the radioactive labelled DNA probe was immediately incubated at 95°C for 5 minutes for denaturation, before rapid adding to the hybridization tube.

2.3.9 Hybridization

Membranes were placed between two hybridization meshes and rolled up tightly, and then inserted into the Hybaid hybridization tube (Thermo). Prior to hybridization, the membranes were pre-hybridized for 1 hour, using 20ml pre-warmed modified church buffer in a circular rotor in a 65°C oven. After the pre-hybridization, the DNA bound membrane was hybridized with the radio-labelled probe using a fresh modified church buffer, and left in a slow rotation in a 65°C oven overnight.

Post-hybridization, the membrane was washed once with NaPi washing buffer for 15 minutes to remove the unbound probe, followed by washing twice with low stringency buffer 2X SSC, 0.1% SDS, for 15 minutes each. A final wash was performed using a high stringency buffer 0.5X SSC, 0.1% SDS, for 15 minutes.

The membrane was dried and wrapped in Saran Wrap before exposure to an Amersham Phosphor cassette or a piece of film. Exposure time varied between experiments, and results imaged using a Typhoon 9400 (GE Healthcare) scanner.

2.4 Western Blot

2.4.1 Solutions

Table 2.7 Solutions used in the western blot experiments

Solution	Constituents
TBS 10X	200 mM Tris 1.5 M NACl Add H_2O to make total volume 1000 ml, adjust the PH to 7.6 by adding HCl
TBS-T	0.1%, Tween-20 50ml of 10X TBS Add H_2O to make total volume 500 ml
25% APS (w/v):	0.2 g of Ammonium persulfate 2 ml H_2O, dissolve well. Aliquot 150 ul to Eppendorf tubes and store at -20 ºC.
Loading buffer	62.5 mM Tris-HCL PH 6.8 2% SDS 0.1% Bromophenol-Blue 10% Glycerol Add H_2O to final volume 20ml, aliqute and store at -20ºC. 0.02% bromophenol blue Mercaptoethanol was added prior use.
10X Transfer Buffer	250 mM Tris-base 1.9 M Glycine Add H_2O to make total volume 1000 ml, adjust PH to 8.5
1X Transfer Buffer:	8 ml 10X Transfer buffer 10 ml methanol and make up the volume to 100 ml H_2O
2X lammeli buffer	4% SDS 20% glycerol Tris HCl pH 6.8

	The solution was stored in aliquots of 50 µl at -20ºC for long-term storage. Defreeze a tube and store at 4ºC for use.
0.15 M Tris-base PH 6.8	
1.5 M Tris-base PH 8.8	181.71g of Tris-base dissolved in 1L of dH_2O, adjust the PH to 8.8 by adding HCl.
10X Running Buffer	250 mM Tris-base Glycine 1.9M Add H_2O to make total volume 1000 ml
1X running buffer	90 ml of 10X running buffer 10 ml 10% SDS, make the total volume to 1L H_2O (freshly prepared).
Stripping Buffer	1% Tween-20 0.5% SDS 15g/L glycine solution

2.4.2 Protein isolation

All protocols were performed on ice to prevent protein degradation, unless stated otherwise. Following transfection, media was aspirated from a reasonably confluent 6 cm plate and cells were washed with PBS. Protein isolation was performed through resuspension of the cells in 100 µl of pre-boiled 2X laemmli buffer added directly, and the cells were scraped using a cell scraper. The buffer containing cellular proteins were transferred to 1.5 ml Bioruptor Microtubes (Eppendorf). Lysates were boiled in 95°C for 5 minutes then sonicated using a Bioruptor Sonicator on a low setting for 5 minutes of 30-second, on/off cycles with a break after 3 minutes for external cooling on ice to shear the DNA.

Samples were kept on ice for 30 minutes, and insoluble fractions were removed by centrifugation at 13,000 rpm for 10 minutes at 4°C to form a pellet. Following centrifugation, the supernatant (containing soluble protein) was transferred to a fresh 1.5ml Eppendorf tube and stored at –20°C (or -80°C for longer storage). Finally, the protein concentration was quantified using a NanoPhotometer (IMPLEN).

2.4.3 SDS-PAGE preparation

As shown in Table 2.8, the composition of the gel varied depending on the molecular weight of the protein being detected. However, a 10% gel was generally used. The gel apparatus was assembled using Bio-Rad plates and 10 well combs. SDS-PAGE was prepared by composing two gels: an acrylamide separating gel and acrylamide stacking gel. The acrylamide separating gel was prepared in a 50 ml falcon tube by adding 1.1 ml of 1.5 M Tris PH 8.8, 1.5 ml acrylamide, 44 µl of 10% SDS, 55 µl of 25% APS, 1.8 ml H2O and 3.7 µl of Tetra methyl ethylene ediamine (TEMED) to polymerize the gel. The solutions were mixed immediately by inverting the tube, and a 1000 µl pipette was used to pour the gel solution between the gel plates, followed by pouring isopropanol (propanol-2) onto the surface of the gel solution to prevent exposure to air. The acrylamide stacking gel was prepared in a 15ml falcon tube by adding 600 µl of 0.15 M Tris PH6.8, 325 µl of acrylamide, 25 µl of 10% SDS, 75 µl of 25% APS, 1.5 ml H2O and 2 µl TEMED, mixed and immediately poured on top of the separating gel. A comb was inserted at an angle to avoid trapping air bubbles under the teeth, and the gel was allowed to set at RT.

Table 2.8 Components and volumes used for SDS-polyacrylamide gel

Constituent	Stacking gel	6% Running gel (60-300kDa)	10% Running gel (15-100 kDa)	12% Running gel (7-70 kDa)	15% Running gel (12-45 kDa)
Water	1.5 ml	2.4 ml	1.8 ml	1.5 ml	1.1 ml
0.15 M Tris PH 6.8	600 µl	-	-	-	-
1.5 M Tris PH 8.8	-	1.1 ml	1.1 ml	1.1 ml	1.1 ml
30% Acrylamide	325 µl	0.9 ml	1.5 ml	1.8 ml	2.2 ml
10% SDS	25 µl	44 µl	44 µl	44 µl	44 µl
25% APS	75 µl	55 µl	55 µl	55 µl	55 µl
TEMED	2 µl	3.7 µl	3.7 µl	3.7 µl	3.7 µl
Total volume (1 Gel)	2.527 ml	4.5 ml	4.5 ml	4.5 ml	4.5 ml

2.4.4 Protein separation by electrophoresis and transfer

1X running buffer was freshly diluted and added to the tank, and the wells were flushed out with running buffer to displace air bubbles. In a clean Eppendorf tube, 40 µg of the protein samples were diluted with laemmlli loading buffer to a final volume of 10 µl, then boiled at 95ºC for 5 minutes. 10 µl of each sample was added into the bottom of the well, alongside the loaded sample 5 µl of BLUeye Prestained Protein Ladder (GENEFLOW, Fisher). Electrophoresis was carried out at 75V for 30 minutes, to allow all samples to migrate through the stacker gel, then at 120V for 1 hour. Gels were then removed from the plates and soaked in transfer buffer, and transferred to a Hybond ECL Nitrocellulose membrane (Amersham biosciences, GE Healthcare) using a semi–dry transfer setup (Bio-Rad apparatus). The transfer was performed by constructing a blotter apparatus consisting of 3 layers of 3 mm Whatman paper, nitrocellulose membrane, SDS-PAGE, and another 3 layers of 3mm Whatman paper (all cut to the size of the gel and pre-equilibrated with transfer buffer). A glass pipette was used to gently remove air bubbles; this is important to achieve good protein transfer. The transfer was carried out using a 400 mA/cm constant for 1 hour, and 1% ponceau S stain was used to visualize quantity of proteins transferred to the membrane.

2.4.5 Immunobloting

Firstly, the membrane was blocked in 5% Marvel skimmed milk in TBST for 1 hour with gentle agitation at RT. The primary antibodies -(1:1000) anti-AID, (1:3000) anti-myc, (1:3000) anti-tubulin- were then added to fresh 2% Marvel milk in TBST and the membrane was immunoblotted overnight at 4°C. Following incubation with the primary antibodies, 3X 10-minute washes were performed in TBST at RT. Then, the secondary antibody – conjugated with horseradish peroxidase, (1:5000) anti-mouse, and (1:5000) anti-rat antibodies – was added to 2% Marvel milk in TBST and incubated for 2 hours at RT. After the incubation, the blot was washed for 3X 10 minutes in TBST.

To create a luminescence signal, detection of the protein was carried out using ECL-plus (Amersham Biosciences, RPN2108), following the manufacturer's instruction. Bands were visualized by incubating for 1 minute with Kodak BioMax XAR films which were then developed. The membrane was stripped of the previous antibodies using a stripping buffer for 15-20 minutes with gentle agitation at RT. The stripped membrane was then re-blocked and re-blotted with a different primary antibody, as above.

2.4.6 Band quantification

Western X-ray films were scanned using an image scanner with a 300dpi resolution and saved as TIFF files. Bands were quantified and analyzed using ImageJ software. The images were converted to black and white 8-bit in ImageJ. The area of each band was determined and a histogram of the intensity of each band was measured. The measurements were then transferred into an Excel program and the values were normalized to the values of a control on the same blot.

2.5 Cell Culture

2.5.1 Solutions

Table 2.9 Materials and solutions used in the cell culture experiments

Solution	Constituents
Tissue culture media	GIBCO®DMEM (Dulbeco's Modified Eagle Medium) for human and mammalian cells, with high Glucose (4.5 g/l) (Invitrogen™) 10% GIBCO® Heat inactivated foetal bovine serum (FBS) (Invitrogen™) 5% of 200 mm L-Glutamine (Invitrogen™) Heated in a water bath at 37ºC prior to use
Trypsin (GIBCO)	Prepared in dated batches by University of Leicester technical service staff, warmed in a water bath at 37°C for 30 minutes prior to use
PBS	Prepared in dated batches and autoclaved by University of Leicester technical service staff
4% Paraformaldehyde	Dilute the 40% PFA (Thermo Scientific) with PBS in a fume hood and allow to dissolve, prior to use.
G418/ Geneticin	0.5 g of G418 in 5 ml disstilled water, filter sterile and stored at 4°C. (100 mg/ml)
Hygromycin B	Gibco® Hygromycin B (50 mg/ml), (Invitrogen™).
10^{-4} M Triamcinolone acetonide (TA)	0.001g of TA in 25 ml of ethanol and stored at -20°C.
Caffeine media	50 ml of DMEM media 97.1 mg of caffeine (sigma) (12.5 mM, Mw=194.19 g/mol) – final concentration of 25 nm. Heat in the water bath until complete dissolved.

Phleomycine media	12 ml of DMEM media 2.4l of Phleomycin (25mg/ml) – final concentration of 5 µg/ml.
Caffeine, Phleomycine media	15 ml of previously prepared caffeine media. 3 µl of phlyomycine (25 mg/ml)
Methanol: acetic acid	Mix methanol and acetic acid in a ratio of 3:1 (Should prepare freshly and stored at -20°C).
Propidium Iodide (PI)	Dilute PI (Sigma#p-4170) to 1 mg/ml with PBS, cover the tube with Aluminum foil to protect from light and store at 4°C.
Ribonuclease A from bovine pancreas (Rnase A)	10 mg/ml stock solution was prepared in water, aliquoted and stored at -20°C.
5% Giemsa	0.4% stock solution; (Sigma G3032) in water
PBS-T-BSA	1% Bovine serum albumin 0.5% triton X-100 PBS, mix and store at 4C.
KU-55933/ ATM	10 mM stock was dissolved in anhydrous dimethyle sulfoxide (DMSO), aliquoted and stored at -20°C.
NU6027/ ATR	10 mM stock was dissolved in anhydrous dimethyle sulfoxide (DMSO), aliquoted and stored at -20°C.
NU7026/ DNA-PKs	10 mM stock was dissolved in anhydrous dimethyle sulfoxide (DMSO), aliquoted and stored at -20°C.
Rad51-02	10 mM stock was dissolved in anhydrous dimethyle sulfoxide (DMSO), aliquoted and stored at -20°C.
Mirin/ MRE11	100 mM dissolved in anhydrous dimethyle sulfoxide (DMSO), aliquoted and stored at -20°C.

Table 2.10 List of all cell lines used in this study.

Name	Discribtion	media
HEK293T	Transformed Human Embryonic Kidney (gift from Dr. John Petrini, Memorial Sloan-Kettering Cancer Center).	DMEM + 10% FBS + 5% Glutamine
HEK293	Human Embryonic Kidney (gift from Dr. Flav Giorgini, University of Leicester).	DMEM + 10% FBS + 5% Glutamine
MEFs	Mouse Embryonic Fibroblast (WT gift from Dr. John Petrini, Memorial Sloan-Kettering Cancer Center. $Ku86^{-/-}$ from Professor Catrin Pritchard, University of Leicester).	DMEM + 10% FBS + 5% Glutamine
U2OS	Human bone osteosarcoma cell (gift from Dr. Nicola Royle, University of Leicester).	DMEM + 10% FBS + 5% Glutamine
Hela CCL-2	Human epithelial cells (gift from Dr. Nicola Royle, University of Leicester). Adenocarcinoma, 31 black female	DMEM + 10% FBS + 5% Glutamine

2.5.2 Mammalian cell culture

Above cells were used for the cell culture experiments performed in a sterile, tissue culture cabinet. 10 ml of supplemented media (see Table 2.9) was transferred to 15 ml falcon tube and 1 ml of defrosted cells were added and centrifuged at 1200 rpm for 4 min. The media was removed and cells were suspended with 5 ml of media. Cells were transferred to T25 tissue culture flask (Greiner) and incubated at 37ºC, in 5% CO_2 for 24 hours.

Cells were passaged twice a week by removing the media from the flask, and washing once with 1X Phosphate buffer saline PBS (SIGMA). Cells were disassociated and detached by adding 1 ml of pre-warmed 1X Trypsin (0.25%) to the cells and the flasks were returned to the incubator for 2 minutes to allow cells detachment.

Cells were visualized using a light microscope to confirm detachment from tissue culture flask and 10 ml of fresh supplemented media was added to the flask to inactivate the trypsin. Cells were titrated before splitting, and an aliquot of cell suspension was added to a new flask containing new fresh media at an appropriate ratio, to obtain approximately 50-60% confluency for cell maintenance or 70-80% for transfection.

2.5.3 Counting cells

Cells were counted either by using the haemocytometer or the Countess Automated cell counter using the cell counting chamber slides (Invitrogen). For both approaches, the cells were trypsinized and centrifuged at 1200 rpm for 4 minutes. The cell pellet was then re-suspended with 5ml PBS. 10 µl of the suspended cells were mixed to 10 µl of 0.4% trypan blue stain (Thermo Scientific) and incubated at RT for 3 minutes. Trypan blue selectively stains the dead cells but the uptake is excluded from live cells. 10 µl of the mixture was loaded to the haemocytometer or the chamber slide for counting.

2.5.4 Transfection

One day prior to transfection, cells were trypsinized and seeded with new growth medium, then plated in a 10 cm tissue culture plate, 6-well plate or 24-well plate (Nunc) to achieve a density of ~2.5 x 10^6, 0.3 x 10^6, and 5.0 x 10^5 cells per plate respectively (70%-80% confluence), and incubated for 24 hours.

The transfections were performed either using Mirus TransIT-2020 transfection reagent (Invitrogen) or FuGENE®HD transfection reagent (Promega), according to the manufacturer's instructions and the results of the optimization. The growth medium was briefly removed from the plate and the cells were seeded with fresh complete growth medium. The transfection reaction was prepared by diluting 2 µg of plasmid DNA with DMEM free serum media, before complexing; this was followed by mixing and incubating for 5 minutes at RT. TransIT-2020 was added to the diluted DNA mixture, vortexed and incubated for 25 minutes at RT (see Table 2.11). The DNA/Lipid complex was introduced dropwise to the appropriate well, and the plate was rocked gently to distribute the transfection mix. For transient transfection, cells were incubated for 48 hours at 37ºC, in 5% CO_2.

In order to ensure stable transfection optimum concentration of Geneticin (G418) or Hygromycin B per ml (sigma) were added 48 hours post transfection. Cells were cultured under selection for 14 days before colonies were isolated either with 3mm Scienceware® cloning discs (Sigma) or using the serial dilution approach.

Table 2.11 Recipe for DNA transfection with TransIT-2020 reagent.

	24-well plate	6-well plate	15cm plate
Complete growth medium	0.5 ml	2 ml	20 ml
Serum free medium	50µl	300 µl	2500 µl
***Trans*IT-2020 reagent**	2 µl	12 µl	100 µl

2.5.5 Cytoplasm to nucleus relocalisation

Cells were plated on sterile glass coverslips in 6-well tissue culture plates to achieve a density of ~3 x 10^5 cells per well, and incubated for 24 hours. Cells were transiently transfected with dsRed-FLPH305L-GR, dsRed-I-SceI-GR and dsRed-GR empty vector, and then incubated for 48 hours' prior to adding Triamcinolone Acetonide (TA). Growth media described above containing 10^{-7} M of TA was freshly prepared and added to the cells then incubated at 37°C with 5% CO_2 for 30 minutes.

Following the required incubation time, the media was removed from each well. 1ml of pre-warmed 4% PFA fixation reagent was added for 20 min at RT. The cells were washed several times with PBS and mounted into microscope slides using ProLong® Gold Antifade Mountant containing DAPI (life technologies) and left to dry for 24 hours in the dark.

2.5.6 Cell cycle analysis

Cell cycle was assessed by propidium iodide (PI) staining and fluorescence-activated cell sorting analysis. Approximately 1.0 x 10^6 cells/ml were harvested after treatment or transfection and collected in a 15ml falcon tube, then pelleted by centrifugation at 200g for 3 minutes. The cells were re-suspended and fixed using ice-cold 70% ethanol in 1X PBS. The samples were vortexed for few seconds and then stored at -20°C overnight. On the day of analysis, the cells were washed with 5X volumes of 1X PBS and centrifuged at 200 g for 3 minutes. After centrifugation, the pellet was treated with RNase A used at a final concentration of 10 µg/ml and re-suspended in PBS containing 50 µg/ml PI buffer solution. Samples were transferred into FACS tubes, vortexed and incubated at 37°C for 30 minutes, and protected from light before the fluorescence-activated cell sorting analysis (Becton Dickinson, BD Biocsiences).

Control cells were prepared without staining and data was acquired for unstained cells, controls and samples. The cell cycle calculations were carried out using the FACSDiva software Version 6.1.3 (BD Biocsiences, San Jose, USA). For cell cycle analysis, MODFIT Program was used, in the Cancer studies department at the University of Leicester.

2.5.7 DDR inhibitor cytotoxicity assay

Cells at the exponential growth phase were harvested with trypsin and counted using a hemocytometer. The cytotoxicity of the DDR inhibitors was assessed by the WST-1 assay. Briefly, cells were seeded in 96-well flat-bottom microtiter plates (Nunc, Fisher Scientific, Leicestershire, UK) at a density of 10×10^3 cells in 100 µl media per well, and placed in incubator at 37°C and allowed to adhere overnight, before being treated with DNA damage response inhibitors (see Table 1.3) at concentrations of 1, 5, 10, 15, 20, 25, 30, 40, 50, 75 and 100µM for 24 and 48 hours. A control-group with the DMSO and zero-adjustment well were also set. 10 µl of wst-1 (10%) solution was added at the end of incubation, and incubation was continued for 4 hours. The absorbance value in 96-well plate was read spectrophotometrically at 570 nm by placing the plate in plate reading spectrophotometer (ELx800, Bio-Tek, UK).
The inhibitory rate for the DDR was calculated according to the formula:
Proliferation = (experimental absorbance value/ control absorbance value) × 100%

2.5.8 Colony formation ability assay

Transfected cells were sorted with fluorescence-activated cell sorting analysis, FACS Aria II (BD Biocsiences, San Jose, USA) by Cancer Studies and Molecular Medicine at the University of Leicester. Following this, cells were diluted and seeded at about 1000 cells per well of a 6-well plate and incubated for 48 hours to allow adhesion. The cells were then treated with DNA damage response inhibitors that were diluted in DMEM media at the indicated concentration prior to use (sigma) and incubated for 1 h at 37°C. The cells were treated with 1 nM TA for 48 hours in the presence or absence of DDR inhibitor.

Following treatment, cells were continuously incubated with normal supplemented media and incubated at 37 °C in 5% humidified CO_2 for 10–14 days in order to instigate colony formation. The medium was aspirated and cells were washed with PBS twice and fixed with (3:1) methanol: acetic acid for 15 min, and stained with 0.5% crystal violet for 15 min at RT.

Plates were placed inverted for air-drying. The colony was determined to consist of at least 50 cells, and visible colonies were counted using an ImageJ macro created by me (Figure 2.1). The plating efficiency and colony formation fraction were calculated based on the survival of non-treated cells by using the following equation:

Colony formation rate = (number of colonies/number of seeded cells) × 100%

Survival fraction = (number of colonies formed)/(number of seeded cells x PE) x 100

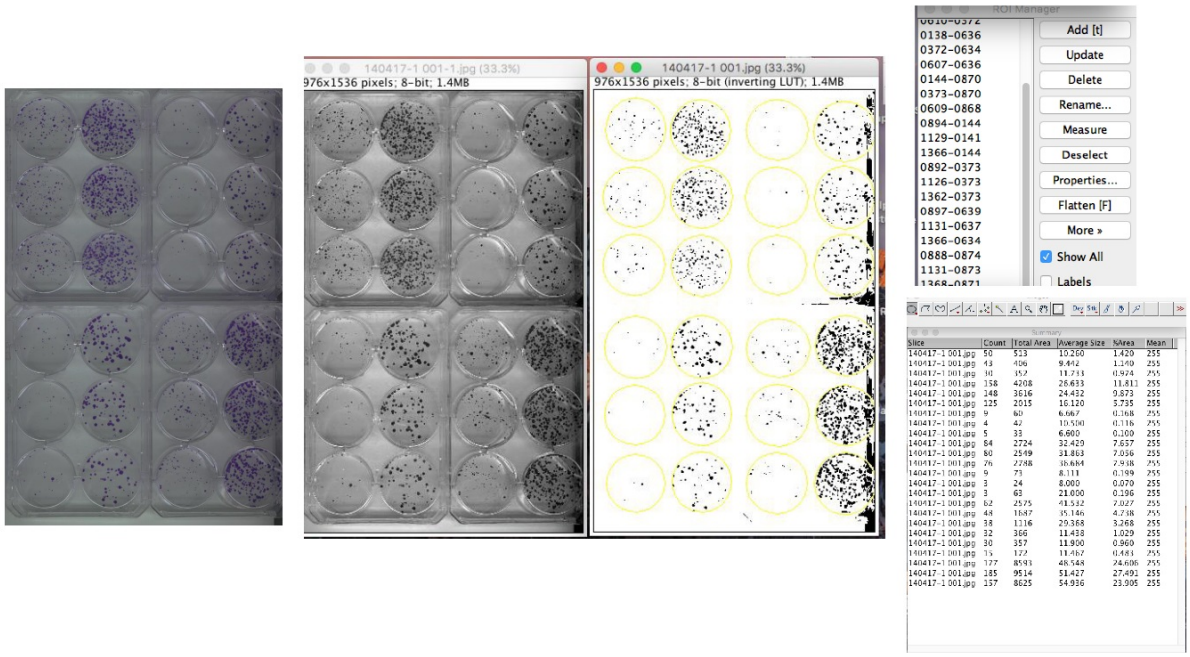

Figure 2.1 Representation of the created automated colony counter macro using imageJ. 6-well plates were scanned and saved as Jpeg-file. Using ImageJ change the image type to 8-bit and adjust threshold to defult black and white. Select the wells and finally analyze particles.

2.5.9 WST-1 cell proliferation assay

The viability of cells was assessed using the the ready-to-use WST-1 cell proliferation reagent (Roche Diagnostics GmbH, Roche Applied Science, Mannheim, Germany) in the process described above (Section 2.5.). Transfected cells were sorted with FACS Aria II (BD Biocsiences). Following this, 10×10^3 cells were seeded into clear flat bottom 96-well plates (Nunc, Fisher Scientific, Leicestershire, UK) and incubated in 100 µl of corresponding complete media and allowed to adhere overnight at 37°C. Following this, cells were treated with 1 nM TA for 48 hours, in the presence or absence of a DDR inhibitor, at the optimized concentration, and incubated in 100 µl of corresponding complete media at 37°C with humidified chamber, 95% air/5% CO_2 for 48 hours. Post incubation, direct addition of 10 µl volume of WST-1 Reagent was added into each well and then incubated for 1 hour.

This was performed in six technical replicates and at least triplicate biological repeats. Cell viability was quantified by placing the plate in a plate-reading spectrophotometer, and measuring the absorbance at 440nm.

Cell viability (%) = (Mean absorbance of treated/Mean absorbance of untreated) × 100%

2.5.10 Cytometric detection of γ-H2AX

Transfected cells were trypsinized and centrifuged at 300g for 4 minutes at RT, then the cell pellet was suspended in 0.5ml 1X PBS. Cells were fixed by transferring the cell suspension into a 6ml polypropylene tube (BD Falcon Cat#352063) containing 4.5 ml ice-cold 70% ethanol diluted in PBS and maintained at -20°C overnight. Post fixation, the cell pellet was then washed in PBS twice and blocked in 2ml of PBS-T-BSA (see table 2.9) for 30 minutes at RT. Following this, the cell pellet was resuspended in 200 µl of anti-γ-H2AX antibody (Millipore 05-636), which was added at a dilution of 1:1000 in 5% PBS-T-BSA and incubated overnight at 4°C. The cells were washed twice in PBS-T-BSA for 10 minutes each, before incubating in the dark with a 200µl of Fluorescein isothiocyanate (FITC)-labeled secondary antibody (Alexa Fluor®488) at a dilution of 1:300 in 5% PBS-T-BSA, for 2 hours at RT with gentle shaking. The secondary antibody solution was removed and the cells were washed in 2 ml of PBS-T-BSA for 10 minutes, then incubated in the dark with 1 ml PI stain solution in PBS for 30 minutes.

Samples were then examined and analyzed for excitation on a flow cytometer with a wave length of 488-nm, in order to measure the intensity of the green (filter: 525/30) of the cells. Samples with no primary antibodies were used as a negative control, which is an important step in setting up quantification gates, as it makes it possible to estimate the nonspecific antibody-binding component and the background signal, as derived from fluorophores. The FITC and PI stain were excited with 488 nm and 405 nm excitation lasers respectively. The emitted light was detected via the filter/bandpass, using a 450/50 and 530/30 filter for FITC and PI respectively. At least 5,000–10,000 events were acquired in a linear side-scatter area (SSC) versus a linear forward-scatter area (FSC) axes. Dual staining revealed a major population of cells, which were gated to omit signals from degraded nuclei debris. Single cells were gated by isolating the cell doublets, and by plotting a linear pulse height (405-H) versus the pulse area (405-A) of the PI channel and setting a gate around single cells (Appendix I).

2.5.11 Metaphase spreads

WT and Ku86$^{-/-}$ MEFs cultured cells at the exponential growth phase were routinely used. 1X 10^6 Cells were plated in 10cm plate, treated for 1 hour with different chemotherapeutic agents - such as phleomycin (5 µg/mL), camptothecin (25 nM) and etoposide (25 µg/mL) - in the presence or absence of caffeine. Following treatment, the cells were treated for 2 h with colcemid (final concentration: 1 µg/mL). Colcemid inhibits the polymerization of microtubules, and hence increase the number of cells in metaphase. For adherent cells; the medium was poured off, and pelleted by centrifugation 1000rpm for 5 min, in order to save cells that may have detached mitotic cells. The adherent cells were then trypsinized and all cells were combined, pelleted and centrifuged at 1000rpm for 5 minutes.

Cells were swelled in 0.075 M freshly-prepared KCL buffer at 37°C for 30 minutes. The KCL was added dropwise for the first 2 ml, then the cell pellet was resuspended in this small volume and the remainder of the 10 ml added. Cells were then fixed in ice-cold (3:1) methanol: acetic acid and centrifuged. The supernatant was removed and the cells were flicked and re-suspended, washed twice with 10 ml fixative very slowly, and incubated on ice for 1-2 minutes after each wash, then left to fix at -20°C overnight. Following this, Spin down cells as above and resuspend in 0.25-0.5 mL of fixative in tube. The fixed cells were dropped in microscope slides and placed to air dry overnight.

The following day, the slides were checked against 10x objectives to ensure quality of preparation, and stained with 5% Giemsa for 10 minutes, before being rinsed under a stream of water in the sink.

Then, the slides were left to dry overnight, and mounted using a ProLong® Gold Antifade Mountant containing DAPI (life technologies) and coverslip, and left to dry for 24 hours in the dark. The experiment was repeated three times.

2.5.12 Anaphase bridges

WT SV40 and Ku86$^{-/-}$ MEFs cultured cells were plated on sterile glass coverslips in 6-well tissue culture plates to achieve a density of ~3 x 10^5 cells per well, and incubated for 24 hours. Cells were treated with caffeine media in a final concentration of 25 nm and incubated at 37°C for 1 hour. The media were replaced with phleomycine media or caffeine/phleomycin media in a final concentration of 5µg/ml before the cells were incubated for 30 minutes at 37°C. Following these treatments and the required incubation time, the cells were then supplemented either with growth media or caffeine media and stored at 37°C for 8 and 12 hours.

The media were removed and cells were washed with PBS. 1ml of pre-chilled (3:1) methanol: acetic acid fixation reagent was used to fix the cells and they were incubated for 10 minutes at RT. The cells were then washed twice with PBS, and 1µl of DAPI stain added to each well in the second wash, before being incubated for 5 minutes at RT. Finally, the cells were washed with PBS and stored at 4°C. The experiment was repeated three times on different days using independent samples to reduce sample-to-sample variability.

2.6 Microscopy

Fixed and live cells were visualized on either an Olympus Cell^R/Scan^R imaging system (Olympus microscope, Xcellence software, version 1.2), or Olympus Cytological imaging system in the Advanced Imaging Facility (AIF) at the University of Leicester. After which, cell images were quantified using the Scan^R analysis software and analysed using the basic, free image processing and analysis software, ImageJ (Schneider et al., 2012). Different ImageJ/macros were created for the automated cell counting.

2.7 Statistical analysis

Statistical analysis was performed using Graph Pad Prism version 6.02. The data were recorded in the text as mean ± standard deviation (SD) of at least three biological replicates or as indicated. The data were analysed by analysis of variance using student's t-test. Statistical significance was represented by a P-value ≤ 0.05.

Chapter 3: Development of an innovative FRT-FLP system to study DNA replication stress

3.1 Introduction

As mentioned in Section 1.11, a number of studies using various genotoxic agents (such as radiation or therapies such as CPT have investigated how cells respond to DNA damage and RS (Kobayashi et al., 2003; Ahn et al., 2011;-Cobb et al., 2005). However, these agents cause genome-wide damage; thereby preventing control over where forks collapse or break, and preventing RS associated events from being studied directly; such as the elucidation of the molecular mechanism underlying se-DSB resolution or misrepair.

To overcome these limitations and establish a new mammalian system to study RS in *vivo*, various principles, ideas, and systems derived from tools available in bacteria and yeast were blended to deliver a novel inducible FRT-FLP system. Attempting to address previous gap, this chapter describes the development of an innovative FRT-FLP system; one that is designed to overcome current methodological limitations through the inclusion of features used in a yeast-based system to induce the generation of single broken DNA RFs at specific loci in mammalian cells. Thus, it is possible to control where a fork breaks, and to study RS-associated molecular events in *vivo*. The first objective when setting up the system was to construct the required FRT and/or FLP plasmids. The second objective was to establish stable FRT-FLP cell lines. Finally, it was necessary to investigate and characterize the cell lines generated by investigating the copy number of integration.

3.2 Results

3.2.1 Designing an FRT-FLP system to generate RS

The FRT-FLP system was developed to permit the precise control of induction of RS; creating either a se-DSB (BF) or direct DSB at a defined locus.

The FRT-FLP cellular system comprises mutant FLP recombinase, FLPH305L, which binds and cleaves at the stably integrated FRT site (Parsons et al., 1988). This action would then induce a se-DSB upon fork collision as demonstrated in budding yeast and as caused by CPT-induced persistent SSBs/ Top1-DNA adducts (Nielsen et al., 2009; 2012).

The integrated FRT sequence was combined with different fluorescent approaches to support microscopic visualization and to observe the fate of the induced broken fork end in real time. The initial visualization strategy utilized the lac-repressor and the tetracycline response element visualization tool. As shown in Figure 3.1, the FRT was designed to be flanked by these operons, and broken fork sites were directly visualized simultaneously, based on binding fluorescent repressor proteins to specific binding sites through expression of the CFP–lac-repressor and the YFP–tet-repressor foci, respectively (Lassadi and Bystricky et al., 2011; Saad et al., 2014).

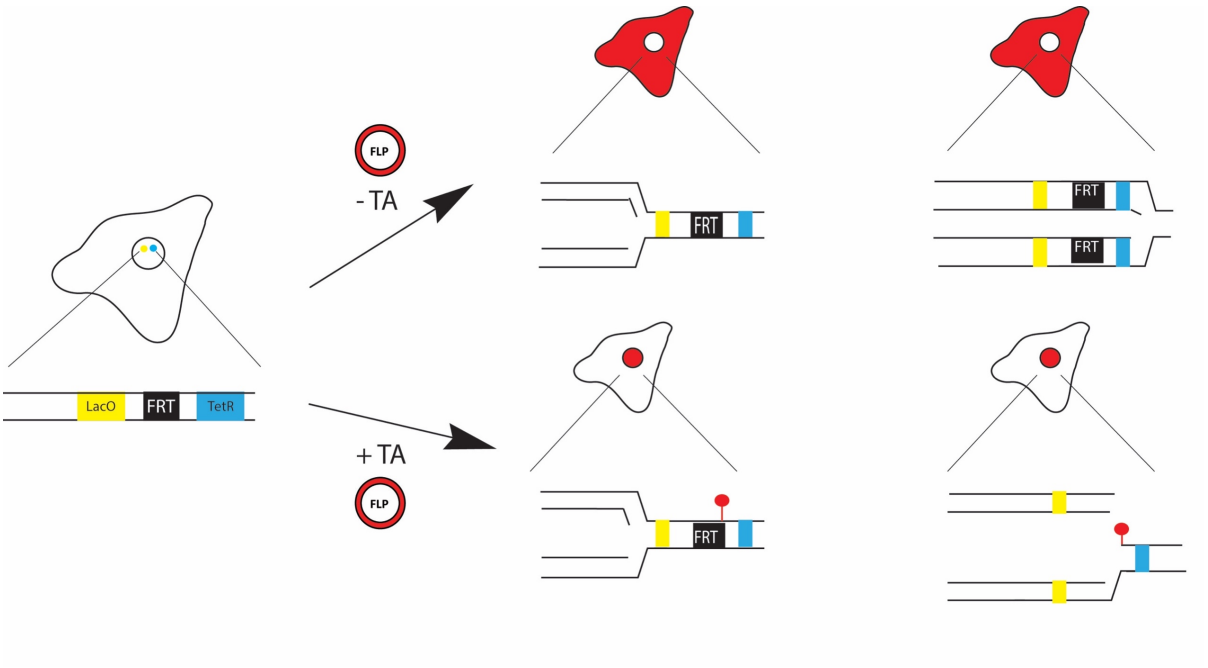

Figure 3.1 Schematic representation of the initial visualization system. The lac-repressor and the tetracycline response element flanking the FLP recognition target site (FRT) are integrated into the genome. Stable lacO-FRT-TetR cells will be subjected to a second transient transfection with the FLPH305L recombinase expression construct that will localize in the cytoplasm in the absence of triamcinolone acetonide (TA). Addition of TA induces re-localisation of FLP recombinase from the cytoplasm to the nucleus. This process generates an irreversible protein-DNA nick and SSB at the integrated FRT locus. Upon replication, the RF will encounter the SSB and form a broken RF.

The second visualization approach involved taking advantage of the recently developed DNA-labelling method, termed the ANCHOR system, through a collaboration with Dr. Kerstin Bystricky (University of Toulouse). The ANCHOR system was adapted from a newly developed DNA labelling system; the ParB-ParS system (Saad et al., 2014). This involves using ParB partitioning proteins derived from the *Burkholderia cenocepacia* bacteria.

The system is based on kinetochore-like nucleoprotein complexes, which ensure stability and faithful mitotic segregation in bacterial replicons by binding to sites (parS) (Khare et al., 2004). The ParB-INT uses the ParB-parS loci of chromosomes c2 and c3 of J231 and employs protein oligomerization in place of operator multiplicity to form visible foci, permitting direct kinetic measurements in single cells (Dubarry et al., 2006).

In the ParB-ParS system, the ParB partitioning proteins (ParB1 and ParB2) can interact with one another via a specific oligomerization domain. A fluorescent focus will subsequently form upon a ParB, which is bound to integrated sites; namely INT1 and INT2 integrated sites (Saad et al., 2014). The ANCHOR visualization system exploits a same principle as the ParB-ParS system; it is based on using a fluorescently labelled "OR" protein, which loosely binds and oligomerizes to integrated specific binding sites, ANCH, creating visible fluorescent foci. GFP-OR3 and YFP-OR4 proteins, which bind and oligomerize at ANCH3 and ANCH4 sites respectively, then create fluorescent foci to allow visualization close to the break site. The non-intrusive weak binding and oligomerization of OR proteins prevent the disruption of DNA replication and repair (Bystricky, unpublished).

In the adapted ANCHOR system, the ANCH3-ANCH4 contains a greatly reduced number of parS binding-sites compared to the ParB-ParS system, facilitating targeted integration and the stability of binding sites in mammalian cells. Moreover, ANCH sequences are not repetitive, and thus it was speculated that their insertion will not alter the chromatin's dynamics, its transcriptional status, or its sensitivity to DNA damage; nor will it disrupt DNA replication and repair as observed in yeast (Saad et al., 2014; Bystricky, unpublished). Notably, an 18 bp unique rare cutting Isce-I site separates these ANCH3-ANCH4 sites. Several studies have involved using mega-nucleases systems such as HO or I-SceI endonucleases to induce DSB unambiguously at defined sites (Jasin, 1996; Bellaiche et al., 1999; Weinstock et al., 2008; Yatagai et al., 2008; Saad et al., 2014; Bindra et al., 2012). The yeast I-SceI is a rare cutting endonuclease, encoded by an intron of the mitochondrial rRNA (Dujon, 1989). It recognizes an 18-base pair sequence (TAGGGATAACAGGGTAAT), cleaving the phosphodiester bond, leaving a 4-5 bp overhang in the 3' hydroxyl group, introducing the DSB to the genome (Colleaux et al., 1988).

Experimentally, and as illustrated in Figure 3.2, the setup of the system involves multiple steps. Stable cell lines were first generated to integrate copies of the FRT sequence into the genome through random integration.

During live cell imaging, and when studying activity at the broken site, co-transfection with the pOR-CFP and pOR-GFP plasmid can be used to generate single CFP and GFP focus in a cell in pre S-phase and post-mitosis when cell division occurred. During S-phase, and in the absence of TA, DNA replication doubles the number of ANCH sites; thus 2 GFP and CFP foci will appear. Hence, duplication will confirm replication has occured. OR proteins bound in a metastable fashion to DNA flanking the ANCH sites and only bind to dsDNA, meaning fluorescent foci will be readily displaced by DNA replication and DNA repair at the site, while remaining available for rebinding as the method to restore a fluorescent focus. The foci will quickly reform once genome integrity is restored. Hence, the features of the ANCHOR system enable tracking of RF-based processes.

As mentioned previously, the devised system regulates the induction of a se- or direct- DSB. This will be achieved by transiently transfection of FRT stable cells with mutant FlP expression constructs “dsRed-FLPH305L-GR” recombinase or “dsRed-I-SceI-GR” endonuclease, which will precisely generate persistant SSB (and ultimately se-DSB) or direct DSB respectively. To initially control the induction of FlPH305L and I-SceI expression we took advantage of the rat glucocorticoid-receptor chimeras (GR), which translocates from the cytoplasm to the nucleus once bound to the synthetic ligand triamcinolone acetonide (TA) (Htun et al., 1995). FlPH305L and I-SceI expression proteins are fused with RFP and GR in a single reading frame; and will be located in the cytoplasm in the absence of TA.

However, the addition of TA to the culture medium will activate GR to stimulate the relocalization of the protein from the cytoplasm to nucleus. Once localized to the nucleus, the FlP binds to the stably integrated FRT sequence, forming a protein-DNA adduct and upon DNA replication, an encountering RF will lead to RF breakage and a se-DSB formed.

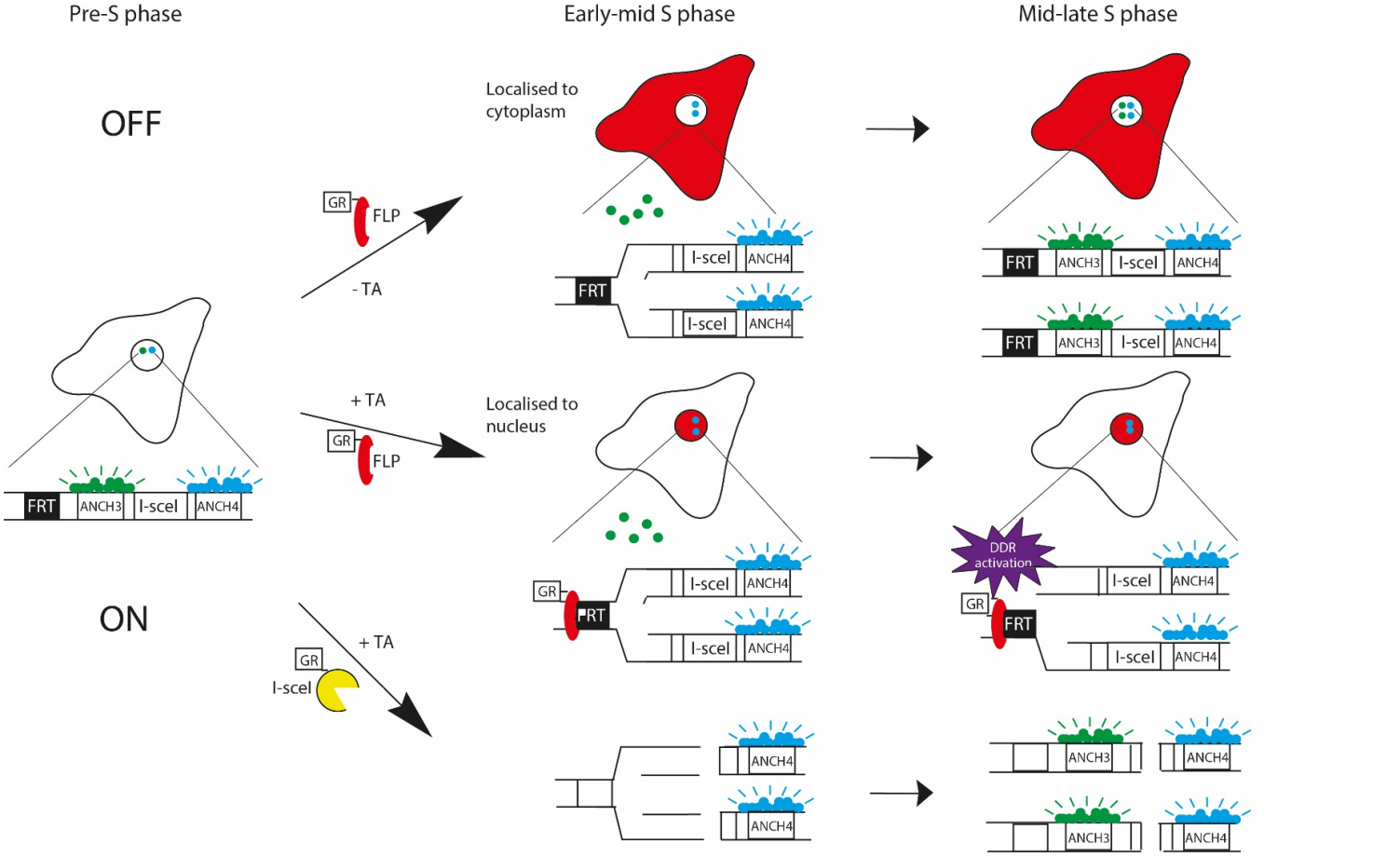

Figure 3.2 Overview of the proposed stages to regulate broken DNA replication fork induction in mammalian cells. The FLP recognition target site (FRT) located upstream of the ANCH3-ANCH4 sequence is randomly integrated into the genome. Stable FRT integrated cells will be subjected to a second transfection with either the dsRed-FLPH305L-GR or dsRed-I-SceI-GR expression constructs that will localise in the cytoplasm (system-OFF) in the absence of triamcinolone acetonide (TA). Addition of TA induces re-localisation of mutant FlP recombinase (FlpH305L) or I-SceI from the cytoplasm to the nucleus. FLP nucleus localization will bind to the integrated FRT sequence and generates an irreversible protein-DNA nick and SSB at the integrated FRT locus. Upon replication, the RF will encounter the SSB and form a broken RF (system-ON). I-SceI nucleus localization will cut the integrated I-SceI sequence and generates a direct DSB.

3.2.2 FRT-FLP plasmid construction

The first step when setting up the system was to construct FLP expression and FRT integration plasmids. To generate these, standard PCR and vector cloning protocols were performed. As listed in Table 3.1, various versions of integration constructs containing FRT sequences were created. An expression construct containing mutant FLP recombinase (dsRed-FLPH305L-GR) was also created. All the plasmids generated were sequence verified.

Table 3.1 List of the FLP-FRT plasmids constructed.

Plasmid	Antibiotic resistance	Size	Description	Schematic map
pUC19-H1-ANCH3-ANCH4-H2	Ampicillin	9111 bp	The original integration plasmid gifted from Dr. Bystricky.	Appendix IV
pUC19-H1-BglII-FRT-ANCH3-ANCH4-H2	Ampicillin	8672 bp	Integration plasmid, FRT located 405 bp from ANCH3 and 1493 bp from ANCH4. Used to generate HEK293-FRT-ANCH3-ANCH4 cell line.	Figure. 3.4
pUC19-H1-BssHII-FRT-ANCH3-ANCH4-H2	Ampicillin	8815 bp	Integration plasmid, FRT located 50 bp from ANCH3 and 1139 bp from ANCH4.	Figure. 3.6
pUC19-H1-BglII-FRT-ANCH3-SacB-ANCH4-H2	Ampicillin	9379 bp	Integration plasmid, FRT located 405 bp from ANCH3 and 3044 bp from ANCH4.	Appendix III
pUC19-H1-BssHII-FRT-ANCH3-SacB-ANCH4	Ampicillin	9522 bp	Integration plasmid, FRT located 50 bp from ANCH3 and 1863 bp from ANCH4. Used to generate U2OS-FRT-ANCH3-ANCH4 cell line.	Figure. 3.7
pdsRed-FLpH305L-GR	Kanamycin	6835 bp	FLpH305L recombination expression plasmid, used to generate	Figure. 3.9.A

			the broken fork.	
pdsRed-I-SceI-GR	Kanamycin	6274 bp	I-SceI endonclease expression plasmid, used to generate the direct DSB, gifted from Dr. Maria Jasin	Figure 3.8
pdsRed-GR	Kanamycin	5550 bp	Empty plasmid used as a negative control plasmid.	Figure. 3.9.B

3.2.2.1 FLP recognition target integration construct

To establish FRT cell lines, different FRT integration plasmids with different visualization tools were generated. The unique FRT sequence is 47 nucleotides long, comprising three symmetrical DNA elements; each 13 bp long (5'-GAAGTTCCTATTC-3'). Two of these elements were inverted with a reverse orientation; this is what the FLP recombinase monomer binds to. However, a third element is also present in tandem, upstream from one of the elements. An 8bp central site-specific recombination spacer (TCTAGAAA) separates the two inverted elements (Figure 1.13.A). This is termed the core crossover region, enabling strand exchange, during which recombination takes place. Inserting an FRT sequence into such orientations will generate a nick (SSB) in the left site of the FRT sequence (Nielsen et al., 2009).

First, a pYFP/LacO-FRT-CFP/tetR integration construct was generated by annealing two FRT oligonucleotides (FRT1_*ISce*I and FRT2_*ISce*I), as previously described in section 2.1.4 (Table 2.2). The annealed FRT overhang insert (64 bp) was digested using the *I-Sce*I restriction enzyme (section 2.1.7), and then cloned and ligated directly into the I-SceI digested pYFP/LacO-I-SceI-CFP/tetR vector. The entire pYFP/LacO-I-SceI-CFP/tetR plasmid encompassed 17 kilobases (kb), containing 256 lac operator repeats (TGGAATTGTGAGCGGATAACAATT) and 96 Tet operator repeats (TCCCTATCAGTGATAGAGA) (Soutoglou et al., 2007) (Appendix II). The ligation reaction was performed and transformed into ElectroMAX™ DH5α-E™ Competent Cells (Section 2.1.8). However, no clones were observed when transforming the ligated construct. This might have resulted from a combination of recombination events and the instability of the original plasmid.

To overcome the transformation difficulties experienced using the Tet and Lac operators, the transformation was repeated using ElectroMAX™ Stbl4™ competent cells. These cells were created specifically to clone unstable DNA sequences, stabilizing direct repeats and retroviral sequences (Al-Allaf et al., 2012). It was expected that plasmid digestion with SacI/ XhoI would give 3 fragments of 10 Kb, 4 Kb and 3 Kb (Figure A). Several colonies were then extracted as described in Section 2.2.4, however, it was observed that each digested clone differed in size (Figure 3.3). This might be due to both recombination events and the instability of the original plasmid.

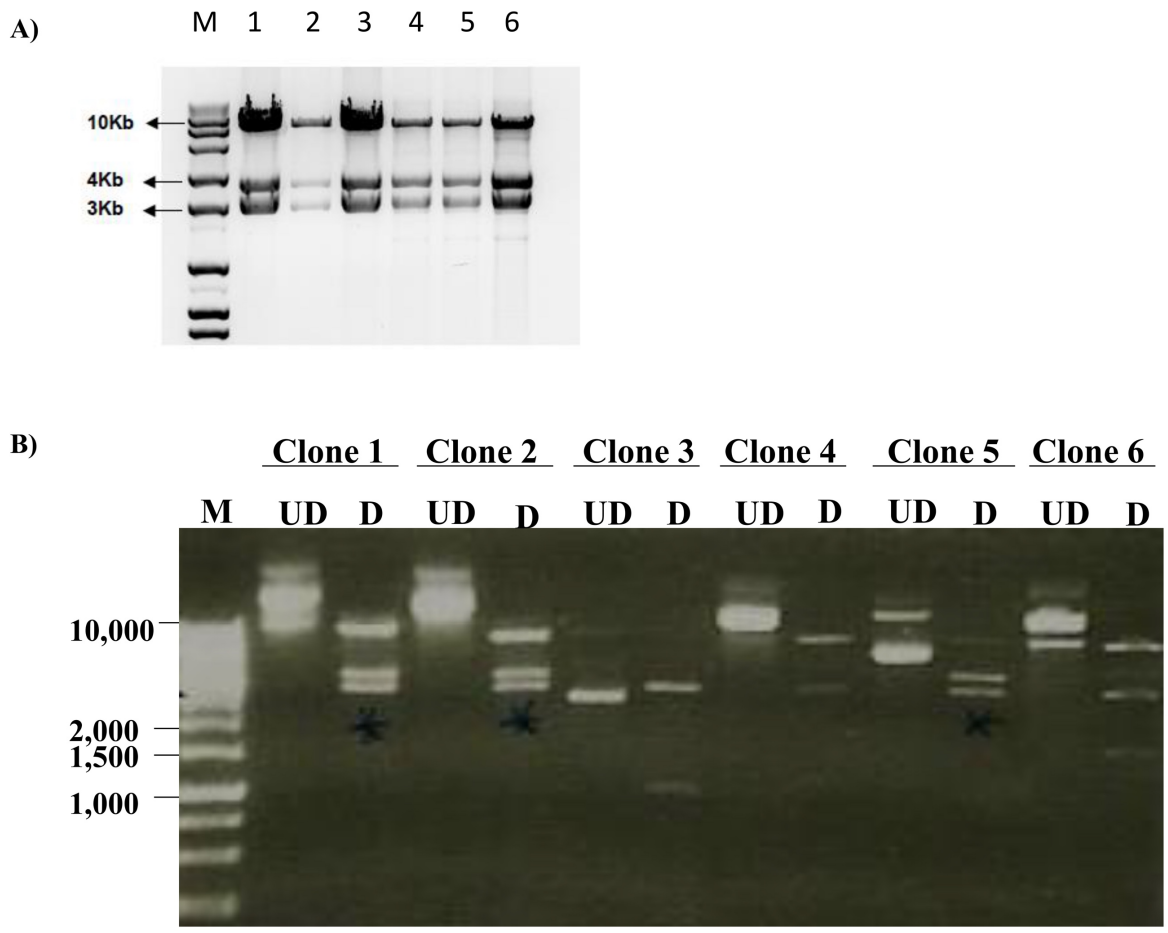

Figure 3.3 Digestion reaction for different pYFP/LacO-FRT-CFP/tetR clones. A) Detection of different pYFP/LacO-I-SceI-CFP/tetR minipreps. **B)** 1% Agarose gel of several selected single clones digested with 10 units of Xhol and SacI restriction enzymes. Digested (D) and Undigested (UD).

A second integration plasmid was created based on the the new ANCHOR visualization tool to avoid the unstability issue of the pYFP/LacO-I-SceI-CFP/tetR plasmid. Different FRT-ANCH3-ANCH4 integration constructs were generated by manipulating the FRT oligonucleotide overhang sequences. This was achieved by inserting the FRT at different sites in the original pUC19-H1-ANCH3-ANCH4-H2 cassette resulting in vectors pUC19-H1-BglII-FRT-ANCH3-ANCH4-H2 (Figure. 3.4), pUC19-H1-BssHII-FRT-ANCH3-ANCH4-H2 (Figure 3.6), pUC19-H1-BglII-FRT-ANCH3-SacB-ANCH4-H2 (Appendix III) and pUC19-H1-BssHII-FRT-ANCH3-SacB-ANCH4 (Figure 3.7) vectors.

In all these constructs the FRT sequence was tagged using two small DNA segments, termed "ANCH", and a single unique 18 bp I-SceI endonuclease site; although it was located in different positions, as described in detail in the following sections. Additionally, all the integration plasmids generated contained the hygromycin (Hygro) resistance marker.

3.2.2.1.1 pUC19-H1-BglII-FRT-ANCH3-ANCH4-H2 integration construct

To allow visualization of GFP and CFP florescent foci near the break site, a FRT sequence was inserted 405 bp from the ANCH3, and 1493 bp from the ANCH4 binding sequence. To generate the pUC19-H1-BglII-FRT-ANCH3-ANCH4-H2 integration construct encompassing 8672 bp. The FRT sequence (48 bp), was created by annealing 100 μM of the two FRT oligonucleotides BglII-FRT-EcoNI primer A and B (106 bp) (Section 2.1.4). The annealed oligonucleotides contained BglII/EcoNI restriction sites and vector homology sequence at each end (Table 2.2). The annealed BglII-FRT-EcoNI oligo's and pUC19-H1-ANCH3-ANCH4-H2 vector (9111 bp) (Appendix IV) were digested with 20 units each of *EcoN*I and *Bgl*II (Section 2.1.7). The ligation reaction was performed at two molar vector to insert ratios, 1:3 and 1:5 with 100ng of total DNA, as described in section 2.1.8. As shown in Figure 3.4, the FRT sequence was inserted upstream of ANCH3-ANCH4. The ligated constructs were then transformed into *E. coli* by electroporation (Section 2.2.3) and transformants were plated on LB media containing Ampicillin. Individual colonies were selected and purified using either the Mini prep or Maxi prep extraction kits (Section 2.2.4). The plasmids were verified by performing a digestion reaction with *Bgl*II and *EcoN*I, and checked on 1% agarose to verify both insert and vector.

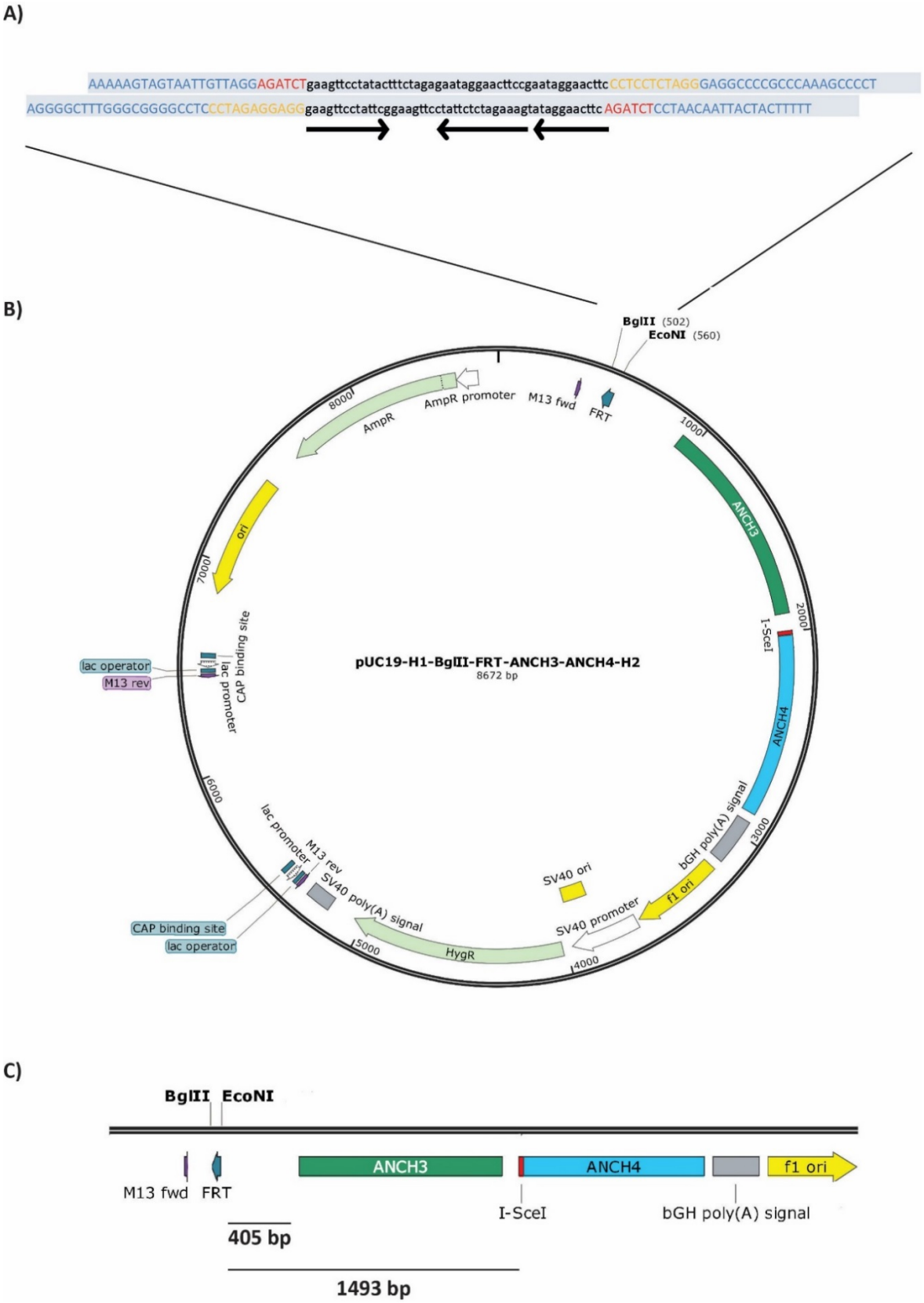

Figure 3.4 Schematic map of the pUC19-H1-BglII -FRT-ANCH3-I-SceI-ANCH4-H2 construct. A) The FRT sequence was generated by annealing 100 µM of two complementary FRT oligonucleotides (BglII-FRT-EcoNI primers A and B). **B)** Map shows the generated construct (8672 bp) **C)** In this construct, the FRT sequence will be 405 bp from ANCH3 and 1493 bp from ANCH4, to allow visualization both at approximately 0.5 Kb and 2 Kb to the break site, respectively.

3.2.2.1.2 pBssHII-FRT-ANCH3-ANCH4 integration construct

To insert the FRT sequence in close proximity to the ANCH3 binding site to visualize occurrences at the break site, a second construct pUC19-H1-FRT-BssHII-ANCH3-ANCH4-H2 was generated. A site direct mutagenesis reaction was performed using a Quick change II kit to insert/add the unique *BssH*II recognition site (CGCGCG) to the vector near ANCH3 using (ins-BssHII-primers), as described in section 2.1.9 in the pUC19-H1-ANCH3-ANCH4-H2 vector (Table. 2.2). The mutated vector was then verified using PCR, followed by sequencing, and the sequences then analysed by aligning them with the original vector and the mutated one. The alignment was performed using BLASTN as shown in Figure 3.5.

In this construct, the FRT sequence was generated by annealing 100 μM of the two complementary FRT oligonucleotides (Section 2.1.4), EcoNI-FRT-BssHII primer A and B. Both constructs contain EcoNI-BssHII restriction sites and a vector homology sequence at each end (Table 2.2). The annealed FRT insert and mutagenized pUC19-H1-BssHII-ANCH3-ANCH4-H2 vector were then digested with *BssHII* (20,000 U/mL) and *EcoNI* (10,000 U/mL) (Section 2.1.7). The digested insert was then annealed and cloned into a digested vector, ensuring the FRT would be 50 bp from ANCH3 and 1139 bp from ANCH4. The generated construct was then transformed into *E. coli*, and individual colonies grown in LB containing Ampicillin. Subsequently, DNA minipreps were prepared from 3 colonies and verified using sequencing (Figure 3.6).

A)

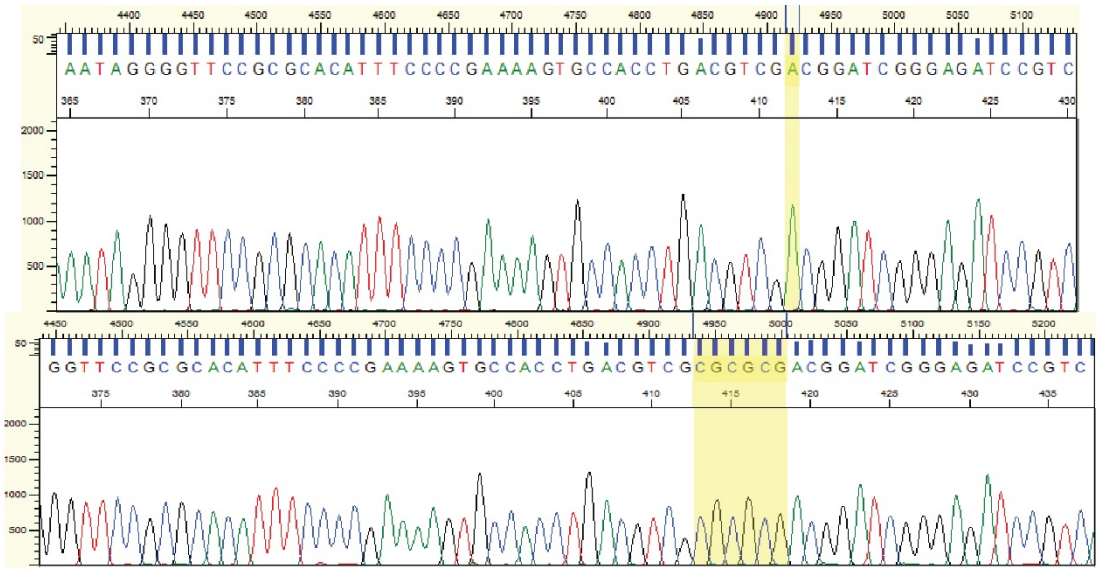

B)

```
ANCH34              ACAAATAGGGGTTCCGCGCACATTTCCCCGAAAAGTGCCACCTGACGTCG------ACGG 1134
mut.ANCH34_cl.4     ACAAATAGGGGTTCCGCGCACATTTCCCCGAAAAGTGCCACCTGACGTCGCGCGCGACGG 422
                    ************************************************      **** 

ANCH34              ATCGGGAGATCCGTCACTTTGGCAGGATCTTCCACAGTTTCAACGTTGAAACTGTGGGGC 1194
mut.ANCH34_cl.4     ATCGGGAGATCCGTCACTTTGGCAGGATCTTCCACAGTTTCAACGTTGAAACTGTGGGGC 482
                    ************************************************************ 

ANCH34              GTAAGCATCAGCGCGGTGGGTGTTTGTGACTGCAACGCTGCGCCAGCAGTTTCAACGTTG 1254
mut.ANCH34_cl.4     GTAAGCATCAGCGCGGTGGGTGTTTGTGACTGCAACGCTGCGCCAGCAGTTTCAACGTTG 542
                    ************************************************************ 

ANCH34              AAACTGAAAGCATTGAGCCGAGTGGCTTGTGGCTCTCTTGCGTTAAGCCTTACAAAAGTC 1314
mut.ANCH34_cl.4     AAACTGAAAGCATTGAGCCGAGTGGCTTGTGGCTCTCTTGCGTTAAGCCTTACAAAAGTC 602
                    ************************************************************ 

ANCH34              CATCTCTACCGGGACGGGGCACTGGCCACGTGCGTCCATCAGGGGGCCAGTTTCAACGTT 1374
mut.ANCH34_cl.4     CATCTCTACCGGGACGGGGCACTGGCCACGTGCGTCCATCAGGGGGCCAGTTTCAACGTT 662
                    ************************************************************ 
```

Figure 3.5 Electropherogram and sequencing alignments of the two plasmid constructs. A) The mutagenic pUC19-H1-ANCH3-ANCH4-H2 plasmid using site direct mutagenesis to insert BssHII at the restriction site. The highlighted square indicates the insertion variants located between the two constructs. **B)** Sequence alignment of pUC19-H1-ANCH3-ANCH4-H2 (ANCH3-4) and the mutagenized pUC19-H1-FRT-BssHII-ANCH3-ANCH4-H2 (mut.ANCH34_cl.4) constructs. The yellow highlighted sequence is the unique BssHII restriction site sequence added to the vector.

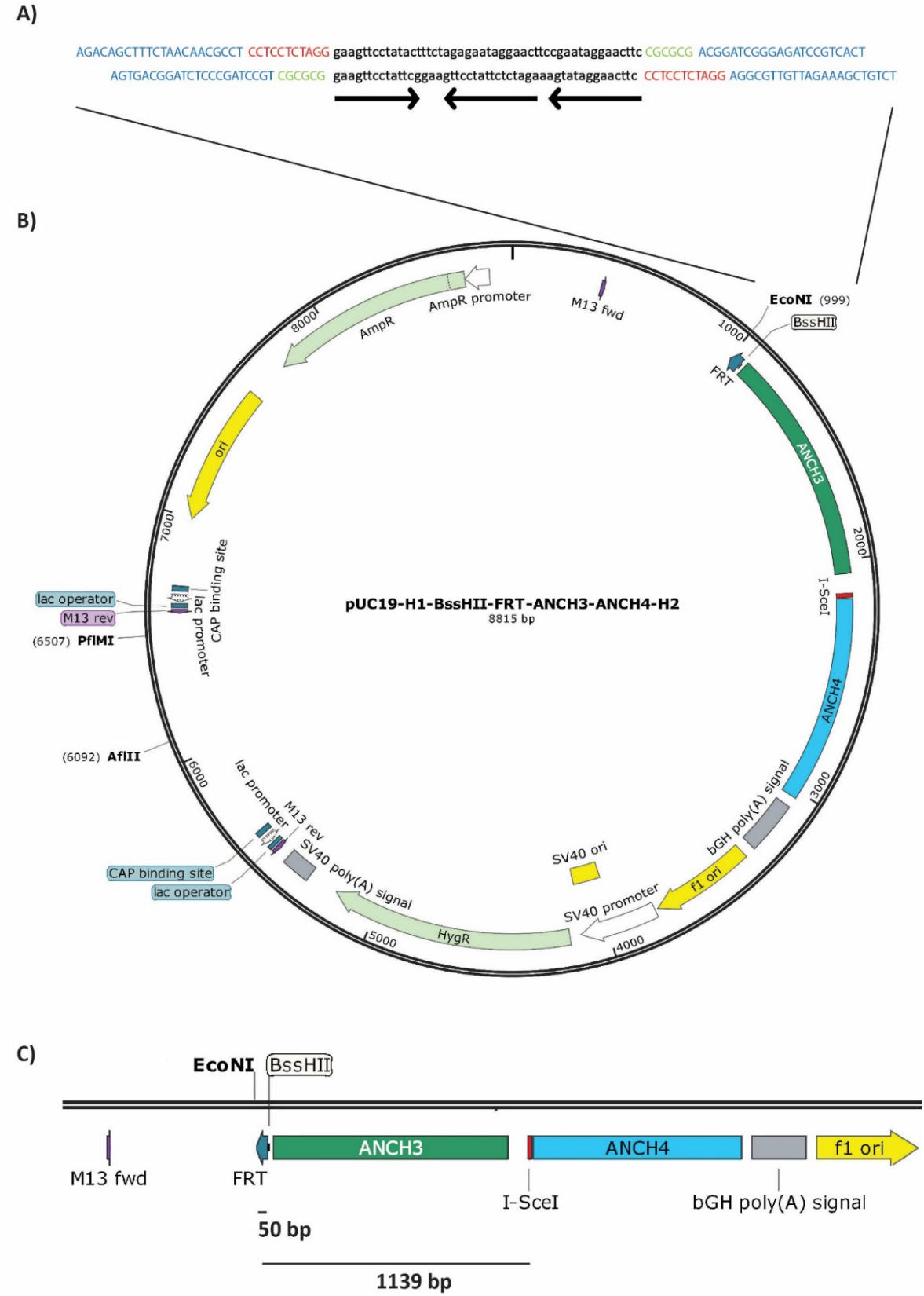

Figure 3.6 Schematic map of the pUC19-H1-FRT-BssHII-ANCH3-ANCH4-H2 construct. A) The FRT sequence was generated by annealing two complementary FRT oligonucleotides (EcoNI-FRT-BssHII primers A and B). **B)** Map shows the generated construct (8815 bp). **C)** In this construct, the FRT sequence will be 50 bp from ANCH3 and 1139 bp from ANCH4 to allow visualization both at and proximate to the break site, respectively.

3.2.2.1.3 pBglII-FRT-ANCH3- spacer-ANCH4 integration construct

As the two previously generated constructs, pUC19-H1-BglII-FRT-ANCH3-ANCH4-H2 (Figure 3.3) and pUC19-H1-BssHII-FRT-ANCH3-ANCH4-H2 (Figure 3.5) have a short 105 bp sequence between the ANCH3 and ANCH4 florescence binding sequences, the resulting fluorescent signals of the two foci in the fluorescence microscope was found to subsequently overlap (Section 3.2.2.1.1 and 3.2.2.1.1). To overcome this and to be able to follow the fate of each florescent foci independently, a random ~720 bp linker sequence in the part of the SacB sequence amplified using the pLEICs-74 vector developed by PROTEX facility, was inserted between the two ANCH sequences. This resulted in the creation of two additional integration constructs pBglII-FRT-ANCH3-spacer-ANCH4 (Appendix III) and pBssHII-FRT-ANCH3-spacer-ANCH4 (9522 bp) (Figure 3.7). In the pBglII-FRT-ANCH3-spacer-ANCH4 vector, the FRT is 1815 bp from ANCH4. Whereas, in the pBssHII-FRT-ANCH3-spacer-ANCH4, the FRT is 1350 bp from ANCH4.

Both constructs were generated by digesting the pUC19-H1-BglII-FRT-ANCH3-ANCH4-H2 and pUC19-H1-BssHII-FRT-ANCH3-ANCH4-H2 with *Not*I and *EcoR*V, which are located between the two ANCH sites, without disrupting the 18 bp I-SceI sequence. The digested plasmids (~6692 bp) were gel purified, and ligation performed using the PROTEX facility to insert the linker sequence when performing ligation independent cloning (LIC). LIC is a cloning method that utilizes the annealing of single-stranded complementary overhangs onto a target vector, and a PCR-generated insert of at least 12 bases. The generated constructs were verified with PCR prior to sequencing.

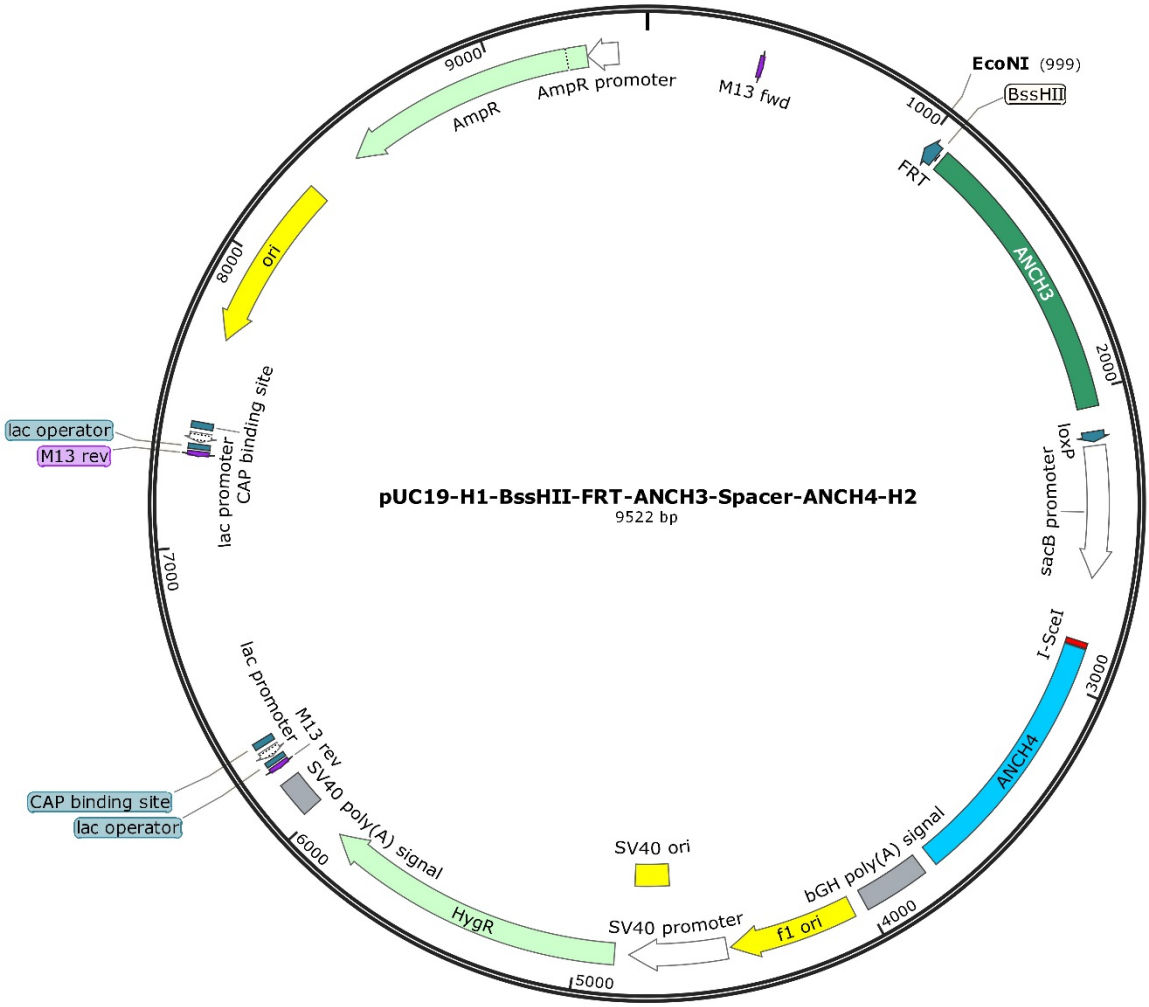

Figure 3.7 Schematic map of the pUC19-H1-FRT-BssHII-ANCH3-SacB-ANCH4-H2 construct. This was accomplished by insertion of a linker of 700 bp from pLEICS2 plasmid (PROTEX) between the ANCH3 and ANCH4 sites, to allow visualization of the two foci in good resolution.

3.2.2.2 I-SceI endonuclease expression construct

In this study, all the expression constructs included were carefully designed to contain components known to play specific roles within mammalian cells. The original pdsRed-I-SceI-GR (6274 bp) expression vector (Figure 3.8.A) was a gift from Dr. Maria Jasin, and has been used to generate proteins linked to the Discosoma sp. red florescent protein (dsRed) for the purpose of visualization. Secondly, the GR sequence was also incorporated, permitting the cytoplasm to achieve nuclear relocalization of the plasmid after the addition of TA (Soutoglou *et al*., 2007). Therefore, once transfected into a mammalian cell, a red fluorescent signal should be visible in the cytoplasm, to indicate expression within the cell. All these components fall within the control of an upstream cytomegalovirus (CMV) promoter, inducing expression across a range of cell types (Qin et al., 2010). This construct contains a neomycin/kanamycin resistant gene (neoR/Kan), which confers resistance on the G418 antibiotic. In this study, the pdsRed-I-SceI-GR vector was also generated to advance cellular experiments that have been conducted to induce direct DSB upon binding to integrated I-SceI sites in a genome, this permits comparisons between induced direct DSB and BF (se-DSB).

3.2.2.3 FLP-recombinase expression construct

To generate an inducible SSB and subsequent broken RF, an expression construct was created. pdsRed-FLpH305L-GR express a Flp "step-arrest" mutant FLP recombinase (FLP305H). The entire FLP305H sequence of 1272 bp was amplified using PCR, as described in Section 2.1.3 using the pBIS-GALkFLP (URA3) plasmid as a template, and using primers specifically applied to amplify FLPH305L, XholSacI_FLP1_FP and KpnlSalI_FLP1_RP primers (Table 2.2). The PCR reaction revealed an amplicon product of expected size of 1272 bp (Figure 3.8.B). As demonstrated in Figure 3.7.C, the purified FLPH305L amplicon and the pdsRed-*I-Sce*I-GR vector were then digested by *Kpn*I and *Sac*I to deliver 5563 and 711 bp products (Section 2.1.7). A ligation reaction was performed (Section 2.1.8) to generate the dsRed-FlpH305L-GR construct (6835 bp), as illustrated in Figure 3.9.A. When generating this construct, the FLpH305L recombinase was tagged upstream with dsRed, and then flanked downstream with GR.

A third empty construct was generated for use as a negative control in subsequent experiments (Figure 3.9.B). The pdsRed-GR empty construct was generated by digesting the dsRed-I-SceI-GR original vector with *Nhe*I and *Xba*l for the purpose of generating blunt ends. The digested vector was run in a 1% gel, and the 3920 bp band purified (Section 2.1.6), and all constructs generated were verified using sequencing primers (Table 2.1).

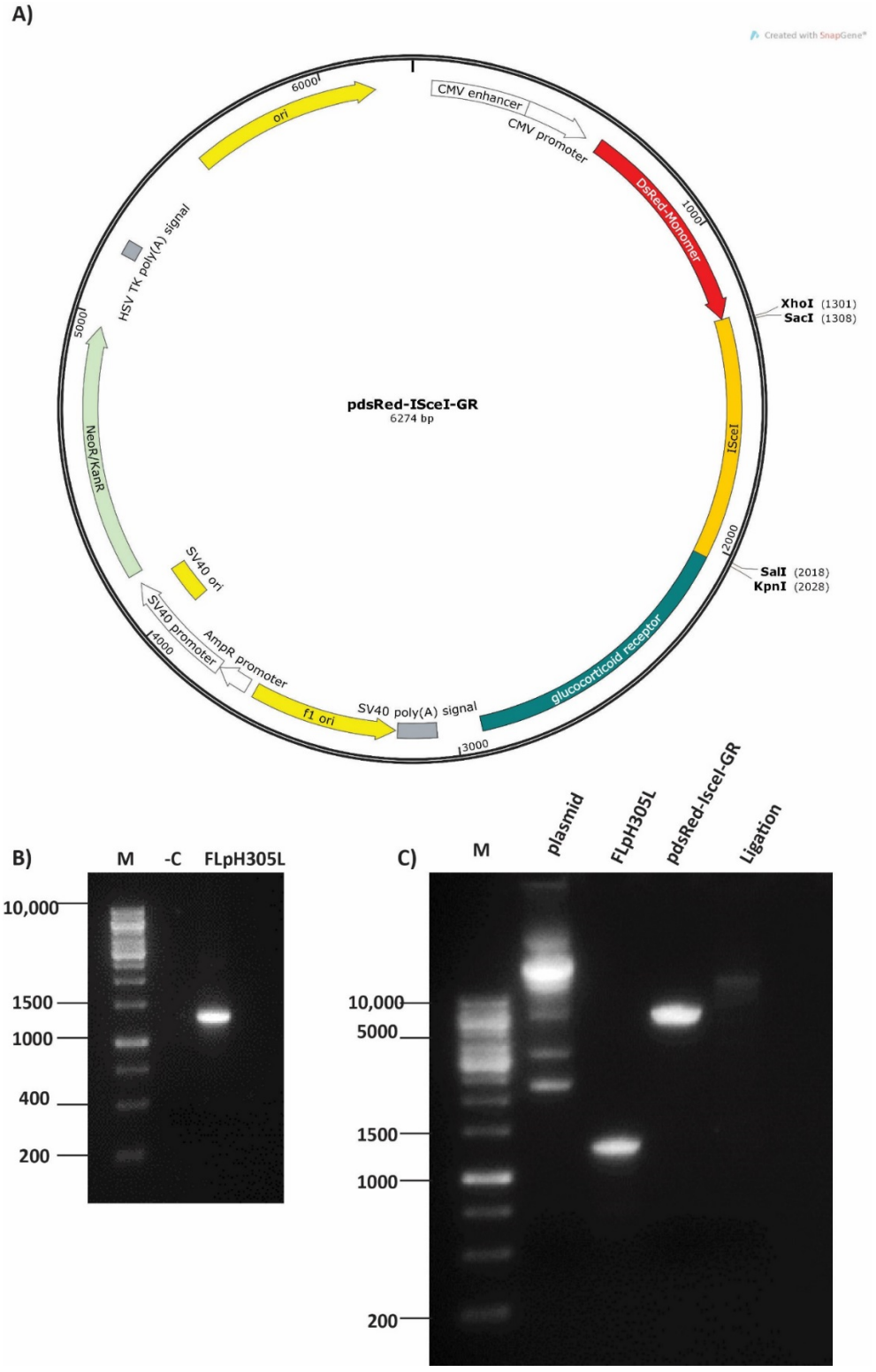

Figure 3.8 Schematic map of pdsRed-I-SceI-GR expression construct. A) Map showing the original pdsRed-I-SceI-GR construct (6274bp), which has been modified to generate the pdsRed-FLpH305L-GR recombinase construct. **B)** 1% gel image, lane 1, the hyper ladder DNA marker, lane 2 is a PCR negative control and lane 3 is PCR product of FLpH305L amplicon, using XholSacI_FLP1_FP and KpnlSalI_FLP1_RP primers. **C)** The digestion reaction, lane 1, the hyper ladder DNA marker, lane 2 is the undigested pdsRed-I-sceI-GR, lane 3, digestion reaction for the insert (FLph305L), lane 4, digestion reaction for the vector (dsRed-I-sceI-GR) using kpnI and SacI restriction enzymes, lane 5, ligation reaction.

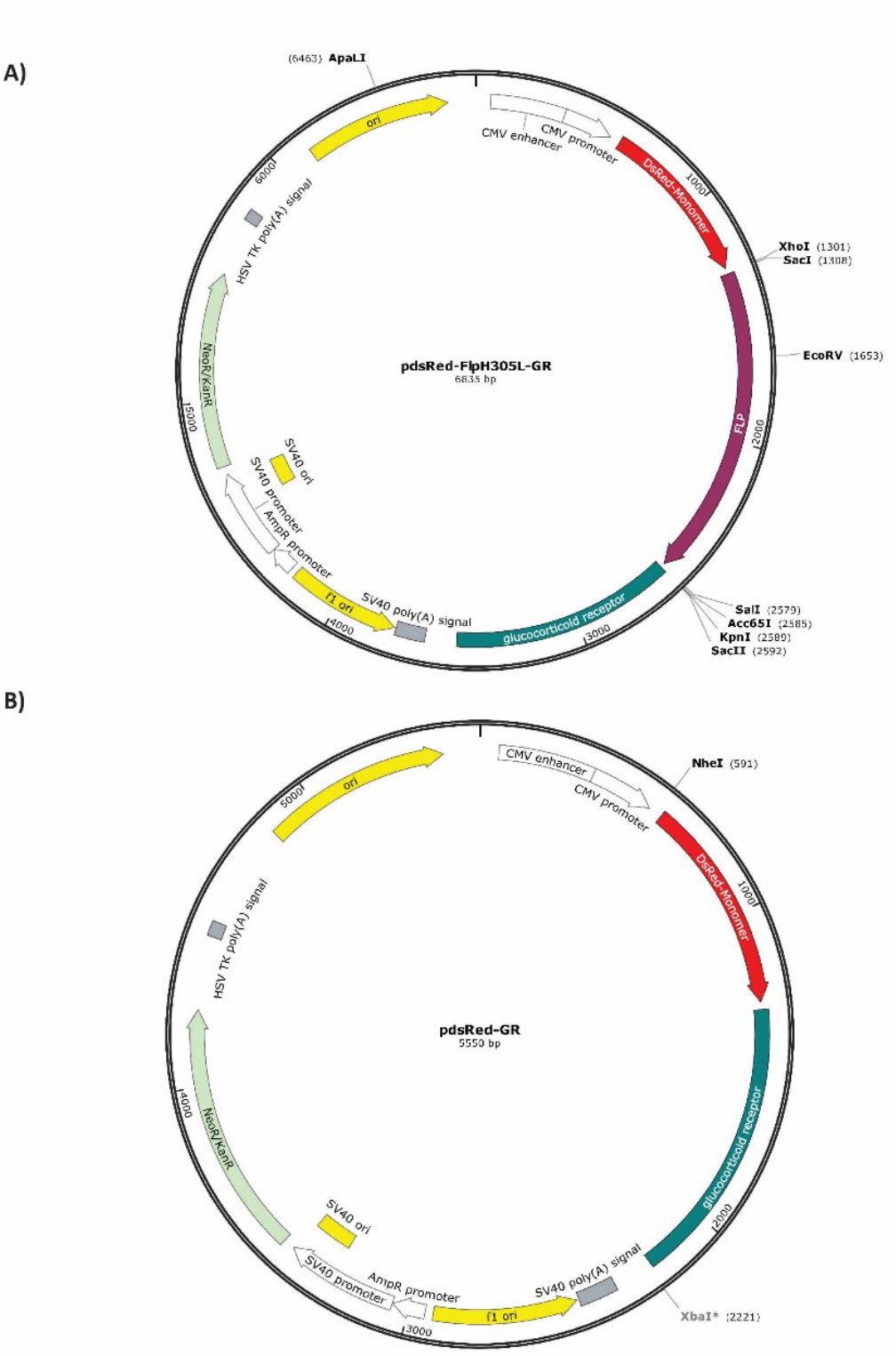

Figure 3.9 Schematic map of the pdsRed-FLPH305L-GR recombinase expression construct. A) Map showing the generated dsRed-FLPH305L-GR construct (6835bp). In this construct, FLPH305L (purple) is tagged with the *Discosoma* red fluorescent protein (dsRed) (red), which was located upstream of the FLPH305L to support visualization of the expression and detection of the transfected cells. The glucocorticoid receptor (GR) receptor was located downstream of the FLPH305L (green). This expression is directed and controlled by an upstream human cytomegalovirus (CMV) promoter (white). **B)** Schematic map of pdsRed-GR empty construct.

3.2.3 Cell immortalization

In T75 tissue culture flasks, primary mouse embryonic fibroblast (MEFs) (used in Chapter 7) and human embryonic kidney (HEK293) cells (gift from Prof Giorgini, University of Leicester) were immortalized through transfection with p129 simian virus 40 (SV40) plasmid (gifted from Mertz's lab), which contains a large T antigen known to inactivate the tumour suppressor gene P53 (Ali and DeCaprio, 2001). 24 hours post transfection, the cells were counted and split regularly at a ratio of 1:10. After 15 passages the growth rate was found to rapidly increase (Figure 3.10), indicating immortalized cells had taken over the culture. The resulting cultures were used for further experiments.

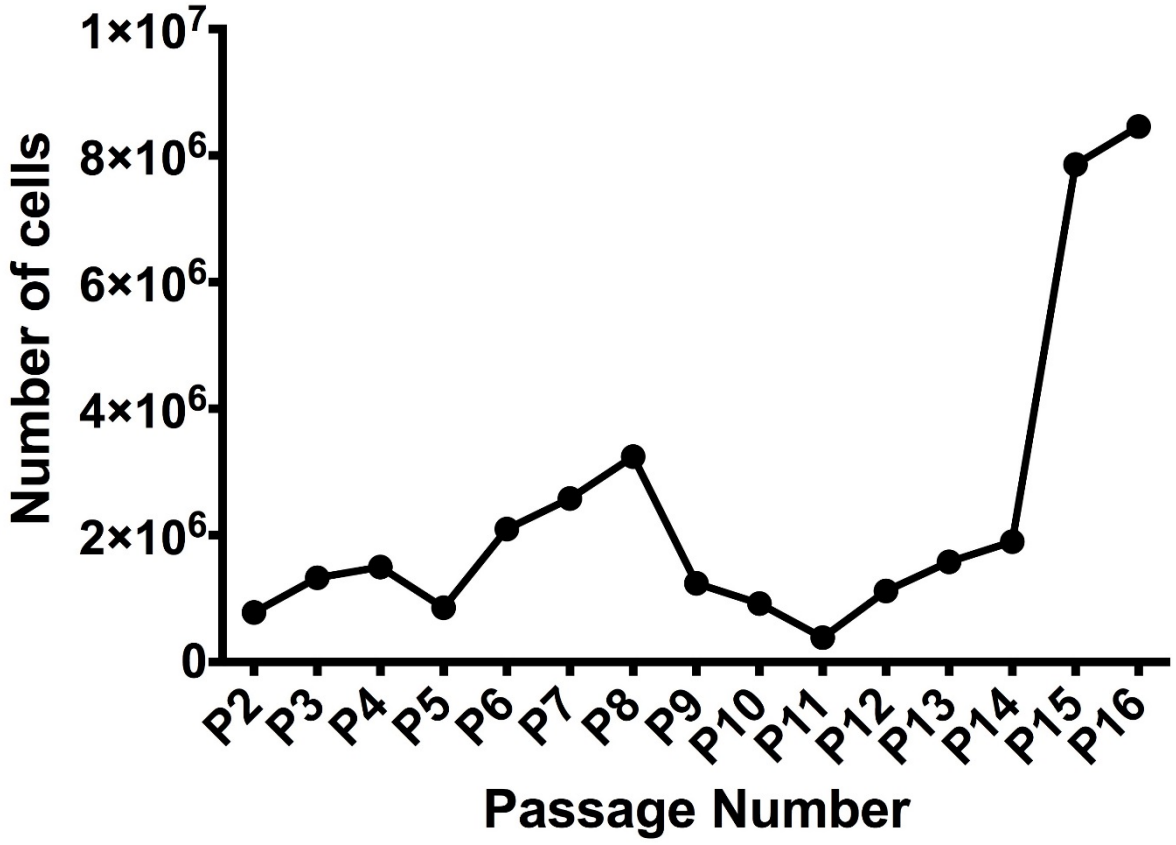

Figure 3.10 Growth curve for immortalization of HEK293 cell. MEFs cells were transfected with pSV40 plasmid carrying the large T antigen for 48 hours. Cells were cultured and the total number of cells was counted in each passage.

3.2.4 Transfection optimization

After successful construction and verification of generated FRT integration and expression constructs, different cell lines were tested to establish which would be the best for setting up the FRT-FLP system. Human epithelial cells, derived from cervical cancer cells (Hela), human bone osteosarcoma cell (U2OS), transformed human embryonic kidney (HEK293T), MEFs, and HEK293 generated in section 3.2.3 were seeded in a 24-well plate. As a starting point, the optimal transfection efficiency was determined by examining the ratio of DNA to transfection reagent. Transient transfection was performed with a constant plasmid concentration (1 µg/ml) of pdsRed-FLPH305L-GR and varied the amount of transfection reagent (1:2, 1:3 and 1:5 ratios of the TransIT-2020 transfection reagent to DNA), as described in section 2.5.4. 1 µg of the original dsRed-I-SceI-GR plasmid was used as a positive control.

Figure 3.11 shows red fluorescence and phase contrast images. As evidenced by the phase contrast images, rounded and dead cells were observed, indicating that toxicity increased in accordance with the amount of transfection reagent. This might be a consequence of the impact of the transfection reagent, or of the lipid-DNA complex incubation time.

It was observed that while there is a detectable and clear expression of dsRed–FlpH305L–GR in the cell lines tested, though the intensity varied between them. The number of red cells were evaluated for red fluorescent protein expression to quantify transfection efficiency. Quantification of transfection efficiencies was assessed by counting the number of red cells present in each well. Figure 3.12 shows a graph that determines the optimal transfection to DNA ratio for all cell lines. Overall, the transfection efficiency was found to slightly vary between the cell lines. The efficiency shows a downward trend when increasing the charge ratio of transfection reagent to DNA. Thus, to minimize cytotoxic effect, it emerged that the optimal ratio is 1:2 DNA to transfection reagent. It was confirmed that 1:2 DNA to transfection reagent, which gave the higher number of transfected cells (red cells) compared to the other ratios.

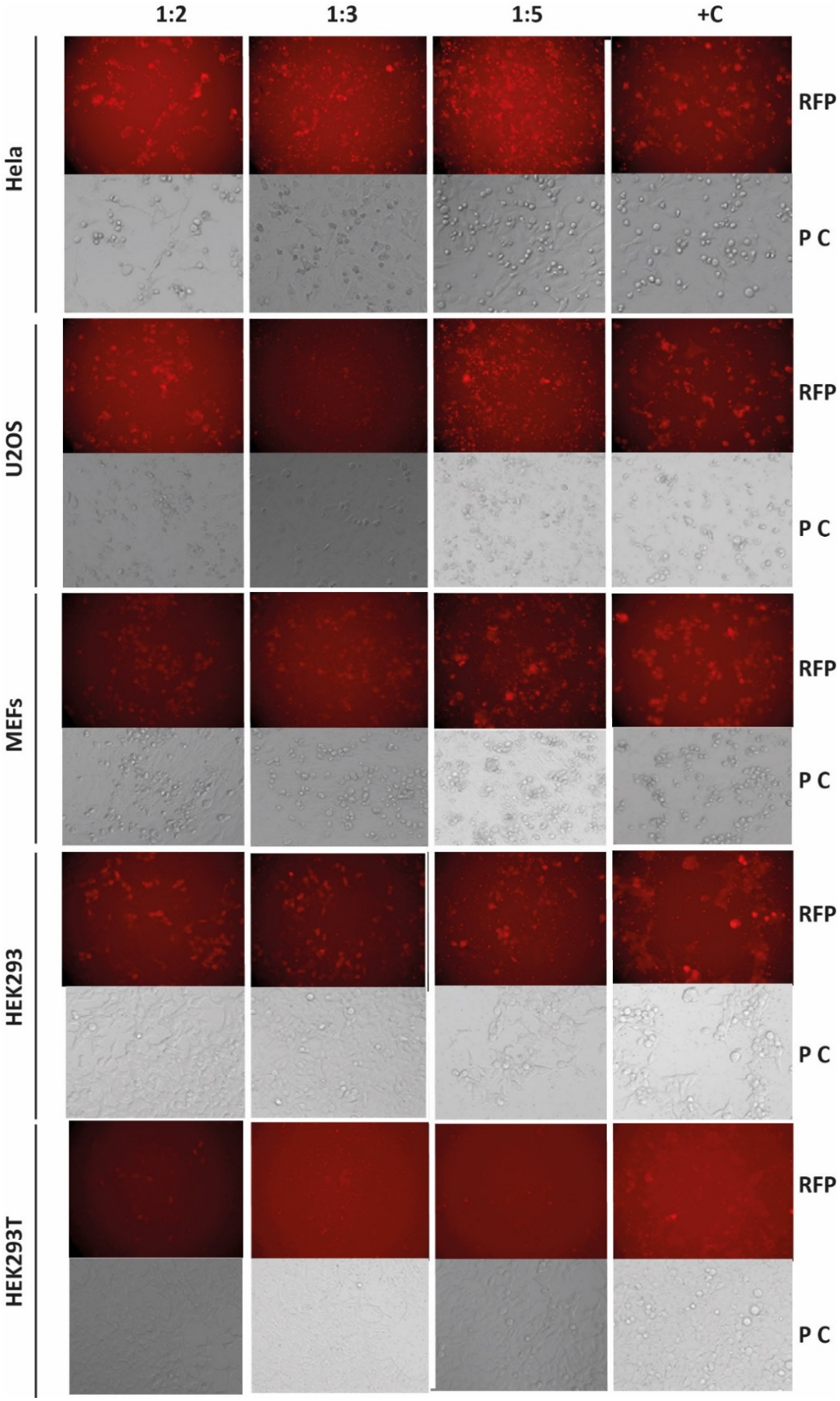
1:2
1:3
1:5
+C
Hela
U2OS
MEFs
HEK293
HEK293T
RFP
P C

Figure 3.11 Transfection optimization using TransIT-2020 transfection reagent. Fluorescence and phase contrast images of Hela, U2OS, MEFs, HEK293T and HEK293_SV40 cells were transiently transfected with the dsRed-FLPH305L-GR expression construct. A Mirus TransIT-2020 transfection reagent was used in various charge ratios relative to transfection reagent to DNA. +C,Cells were transfected using dsRed-I-SceI-GR as a positive control. The cells were visualized with a fluorescence microscope 24 hours' post transfection. The images were taken using the Olympus Cell^R/Scan^R system.

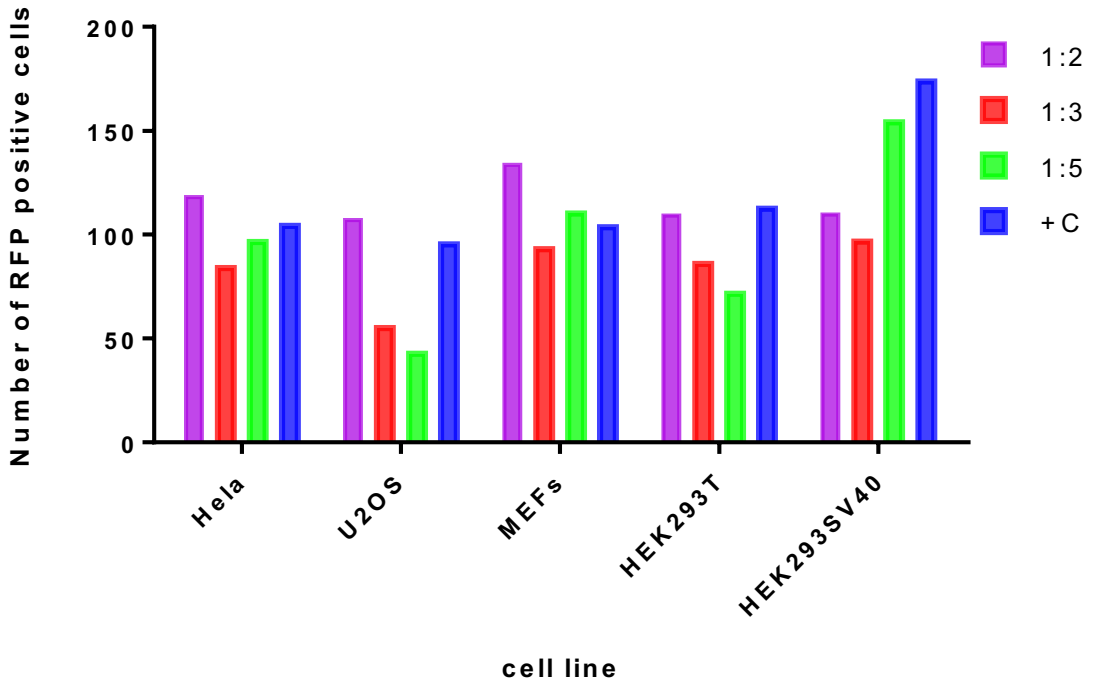

Figure 3.12 Quantification of transfection efficiency. A comparison of the percentage of RFP positive cells in different cell lines. Hela, U2OS, MEFs, HEK293T and HEK293_SV40 were transiently transfected with dsRed-FLPH305L-GR construct, using the Mirus transIT-2020 transfection reagent in various ratios of DNA to transfection reagent. Purple bars represent a 1:2 ratio; red bars represent a 1:3 ratio and green bars represent a 1:5 ratio. +C, cells were transfected using a dsRed-I-SceI-GR vector as a positive control in 1:2 DNA to transfection reagent ratio. Fluorescence was then quantified by counting the RFP-expressing cells, relative to the total number of cells using Scan^R analysis software.

To improve transfection efficiency, and reduce the toxicity arising from the former transfection reagent, several parameters were examined for HEK293-SV40 cells as they prove to be easily transfect. Transfection optimization was performed by using different transfection reagents, varying the amounts of plasmid DNA and varying the incubation time following transfection. Cells were first seeded for 24 hours in a 6-well plate, and transfected with different pdsRed-FLPH305L-GR plasmid concentrations, ranging between 1-3 µg/ml. The transfection was performed using FUGEN versus Trans-IT2020 (Section 2.5.4). The cells were incubated for either 24 or 48 hours to establish the optimum incubation time post transfection.

The cells were evaluated for dsRed expression using the Olympus ScanR screening station and the quantification of transfection efficiencies assessed using the Scan^R analysis software; this involved measuring the percentage population of red cells relative to the total number of cells present in each well (Section 2.6). Overall, the results showed transfection efficiency in all conditions increased after the cells had been incubated for 48 hours; this compared with 24 hours post transfection. The transfection efficiency of Trans-IT2020 was approximately 18-55 % after 24 hours incubation, then it rose to almost 50-70 % Post 48 hours incubation. Whereas, FUGEN revealed a transfection efficiency of 20-35 % post 24 and it increased to 50-75 % post 48 hours incubation. Although the transfection efficiency of Trans-IT2020 was higher than FUGEN after 24 hours incubation, no notable differences were revealed between the two reagents 48 hours post incubation (Figure 3.13).

It was revealed that using 1 µg of plasmid gave the lowest transfection efficiency in all conditions. However, a sharp increase in the efficiency was revealed when using 2 µg of plasmid to give an efficiency of approximitly 70%. This increase experienced a steady growth in the efficiency when increasing the amount of plasmid to 2.5 or 3 µg. It was visually noted that FUGENE was less toxic to cells than using a Trans-IT2020 reagent.

In conclusion, using HEK293-SV40 cells with a 48 hour incubation period, in combination with FUGENE, deliver high transfection efficiency and thus were used in all further experiments.

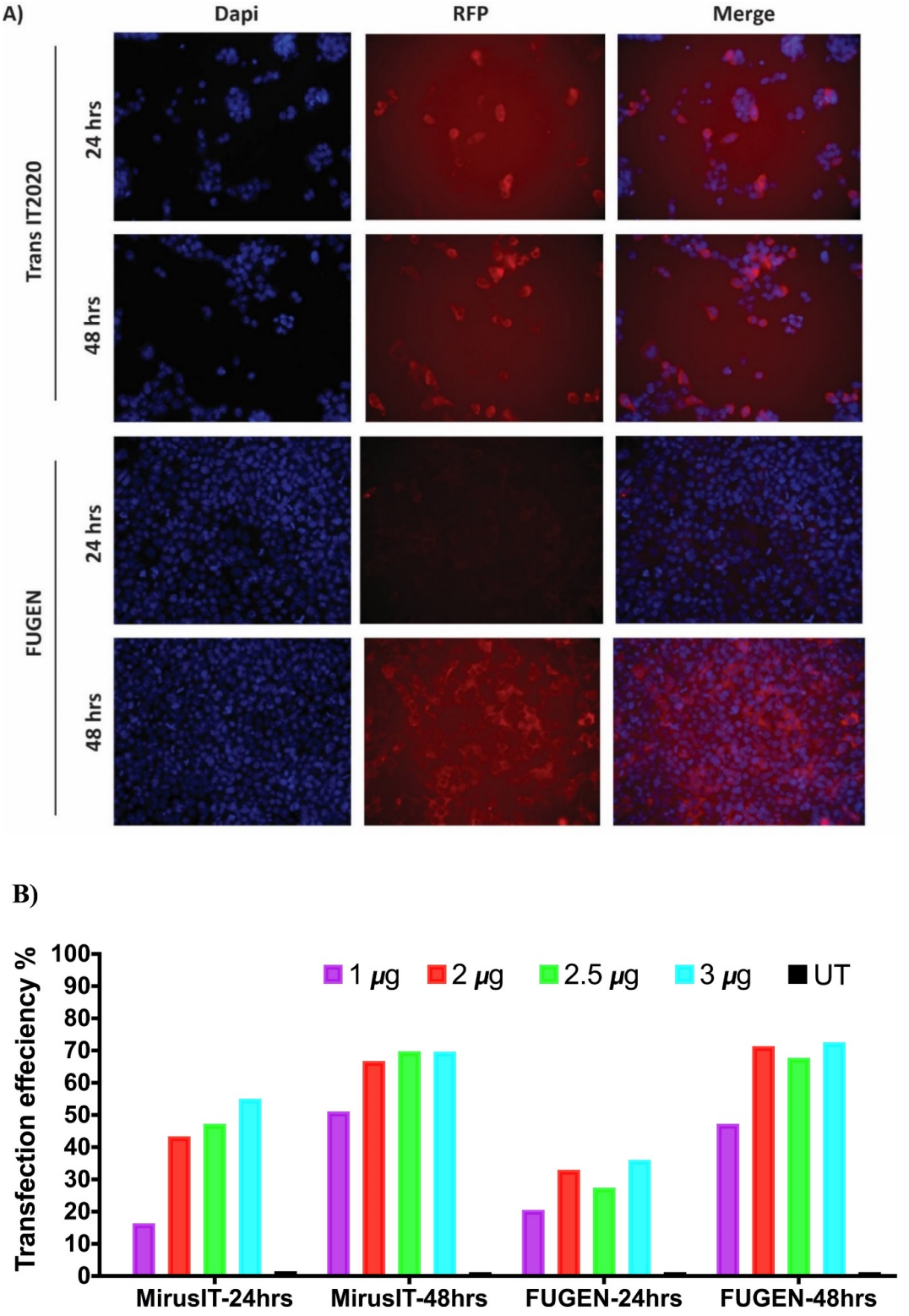

Figure 3.13 Determination of the optimal transfection condition for HEK293 cells. A comparison of the percentage of RFP positive cells in HEK293_SV40. Cells were transiently transfected with dsRed-FLPH305L-GR construct, using either the Mirus transIT-2020 or FUGEN transfection reagent in various DNA amount. UT, untransfected cells. **A)** Presentative images of cells transfected with 2 µg of pdsRed-FLpH305L-GR using Mirus IT or FUGEN transfection reagents, and incubated for 24 and 48 hours. **B)** Fluorescence was quantified by measuring the percentage of RFP-expressing cells relative to the total number of cells stained with DAPI stain, using Scan^R analysis software.

3.2.5 Determination of the optimal selection concentration

Before performing a stable transfection experiment to generate stable cell lines, determining optimal antibiotic concentrations for the selection markers used is a vital step in efficiently selecting stable single cell clones. This step was achieved by performing a kill curve experiment. This is a dose-response experiment, whereby Hela, U2OS, MEFs, HEK293T and HEK293SV40 cell lines are subjected to increasing amounts of G418/Geneticin and/or Hygromycin-B selection reagents. These are selection drugs used for the selection of stably expressed FlpH305L and FRT, respectively.

The cells were evaluated for their resistance and sensitivity, and for efficient antibiotic selection. This involved growing a constant number of cells in a complete media containing various concentrations of the selection reagent, as illustrated in Figure 3.14. G418 ranged from 0.5 -1.0 mg/ml; whereas Hygromycin B ranged from (0.5 - 500 µg/ml), and non-antibiotic containing cells were used as a negative control. Media that contained selected antibiotics was replaced every two days. High, optimal, and low antibiotic concentrations were determined by assessing levels of cell detachment. When cell death was evident within 2-3 days of antibiotic selection, the concentration was deemed high. Optimal concentration (Table 3.2) was defined as the lowest antibiotic concentration found to kill the majority of cells within seven days when compared to untreated control cells.

It was observed that optimal concentrations were cell type dependent. All the tested cells showed an increased sensitivity toward the highest concentration of selection reagent. Surprisingly, the HEK293T cells persisted, proving resistant to higher selected concentrations of G418. This suggests that this cell line was already resistant to the selection reagent and thus unsuitable for use with this construct. This confirms this cell line cannot be used to isolate stable single-cell FLPH305L clones.

To confirm the visually recorded toxicity results, and to obtain an accurate determination of optimal antibiotic concentration for HEK293 cells, cells were seeded into a 6-well plate and subjected to a range from 50- 300 µg/ml hygromycin B. The cells were trypsinized and counted as described in section 2.5.3, and a kill curve plotted, as shown in Figure 3.15. 200 µg/ml of hygromycin B was confirmed to be the optimal dose for use with HEK293 cells.

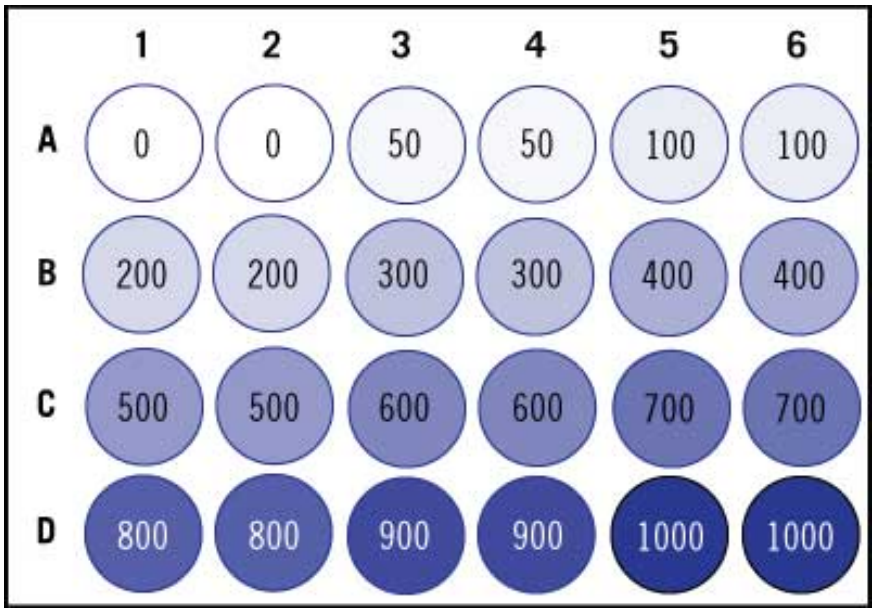

Figure 3.14 A schematic illustration of the strategy used to determine the optimal antibiotic selection dose for G418. Cells were seeded equally between the wells, and subjected to different antibiotic concentrations ranged from 0.5 -1.0 mg/ml in duplicate wells.

Table 3.2 Optimal antibiotic dose concentration for different cell lines. [a]

Cell line	Optimal dose concentration	
	Hygromycin B	G418
Hela	250 µg/ml	900 µg/ml
U2OS	150 µg/ml	500 µg/ml
MEFs	200 µg/ml	300 µg/ml
HEK293	200 µg/ml	700 µg/ml
HEK293T	350 µg/ml	>1000 µg/ml

[a] This table lists the optimal dose concentrations for G418 and Hygromycin B, which were used to select stable cell clones and transfectants.

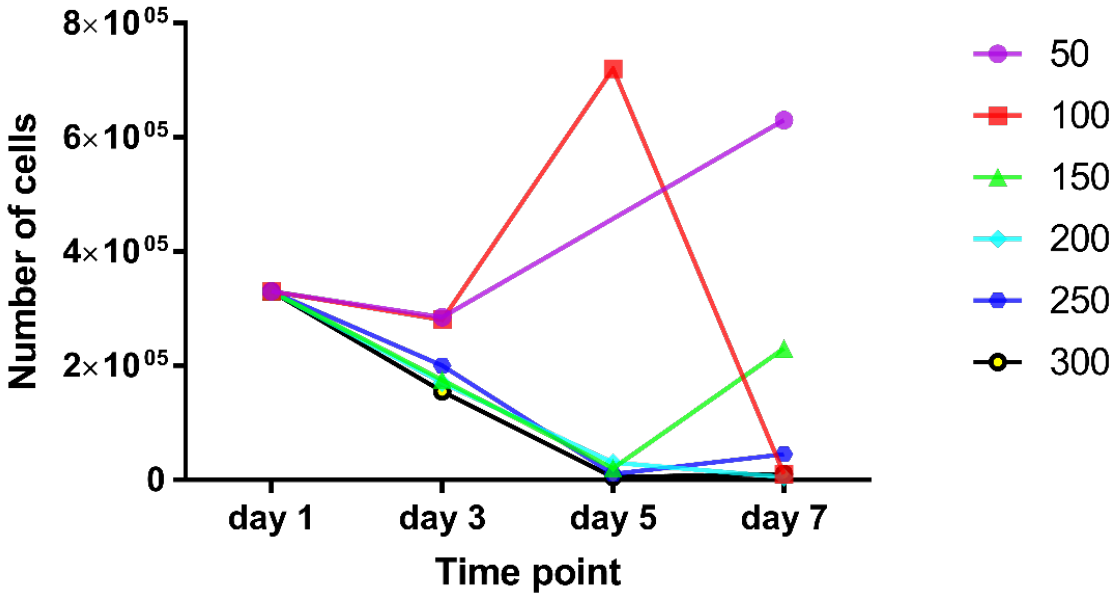

Figure 3.15 Determination of optimal Hygromycin B concentration. The kill curve for HEK293 cells subjected to various selection drug concentration ranged from (50-300 µg/ml) at different time points.

3.2.6 Stable transfection and selection

To set up the FRT-FLP system, stable transfections were performed using a FUGEN transfection reagent for Hela, U2OS and HEK293 cell lines. To generate stable cells lines two approaches were designed, the first attempted to generate cell lines stably expressing dsRed-FLPH305L-GR, and the second approach involved generating an FRT cell line.

3.2.6.1 Stable FLP cell line

Hela, U2OS and HEK293-SV40 cells were transfected with dsRed-FLPH305L-GR (1:2 DNA to transfection reagent). The original dsRed-I-SceI-GR plasmid was used as a positive control, and a plasmid free transfection used as a negative control. Transfection was performed using optimal transfection conditions in 15 cm plates, and propagation at 37°C. 48 hours after transfection, stable transfectants were maintained in medium containing optimum concentrations of the G418 selection drug (Table 3.2). G418 was used as a selection marker, because the transfected cells possessed the neomycin resistance gene, while the un-transfected cells did not. The selection media was also replaced every three days.

Transfection efficiency was assessed using the ScanR screening station, which involved detecting those cells expressing red fluorescent protein at time points before and after the addition of the G418 selection drug, and comparing the total number of cells present every two days. By visualizing the transfection plate using live cell imaging (Figure 3.16), 48 hours' post transfection, the percentage of RFP was found to be 80, 60 and 30 for Hela, U2OS and HEK293 respectively. As shown in Figure 3.16.A, the transfection efficiency for Hela cells transfected with both dsRed-FLP-GR and dsRed-I-SceI-GR was high post 48 hours incubation and before adding the selection drug (0-times point). The percentage of red cells gradually decreased over time, it reached about 10% and 30% with dsRed-I-SceI-GR and dsRed-FLPH305L-GR, respectively, after a week (192 hours) of adding G418. U2OS (Figure 3.16.B) and HEK293 cells (Figure 3.16.C) followed a similar pattern; both showing an increase in the number of red cells after the addition of the selected antibiotic and a reduction in cell numbers on the fifth day (144 hours) after adding the drug. However, the percentage of red cells after six days and continued to decline steadily to ten days. By day 10, the percentage of cells with a red signal had dropped hitting a low-point of about 30%.

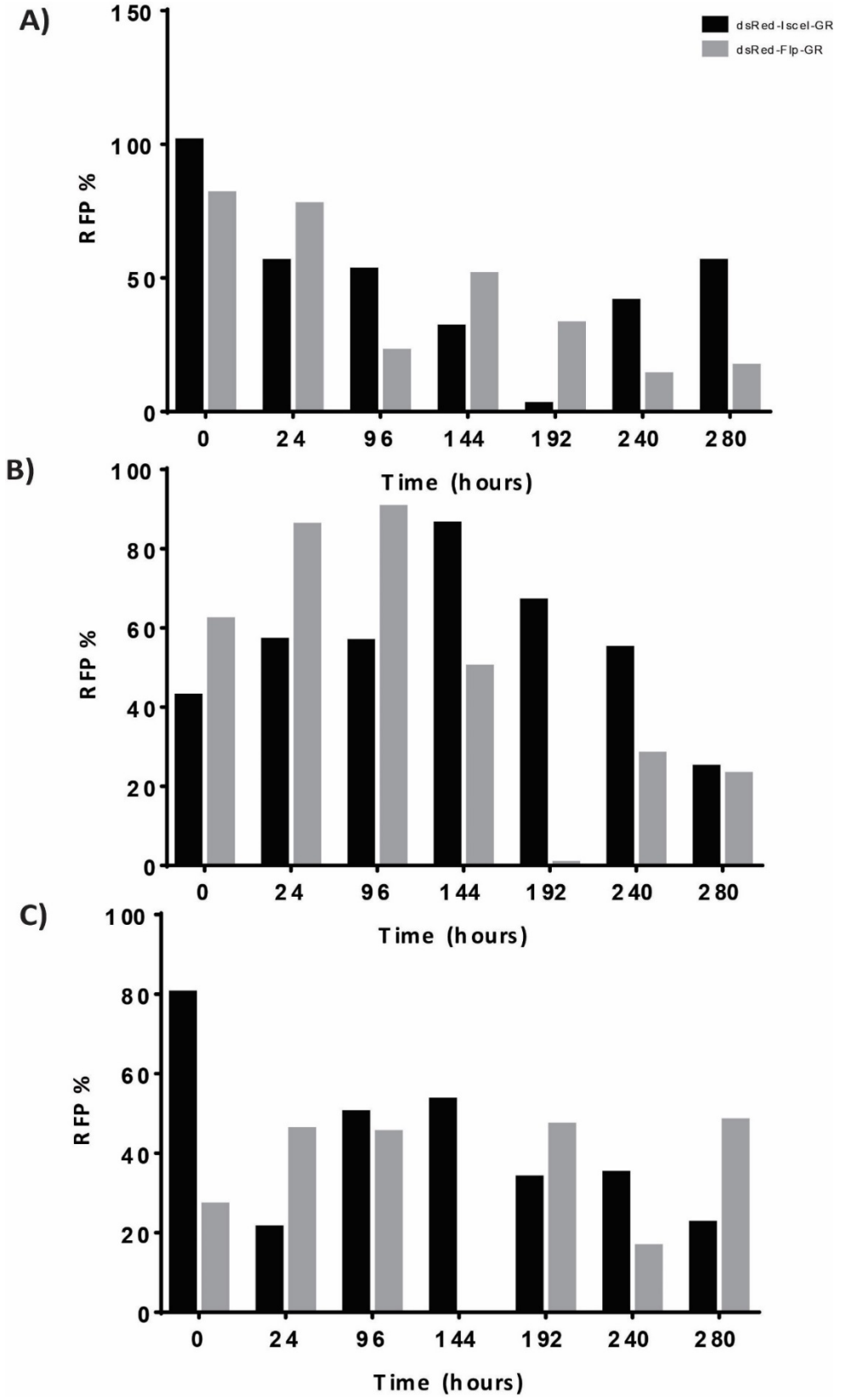

Figure 3.16 Percentage of red fluorescent protein (RFP) expression for transfected cells. The percentage of RFP expression was compared over time for **A)** Hela cells, **B)** U2OS cells, and **C)** HEK293s cells. The black bars represent the values of dsRed-I-SceI-GR vector and the grey bars represent the values of dsRed-FLPH305L-GR construct. Time zero indicates 48 hours' post transfection before addition of the G418 selection drug.

Ten days post transfection and selection with G418, HEK293 cells were 70% confluent, and single clones had formed and were countable for all the cells transfected with dsRed-FLPH305L-GR and dsRed-I-SceI-GR (Figure 3.17.A). Additional to the transfection plates, plasmid free transfection was used as a negative control; which involved plating cells in a 6-well plate and adding appropriate concentrations of G418 for each cell line.

Difficulties arose when aiming to isolate single clones from the polyclonal, confluent plate, as this prevented the accurate isolation of single-cell clones. Therefore, cells were split, and limiting dilution performed for the original transfection plates, by plating 2,500 and 25,000 cells per 15 cm plate.

Figure 3.17.B shows a kill curve performed by counting the total number of cells over each time point (Section 2.5.3). A similar pattern was observed concerning the impact of G418 selection antibiotic in all cell lines; where the cells' growth rate was reduced after adding G418. As shown in Figure 3.17.C, 106 and 90 colonies formed per million cells for dsRed-FLPH305L-GR and dsRed-I-SceI-GR respectively. Suggesting expression of FLp and I-SceI did not confer differing toxicities. In conclusion, the loss of expression of red signal during time was an issue and indicate that generation of cells stably expressing FLP is impossible, as the expression of the RFP was decresed over time, and subsequently an alternative strategy was used to generate a FRT stable cell line.

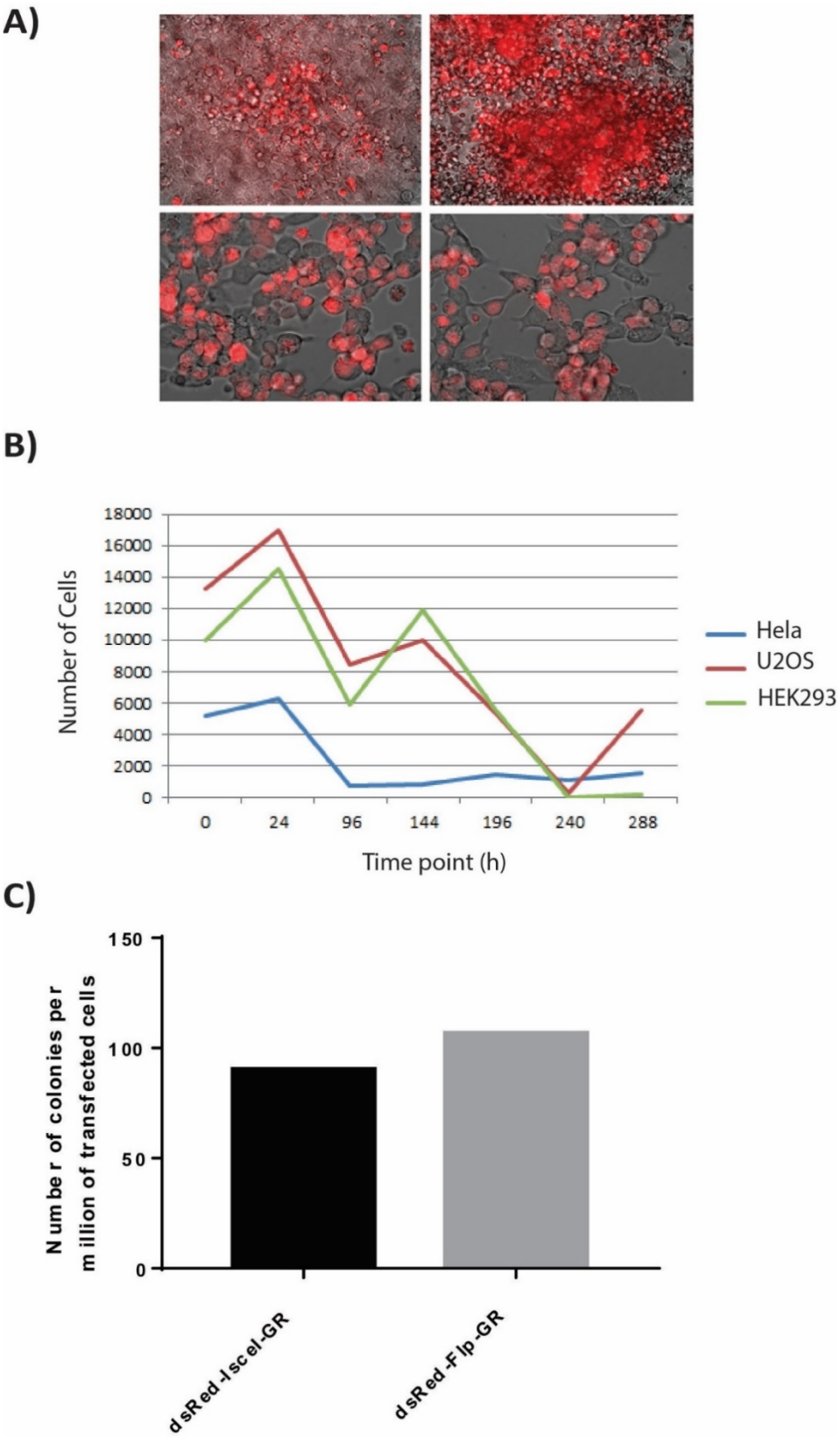

Figure 3.17 FLpH305L stable transfection. A) HEK293T cells were stably transfected with dsRed-FLPH305L-GR and maintained in media containing 1000µg/ml G418. Visualization of the original 15cm transfected plate after 10 days of selection. Limiting dilutions of transfected cells. **B)** Kill curve for Hela, U2Os and HEK293 cells transfected with dsRed-FLpH305L-GR and subjected to G418. **C)** Number of FLP and I-SceI colonies generated after stable transfection and selection of HEK293 cells.

3.2.6.2 Stable FRT cell line

To begin setting up the FLP-FRT system according to an alternative approach, stable FRT-ANCH3-ANCH4 cell lines were generated by selecting resistant clones, following random integration with the lipofectamine transfection. The HEK293 cell line was stably transfected with pANCH3-ANCH4 and pUC19-H1-BglII-FRT-ANCH3-ANCH4-H2 constructs to generate the HEK293-ANCH3-4 (Figure 3.18) and HEK293-FRT-ANCH3-4 (Figure 3.19) cell lines, respectively. Stable transfections were performed as described in section 2.4.5, and the cells maintained for 10 days in a medium containing an optimal hygromycinB concentration (200 µg/mL) (the selection marker for the ANCH3-ANCH4 construct). Selection and single clone isolation were performed successfully using serial dilutions in a 96-well plate to select resistant transfected cells. Fifty isolated single clones were further expanded prior to collection for further validation experiments. Several cell lines comprising a stably integrated FRT were established.

To check and detect the integration of plasmid DNA, genomic DNA was extracted from 50 isolated clonal cell lines using a Maxwell 16 cell DNA purification kit, as described in Section 2.3.2. Screening of the genomic DNA for the 50 expanded clones was conducted using PCR (Section 2.1.3). The PCR reaction was performed using equal amounts of gDNA (50 ng/µl) and the ANCH3-4 _406_FP and ANCH3-4_2977_RP primer set (Table 2.2), to detect the complete integration for the entire FRT-ANCH3-ANCH4 integration (Figure 3.18 and Figure 3.19). The parental HEK293 cell line was used as a negative cell line showing no band. Twenty-eight of the 50 clones delivered an expected band size of 2589 bp. Stable lines were then used in subsequent experiments to incorporate dsRed-Flp-GR and OR3-GFP/OR4-CFP.

A)

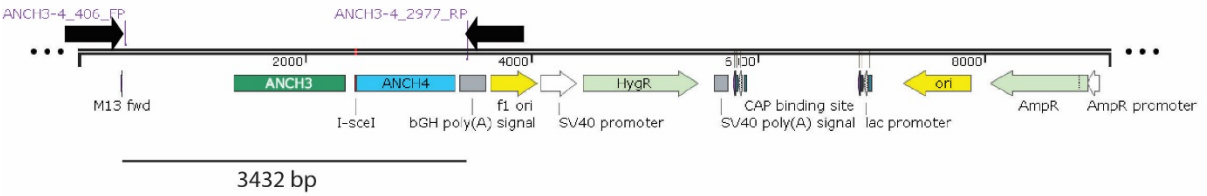

B)

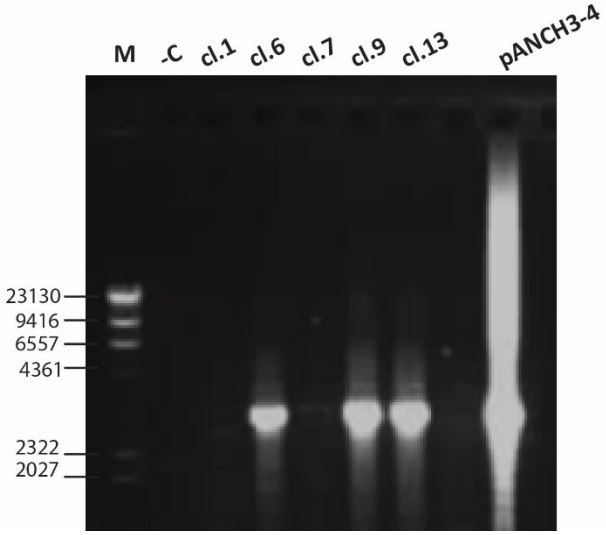

Figure 3.18 Detection of the ANCH3-ANCH4 integration site for stable isolated clones. The gDNA of several clonal cells was extracted. **A)** A schematic showing the pair of primers (black arrows) flanking the ANCH3-I-SceI-ANCH4 region used to detect the integration. **B)** The PCR product for several selected clones resolved in 1% agarose gel. M is a lambda DNA ladder. -C is the parental HEK293 cell line was used as a negative cell line. P is pUC19-H1-BglII-FRT-ANCH3-ANCH4-H2, which was used as a positive control.

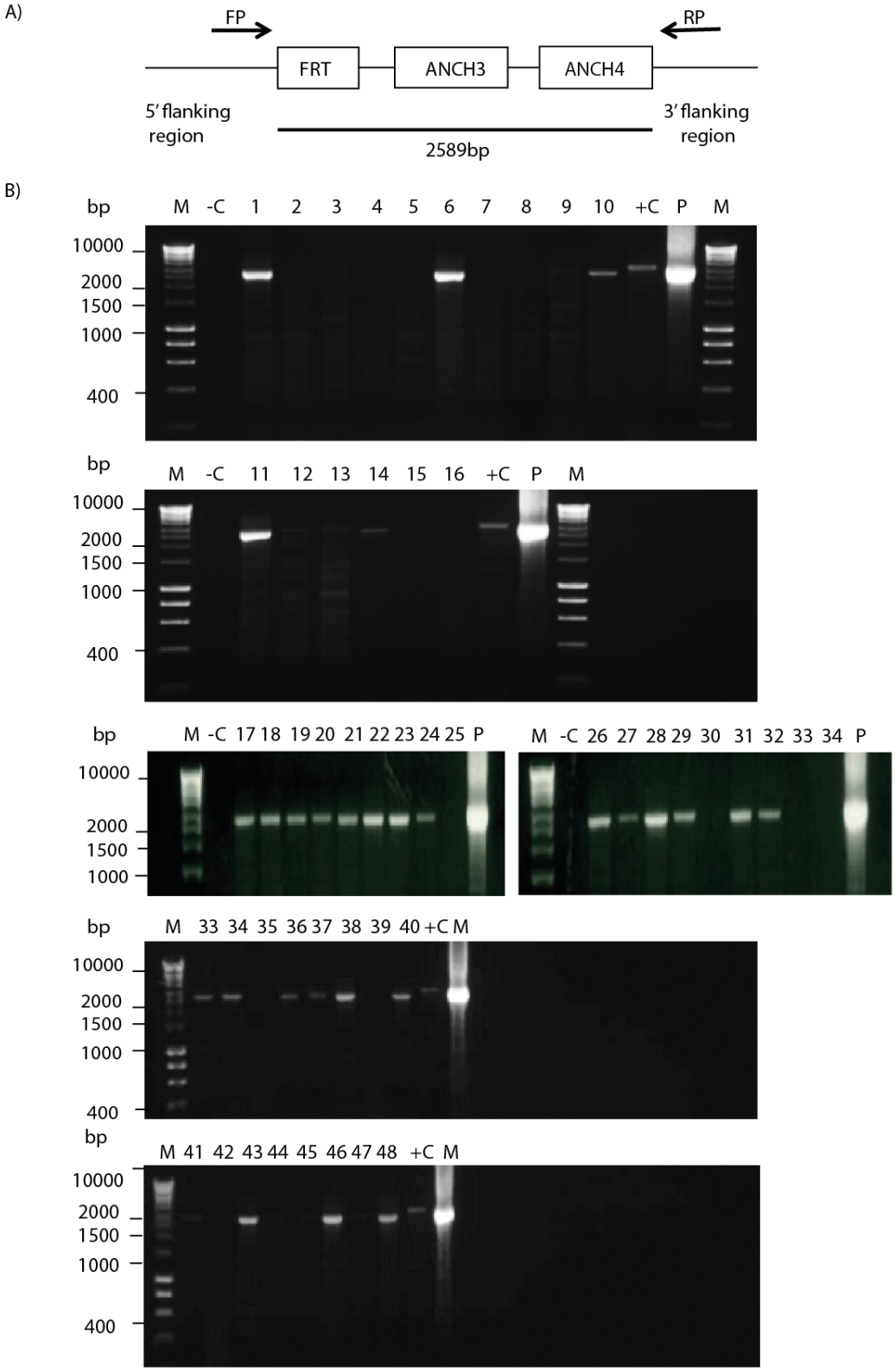

Figure 3.19 Detection of the FRT-ANCH3-ANCH4 integration site for stable isolated clones. The gDNA of the 50 expanded clones was extracted. **A)** A schematic showing the pair of primers flanking the FRT-ANCH3-ANCH4 region was used to detect the integration. **B)** The PCR product for the 50 isolated single clones resolved in 1% agarose gel. M is a DNA hyper ladder. –C is the un-transfected HEK293. +C is the HEK-ANCH3-ANCH4 (cl.9) cell line generated. P is pUC19-H1-BglII-FRT-ANCH3-ANCH4-H2, which was used as a positive control.

3.2.7 Stability of the FRT-ANCH3-ANCH4 integration

To examine the stability of the integration of FRT-ANCH3-I-SceI-ANCH4 clones, random clonal cells were selected. Clones 14, 19, 21 and 31 were expanded then split and cell pellets collected from different passages. DNA extraction was performed using the max-well extraction method, as described in section 2.3.2. Standard PCR reaction of gDNA was performed to confirm the stability of the FRT-ANCH3-ANCH4 integrants following six passages. As shown in Figure 3.20, the presence of a band of 2589 bp indicates complete and stable integration of the FRT across all selected clonal cell lines.

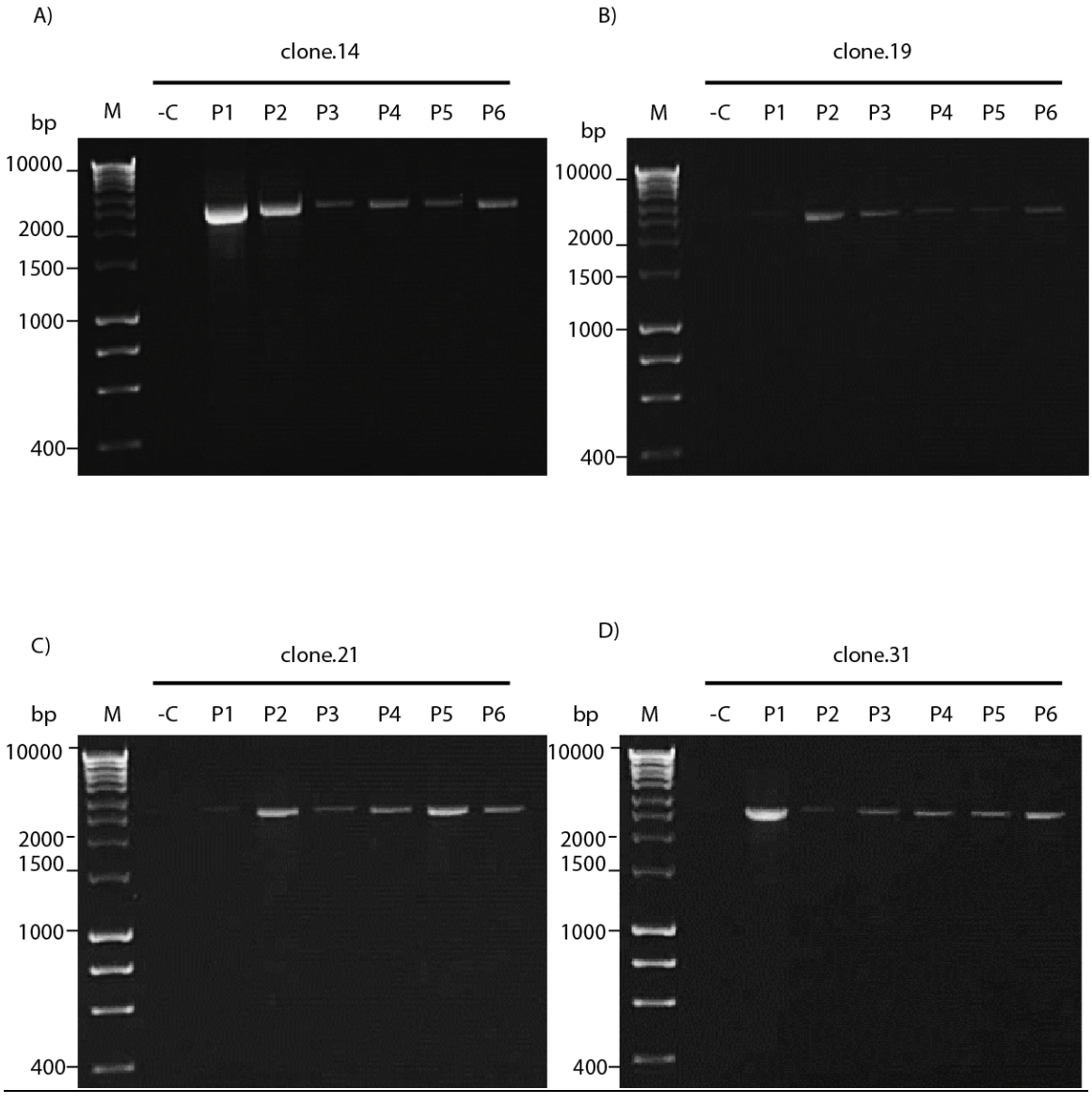

Figure 3.20 Stability of the FRT-ANCH3-ANCH4 integration. The cells were collected in different passage numbers. PCR reaction was performed with the same quantities of gDNA (20 ng) and primers. **A)** PCR product for clone 14. **B)** PCR product for clone 19. **C)** PCR product for clone 21. D) PCR product for clone 31. Clones resolved in a 1% agarose gel. M is the DNA hyper ladder. –C is the un-transfected HEK293. P is the passage number.

3.2.8 Characterization of isolated clones

Following successful FRT integration into the genome, it was of interest to detect the number of integrations in each of the established clonal cell line to compare clones. Two techniques were performed to determine this, southern blotting and metaphase fluorescence in situ hybridization (FISH) using a labelled FRT probe, were selected for the identification of single integration clones.

To perform the southern blot; genomic DNA (gDNA) from the established HEK293-FRT-ANCH3-ANCH4 was extracted from each clonal cell line (clone 14, 19, 21, 31) using the phenol: chloroform method, as described in Section 2.3.2, to gain a higher yield of DNA. The principle of the technique involves digestion of DNA with a restriction endonuclease enzyme, gel electrophoresis, and blotting by transferring fragmented DNA into a Hybond membrane. This process is then followed with hybridization steps, using a labelled DNA probe (all the different steps were described in Section 2.3). Finally, the targeted region can be detected and visualized with exposure to film.

Several restriction enzymes, as listed in Table 3.3 were used to determine which enzymes completely digest the gDNA. Equal amounts of restriction enzymes were added to the digestion reaction. The digestion efficiency differed between these enzymes. As shown in Figure 3.20, it was revealed that *Ase*I and *BamH*I did not digest the gDNA completely, relative to the other selected enzymes; thus, they were excluded. *Bgl*II digest the gDNA more than other enzymes and thus the gDNA was spread giving a very faint smear. However, although the *Hinf*I digested the genomic DNA, it did not digest the plasmid, and thus will not cut into the integrated sequence. Given the results shown in Figure 3.21, *Pst*I and *EcoR*I were used to restrict digested gDNA in subsequent southern blot experiments.

Table 3.3 List of the restriction enzymes used for gDNA digestion.

Restriction enzyme	Sequence	Number of sites within plasmid
BglII	5'… AGATCT…3'	1 site
AseI	5'… ATTAAT…3'	2 sites
BamHI	5'… GGATCC…3'	3 sites
XhoI	5'… CTCGAG…3'	1 site
PstI	5'… CTGCAG…3'	2 sites
EcoRI	5'… GAATTC…3'	4 sites
HinfI	5'… GANTC…3'	0 sites

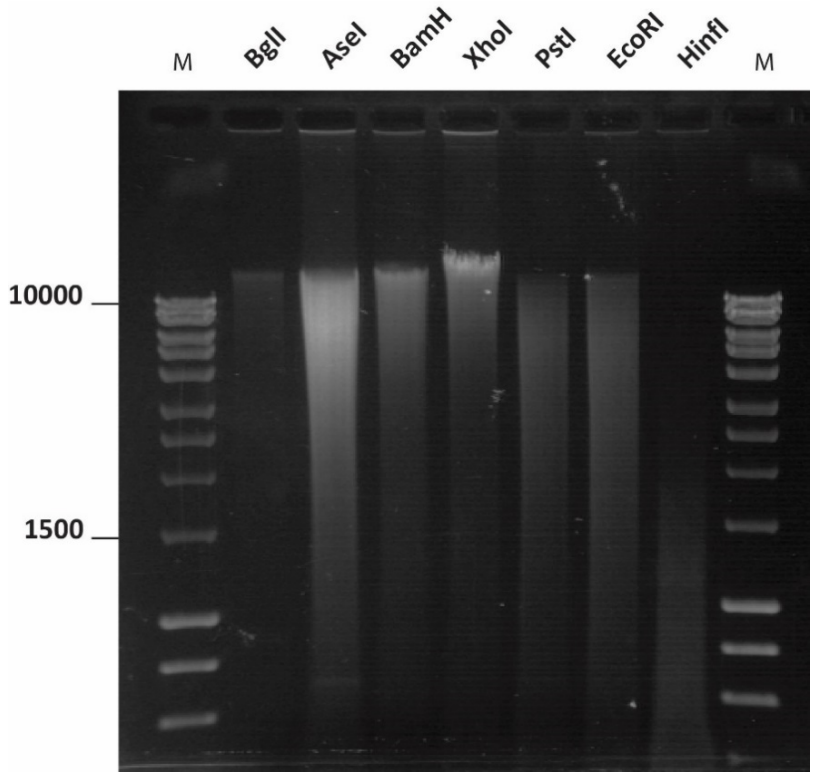

Figure 3.21 Restriction endonuclease digestion of genomic DNA. gDNA extracted from HEK293-FRT-ANCH3-4 cells was digested using respective restriction enzymes. Equal amounts of digested DNA were then loaded into a 0.8% agarose gel.

10 µg of gDNA per lane was digested by either *Pst*I or *EcoR*I, as described in Section 2.3.3 (Figure 3.22). Quantification occurs when comparing the hybridization bands between the original plasmid (pUC19-H1-BglII-FRT-ANCH3-ANCH4-H2) and established clonal cells. *EcoR*I will cut the circular plasmid at four sites, resulting in four bands with 1553 bp, 2171 bp, 4728 and 220 bp size. Whereas, the *Pst*I cuts the plasmid at two unique sites giving two bands with 2388 bp and 6284 bp, as illustrated in Figures 3.22.A and B respectively. The blots were initially hybridized with a DNA probe labelled with a random prime-32P-dCTP. A FRT-ANCH3-ANCH4 probe (406/2977) was used to detect the entire FRT-ANCH3-ANCH4 integration site.

It was expected that post hybridization, the EcoRI digested plasmid will reveal 3 fragments while, the *Pst*I-digested plasmid will reveal 2 fragments. As shown in Figure 3.22.D, the plasmid digested with *EcoR*I reveled 4 fragments and 2 unexpected faint bands. While *Pst*I-digested plasmid revealed 2 fragments, as expected. The clonal cells digested with *EcoR*I revealed 2 faint fragments for clone 14, 4 faint fragments for clones 19 and 21, and 1 faint band for clone 31. Among these bands; one band with a ~1500 bp band was detected in all cell lines. Other fragment with an expected size of approximately 2300 bp was detected in clones 14, 19 and 21. By contrast, the *Pst*I revealed two fragments in all clonal cells as expected. One band with an expected product sized at 2400 bp, and a second band with unknown product size. This difference in detected band size suggests that the FRT-ANCH3-ANCH4 sequence is present at different integration sites within the genome. It was concluded that these results were inconclusive.

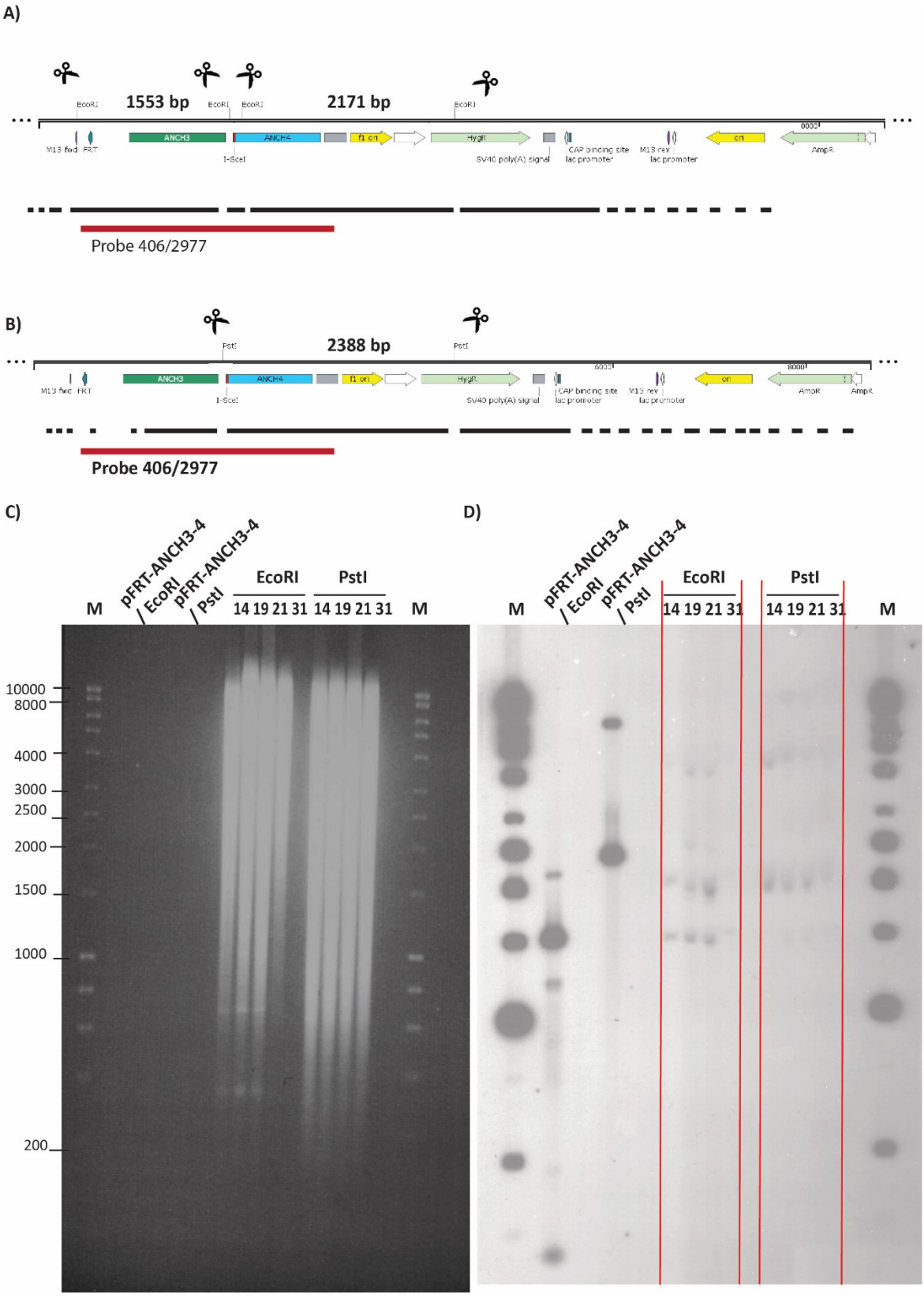

Figure 3.22 Determination of the FRT copy number integration using 406/2977 probe. A) Schematic showing the EcoRI restriction sites and the probe location (red) used to detect integration. **B)** Schematic showing PstI to detect number of integration. **C)** 0.8% Agarose gel electrophoresis showing the digestion reaction for respective clonal cell lines. **D)** Blot hybridized with probe FRT-ANCH3-ANCH4. M is a 1KB DNA hyper ladder.

To attempt to observed the integration results, a second blotting was performed, but using a different probe (Figure 3.23). ANCH3-4_406-FP and ANCH3-probe_RP primers were used to amplify the FRT-ANCH3 sequence. a FRT-ANCH3 (406/ANCHR) probe was labelled and applied in the same way as the previous probe. It was expected that post hybridization, the *EcoR*I- or *Pst*I- digested pUC19-H1-BglII-FRT-ANCH3-ANCH4-H2 plasmid will reveal a single fragment. PstI-digested plasmid revealed 1 fragment, as expected. However, as shown in Figure 3.23.D, the plasmid digested with EcoRI reveled 2 fragments, which might be due to the probe binds to the plasmids' backbone. Similarly, the clonal cells digested with *EcoR*I revealed two fragments in all clonal cells. By contrast, the *Pst*I revealed one faint fragment in all clonal cells as expected.

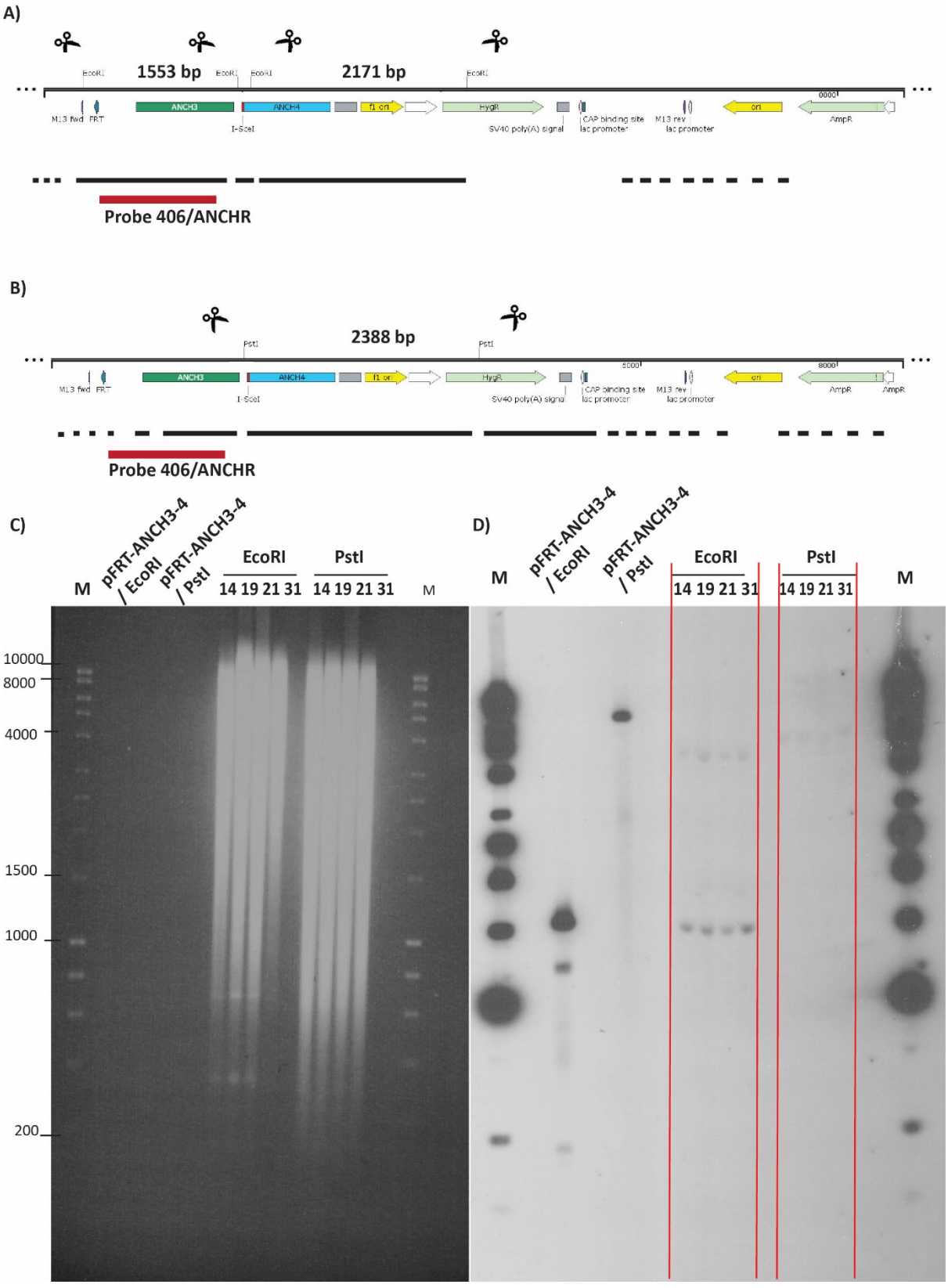

Figure 3.23 Determination of FRT copy number integration using 406/ANCHR probe. A) Schematic showing EcoRI restriction site and the probe location (red) used to detect the integration. **B)** Schematic showing PstI. **C)** 0.8% Agarose gel electrophoresis showing digestion reaction for respective clonal cell lines. **D)** Blot hybridized with probe FRT-ANCH3. M is a DNA hyper ladder.

To attempt to detect the number of FRT integrations using an alternative approach, and to visualize and determine their location within the genome; a FISH was attempted. The principle of this technique involved fixing DNA molecules within metaphase spreads onto a slide. This was followed with hybridization with fluorochrome-labeled DNA probes, to produce a distinguishable florescent signal. Two approaches were attempted for hybridization; either using a single fluorescent ANCH3 probe or combined multiple probes in order to enhance the florescent signal. Although the DAPI stained metaphase spreads were performed successfully, the detection and visualization of the entire length of the integrated FRT sequence was not possible when employing either hybridization approach (Figure 3.24).

The copy number integration was examined by visualizing the oligomerization of OR proteins to the integrated ANCH locus (ANCHOR labelling system), as described in Chapter 4.

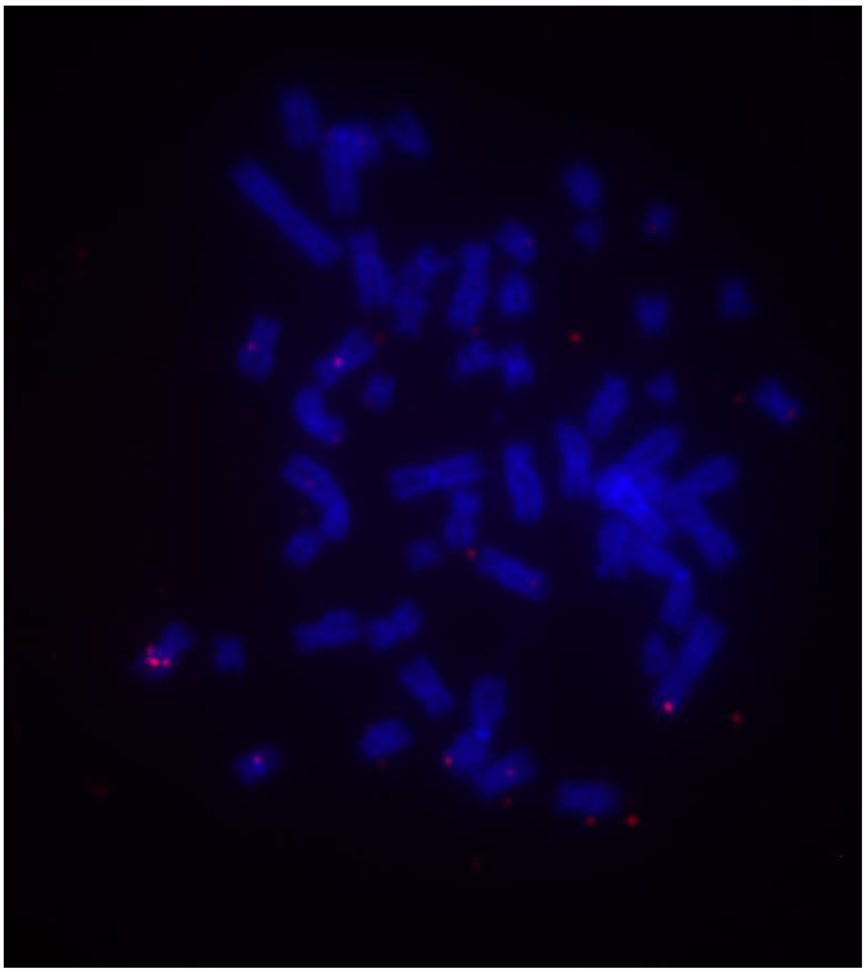

Figure 3.24 Cytogenetic characterization detecting FRT-ANCH3-ANCH4 integration sites. FISH of DAPI stained metaphase chromosomes from HEK293-FRT-ANCH3-ANCH4 cells (clone 19). Red signal correspond to the FRT-ANCH3-ANCH4 sites.

3.3 Discussion

A number of studies using various genotoxic agents (such as radiation or therapies such as CPT have investigated how cells respond to DNA damage and RS (Cobb et al., 2005). These agents cause genome-wide damage; thereby preventing control over where forks collapse or break, and preventing RS associated events from being studied directly; such as the elucidation of the molecular mechanism underlying se-DSB resolution or misrepair.

This chapter presented the development and set up of an inducible FRT-FLP system. This was based on utilizing a mutant FLP recombinase (FLPH305L) to induce RS (Parsons et al., 1988). FLPH305L will bind to FRT site introduced into the genome, subsequently attacking DNA phosphodiester bonds, and generating an irreversible DNA-protein adduct and SSB (Nielson et al., 2009). Upon DNA replication, the RF will encounter the SSB, leading to fork breakage and the formation of se-DSB. Nielson et al. (2009) demonstrated se-DSB generation by FLPH305L in *Saccharomyces cerevisiae* budding yeast, and CPT treatment of human cells includes DSB generation.

The FRT-FLP system allows the induction of a single genomic insert into mammalian cells, thus providing a unique tool to extend capacity to directly dissect and study diverse RS-associated processes, such as repair pathways and checkpoints in mammalian cells *in vivo*.

The FLP-induced irreversible protein-DNA adducts and single-stranded break mimics oncogene- and therapy-induced RS, such as CPT (Koster et al., 2007). It has been speculated that positive supercoils accumulate in front of moving replication forks, rather than colliding between replication forks and trapping Top1-cleavage complexes causing stalling and collapse of replication forks and consequently cell death in CPT-treated cells. This is highly unlikely to occur in cells within the FRT-FLP system, as only one insult is generated, and active Top1 remains present as a means to remove topological stresses in replicating DNA. Thus, the FRT-FLP system will allow to overcome the two effects resulting from defective topoisomerase activity, affording the system advantages over CPT studies (Nielson et al. 2009).

When setting the system up, different FLP and FRT constructs were generated for various reasons. These involve integrating plasmids containing FRT sequences, and expressing plasmids that contain either an I-SceI endonuclease or a mutant FlPH3005L recombinase.

The generation of an FRT integration construct (YFP/LacO-FRT-CFP/tetR) proved unsuccessful due to several reasons. First, regarding the LacO/ TetR system, although the digestion and ligation steps were successful, problems arose when we trying to propagate it in bacteria (Soutoglou et al., 2007; Tsukamoto et al., 2000). Using the ElectroMAX™ Stbl4™ Competent cells is known to overcome propagation difficulties. These cells were created specifically to clone unstable DNA sequences, stabilizing direct repeats and retroviral sequences (Al-Allaf et al., 2012). Thses cells derivative of JM109/J5 (STBL2 strain) and contain direct repeat sequence that are stable compared to other E.coli strains (Schmidt and Bloom, 1999). Surprisingly, digestion of the selected clones resulted in different product sizes, indicating differences in their sequences. Thus, the generation of LacO-FRT-TetR ultimately failed because of the instability of the lacO/tetR plasmid.

This drawback likely arose due to the presence of the large number of highly repetitive DNA sequences of Lac (256 bp) and Tet (96 bp), and the operators of the original plasmid (YFP/LacO-I-SceI-CFP/tetR). We concluded that the plasmid is unstable, and frequently implicated in recombination events when attempting to propagate in bacteria. Extensive use was made of the visualization of fluorescent repressor/operator tools (i.e. binding of repressor proteins to specific DNA binding sites) in order to tag genomic loci in eukaryotes (Strauight et al., 1996). However, despite their general utility as a means of monitoring chromatin dynamics, these systems prevented the direct dissection of BF replication, and the onset of repair in vivo. In addition to its repetitive nature, and the large sized operator arrays, the lengthy stretches of tightly bound LacO and TetR repressors proteins are capable of creating a barrier both large and complex and capable of obstructing chromatin function. This can alter short-range DNA processes, such as the gene domain structure, intragenic looping or DNA maintenance, also provoking disruptive recombination events (Possoz et al., 2006; Jacome and Fernandez-Capetillo, 2011). Moreover, these repressors create traceable fragile sites, and constitute a barrier of unknown penetrability, affecting the DNA processing enzymes; thus, they might disrupt DNA replication and obstruct chromatin function (Sofueva et al., 2011; Jacome and Fernandez-Capetillo, 2011). Given the instability of the lacO/tetR plasmid in bacteria, and the fact that similar stability problems might continue to arise during replication in mammalian cells, it was decided not to use this plasmid, as it is inappropriate for use in visualizing and analysing BF and might cause problems during DNA replication in mammalian cells even if pLacO-FRT-CFP was successfully generated and integrated. Thus, this approach was abandoned.

In order to address drawbacks associated with the lacO/tetR system, an alternative visualization approach was implemented, involving tagging the FRT with the newly developed ANCHOR system. This work was conducted collaboratively with Dr. Kerstin Bystricky, from the University of Toulouse, by applying a stable strategy, using the recently developed protein oligomerization as a non-intrusive DNA labelling tool (known as the ParB-INT system). The ParB system has been demonstrated as best suited to fine-scale studies, as they circumvent the previous technical limitations that arise when employing traditional visualization systems (Saad et al., 2014). The ANCHOR system involves using fluorescently labelled "OR" proteins that loosely bind and oligomerize to small integrated DNA segments, termed "ANCH", creating fluorescent foci. ANCH sequences are not repetitive, and it has been shown that they do not disrupt DNA replication or repair (Saad et al., 2014). Overall, it was concluded that adapting the ANCHOR labelling approach might prove a suitable strategy for generating an integration vector for mammalian cells.

We adapted the fluorescent protein tag system originally developed for prokaryotes for use in eukaryotes. Construction of FRT into the ANCHOR plasmid was successfully accomplished, and the FRT oligonucleotides sequence inserted at different sites in the original pUC19-H1-ANCH3-ANCH4-H2, to construct a series of FRT integration plasmids, each with a specific feature.

Conversely, various expression plasmids were successfully generated, to induce either a direct DSB or a BF (se-DSB). A dsRed-I-SceI-GR construct gifted by Dr. Maria Jasion was used to induce a direct DSB. In this construct I-SceI is tagged with Discosoma red fluorescent protein (dsRed), which allows visualization of expression and the detection of transfected cells (Bevis and Glick, 2002). Moreover, the GR receptor was located downstream of I-SceI allowed relocation from the cytoplasm to the nucleus (Htun et al., 1996) following addition of the TA and control over the induction of RS and a DSB (Soutoglou et al., 2007). By manipulating this construct, the I-SceI sequence was removed and the mutant FLPH305L cloned into the plasmid to successfully generate dsRed-FLPH305L-GR construct. A negative control plasmid was generated from the dsRed-I-SceI-GR by removing the I-SceI to generate dsRed-GR. Thus, the negative plasmid will have the same backbone as the expression plasmid, without causing DNA damage or RS. Thereby serving as a useful control in subsequent experiments.

The second step when developing the system involved generating a FRT-FLP stable cell line. Initially, to test which cell lines would be the most suitable for the system, Hela-CCL2, U2OS, MEFs, HEK293T and a HEK293 cell lines were cultured and transfection conditions optimized to achieve high (80-90%) efficiency. Transient transfection with an expression vector designed to encode FLPH305L and I-SceI was successful, delivering similar efficiency in all cell lines. The efficiency was monitored by visualizing the red fluorescent signal using a fluorescence microscope. However, inconsistencies were observed between cell lines as regards the expression level. Notably, most cells found to have a strong red fluorescent signal. In contrast, MEF cells were found to have a weak signal relative to other human cell lines. This was possibly due to variability in the constitutive human cytomegalovirus (CMV) promoter, which derives RFP expression, across different cell types (Qin et al., 2010). Therefore, we decided to exclude MEF cells. Visually, it emerged that the transfection reagent induced cell toxicity. Thus, a different transfection reagent was used and conditions were optimized using HEK293 cells. The results showed expression increased after 48 hours compared with 24 hours, and FUGENE was visuly less toxic than using a Trans-IT2020 reagent. Thus a 48 hour incubation period, in combination with FUGENE, was used for all further experiments.

Given the transfection result we moved forward using HEK293, Hela, U2OS and HEK293T cells. To begin generating stable FLP cells, we aimed to test and determine efficient selection concentrations. The addition of a G418-selection antibiotic (the selection marker for dsRed-FLPH305L-GR construct) was conducted to select resistant transfected cells. It was anticipated that this would kill all the untransfected cells, because they do not express the kanamycin resistance gene (neoR); whereas, transfectants would be expected to survive. However, surprisingly, it was revealed that untransfected HEK293T cells survive and grow, even after maintaining cells using media supplemented with higher concentrations of G418. The HEK293T cells were resistant to the highest concentrations of G418, and difficulties arose when seeking to select single clones. Therefore, HEK293, Hela, and U2OS cells were considered the most suitable cell lines to use, as the RFP signal was detectable and proved sensitive to the selection drug.

The selected cells were stably transfected with FLPH305L and monitored in a media supplemented with an optimal concentration of the selected drug. Although transfection and selection was performed successfully, there were difficulties generating stable expression FLP, and it was not possible to obtain a single stable red clone; as the expression of the RFP reduced over time.

Consequently, the isolation of single red clones from the polyclonal plate was deemed impossible, leading to transient transfection being performed in subsequent experiments. As expected, it was deduced that using the mutant FLP recombinase in mammalian cells would not have any effect on the cells. However, use of Flp1 technology for site-directed recombination in mammalian cells meant that no problems were anticipated when using FLP.

Due to difficulties generating stable expressing FLP cell lines, it was decided to use another approach; this involved establishing FRT-ANCH3-ANCH4 cells, which would then be transiently transfected with FLP. HEK293 cells were successfully transfected with pUC19-H1-ANCH3-ANCH4-H2 and pUC19-H1-BglII-FRT-ANCH3-ANCH4-H2 generating HEK293-ANCH3-4 and HEK293-FRT-ANCH3-4 cell lines, respectively. These stable cell lines contained a 48 bp FRT sequence, and a unique 18 bp nucleotide I-SceI restriction site, flanked by ANCH3 and ANCH4 sites. Resistance selection was proceeded by the addition of a hygromycin-selection antibiotic (the selection marker for pUC19-H1-BglII-FRT-ANCH3-ANCH4-H2) to the transfected cells. After transfection and selection with hygromycinB, single clones were isolated using serial dilution. Another cell line was then generated by transfecting U2OS cells with pUC19-H1-BssHII-FRT-ANCH3-SacB-ANCH4, as performed by Cellomics Technology.

Single FRT-ANCH3-ANCH4 clones were expanded, and then collected for experiments designed for validation purposes. The genotype for the generated clonal cell lines was checked with the genomic PCR, following sequencing to confirm the complete insertion of the FRT sequence. To determine the copy number of the integrated locus restriction digests of genomic DNA, Southern blotting and FISH with labelled FRT probe was used to confirm single site integration, and to identify single FRT integration clones. Based on the southern blot results, we attempted to estimate an integrated copy number for the four clones. However, determining the copy number was not straight forward. It was further concluded that it was difficult to determine the number of integrations at this stage and further optimization of the approaches will be required. However, despit not confirming yet the number of integration, the cell lines can still be used for experiments as the FLP, I-SceI and dsRed-GR constructs can be transfected into the same clonal cell line meaning the number of FRT site is same. In all subsequent experiment HEK293-FRT-ANCH3-ANCH4 cell line (clone.19) was used as it was growing fine.

In conclusion, the novel inducible system designed for this program combines principles that can be used to regulate the induction of broken DNA replication forks at specific genomic loci in mammalian cell-types. Moreover, the location of the damage can be visulized, so that genetic analyses can easily be coupled to microscopy analyses. This facilitates pioneering studies that can be used to elucidate molecular mechanisms that act to restart DNA replication forks, and to suppress tumourigenesis, and those causing misrepair, driving cancer progression. Understanding these processes will illuminate RS responses and assist the development of more efficient preventative and therapeutic strategies.

Chapter 4: Validation of different features of the FRT-FLP system

4.1 Introduction

In many studies examining protein function, the researchers control the expression of the protein of interest either at the DNA or RNA level (Gossen and Bujard, 1992; Elbashir et al., 2001). Successful control of the protein expression at the DNA level can be achieved by altering the coding sequence of a gene (Saure and Henderson, 1988). However, this technique has a number of limitations, partially resulting from the protein depletion being indirect. In addition, protein level controled at the RNA level using siRNA suffers from off-target leakiness of silencing or may not significantly reduce expression (Bartlett and Davis, 2006). Further systems have also been developed that having directly deplete a target protein by exploiting the specific protein degradation pathway (Iwamoto et al., 2010; Bonger et al., 2011; Banaszynski and Chen, 2006).

Systems permitting the conditional control of localization of the protein of interest have also been utilized, developed by fusing the targeted protein to the binding domain of steroid hormones or rapamycin systems (Picard et al., 1988; Haruki et al., 2008; Picard, 2000). The GR is a well-studied member of the hormone receptor superfamily, which also includes steroid receptors (Rousseau et al., 1979). GR is ubiquitously expressed in all cells, while also regulating the expression of genes through transrepression or transactivation. The Un-liganded (i.e. inactive state) of GR is (unlike many other constitutively nuclear receptors shuttling between the cytoplasm and the nucleus) localized exclusively in the cytoplasm, where it forms a multi-protein complex, with heat shock proteins (i.e. Chaperon proteins) in quiescent cells in the absence of glucocorticoids hormone (GC) (Gasc and Baulieu, 1987; Pratt and Dittmar, 1998). This steroid receptor only translocates and accumulates in the nucleus in response to the GC ligand binding after exposure to a steroid (Martinez et al., 2005). Following the binding and activation of the ubiquitously expressed intracellular GR receptor to GC, ligand activated GR is released from this multi-protein complex and translocates to the nucleus (Picard and Yamamoto, 1987), where it can then modulate cellular events by altering to gene transcription and activation through binding to glucocorticoid-responsive elements (GREs) in the promoter region of the target genes, where it interacts with transcriptional coactivators (Stevens et al., 2004).

The designed FRT-FLP system (Chapter 3) combines multiple features, each with unique advantages. We took advantage of the GR chimeras, which translocate from the cytoplasm to the nucleus when bound to the synthetic ligand TA. FLP recombinase or I-SceI restriction endonuclease were cloned as required and fused at the ligand-binding domain of the GR, in a single open reading frame with monomeric RFP. It was hypothesized that utilizing the GR tagging system with the FRT-FLP system would permit inducible induction of a BF or DSB at the FRT-ANCH3-I-SceI-ANCH4 site in single living cells. Upon nuclear localization of the I-SceI endonuclease or FLPH305L recombinase, respectively.

In the FRT-FLP system, the adapted ANCHOR labelling shared a similar concept with the ParB-INT system (Saad et al., 2014). It was hypothesized that inserting the FRT sequence proximate to a small DNA sequence containing ANCH sites (i.e. the ANCH3 and ANCH4 sequence) would enable visualization of BF repair in a more extensive and attainable resolution. In addition, the employment of the florescent 'OR' protein (which oligomerizes to ANCH sites, creating a fluorescent focus), enables the observation of the BF repair kinetics in a single cell without interfering with the replication processes (Saad et al., 2014).

The current chapter focusses on assessing and validating the effectiveness of the different features of the FRT-FLP system to confirm its potential as a tool to study both BF and DSB processing. The aims here can be separated into three objectives. The first was to examine the effectiveness of GR relocalizing FLP and I-sceI. The second was to validate the capacity to utilize the adapted ANCHOR system in combination with the designed FLp-FRT system for the visualization and analysis of the FRT-ANCH3-I-SceI-ANCH4 site. The third aim was to demonstrate FLP features that were DNA-replication-dependent to detect SSB and DSB generation by alkaline gel electrophoresis followed by southern blot validation.

4.2 Results

4.2.1 Preliminary validation of GR-mediated cytoplasm to nucleus relocalization

In the first GR system validation, HEK293-FRT cells were used to verify the red signal moved from the cytoplasm to the nucleus following addition of TA. Cells were transiently transfected for 48 hours using dsRed-FLPH305L-GR and dsRed-I-SceI-GR constructs. Cytoplasm to nucleus re-localization was monitored using an Olympus Cell^R/Scan^R microscope, and the slides were imaged and examined using RFP and DAPI filters prior to and after the addition of the TA. Figure 4.1 shows RFP and merged RFP/DAPI images, which were captured to detect the dynamics of a tagged red fluorescence signal.

Overall, cells transfected with dsRed-I-SceI-GR revealed higher transfection efficiency (about 70%) than the dsRed-FLPH305L-GR (about 48%). In the absence of TA, the cytoplasmic localization of dsRed-I-SceI-GR was clearly observed in all transfected cells (Figure 4.1). Nevertheless, 6-hours post TA addition a clear shift to nuclear signal as expected from previous work (Soutoglou et al., 2007). However, it was observed that patterns of intracellular distribution of GR was not form consistently between adjacent cells. In some cells, strict nuclear exclusion was observed, and others showed nuclear and cytoplasmic partition without TA. In contrast, there was no obvious relocalization of dsRed-FLPH305L-GR transfected cells upon addition of TA. Nuclear RFP was observed, even under TA free conditions, preventing the observation of red movement in cells (Figure 4.1). This suggested either FLP disrupted the function of GR, or there was an issue with the construct.

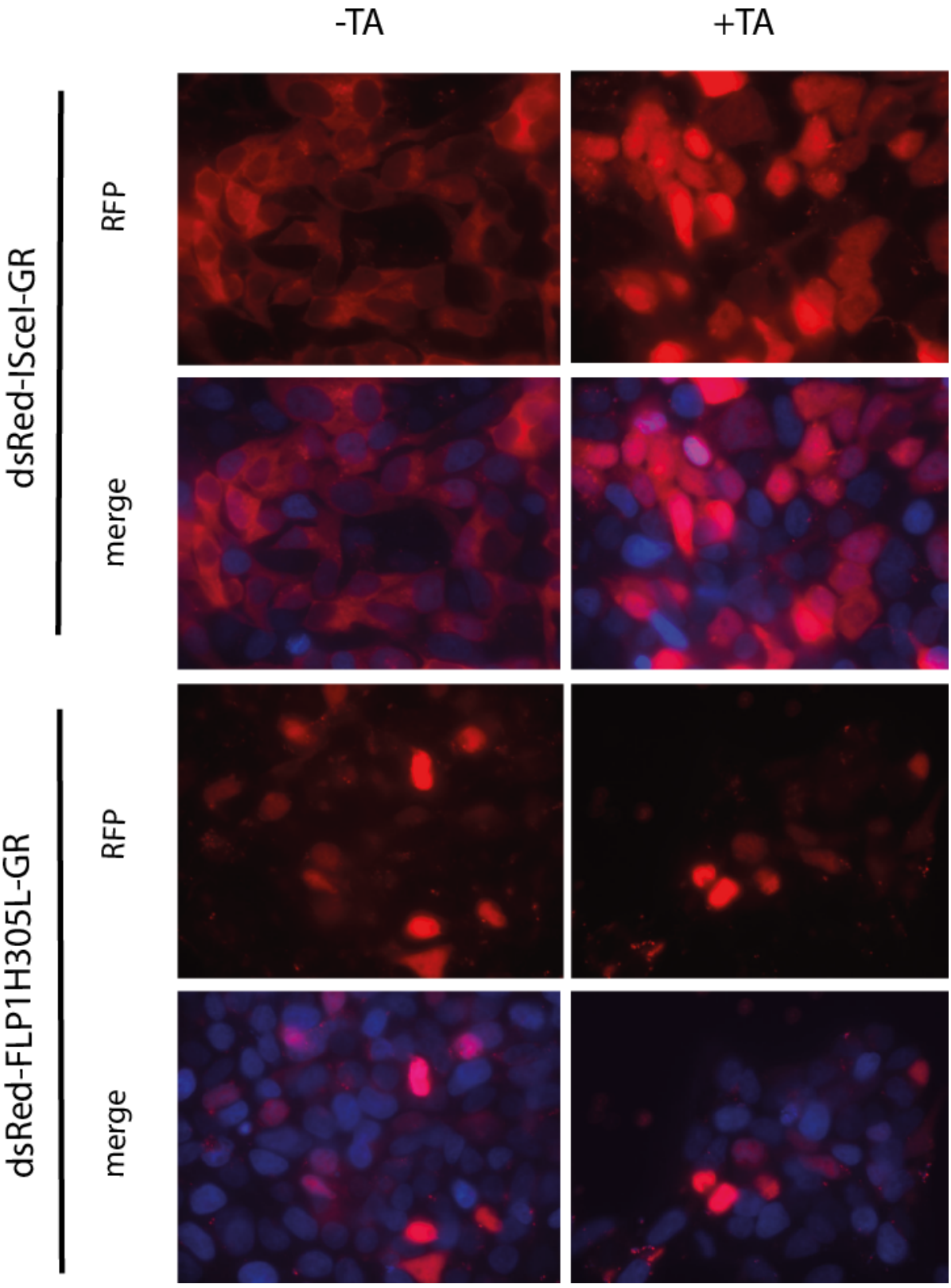

Figure 4.1 Visualization of cytoplasm to nucleus relocalization of the dsRed-GR tagged protein. HEK293-FRT cells were transiently transfected for 48 hours with the generated expression constructs dsRed-I-SceI-GR or dsRed-FLPH305L-GR. Media containing 10^{-7} M of Triamcinolone acetonide (TA) was then added and incubated for 6 hours.

Following sequence analysis of the generated pdsRed-FLPH305L-GR construct, a start codon (ATG) and a stop codon (TAA) were flanking FLPH305L (Figure 4.2.A). The presence of a stop codon after the FLPH305L sequence would mean the transcription factory would encounters a stop codon before the GR sequence, promoting ribosome dissociation, before GR translation. This means dsRed-FlpH305L would be generated without GR, abolishing the GR translocation receptor mobility. This explains the detection of the red signal in the nucleus before TA treatment, and prevents the observation of red signal relocation in cells transfected with dsRed-FLPH305L-GR.

To generate a new dsRed-FLPH305L-GR (no ATG/TAA) plasmid; site direct mutagenesis was performed (Section 2.1.9) on the previously constructed pdsRed-FLPH305L-GR to remove the stop and start codon flanking the FLPH305L (Figure 4.2.A and Appendix V). This new dsRed-FLPH305L-GR construct was achieved using Xho1Sac1.FLP No-ATG F.P. and Kpn1Sal1.FLP1 No-TAA R.P primers (Table 2.2).

To examine cytoplasmic nucleus localization in a newly generated plasmid the previous experiments were repeated. Though the transfection efficiency was low (about 25%), yet TA-induced red signal relocalization from cytoplasm to the nucleus was successfully observed over an extended period in all transfected cells (Figure 4.2.B).

A)

```
pdsRed-FLp-GR      1 ---GAGCACGCCGAGGCCCGCCACTCCGGCTCCCAGTCCGGACTCAGATC     47
                     |||||||||||||||||||||||||||||||||||||||||||||||||||
no ATG/TAA         1 TANGAGCACGCCGAGGCCCGCCACTCCGGCTCCCAGTCCGGACTCAGATC     50

pdsRed-FLp-GR     48 TCGAGCTCAAATGCCACAATTTGGTATATTATGTAAAACACCACCTAAGG     97
                     ||||||||||    ||||.||||||||||||||||||||||||||||||||
no ATG/TAA        51 TCGAGCTCAA---CCACNATTTGGTATATTATGTAAAACACCACCTAAGG     97

pdsRed-FLp-GR     98 TGCTTGTTCGTCAGTTTGTGGAAAGGTTTGAAAGACCTTCAGGTGAGAAA    147
                     |||||||||||||||||||||||||||||||||||||||||||||||||||
no ATG/TAA        98 TGCTTGTTCGTCAGTTTGTGGAAAGGTTTGAAAGACCTTCAGGTGAGAAA    147

pdsRed-FLp-GR    148 ATAGCATTATGTGCTGCTGAACTAACCTATTTATGTTGGATGATTACACA    197
                     |||||||||||||||||||||||||||||||||||||||||||||||||||
no ATG/TAA       148 ATAGCATTATGTGCTGCTGAACTAACCTATTTATGTTGGATGATTACACA    197

pdsRed-FLp-GR    198 TAACGGAACAGCAATCAAGAGAGCCACATTCATGAGCTATAATACTATCA    247
                     |||||||||||||||||||||||||||||||||||||||||||||||||||
no ATG/TAA       198 TAACGGAACAGCAATCAAGAGAGCCACATTCATGAGCTATAATACTATCA    247

pdsRed-FLp-GR   1198 ATTGAGGAGTGGCAGCATATAGAACAGCTAAAGGGTAGTGCTGAAGGAAG   1247
                     |||||||||||||||||||||||||||||||||||||||||||||||||||
no ATG/TAA      1198 ATTGAGGAGTGGCAGCATATAGAACAGCTAAAGGGTAGTGCTGAAGGAAG   1247

pdsRed-FLp-GR   1248 CATACGATACCCCGCATGGAATGGGATAATATCACAGGAGGTACTAGACT   1297
                     |||||||||||||||||||||||||||||||||||||||||||||||||||
no ATG/TAA      1248 CATACGATACCCCGCATGGAATGGGATAATATCACAGGAGGTACTAGACT   1297

pdsRed-FLp-GR   1298 ACCTTTCATCCTACATAAATAGACGCATATAATGTCGACGGTACCGCGGG   1347
                     |||||||||||||||||||||||||||||   ||||||||||||||||||||
no ATG/TAA      1298 ACCTTTCATCCTACATAAATAGACGCAT---ATGTCGACGGTACCGCGGG   1344

pdsRed-FLp-GR   1348 TATCGGAAATGTCTTCAGGCTGGAATGAACCTTGAAGCTCGAAAAACAAA   1397
                     |||||||||||||||||||||||||||||||||||||||||||||||||||
no ATG/T        1345 TATCGGAAATGTCTTCAGGCTGGAATGAACCTTGAAGCTCGAAAAACAAA   1394
```

B)

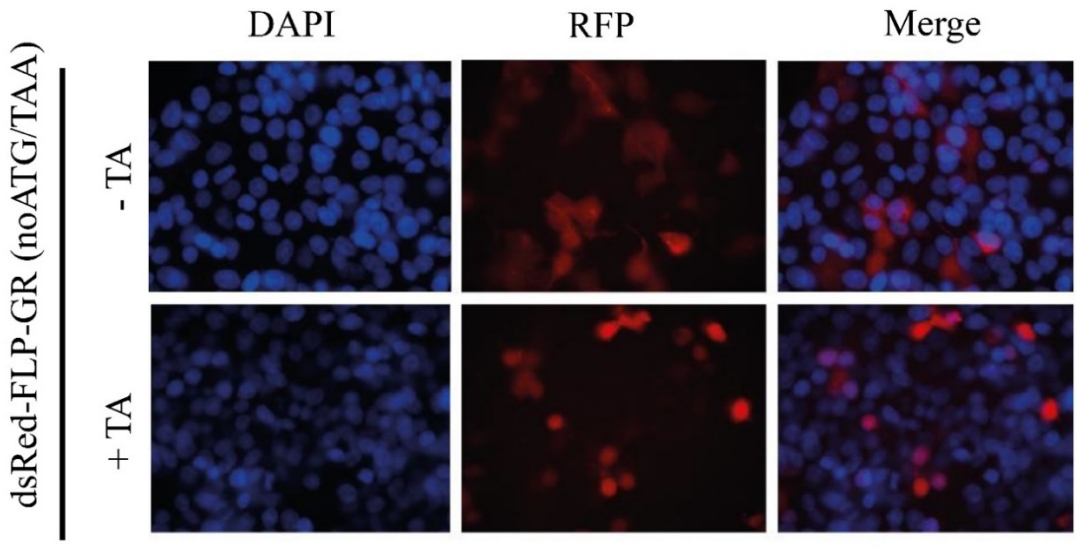

Figure 4.2 Visualization of cytoplasm to nucleus relocalization of the dsRed-FLPH305L-GR (no ATG/TAA). (A) Sequence alignment analysis of new site-directed mutagenized dsRed-FLP305H-GR (no ATG/TAA) and the original dsRed-FLPH305L-GR. Site direct mutagenesis was achieved by removing the start (ATG) and the stop (TAA) codon flanking the FLPH305L sequence (yellow highlighted sequence). **(B)** HEK293-FRT cells were transiently transfected with a newly generated dsRed-FLPH305L-GR (noATG/ATT) expression construct for 48 hours. Media containing 10^{-7} M of Triamcinolone acetonide (TA) was then added and incubated for 6 hours.

It has been demonstrated that the rate of the cytoplasm-to-nucleus translocation of GR is determined by ligand concentrations and affinity (Schaaf and Cidlowski, 2003). Moreover, given the fact that the patterns of intracellular distribution of GR was not completely consistent between cells (Figure 4.1), it was interesting to examine whether using different classes of steroid hormones would induce more efficient RFP-GR translocation. A comparative ligand response translocation was performed. HEK293-ANCH3-ANCH4 cells were transfected with newly constructed dsRed-FLPH305L-GR, and the efficiencies of two high-affinity glucocorticoid ligands were evaluated. Post transfection, cells were treated with 10^{-7} M TA (Soutoglou et al., 2007) or 1μM dexamethasone (Dex) (Schaaf and Cidlowski, 2002).

As shown in Figure 4.3, the cellular localization of the expressed RFP was monitored with fluorescence microscopy. This experiment assessed the time-dependent induction of FLP from the cytoplasim to the nucleus induced by TA or Dex. Red signal predominated in the cytoplasm after 30 minutes of steroid addition, and relocated to the nucleus when either TA or Dex were added. The rate of relocalization was visualized over an extended period and red nuclear signal was observed to increase with longer the incubation time. In conclusion, there was no obvious difference between TA and Dex, TA was used for further experiments.

Given previous observation in published literature (Soutoglou et al., 2007), it was expected that approximately one third of the red signal would have translocated after 2 hours, and that after 24 hours' incubation the red fluorescence signal would become mainly nuclear in the presence of Dex or TA. Our data agreed with this (Figure 4.3), though a sub-set of cells did not demonstrate relocalization by 24 hours. Thus, it was decided to incubate the cells for 48 hours in subsequent experiments.

To quantitatively assess the mobility and nuclear translocation of RFP-tagged GR in the nucleus of transiently transfected HEK293-FRT cells, cells were transfected with pdsRed-GR, pdsRed-I-sceI-GR, or dsRed-FLPH305L-GR and computer-controlled high-resolution microscopy live cell imaging was used to monitor RFP signal. Unexpectedly, it emerged that the RFP signal accumulated in the nucleus for all constructs, even under ligand-free condition (Data not shown). Possible reasons for this discussed in section 4.3. The media was replaced for cells with media containing TA, and live cell imaging was used to image cells every 30 minutes overnight post-TA treatment (24hrs). Analysis of the time-lapse series revealed that during translocation, cells were frequently rounding up and detaching. Nevertheless, significant nuclear GR relocalization was observed in remaining attached cells. This

experiment suggested the conditions within microscope incubator affected the cells and lead them to start detaching, despite the conditions being set the same as the normal incubators. The reasons for this were therefore not clear, but meant it was difficult to use confocal and time-lapse microscopy to quantify RFP-GR localization over extended periods of time post-TA addition.

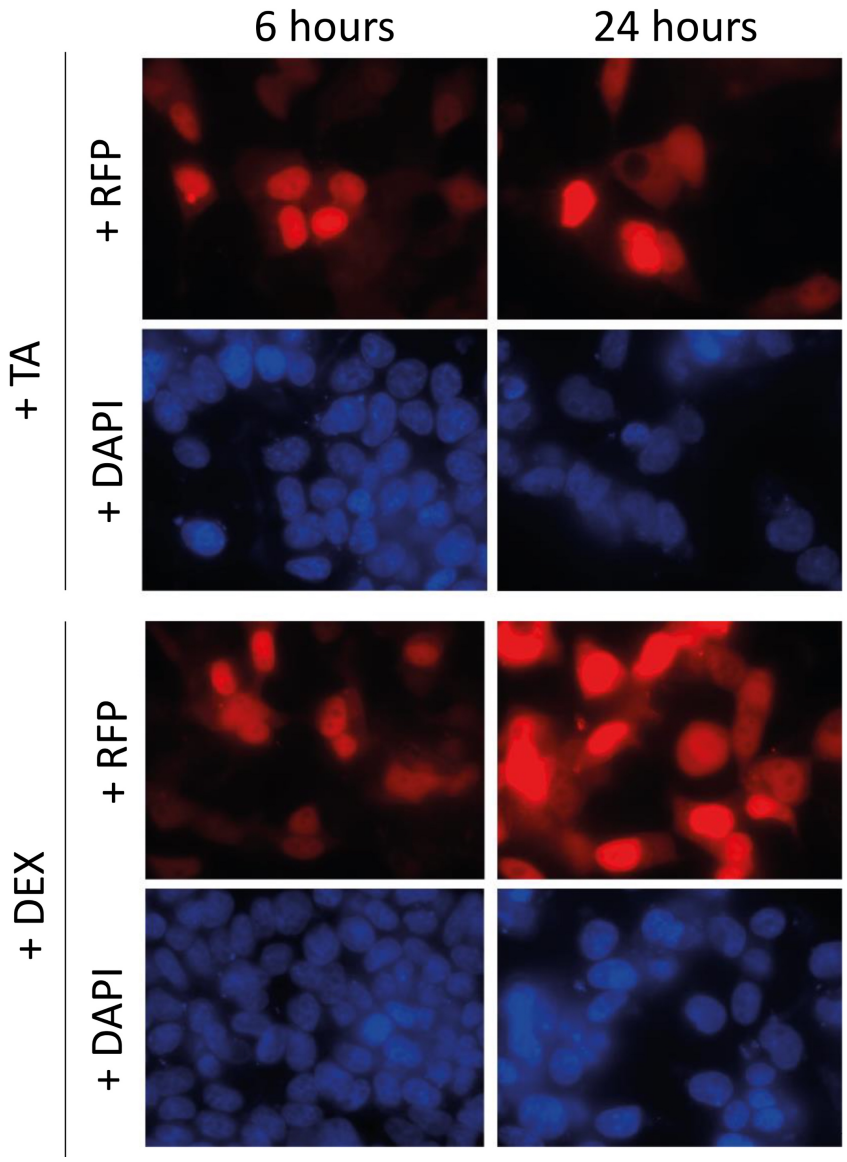

Figure 4.3 Validation of the GR system's effecicny using different steroid ligands. Validating the steroid-induced red signal re-localization from the cytoplasm to the nucleus RFP and merging (RFP/DAPI) images that detect the dynamics of the red fluorescence that tagged the FLPH305L protein before and after steroid addition. HEK293-FRT cells were transiently transfected with the expression generated constructs dsRed-FLPH305L-GR for 48 h. Media containing 10^{-7} M of TA and 1 µM of dexamethasone (Dex) were added and incubated for 24 hrs at 37°C with 5% CO_2. FLPH305L re-localisation was monitored with an Olympus Cell^R/Scan^R microscope, and the resultant slides imaged and examined with RFP and DAPI filters before and after steroid addition. The cells were visualised with an Olympus Cell^R/Scan^R imaging system and Olympus FV1000 confocal microscope, provided by the Advanced Imaging Facility at the University of Leicester.

4.2.2 Improvements to the FRT-FLP system to better regulate RS induction

The previous results appear to suggest the GR tag does not suppress completely nuclear localization when TA is not present, and that addition of TA does not lead to nuclear relocalization in 100% of transfected cells. Therefore, to tightly control the induction of RS we utilized the adaptable auxin-inducible degron (AID) system outlined by Kanemaki (2009). The AID system originated from the plant *Arabidopsis Thaliana* (Nishimura et al., 2009). This specific degradation pathway relies on the induction of the ubiquitous plant hormone (auxin), or indol-3 acetic acid (IAA), which mediates interactions between auxin specific E3 ubiquitin ligase SCF^{Tir} and auxin responsive plant transcription repressors (AUX/IAAs), leading to relatively swift proteasome-dependent degradation of the target protein fused with the degron (Figure 4.4).

Eukaryotes lack the specific plant orthologues for both auxin and F-box transport inhibitor response-I (TIR1), despite sharing multiple forms of the evolutionarily conserved Skp1-Cullin-F-box (SCF) degradation pathways. In principle, and as illustrated in Figure 4.4, the AID cassette allows the expression of the TIR1 protein and FLPH305L protein fused with AID degron; a small auxin-responsive AUX/IAA sequence that can directly control protein levels for study. TIR1 is plant specific, and binds to the endogenous SCF complex via the F-box domain (Dharmasiri et al., 2005). When utilizing endogenous SCF subunits in cells, TIR1 forms an auxin binding domain, affecting the E3 ubiquitin ligase complex SCFTIR1 (Abel and Theologis, 1996). The genes encoding these two proteins are transcribed as bicistronic mRNA, which forms two proteins simultaneously, using an internal ribosome binding site (IRES).

In the presence of auxin, SCFTIR1 recognizes and recruits the E2 ubiquitin ligase enzyme. This results in poly ubiquitinatylate and AID degron, and the fusion protein being immediately degraded by the proteasome.

We hypothesized that combining the GR and AID tag systems might deliver a more powerful method by which to facilitate efficient conditional control over Flp1 activity, to overcome the possibility of background Flp1 binding, thereby maintaining a (RS-OFF) phenotype.

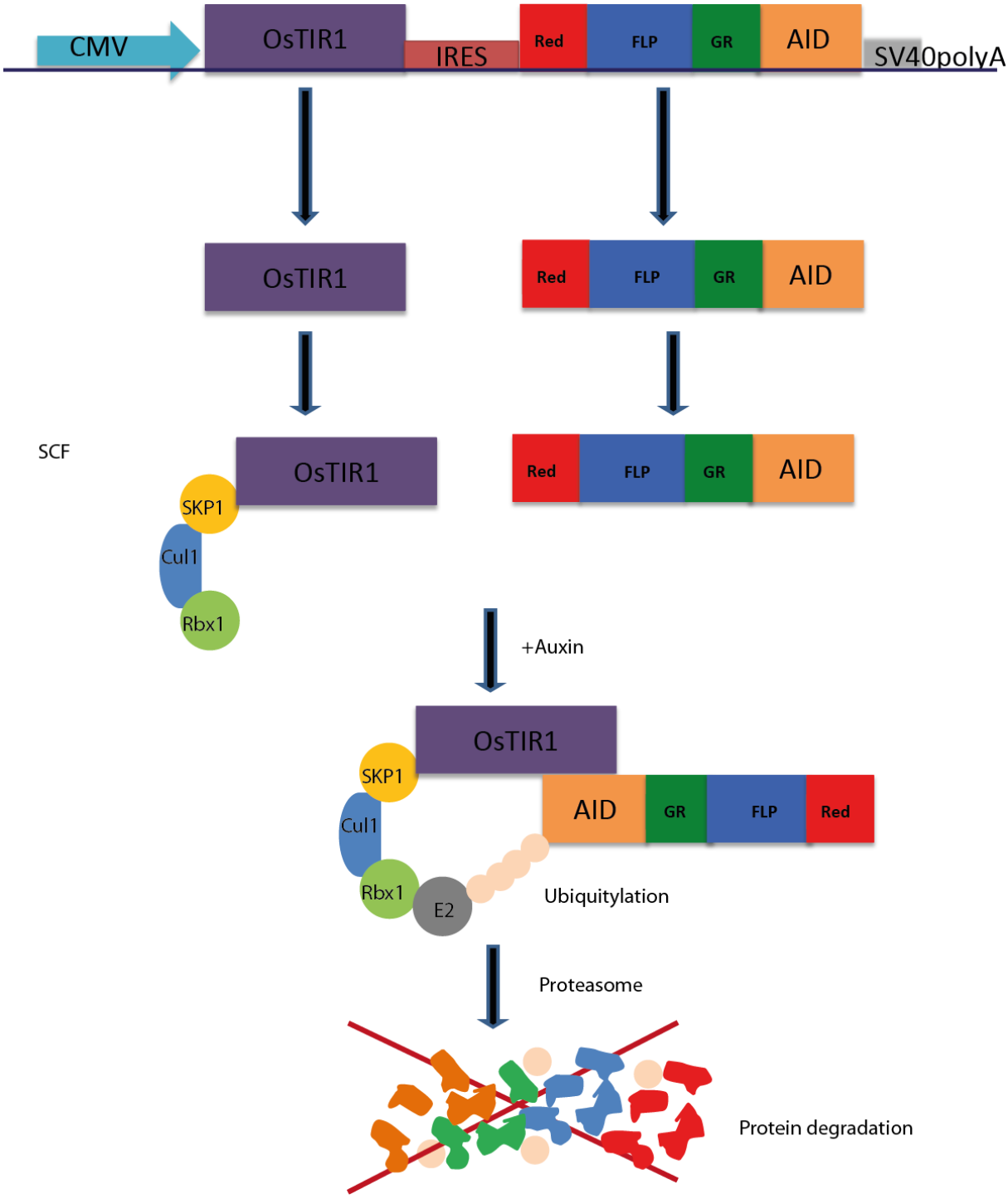

Figure 4.4 Schematic illustration of the principle of AID auxin system. The dsRed-FLPH305L-GR incorporated in the N- terminal of the original Auxin-induced degron cassette (AID- pMK107) vector. Expression deriven by the immediate early promoter of cytomegalovirus (CMV promoter) at the 5' terminus, which is processed by the poly-adenylation signal from the SV40 T antigen. The internal ribosome entry binding sequence (IRES) site would permits simultaneous translation of the aid fused protein and OsTIR1. This will allow expression of two proteins; the OsTIR1 protein and the dsRed-FLP-GR fused to the 25 KD AID degron. The TIR1 forms auxin dependent E3 ubiquitin using the SCF subunit. Following Auxin addition, the SCF-TIR1 complex binds to the AID degron and polyubiquitilates it, finally degrading the FLP protein via the proteasome.

4.2.2.1 Preliminary validation of AID Degradation

To assess whether the HEK293-FRT cells established were appropriate for the AID system and sensitive to the addition of auxin; cells were transfected with the original pMK106 (Figure 4.5.A) or pMK107 (Figure 4.6.A) plasmids gifted from Dr. Masato Kanemaki, at the National Institute of Genetics, with the intention of verifying if they worked as outlined. Both constructs expressed a plant specific F-box TIR1 protein comprising 9 repeats of Myc tag (TIR1-9Myc), producing an SCFTIR1 complex, and working as auxin-dependent E3 ubiquitin ligase for the degradation of the target protein. Fusion genes could then be derived from the immediate early promoter of cytomegalovirus (CMV promoter) at the 5' terminus, processed by the poly-adenylation signal from the SV40 T antigen. The internal ribosome binding sequence (IRES) permits translation of the aid fused protein. The plasmids also contain an SV40 origin (SV40 ori) for replication in cells expressing the SV40 T antigen. When selecting *E. coli* and mammalian cells, the vector contains a kanamycin/neomycin-resistance cassette, conferring resistance onto kanamycin and G418, respectively. This also comprises both a pUC origin of replication for propagation in *E. coli*, and an f1 origin for single-stranded DNA production.

Post transfection, the cells were exposed to either 500 μM or 1000 μM auxin (IAA) for different incubation times. Cell lysate was then collected as described in Section 2.4.2, and AID-mediated degradation was detected with immunoblotting using an anti-AID and anti-Myc antibodies (Section 2.4.5). CENP-H protein levels Markedly decreased 5 hours post the addition of IAA (Figure 4.5.B and C), with the higher IAA dose leading to increased degradation; demonstrate a dose dependency. However, levels increased again 24 hours post IAA addition. The reversibility of protein depletion and the re-expression of degraded proteins was then assessed by putting cells back in normal media lacking auxin. Figures 4.5.D and E reveal that using 500 μM IAA does not necessarily result in complete degradation. There was a 50% reduction in AID-CENP-H expression in IAA treated cells relative to untreated cells, again indicating that the use of higher concentrations is more efficient as a means of protein degradation. However, the AID-CENP-H protein was successfully re-expressed a short time (between 3-6 hours) after auxin removal.

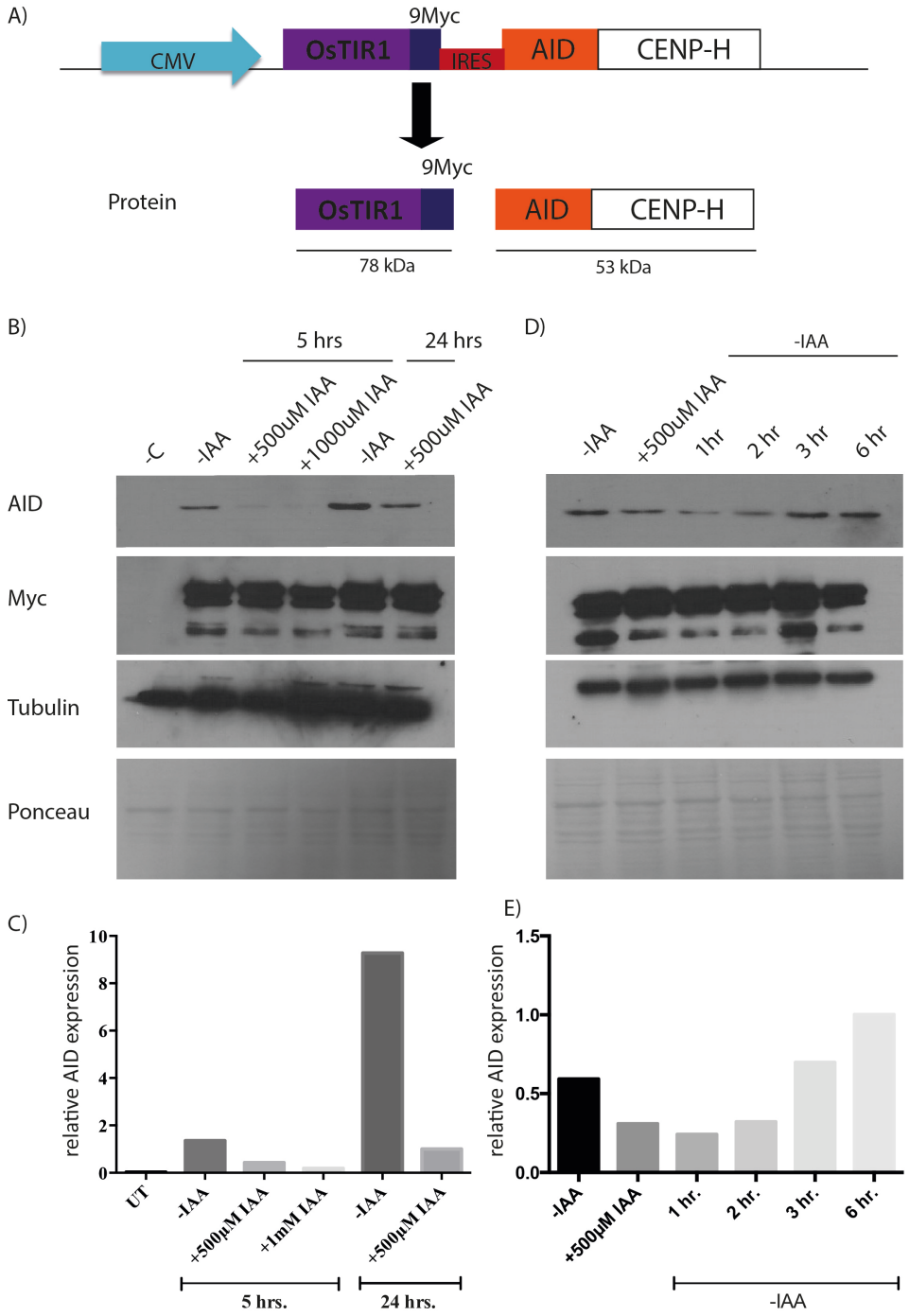

Figure 4.5 Controlling protein expression with the AID system of the N-terminal AID degron (pMK106). A) Schematic of the generated vector allowing the simultaneous expression of two proteins, namely, the TIR1 protein (78 kDa) and the AID protein (53 kDa). **B)** Immunoblotting detection of AID expression and degradation detected by the AID antibody. TIR1 expression was detected with the Myc antibody. HEK293 cells were transiently transfected with pMK106 to express the AID protein for 24 hrs. The cells were treated with different auxin (IAA) final concentrations of 500 µM and 1 mM for 5 hrs or 24 hrs. The cells were collected for immunoblotting in the presence of auxin (+IAA) or the absence of auxin (-IAA); non-transfected cells were used as a negative control. **C)** Quantification analysis of AID expression to the control protein (tubulin). **D)** Immunoblotting detection of 293 cells transfected as above and treated with 500 µM IAA for 24 hrs. Auxin media were replaced with normal growth media; the cells were collected at different indicated times. **E)** Quantification analysis of the re-expression of the AID protein to the control protein (tubulin).

Similarly, and as shown in Figures 4.6.B, the protein level for cells transfected with N-terminal AID degron degraded completely after the IAA addition. Overall, it was observed that the degradation of the N-terminal AID cassette was more efficient than that of the C-terminal AID cassette, even when using a low IAA dose concentration (500 µM). Visually inspection revealed that transfecting cells with an empty AID cassette or adding auxin hormone did not affect cell growth or viability.

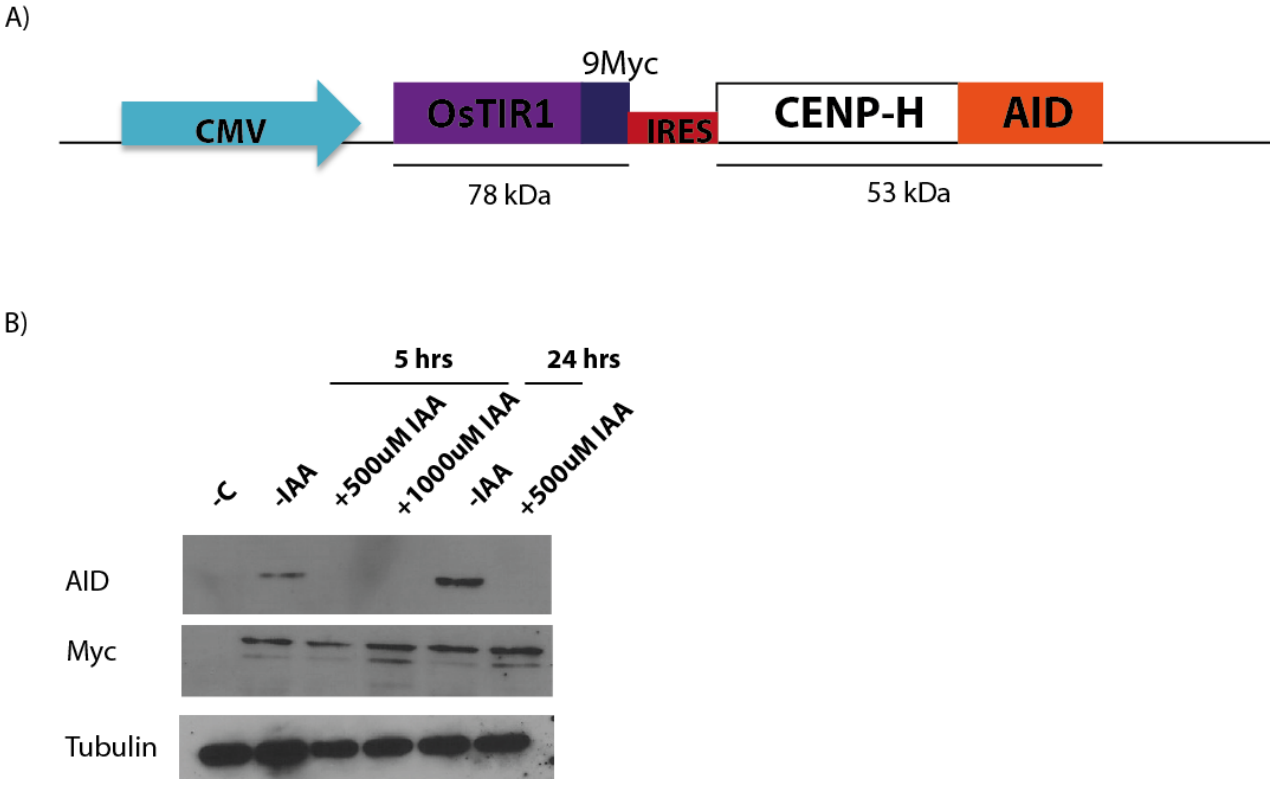

Figure 4.6 Controlling protein expression with the AID system of the C-terminal AID degron (pMK107). A) Schematic illustration of the generated vector permitting the simultaneous expression of two proteins; namely, the TIR1 protein (78 kDa) and the AID protein (53 kDa). **B)** Immunoblotting detection of AID expression and degradation as detected by the AID antibody. TIR1 expression was detected by the Myc antibody. A total of 293 cells were transiently transfected with pMK107 to express the AID protein for 24 hrs. The cells were treated with different auxin (IAA) final concentrations of 500 µM and 1 mM for 5 hrs or 24 hrs. The cells were collected for immunoblotting in the presence of auxin (+IAA) or absence of auxin (-IAA); non-transfected cells were used as a negative control.

4.2.2.2 Insertion of the dsRed-FLPH305L-GR into the AID cassette

Studies have revealed that using the AID system can deliver control of protein levels (Nishimura et al., 2009). Hence, we tested the AID tag system, as a tool for more tightly controlling the expression of I-SceI and Flp, to add an extra level of regulation during the induction of DSB and se-DSB, respectively.

Two additional FLP recombinase expression vectors were generated by cloning dsRed-FLPH305L-GR (no ATG/TAA) into AID degron either at the carboxyl N-terminus (AID-PMK106), or at the amino C- Terminus (AID-PMK107)

The cloning primers were designed to include vector homology (N-ter:...), (C-ter:...) in the 5' end of each primer. This allowed generation of complementary and suitable ends when cloning the amplicons to the target vector. The generation of these constructs was achieved by amplifying the dsRed-FLpH305L-GR from pdsRed-FLPH305L-GR, using either the pMK106_EcoRI_dsRed_FP/pMK106_ScaI_GR_RP or pMK107_EcoRI_dsRed_FP/pMK107 _ScaI_GR_RP primer sets (see Section 2.1.3). The PCR product (insert) was also gel purified and sequence verified before proceeding with cloning. The pMK106/ PMK-107 vectors were digested using 20,000 U/ml of *Sca*l and *EcoR*I (Section 2.1.7). As the inserted sequence contained multiple *EcoR*I sites, cloning was performed using LIC in PROTEX (Figur 4.7). The generated FLP-AID constructs were sequenced verified.

A)

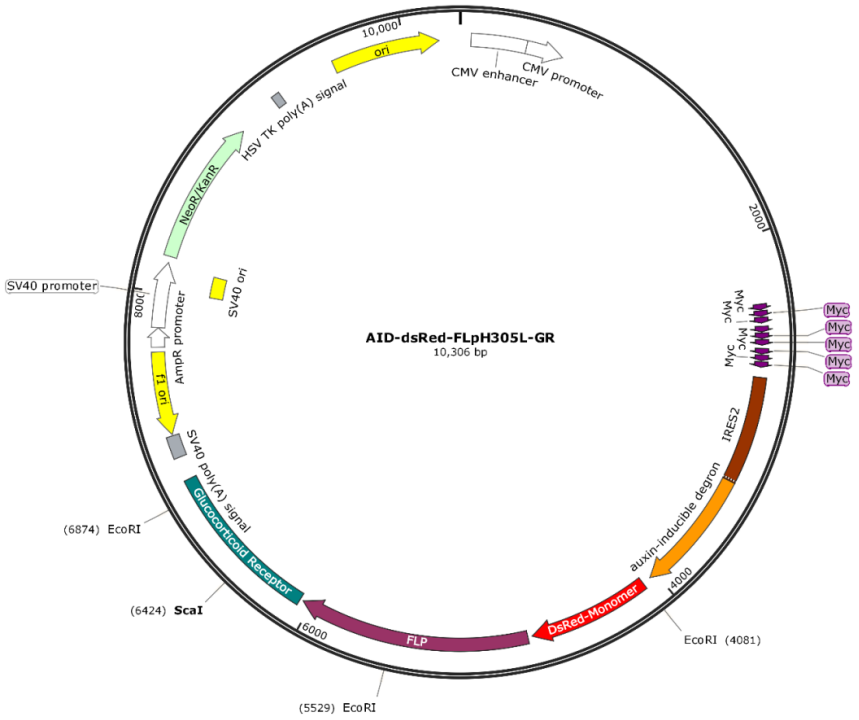

B)

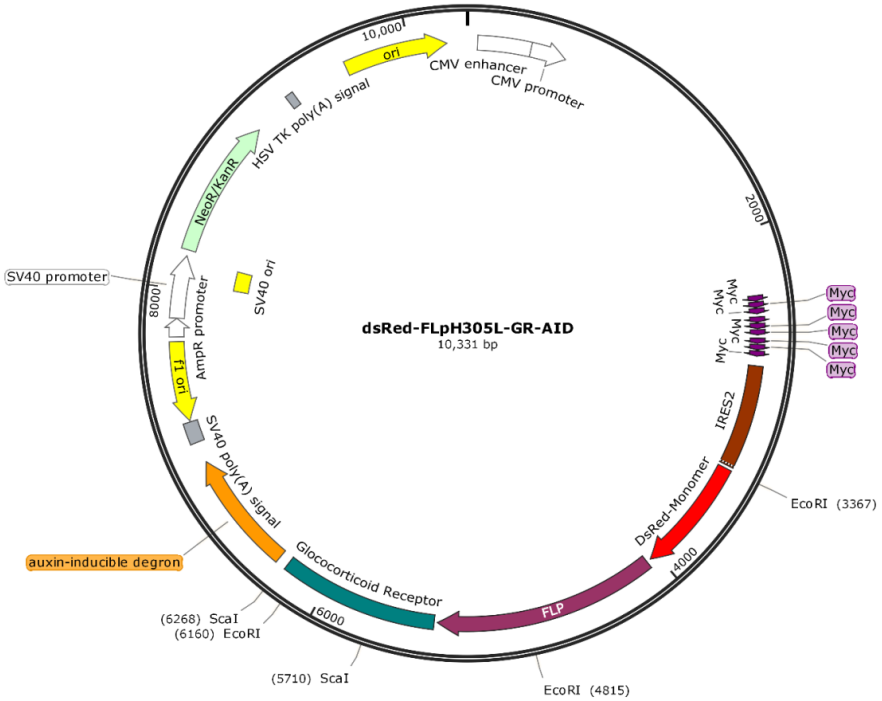

Figure 4.7 Schematic of the AID-FLPH305L recombinase expression constructs. A) The constructed N-terminal AID-dsRed-FLPh305L-GR. The dsRed-FLPH305L-GR amplicon was inserted as *EcoR*I/*Sca*I, downstream of the AID sequence (orange). **B)** The constructed C-terminal dsRed-FLPh305L-GR-AID. The dsRed-FLPH305L-GR amplicon was inserted as *EcoR*I/*Sca*I upstream of the AID sequence (orange). In both constructs, the AID is tagged upstream, with the OsTIR1 sequence (purple). This construct contains a kanamycin-resistant gene. The expression was controlled with a CMV promoter located upstream of OsTIR1.

4.2.2.3 Validation of the AID-tagged FLPH305L degradation

The expression and degradation of the AID-tagged FLPH305L protein was examined to test the applicability of combining the FLP-FRT and AID degron systems. HEK293 cells were transfected with pAID-dsRed-FLPH305L-GR or pdsRed-FLPH305L-GR-AID for 48 hours to achieve maximum transfection efficiency based on the optimization experiment (Figure 4.8). Post transfection, the cells were exposed to 1000 µM auxin (IAA). As the constructed vectors were tagged with RFP, the degradation was detected by means of loss of red fluorescence and the anti-AID antibody. The transfection efficiency proved too low, possibly due to the large size of the polycistronic expression vectors. In addition, and unexpectedly, the constructs generated increased the toxicity of the cells, as the cells died post transfection. This constrained the number of cell pellets collected for immunoblotting detection.

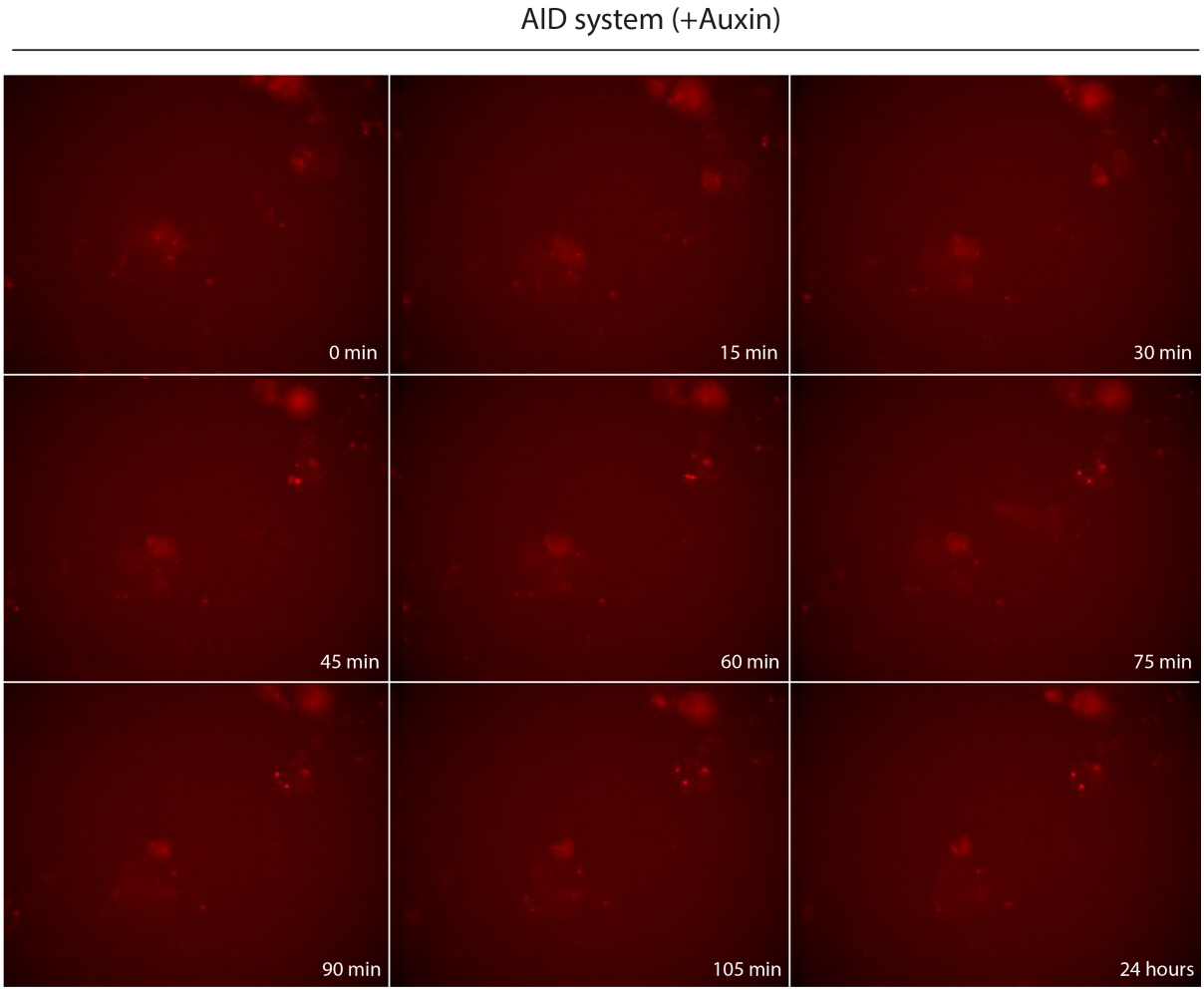

Figure 4.8 Depletion of RFP fused to AID after the addition of auxin in HEK293 cells. Fluorescent images of HEK293 cells transiently transfected with the dsRed-FLPh305L-GR, fused to AID degron for 48 hrs. 1000µM was added to the media and live cell imaging performed to visualize the depletion of RFP for 24 hrs.

4.2.3 Assessing the effect of triamcinolone acetonide on cell cycle

To investigate the effect of TA on cells more precisely; analysis of the effect of TA on cell cycle profile was examined, it was important to do this as the FRT-FLP system requires cells to be cycling. The cell cycle distribution of ethanol fixed and PI stained cells (Shichiri et al., 1993) was analysed using the Aria FACS flow cytometry system, and cell cycle distribution analysed using the MODFIT Program. To understand cell cycle progression, it was necessary to synchronize the cells into two frequently used points; the G0/G1 and M phase to be used as reference points. The cells were arrested in the G0 phase by growing to confluence un-transfected HEK293-FRT cells in a serum deprivation medium for 48 hours. Additionally, to synchronize the cells in the M phase, the commonly used microtubule inhibitor Nocodazole was used. The cells were incubated in a medium containing 1μM of Nocodazole for 24 hours. The degree of growth arrest was determined according to the controls, yielding a result with high synchrony for cells with G0/G1 and M phase DNA content. This permitted a more accurate assessment of the cell cycle position in the test samples (Figure 4.9).

Un-transfected HEK293-FRT cells (clone 19) were seeded for 24 hours. Normal cycling cells were then compared to cells stimulated with 10^{-7} nM TA and incubated at different time points, before the medium was replaced with a TA-free medium and the cells observed for another 48 hours. Cells were collected either immediately after TA addition (0 hours), or at indicated time points, or were alternatively released from TA. This process was accompanied by controls (un-treated cells) that were collected simultaneously at each time point. The cell cycle profiles were examined with flow cytometry. There was no impact from the addition of TA on the cell cycle profile, demonstrating the suitability of the TA/GR system for analyzing cycling cells (Figure 4.10).

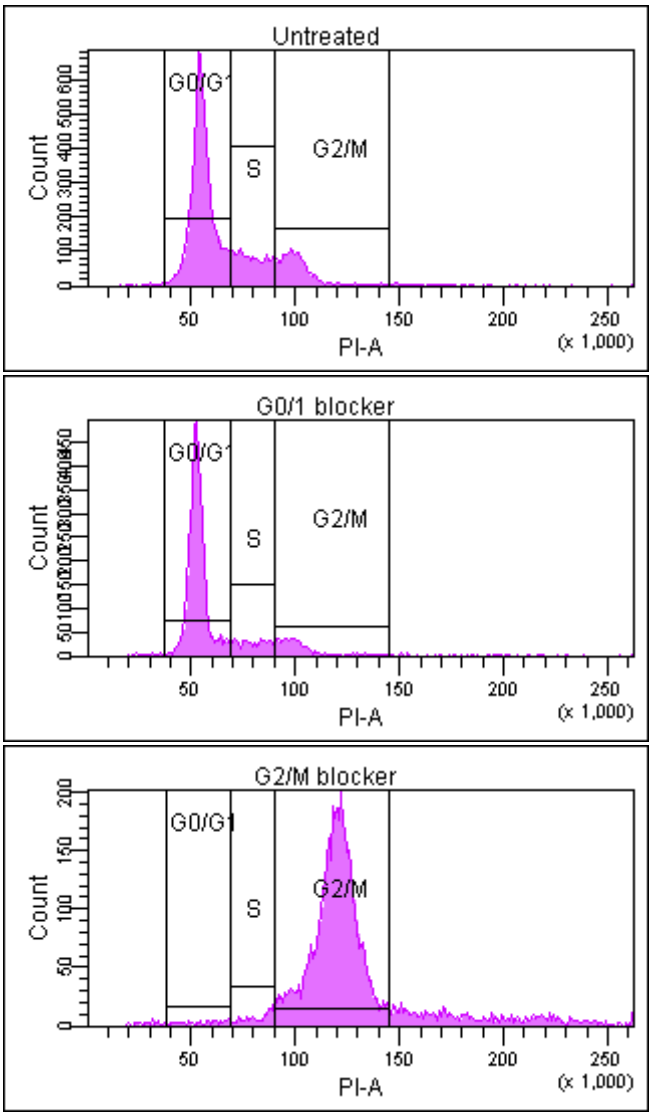

Figure 4.9 Cell synchronization in the G0/G1 and M phase of the cell cycle. HEK293-FRT were treated with serum deprivation medium or 1 μM Nocodazol for 48 hours to arrest cells in G0/G1 or G2/M phase, respectively.

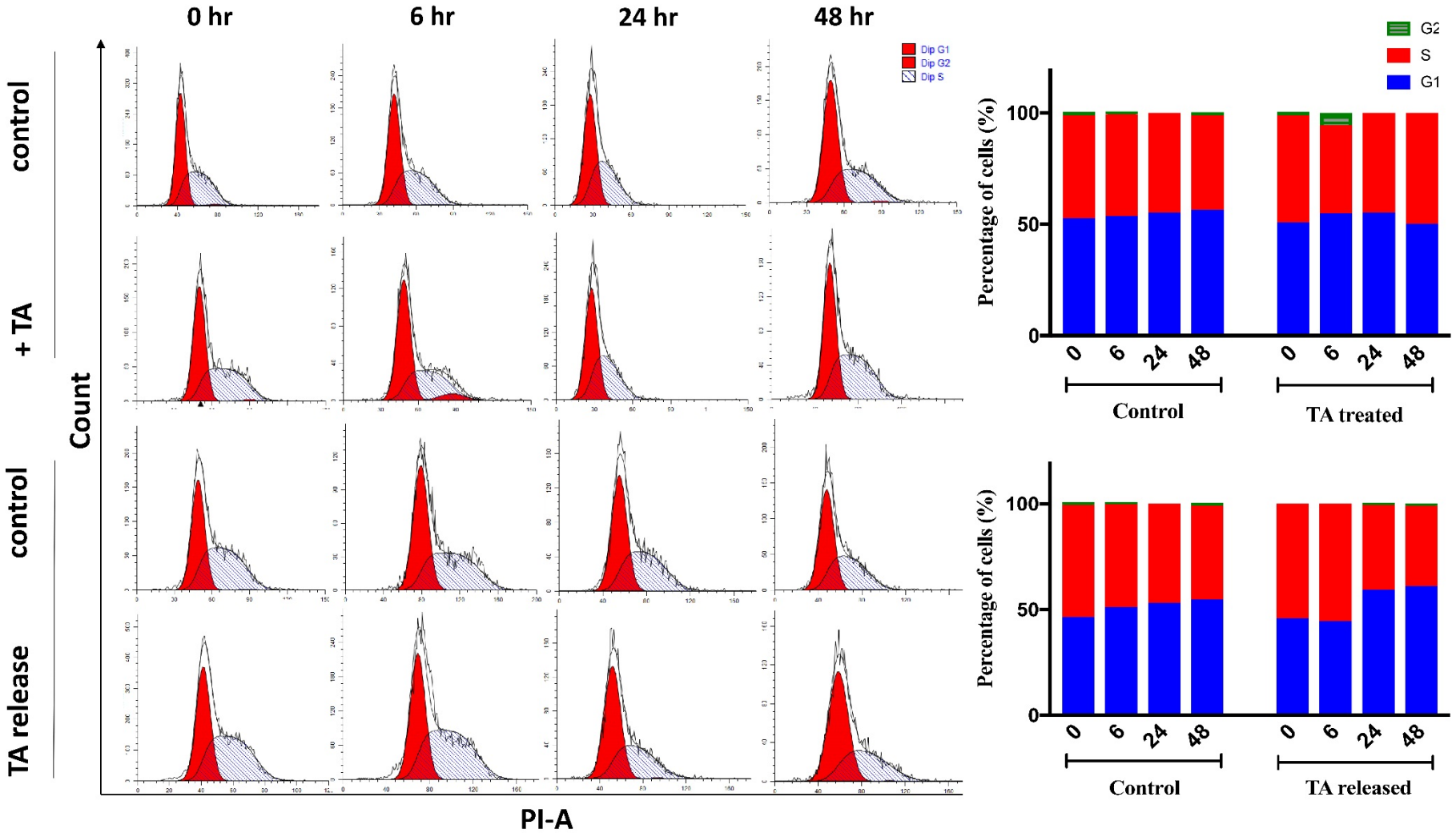

Figure 4.10 Cell cycle analysis of un-transfected HEK293 cells in response to TA addition and release. Representative plots of cell cycle distribution for cells stimulated with 10^{-7} nM TA for up to 48 hours. The cells were collected either immediately following TA addition, or TA was released at the indicated time points. Experiments independently repeated three times.

4.2.4 Validation of the ANCHOR labelling system

The ANCHOR labelling system employs fluorescently labelled 'OR' proteins that bind loosely and oligomerize to small integrated DNA segments called 'ANCH', creating fluorescent foci. To test the adapted ANCHOR system, efficiency of the OR3-GFP/OR4-CFP expression was tested, and its binding to the integrated ANCH3 and ANCH4 was examined. In the stable HEK293-ANCH3-ANCH4 cell lines, the FRT site was integrated 405 bp from ANCH3, and 1493 bp from ANCH4. The cells were transiently transfected with one or more of the pOR florescent plasmids. The parental HEK293 cells were employed as negative control cells, which lacked the FRT-ANCH3-ANCH4 sequence in their genome. The ANCH3-GFP and ANCH4-CFP upstream of the FRT site were simultaneously visualized, employing an Olympus Cell^R/Scan^R microscope. Figure 4.11.A demonstrates that CFP and GFP signals were distributed in the negative control HEK293 cells, as no foci were formed or visualized within the cells. By contrast, in the established HEK293-FRT-ANCH3-4 cells, the oligomerization and binding of the fluorescent OR3-GFP and/or the OR4-CFP to the ANCH3 and/or ANCH4 sequence sites was successfully confirmed by the formation of visible green and/or cyan foci, respectively (Figure 4.11.B). In addition, the presence of a single GFP and CFP nuclear focus indicated that a single integration event had taken place of this single cell clone. However, due to the low-level transfection efficiency, many cells do not contain foci, making it difficult to analyse several cells.

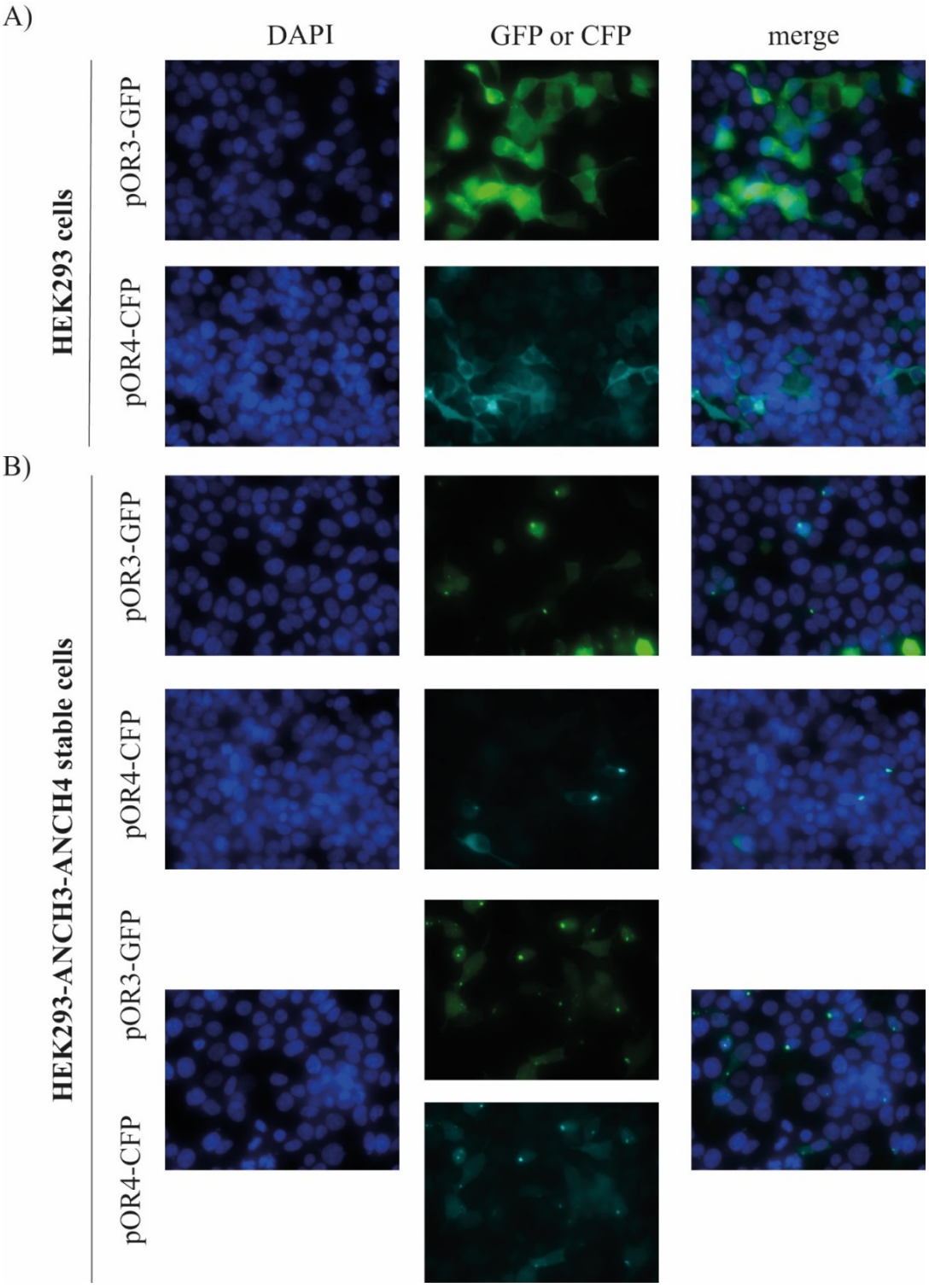

Figure 4.11 Validation of the ANCHOR DNA labelling system. A) Parental HEK293 cells were transiently transfected with pOR3-GFP (300ng) and/or pOR4-CFP (500ng) for twenty-four hours. Post transfection cells were stained with DAPI. The cells were examined with an Olympus Cell^R/Scan^R microscope employing GFP, CFP and DAPI filters. **B)** Stable HEK293-ANCH3-ANCH4 cells were transiently transfected with pOR3-GFP (300 ng) and/or pOR4-CFP (500 ng) for twenty-four hours.

The ANCHOR visualization system was applied to test whether both OR constructs could be expressed simultaneously in living cells, with the Red-FLPH305L-GR recombinase expression plasmid. To visualize the complete FRT-FLP system, HEK293-FRT-ANCH3-ANCH4 and U2OS-FRT-ANCH3-ANCH4 single clonal cells were transiently co-transfected with dsRed-FLPH305L-GR, pOR3-GFP and pOR4-CFP expression constructs for 24 hours and were then permitted to grow in the presence or absence of TA for 48 hours. Alongside these FRT-cell lines the parental HEK293 cells were employed as negative control cells, which lacked the FRT-ANCH3-ANCH4 sequence in their genome.

The cells were subsequently fixed and visualized using a computer-controlled high-resolution confocal fluorescence laser microscopy (i.e. Leicester's Core Biotechnology Services). Figure 4.12 demonstrates that CFP and GFP signals were distributed in the negative control HEK293 cells, as no foci were formed or visualized within the cells. While, the oligomerization and binding of the fluorescent OR3-GFP and/or the OR4-CFP to the ANCH3 and/or ANCH4 sequence sites was successful and a nuclear CFP and GFP foci on the HEK293-FRT-ANCH3-ANCH4 cells was clearly formed. As mentioned previously (Section 3.2.2.1.1) these cell line has a short ~105 bp sequence between the ANCH3 and ANCH4 sequence and subsequently an overlap of CFP and GFP signal was observed. In some cells, false positive foci were also exhibited in the RFP signal (circled in Figure 4.12). Similar to the preliminary experiment (Figure 4.11), it was observed that some cells have successfully transfected with all three plasmids, which clearly indicate the system can be utilized. However, due to the low-level transfection efficiency, many cells do not contain any foci. Moreover, many of the transfected cells did not exhibit all three signals. In addition, the degree of decondensation was observed to vary between the transfected HEK293-FRT-ANCH3-ANCH4 cells, due to their foci being of different sizes (more images can be found in Appendix V).

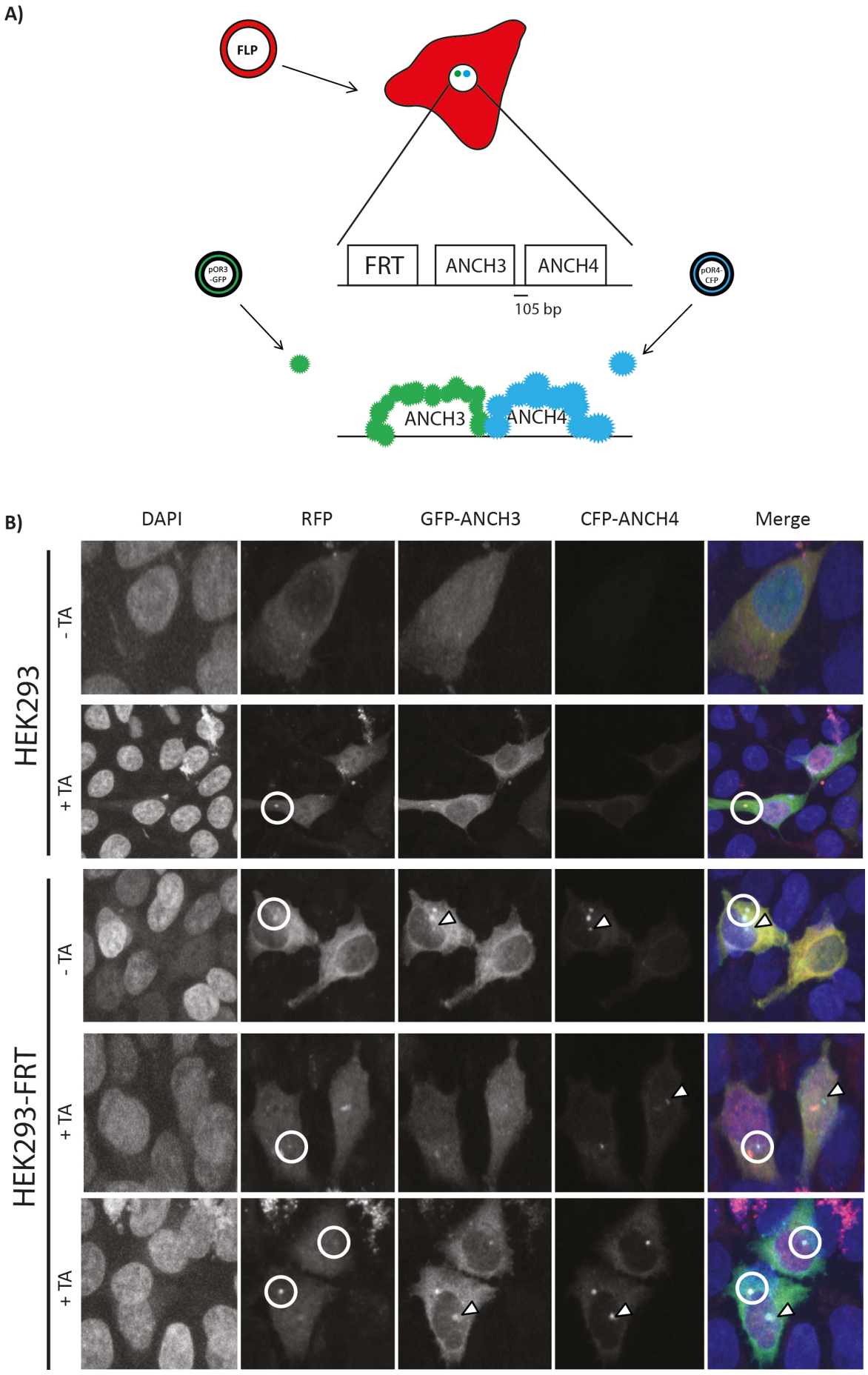
A)
FLP
FRT
ANCH3
ANCH4
105 bp
pOR3-GFP
pOR4-CFP
ANCH3
ANCH4
B)
DAPI
RFP
GFP-ANCH3
CFP-ANCH4
Merge
HEK293
- TA
+ TA
HEK293-FRT
- TA
+ TA
+ TA

Figure 4.12 Co-expression of dsRed-FLP-GR, OR3 and OR4 in HEK293-FRT cells. A) Experimental representation of the ANCHOR system. In HEK293-FRT cells, the ANCH3 and ANCH4 sites for binding with their OR proteins are inserted 405 bp and 1493 bp downstream from the FRT site. The ANCH sequences are separated by 105 bp. Post transfection, OR3-GFP and OR4-CFP bind to their ANCH specific sites to produce visible GFP and CFP foci. **B)** Representative Florescent confocal microscopy images of OR3-GFP and OR4-CFP distribution in cells labelled at ANCH3 and ANCH4 sites flanking the FRT sequence. HEK293 and HEK293-FRT-ANCH3-4 cells transiently transfected with OR3-GFP, OR4-CFP and dsRed-FLPH305L-GR in the presence or absence of TA to regulate dsRed-FLP-GR cytoplasmic to nuclear localization. The arrowhead shows the GFP/CFP formed foci that indicate the position of the ANCH3-4 site. White circle shows the false positive RFP-foci. The FLP recombinase localizes in the cytoplasm (system-OFF) in the absence of TA.

Figure 4.13, depicts the visualization of U2OS-FRT cells. These cells have a ANCH3 and ANCH4 separated from each other with ~720 bp (Section 3.2.2.1.3). However, although U2OS contain separated ANCH3 and ANCH4 sites, the CFP and GFP signals did not separate clearly as expected, and so an overlap was observed in the GFP and CFP signals. It was observed that a number of cells exhibited both GFP and CFP signals, though some only exhibited only the CFP signal. In summary, these data indicate that dsRed-FLP-GR, OR3 and OR4 can be co-expressed and ANCHOR foci mark the FRT site. However, giving that the number of cells with all three colors are relatively few, it may not be possible to analyse high numbers. (more images can be found in Appendix VI).

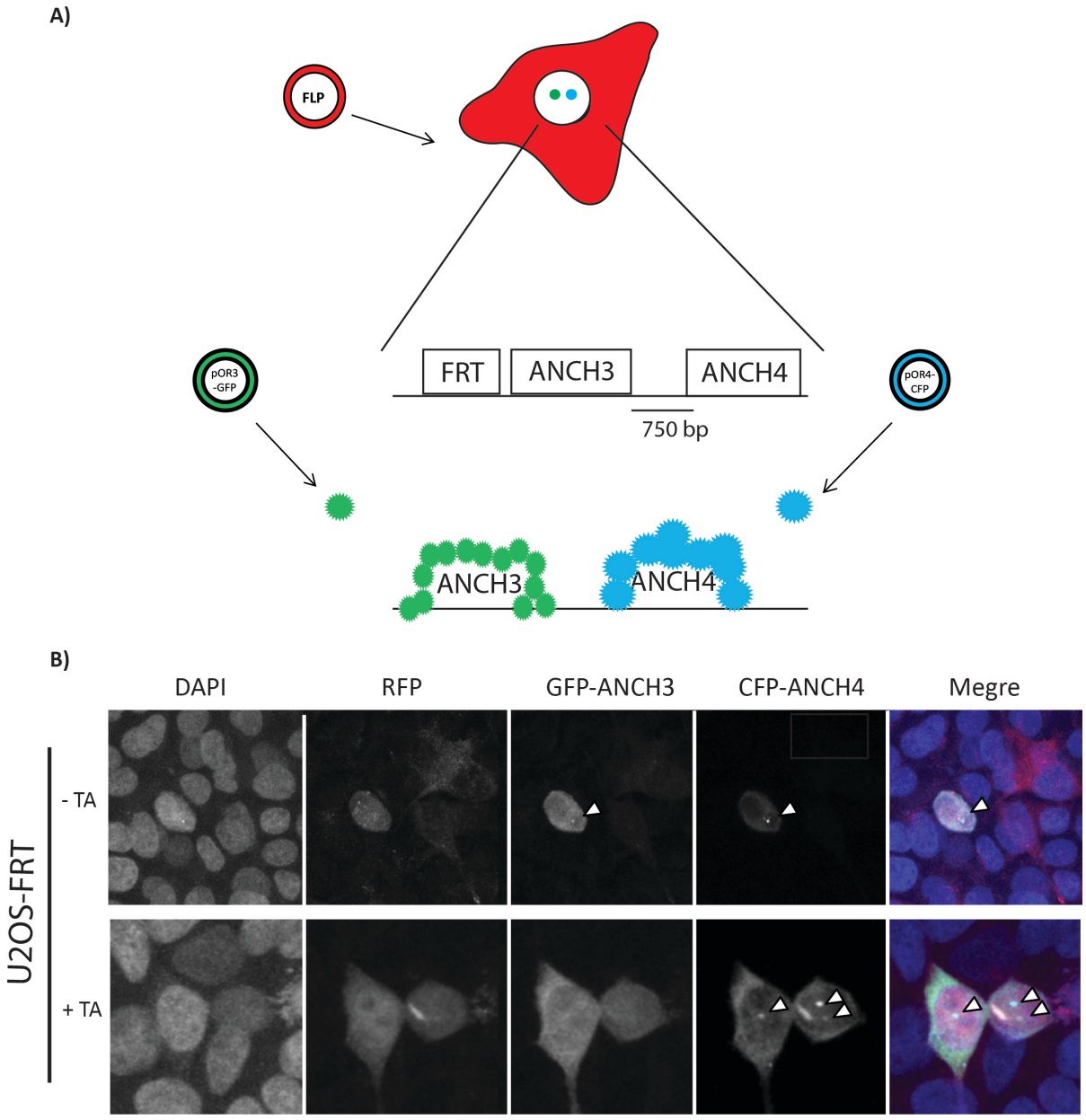

Figure 4.13 Co-expression of dsRed-FLP-GR, OR3 and OR4 in U2OS-FRT cells. A) Experimental representation of the ANCHOR system. In U2OS-FRT generated cells, the ANCH3 and ANCH4 sites for binding with their cognate OR proteins are inserted 50 bp and 1139 bp downstream from the FRT site. The ANCH sequences are separated by 750 bp. Post transfection, OR3-GFP and OR4-CFP bind to their ANCH specific sites to produce visible GFP and CFP foci. **B)** Representative florescent confocal microscopy images of U2OS-FRT-ANCH3-4 cells transiently transfected with OR3-GFP, OR4-CFP and dsRed-FLPH305L-GR in the presence or absence of TA. The arrowheads show GFP/CFP formed foci indicating the position of the ANCH3-4 site. The FLP recombinase localizes in the cytoplasm (system-OFF) in the absence of TA.

4.2.5 Visualization of FLPH305L induced SSB at FRT site

Alkaline denaturing gels electrophoresis are run at a sufficiently high pH to denature double-stranded DNA. The denatured DNA is maintained in a single-stranded state and migrates through the gel. It was previously used to succesfuly visualize the DNA nick generated by the FLP-nick system in budding yeast (Nielson et al., 2009). This was accomplished by collecting cells in different time point post- the induction of FLPH305L to generate the nick in G1-arrested as well as after release into S-phase cells. As shown in Figure 4.14, a band of ~2000 bp was revealed in G1-arrested cells post 180 minutes of galactose induction. This validate the cleavage of FRT upon FLPH305L induction.

Similarly, to confirm the induction of the FLPH305L-induced SSB at the FRT site in our system; alkaline denaturing gel electrophoresis was performed using a specific probe for the FRT integrated site. HEK293-FRT cells were transfected for 48 hours with empty GR, I-SceI or FLPH305L plasmids. Post transfection, to create a SSB or DSB, cells were allowed to grow in the absence or presence of TA for the time points indicated. gDNA was isolated from GR-, I-SceI- or FlpH305L-transfected cells as well as from the untransfected ANCH3-ANCH4 cell line, which was used as a negative control. Phenol/chloroform/isoamyl alcohol DNA extraction method was performed (as described in Section 2.3.2), to obtain the highest yield of DNA. 10 µg samples of dissolved DNA were digested with *EcoR*I, which flanks the FRT site, resulting in a DNA fragment of 1565 bp. To establish if all samples had been completely digested, 10 µl of the digested DNA reaction was applied on a 0.8% agarose gel with ethidium bromide. As described in Section 2.3.3, the remainder of the digested DNA reaction was precipitated using 0.3 M sodium acetate and then dissolved in 20 mL 1X alkaline loading buffer, and run in an alkaline or native gel.

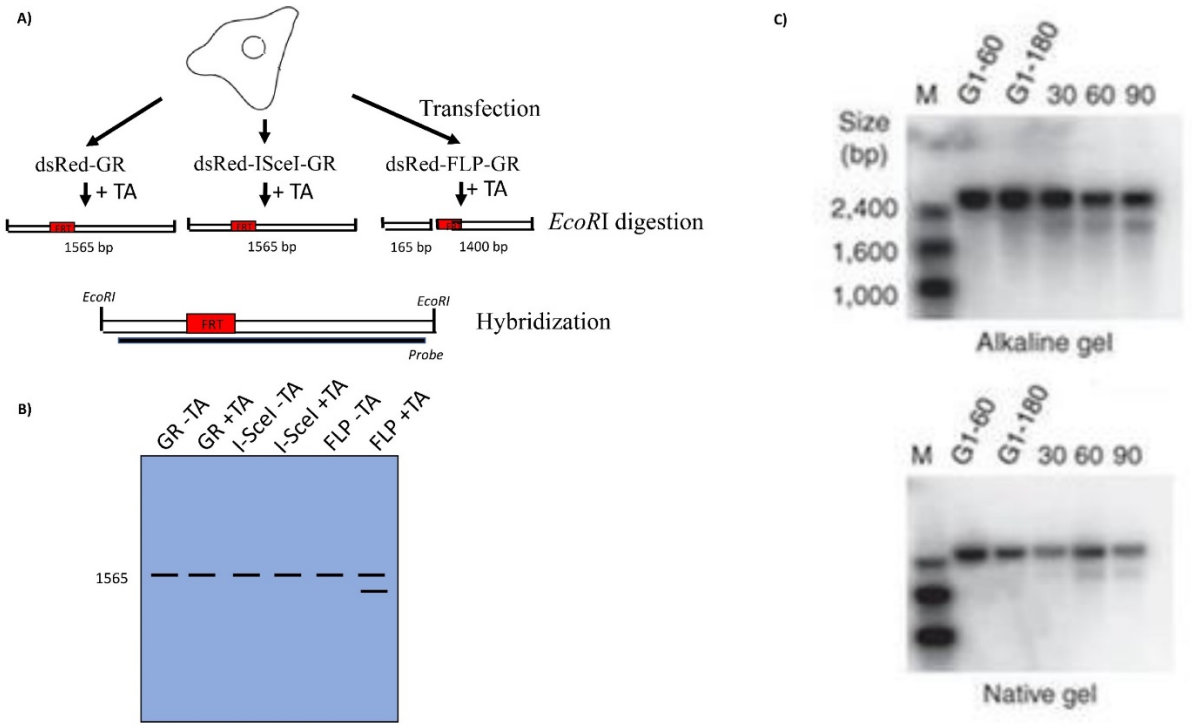

Figure 4.14 Principle of alkaline denaturing gels electrophoresis to detect the induced single strand breaks. (A) FRT stable cell lines were transiently transfected with different expression plasmids; the pdsRed-GR, pdsRed-I-SceI-GR and pdsRed-FLP-GR. Post TA addition, I-SceI will bound to the integrated Isce-I endonuclease site, and generates a direct DSB, the FLpH305L recombinase binds to the integrated FRT site and generates a stable SSB that leads to a broken Fork (se-DSB). Genomic DNA extracted from GR-, I-SceI- and FLP- were digested with EcoRI restriction enzyme that will cut around the FRT site. **(B)** Digested DNA were separated in alkaline or native gel to detect SSB or DSB, respectively, followed by capillary transfer into membrane. Membranes were hybridized using Radio labelled FRT probe. If SSB occur in the FRT site two fragments will be detected. **(C)** Detection of SSB and DSB by alkaline and native gel using FLP-nick system in budding yeast (Nielson et al., 2009).

As shown in Figure 4.14, it was expected that the addition of TA into the untransfected ANCH3-ANCH4 cell line will not generate any SSBs and thus, a single band with a ~1500 bp either in the presence or absence of TA will observed. In FLP-transfected cells a single band was expected in the absence of TA, whereas the presence of a second band (bp) during the induction of TA demonstrated that cleavage occurred. Notably, a single band would appear for cells transfected with either dsRed-GR or dsRed-I-SceI-GR either in the presence or absence of TA. However, using the native agarose gel electrophoresis will detect the DSB generated in the I-SceI-transfected cells if the probe was designed to hybridize to the I-SceI site in these experiments, the FRT site only were examined.

To examine the induction of SSB in all three cell lines. gDNA purified from the established HEK293-FRT (cl.19) cells was used as a template for the PCR reaction to generate the hybridization probe. Initially both alkaline and native membranes were hybridized with probe 3 that recognize approximately the complete FRT-ANCH3 sequence, which is equal to a DNA fragment of approximately 1143 kb. Figure 4.15 shows southern blot membranes from both alkaline and native gels.

The negative control cells (ANCH) revealed a band of ~1500 bp as expected. This demonstrate that the generated probe had successfully worked. However, a very faint bands were revealed with the expected size in all transfected cells (Figure 4.15.B). To identify the subsequent generation of DSB, the experiment was repeated with the samples run in a native gel instead of an alkaline gel. As shown in Figure 4.15.B, no bands with the expected product size were obtained. Unexpectedly, clear bands ~ 5000-6000 bp were appear in all transfected cells, which might indicate that the probe hybridized to the plasmids' backbone.

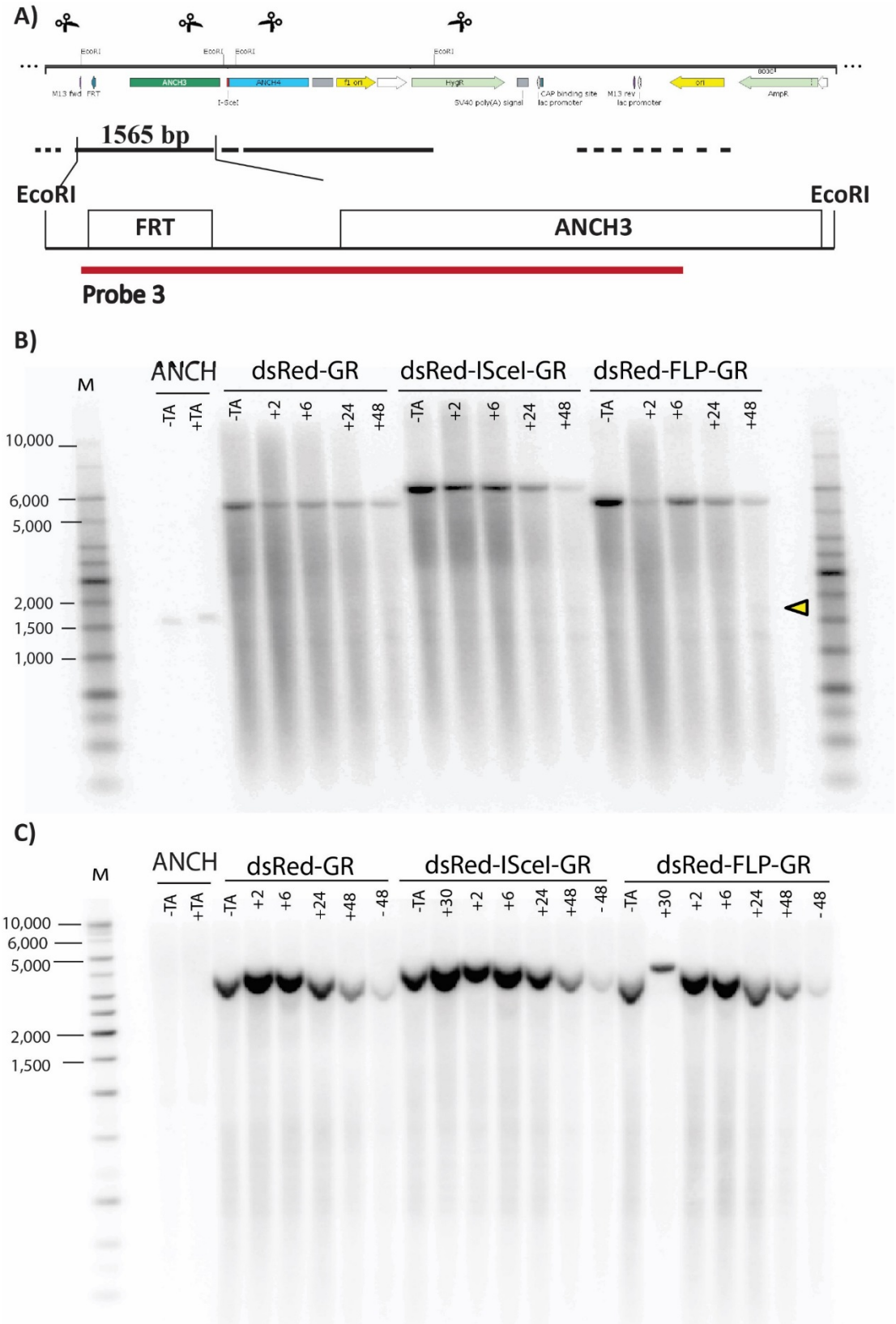

Figure 4.15 Detection of SSB generation at the FRT site. (A) Schematic of the FRT-ANCH3-ANCH4 integrated sites, showing the EcoRI site and DNA hybridization probe 3. **(B)** Analysis of gDNA restricted with EcoRI ran in alkaline gel electrophoresis. **(C)** Analysis of gDNA restricted with EcoRI ran in native gel electrophoresis. Membranes were hybridize with radiolabeled probe 3. Yellow arrow shows the expected revealed band of 1500 bp.

To overcome this technical issue, different primers located in the FRT-ANCH3 site were designed to generate different PCR products that could be used as probes to hybridize to regions of interest (Figure 4.16). The generated probes were bioinformatically analysed by blasting them with the original plasmid and the human gDNA sequence, to choose a more specific hybridizing probe (Appendix VII). The results showed that probe 4 was the most specific to bind to the integrated sequence and had less tendency to nonspecifically bind to the human genome. While, probe 3 was less specific and had a tendency to bind to the backbone of the plasmids.

Therefore, the experiment was repeated using probes 4 (613 bp), which hybridized only to ANCH3 sequence. As illustrated in Figure 4.17, a DNA fragment of approximately 1565 bp was positioned around the nick prior to the induction of TA, whereas a faint band of ~1400 bp was revealed post-TA induction, indicating the generation of SSB nick. The ANCH3-4 cell line revealed an unexpected band of approximately 5000 or 6000 bp in all lanes, which reflected the plasmid backbone and was detected in both membranes. This is an inconclusive and the generation of SSB and DSB have been not detected yet.

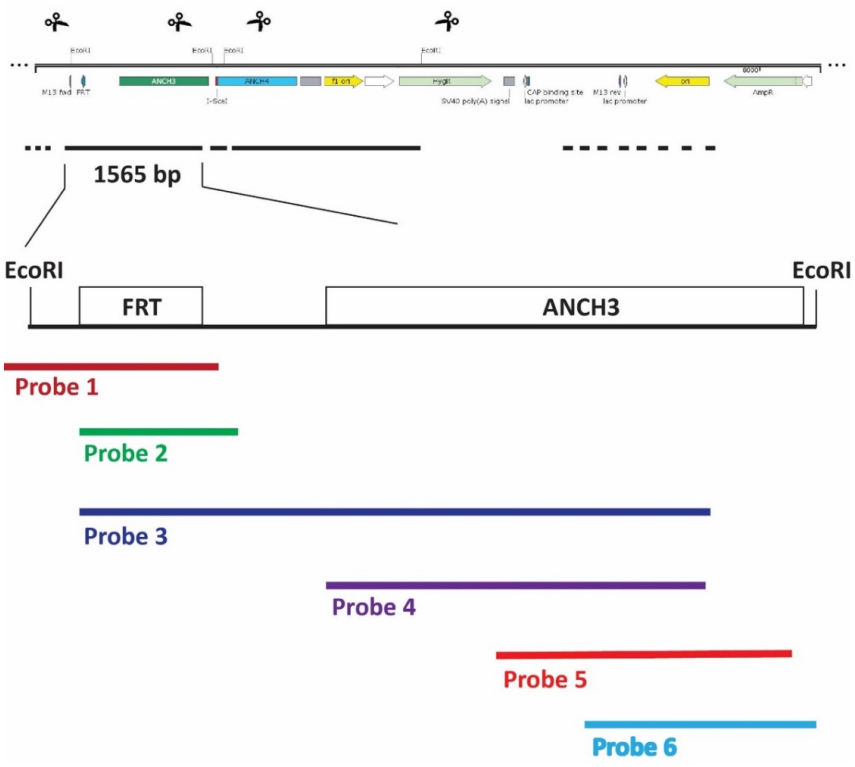

Figure 4.16 Schematic showing the various designed DNA probes.

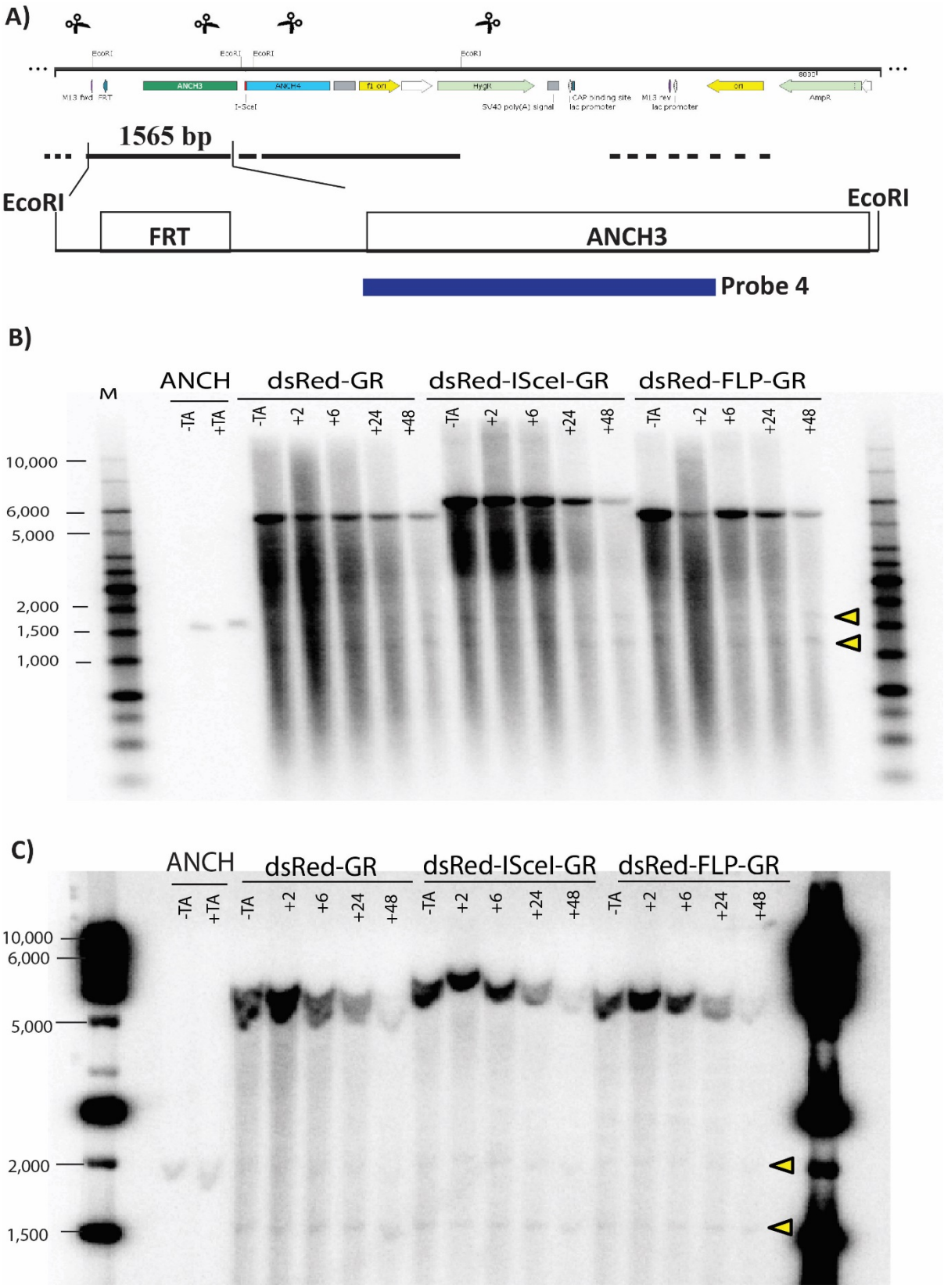

Figure 4.17 Detection of DSB generation at the FRT site. (A) Schematic of the FRT-ANCH3-ANCH4 integrated site, showing the EcoRI site and DNA hybridization probe 4. **(B)** Analysis of gDNA restricted with EcoRI ran in alkaline gel electrophoresis. **(C)** Analysis of gDNA restricted with EcoRI ran in native gel electrophoresis. Membranes were hybridize using radiolabeled probe 4. Yellow arrow shows the expected revealed band of 1500 bp.

4.3 Discussion

The previous chapter discussed the design of a new mammalian cell-based assay, in which the inducible FRT-FLP system consisted of a number of features that facilitated the analysis of BF repair beyond what was impossible previously. This current chapter discusses the validation of the different components of this novel FRT-FLP system.

The system was designed to conditionally control the induction of BF during DNA replication and direct DSBs at specific genomic loci; thereby, making it possible to assess the role of different types of DSBs. The GR tag system was proposed as a suitable tag to enable conditional control of FLP and I-SceI cellular localization to generate SSB (and ultimately BFs) and DSBs respectively allowing the system rapid switching control, i.e. ON/OFF. There was successful fusion between FLPH305L or I-SceI and GR and dsRed in a single open reading frame. A significant florescence in the cytoplasm was visualized and confirmed using the dsRed-I-SceI-GR plasmid. However, the cytoplasmic localization of the first generated dsRed-FLPH305L-GR was not as expected. This was due to the presence of stop and start codons (ATG/TAA) flanking the FLPH305L sequence, resulting in technical limitations. All the codons following the starting codon identified were translated sequentially, and the ribosome was dissociated when the termination factory encountered a stop codon (i.e. the dsRed-FlPH305L generated in the absence of GR). This explained detection and presence of the red signal, and prevented the observation of red movement in cells transfected with dsRed-FLPH305L-GR. Thereby, and in order to overcome this limitation, site direct mutagenesis was performed. Generation of a new dsRed-FLPH305L-GR with no ATG/ATT was performed and the sequence verified successfully for use in subsequent experiments.

Despite these precautions, there was some heterogeneity in the GR localization in some cells where cells with both nuclear and cytoplasmic localization, while a minority of cells did not exhibit nuclear relocalisated. Nevertheless, most cells exhibited higher nuclear signal relative to cytoplasmic signal in TA. It was deduced that the intracellular distribution of tagged GR is not complete with a minimal leakiness of the RFP signal in some nuclei noted under no ligand conditions. In addition, it was concluded that, upon the addition of TA, GR localization was not as rapid a process as had been previously reported (Soutoglou et al., 2007). In the current system the translocation of the GR import proved a lengthy process; i.e. taking a number of hours rather than minutes. This slow cytoplasmic to nucleus import is likely due to the efficiency of the agonists ligand used (Martinez et al., 2005).

Given the slow kinetics result, two different classes of steroid hormones were evaluated to induce translocation. Following transfection, the cells were stimulated to either the TA or dexamethasone steroid ligands. The red signal expressed was predominantly found in the cytoplasm, while movement from the cytoplasm (prior to the addition of the steroid) to the nucleus (following the addition of the steroid) was successfuly observed in both the ligands employed. Translocation of the expressed protein fused to the GR was monitored up to a period of twenty-four hours. It was observed that the RFP signal remained within the cytoplasm of the incubating the cells after two hours, and that approximately half of the cells experienced observable nuclear accumulation (visibly more signal in nucleus than cytoplasm) at six hours, while complete translocation was induced within twenty-four hours. In contrast, un-liganded GR fused to green fluorescent protein (GFP) has been previously shown to be predominantly residual in cytoplasm, translocating rapidly (complete translocation after 30 minutes) to the nucleus in a hormone-dependent manner when binding to the synthetic ligand TA (Htun et al*.,* 1996; Ogawa et al., 1995). There have also been a number of earlier studies demonstrating that the cytoplasmic to nucleus mobility of GR works upon ligand binding with rapid kinetics, with translocation being completed thirty minutes after the addition of the hormone (Soutoglou et al., 2007). Ideally, activation of FLP recombinase and I-SceI endonuclease expressed proteins should be uniformly rapid and efficient, so that the consequences can be induced (i.e. SSB or DSB) in majority of cells at the same time, though the timing of BF will not occur until a cell is undergoing replication anyway and it is difficult to have this occure in most cells at the same time without synchronizing the cultures.

Given these results, experiments were initiated to precisely monitor the subcellular trafficking of GR in live cells, to quantify the accumulation of fluorescence in the nucleus and determine the efficiency of the GR tagging system relative to the current system. Unfortunately, the use of live cells brings about difficulties in the observation of any cytoplasmic to nuclear translocation dynamics of a fluorescently labelled receptor as cells rounded and detached during the course of experiment. The inability to directly observe living cells impeded completing the time-lapse series of dynamics related to the red signal and prevented the quantitative analysis. Moreover, in the live cell experiment there was nuclear accumulation of the red signal even under TA-free conditions. These results suggest that these conditions somehow activated the RFP-GR chimeric protein even prior to the addition of steroids.

Studies have demonstrated the shuttling of unliganded-GR from cytoplasmic to nucleus, and vice versa. This has been suggested due to its association with the heat shock protein complex (Hache *et al*., 1999). It was also observed that GR can also be translocated into the nucleus in steroid free conditions through interaction with the heat shock protein Nup62 (Echeverria *et al*., 2009).

The GR was demonstrated to be a potent cell cycle regulator, interacting with cell cycle regulatory kinase and inducing arrest at the G0/G1 checkpoint (Rogatsky *et al*., 1997). Though I did not observe G1 arrest upon TA addition (Figure 4.10). Live cell imaging using fluorophore-tagged GR revealed the panel of GR distribution, as a reflection of cell cycle progression. The impact was profiled according to cell cycle progression driven by physiological GR trafficking on the panel of GCs action (Matthews *et al*., 2011). It was deduced that GR was tightly accumulated in the nucleus through the G1 interphase, prior to the cell division and strictly cytoplasmic translocation with rapid exclusion during mitosis following cell division in G2/M ligand independent induction of GR. Suggesting that future experiments could be performed with our cells while using cell cycle marker such as EdU for S-phase cells to determine if cell cycle stage correlates with RFP localization patterns.

As a consequence, it was concluded that the utilization of GR in the system would not result in powerful conditional control over the RFP localisation, as the intracellular distribution of the RFP signal without steroid was not as consistently cytoplasmic, as previously suggested (Soutoglou *et al*., 2007). The GR leakiness of localization and slower than expected TA-induced relocalisation not the nucleus caused a technical limitation in the current system, as a result of the inability to precisely control induction of the expression proteins that caused RS or DSB in case of I-SceI. Ideally, the inactivation of the FLP fused to the GR should be precisely controlled, to provide a RS-OFF phenotype in the absence of TA, or a RS-ON phenotype upon the addition of TA.

It was considered important to maintain a 'RS-OFF' phenotype; thus, it was necessary to control Flp recombinase and I-SceI endonuclease activity to achieve conditional induction of RS using systems that can manipulate protein localization, inactivation or depletion. Several systems have been published to control and mediate protein localization, based on fusing target proteins into the binding domains of steroid hormones, or rapamycin-dependent dimerization domains, to control nuclear localization (Haruki *et al*., 2008; Picard *et al*., 1988). However, these processes rely on protein activity that is restricted to a specific cellular compartment.

Therefore, in order to conditionally inactivate and tightly control protein level, advantage was taken of protein depletion methods to control FLP or I-SceI break induction, and to add an additional level of regulation for the induction of DSB and se-DSB. In general, a variety of efficient techniques have been used to control protein expression; these involved altering the DNA coding sequence, deleting relevant genes or down regulating gene expression by suppressing the mRNA via RNAi (Gossen and Bujard, 1992; Elbashir *et al*., 2001). However, these methods were found not to be suitable or applicable within the FRT-FLP system, due to a lack of reversibility. A variety of systems have been published to allow the depletion and degradation of the protein of interest. Previous studies have illustrated the importance of the rapid depletion of proteins for the interpretation of the subsequent phenotype and to characterize a large number of essential proteins (Iwamoto *et al*., 2010; Bonger *et al*., 2011; Banaszynski and Chen, 2006). Some systems have achieved the degradation and depletion of targeted proteins by means of an inducible degradation signal, or degron by modulating ubiquitin ligase, i.e. the SCF complex (Dohmen *et al*., 1994). It has been established that endogenous proteins can therefore be directly controlled through the employment of such systems. The most generally applicable approaches for controlling the activity of a protein have been developed in yeast. Three degradation systems have been characterized in S. cerevisiae, based on the use of either a N-end rule domain, capable of inducing protein degradation (Dohmen *et al*., 1994), or an auxin inducible degron (Nishimura et al., 2009). The original N-end rule degron system approach proved highly efficient and reversible in yeast. It is reliant on the exposure of a destabilizing amino (N)-terminal residue to a temperature shift, and is therefore limited to use in mammalian cells (Holland et al., 2011).

The AID degradation has been used to deplete proteins of interest by directly exploiting a specific protein degradation pathway, which induces ubiquitination and subsequent proteasome degradation (Zhou, 2005; Banazynski and Wandless, 2006). This method has been employed as a means of controlling protein expression in mammalian cells.

The recently adaptable auxin-inducible degron (AID) system was employed to provide an 'RS-OFF' phenotype. It was observed by checking the original plasmids when transfecting cells with an empty AID cassette, or adding the natural plant auxin hormone, had no impact on cell growth or cell viability. This immunoblotting result indicated that the protein level can be directly controlled and degraded in a dose-dependent manner. Collectively, these results revealed that the AID system can be used to control the stability of proteins localized either in a nuclear or cytoplasmic membrane and induce degradation.

The utilization of the auxin resulted in a number of additional advantages, as the protein depletion was both rapid and reversible. New expression constructs were successfully generated by combining the current GR system with the AID degron. However, it emerged that the transfection efficiency proved too low, potentially because of the large size of the polycistronic expression vectors. In addition, the construct appeared to be toxic as cells died post transfection. Subsequently, the low number of cells constrained the number of cell pellets collected. Therefore, immunoblotting detection was difficult to perform. It was generally challenging to facilitate the combined FLP-GR system with the AID system. In future work, different vectors could be constructed; such as the use of the auxin without the GR, which might significantly enhance the versatility of the AID degron system; thus, minimizing the size of the construct. Though if degradation is being induced, the RFP signal to identify transfected cells may have to be expressed independently of FLP.

Overall, a major limitation of the generated system consisted of the inability to precisely overcome the leakiness of the GR fused protein, along with difficulties combining it with a degron system. Despite these, in subsequent experiments, we concluded that the GR system still provided sufficient control and still employed the GR system but always carefully considered its limitations regarding the control localization of the protein and the induction of RS, when assessing phenotypes data.

The FRT-FLP system proved to have an additional advantage, which involved using the ANCHOR labelling system, and fluorescent-labelled ‘OR’ proteins that loosely bind and oligomerize to integrated small DNA segments called ‘ANCH’ to create fluorescent foci. The efficiency of the OR3-GFP/OR4-CFP expression plasmids was estimated, and their binding to the integrated ANCH3 and ANCH4 examined respectively. A preliminary experiment was performed using the HEK293-FRT-ANCH3-4 established cell line. Although the transfection efficiency was relatively low, the oligomerization and binding of the fluorescent OR3-GFP and/or OR4-CFP to their unique ANCH3-ANCH4 sequence sites was successfully confirmed by the formation of visible green and/or cyan foci, respectively. Single ANCH3-GFP and ANCH4-CFP foci that co-localised were simultaneously visualized in clone 19, indicating a single integration site comprising FRT-ANCH3-I-SceI-ANCH4. Moreover, the parental HEK293 control cells did not exhibit either green or cyan foci due to the lack of ANCH3 and ANCH4 sequences. Providing further strong evidence that the foci in HEK293-FRT cells were real.

The employment of the ANCHOR system combined with the expression of the FLPH305L recombinase plasmid to visualize the site where a SSB (se-DSB) should occur was achieved in both HEK293 and U2OS cells. An experiment was performed utilizing both HEK293 and U2OS fixed cells post-transfection with three expression plasmids: OR3-GFP, OR4-CFP and dsRed-FLPH305L-GR. In both the cell lines used, the FLP recombinase was largely localized in the cytoplasm (system-OFF) in the absence of TA. In HEK293-FRT-ANCH3-4 cells, transfection efficiency was poor again and single nuclear GFP and CFP overlapping foci were observed in only some of the transfected cells. The majority of the fluorescent foci unexpectedly appeared in the cytoplasm as large foci, rather than the nucleus, of some of the transfected cells. This indicates OR proteins may oligomerise in cytoplasm. Inserting the nuclear localization sequence (NLS) into the OR expression protein may be a possible way of increasing the nuclear localization efficiency of the formed foci (Lange et al., 2007). Conversely, although the generated U2OS-FRT-ANCH3-4 cells have two integrated ANCH sites separated by 750 bp, which is theoretically sufficient to visualize two separated but adjacent foci, the two formed GFP and CFP foci still overlapped. No significant separation was observed, perhaps because the OR proteins can spread along the adjacent DNA. An association of the 100-200 ParB molecules was shown to spread with at least 1 kb of adjacent DNA observed in the living *S. cerevisiae* (Saad et al., 2014).

If the transfection efficiency and nuclear localization of OR proteins can be improved, then the ANCHOR system could be an excellent tool for visualising the disappearance and appearance of the loosely bound OR3-GFP/OR4-CFP proteins at RFs and BF undergoing repair. In addition, the disappearance of the fluorescent GFP foci inserted immediately at the break site makes it possible to distinguish cells that that have incurred a BF from normally replicating cells (further discussion and details will be found in Section 8.2). Interestingly, any observed loss of the GFP signal while the CFP foci remains might be due to OR proteins only binding to the dsDNA, meaning the loss of focus indicates BF has occurred in a particular cell and that the ANCH3 sequence has become ssDNA, which is consistent with results obtained from the ParB-INT system. Similarly, ParB proteins were shown to bind only to the dsDNA. Loss of focus indicates that the INT1 sequence became single-stranded (Sadd *et al*., 2014). As the preliminary validation was conducted with fixed cells, the loss of a GFP fluorescent foci was found to be not due to photo bleaching during the experiment.

Thus, it was speculated that OR proteins only bind to dsDNA, meaning that during replication and repair in the S-phase, foci will be removed from the site, although when a repair occurs those foci will form again, meaning genome integration is restored

Collectively, the ANCH3-ANCH4 site upstream the FRT sequence were simultaneously visualized using the ANCHOR labelling tool. These features would make the system widely applicable to the study fine-scale analysis of BF dynamics and repair process by visualising the disappearance and appearance of the loosely bound OR3-GFP/OR4-CFP proteins at RFs and BF undergoing repair. In addition, the disappearance of the fluorescent GFP foci inserted immediately at the break site makes it possible to distinguish cells that that have incurred a BF from normally replicating cells. Employing this feature in future experiments will serve to distinguish between cells that have undergone replication at the FLP-DNA adduct site following TA-induced FLP nuclear localization from those that have not. In addition, accurate measurement of the kinetics of induction, and resolution of broken forks (se-DSB), will be monitored over time. This can be achieved by monitoring changes in OR-foci after switching on to monitor repair kinetics at site. However, due to cell-to-cell variability at the time of break induction and repair, disappearance of the GFP signal from the ANCH3 site must be studied in single cells to illustrate the relative speed at which focus is lost and regained. Due to the possibility that GFP disappearance occurred at the earliest point following TA induction, the CFP and GFP can be tracked three dimensionally in live cell imaging by acquiring up to 24 hours over the time frame to monitor focus intensity and changes to the overlapping degree of individual cells. Additionally, intrusive weak binding and oligomerization of OR proteins means there is no disruption of DNA replication and repair. Thus, this visualization feature provides the ability to accurately track repair kinetics of se-DSB induction and resolution, and of the replication completion by monitoring the appearance of two CFP foci.

Chapter 5: Assessing the cytotoxicity and genotoxicity of Flp-induced replication stress relative to direct DSBs

5.1 Introduction

DNA-damaging agents, errors in DNA replication and sporadic repair errors represent a continuous threat to mammalian cells (Lindhal and Barnes, 2000). The action of these sources can causes aberrant RFs and DSBs to appear within the genome (Kastan and Bartek, 2004). These defective DNA structures have the potential to subsequently cause mutagenicity, cellular changes or cellular death (Ciccia and Elledge, 2010). The DDR mitigates the genotoxic potential of DSBs via a robust sensing/detection system that regulates cell cycle arrest, either by facilitating a DSB repair mechanism, or by activating alternative cell pathways such as senescence and apoptosis, to prevent any genomically unstable cells from proliferating (Zhou and Elledge, 2000; Harper and Elledge, 2007). RS is related to spontaneous GIN, and is a major source of chromosomal re-arrangements and unscheduled recombination events (Zeman and Cimprich, 2014). Several studies have indicated that low-fidelity replication mechanisms can lead to toxicity and large-scale sequence rearrangements that contribute to a wide range of complex human genomic rearrangements, potentially resulting in cancer and premature ageing (Lee et al., 2007; Arlt et al., 2011; Zhang et al., 2009; Liu et al., 2011; Kastan, 2007). Studies have indicated that human pre-malignant lesions exhibit RS-associated DNA damage (Bartkova et al., 2005; Gorgoulis et al., 2005). This suggests that RS is a major source of the mutations that are associated with cancer initiation and tumourigenesis (Bartek et al., 2007; Halazonetis et al., 2008).

It has been recognised that DSBs function as both initiators and intermediates of a wide range of chromosomal rearrangements. However, it was hypothesised that broken RFs (se-DSBs) might be considered more genotoxic than the direct DSBs, posing resolution problems in the absence of a second DSB-end. Subsequently, may anneal to another sequence in the genome leading to unscheduled events of genomic rearrangements (Figure 5.1) (Cobb et al., 2005). Moreover, difficulties may arise when attempting to simultaneously repair several se-DSBs on replicating chromosomes. The failure to repair this type of RS threatens genome stability and may result in tumorigenic translocations and various other types of mutations (Zhang et al., 2009). Concordantly, if these DNA breakages are incorrectly repaired by HR and NHEJ repair mechanisms, these lesions may lead to the loss of genetic information, the accumulation of point mutations or may pose a serious threat to chromosomal translocations. When a cell continues to divide, the broken chromosome fragments will missegregate, leading to aneuploidy (Gelot et al., 2015).

There is strong evidence linking se-DSBs with several cancer-associated mutations, including translocation, CNV and LOH (Burrell et al., 2013; Peto, 2001; Sakofsky et al., 2012). Collectively, these studies serve to highlight how critical it is to understand the molecular events surrounding RS. The presence of an unrepaired DSB or se-DSB poses a hazard to genomic integrity and can trigger the DDR, resulting in cell cycle arrest, cell death or hereditary changes if DDR is ineffective at counteracting the damage (Jackson and Bartek, 2009).

The aim of this chapter was to facilitate the direct study of phenotypic and genotypic comparison between the induced DSB and BF. The primary objective was to understand the phenotypic effects of the induced FRT-FLP system, to initiate the generation of either a DSB or a BF, to establish whether se-DSBs are more cytotoxic than the direct DSBs. This involved conducting genome stability assays, such as viability assays. The secondary objective was to assess the genotoxicity of the induced se-DSBs in causing mutations relative to direct DSB.

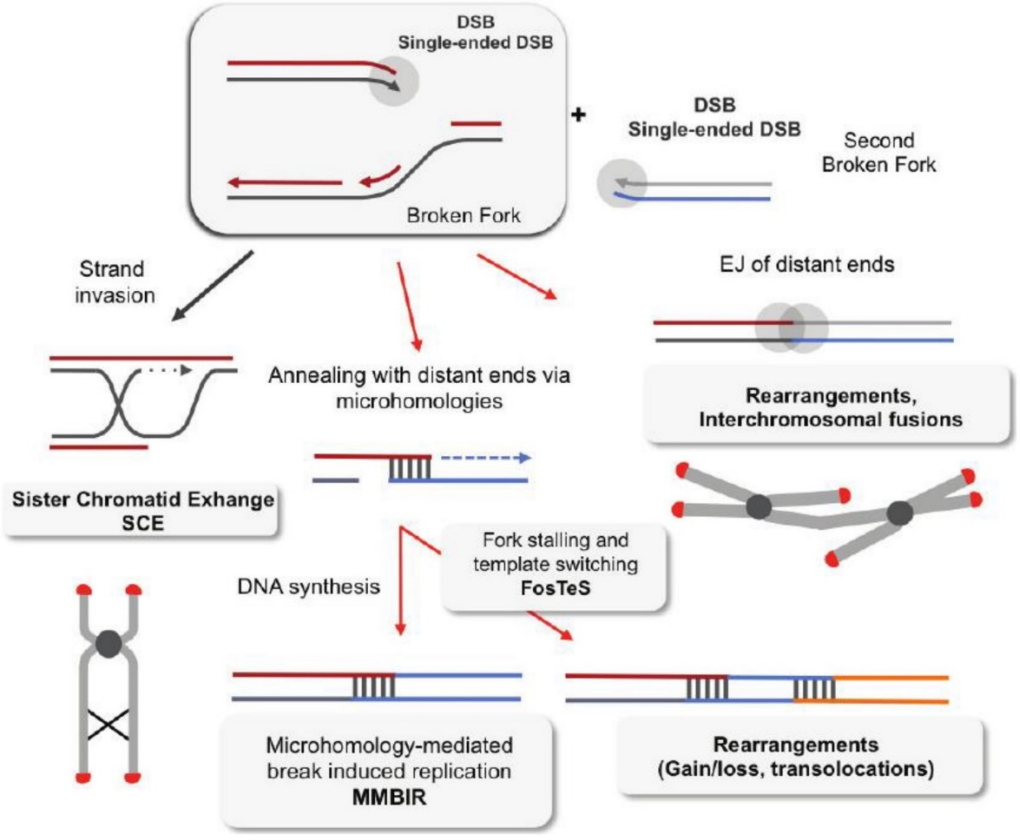

Figure 5.1 proposed consequences of se-DSB generated by replication stress. Se-DSB may repaired by strand invasion leading to sister chromatid exchange. Se-DSB may anneal to another distant se-DSB leading to complex chromosomal rearrangements such as translocation. The annealing of two distal se-DSB by c-NHEJ or A-NHEJ lead to dicentric chromosome formation such as intrachromosomal fusion. (Adapted from Gelot et al., 2015).

5.2 Results

5.2.1 Characterization of phenotypes induced by broken RFs vs. direct DSBs

This section examines the phenotypic differences induced by se-DSBs and DSB (Figure 5.2). This was accomplished by using the following assays: cell cycle changes analysed by flow cytometry, cell viability and the clonogenic survival assay.

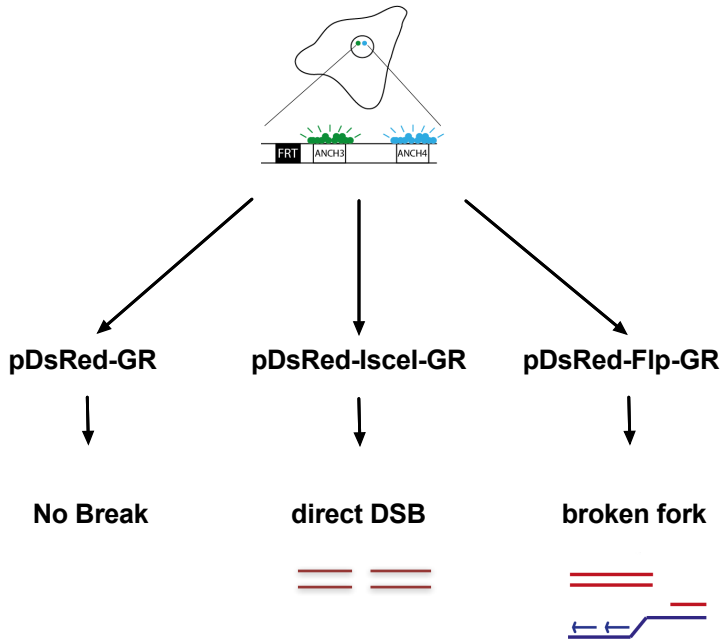

Figure 5.2 Scheme elucidating the induction of various forms of replication stress in a living cell. FRT stable cell lines were generated and transeintly transfected with different expression plasmids; the pdsRed-GR empty vector was used as a negative control where no DNA break will be generated ; transfecting the cells with the pdsRed-I-SceI-GR will generate a direct DSB in the integrated Isce-I endonuclease site, transfecting the cells with pdsRed-FLP-GR will generate a stable SSB in the integrated FRT site and that leads to a broken Fork (se-DSB) upon collision with a DNA replication fork (Nielsen et al., 2009).

5.2.1.1 Evaluation of cell cycle progression of broken RF versus direct DSB

Several studies have concluded that inducing a single DNA DSB is sufficient to cause cell cycle arrest in yeast (Sandell and Zakian, 1993; Nielsen et al., 2009). In order to examine whether an induced DSB or BF (assuming at this point that FLP binds to FRT and leads to se-DSB generation upon replication) caused an alteration in the cell cycle profile in the generated HEK293-FRT cells. HEK293-FRT cells were transiently transfected with pdsRed-*I-Sce*I-GR and pdsRed-FLPH305L-GR in the presence or absence of TA, respectively.

Non-transfected cells were used as a negative control, and cells transfected with dsRed-GR (mock) served as another negative control in order to determine any unexpected non-specific effects of dsRed-GR re-localization.

Figure 5.3 shows the cell cycle distribution 48 hours after TA addition, which would be long enough for all cells in culture to enter S-phase. Overall, the induced DSB or se-DSB did not show any significant changes in cell cycle profile compared to the un-transfected cells in the presence or absence of TA.

Un-transfected cells had a lower percentage of cells in the G0/G1 phase (61.403±3.942%) when compared with the control groups (GR-only mock cells) (62.8±6.1% in G0/G1), the generated DSB cells (65.5±5.4% in G0/G1), or the induced BFs cells (66.0±6.5% in G0/G1) (see Table 5.1). This suggests that transfection of the HEK293-FRT cells with dsRed-GR, dsRed-I-SceI-GR or dsRed-Flp-GR induces a small increase in cells at the G0/G1 phase. However, the increase was more pronounced in I-SceI- and FLP- transfected cells than the GR-mock transfected cells.

In the untransfected samples, there was a small TA-induced increase in G0/G1 cells (approximatly 1%). Whereas, there was only a 8% increase in the number of cells in the G0/G1 phase for the control cells (cells transfected with dsRed-GR) post-TA addition, the number of cells in the G0/G1 phase rose only from 65.5±5.4% to 68.8±3.4% in dsRed-I-SceI-GR, and from 66.0±6.5% to 68.7±3.5% in dsRed-Flp-GR in cells treated with TA (Figure 5.4). This confirms that TA addition did not have a major effect on the cell cycle profile (as observed in Figure 4.10).

On the other hand, in the absence of TA the un-transfected cells had a similar percentage of cells in the S-phase (30.4±2.3) when compared with other control groups (30.8±8.5 %). However, a reduction in the percentages were observed compared with the GR-only generated DSB cells (28.3±7.0 % in S) and induced BFs cells (26.3±7.5 % in S).

Collectively, these results indicate that induced DNA damage (either a DSB or BF) in HEK293-FRT cells slightly altered, but produced no noticable changes to cell cycle progression at the G0/G1 phase, or cell cycle arrest, in comparison to the GR-mock transfected cells and thus, might not inhibit cell proliferation.

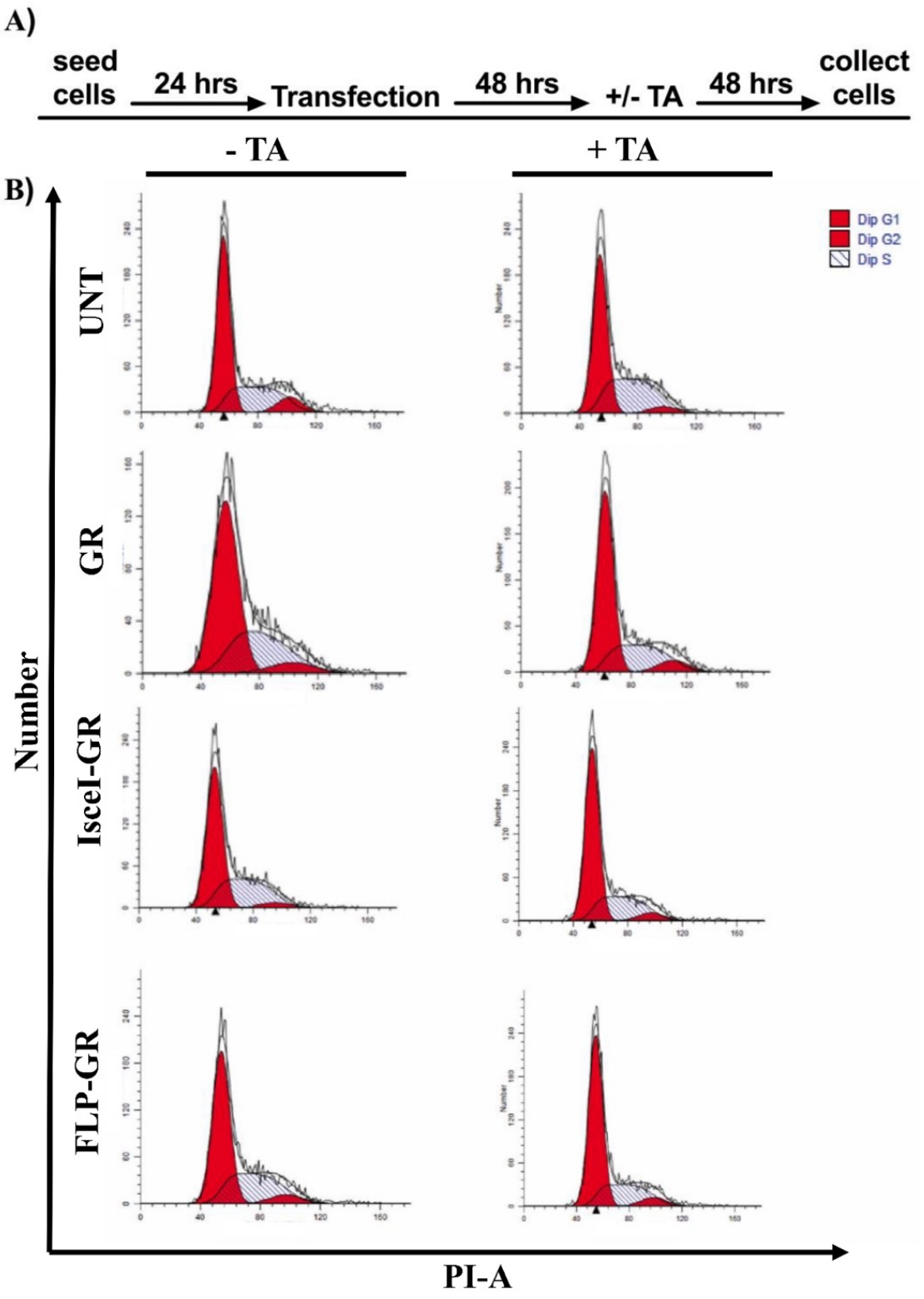

Figure 5.3 Cell cycle distribution of direct DSB versus Broken Fork. Flow cytometric analysis of cells transiently transfected with pdsRed-GR, pdsRed-I-SceI-GR and pdsRed-FLPH305L-GR in the presence or absence of TA for 48 hr. Cells were collected by centrifugation, ethanol fixed, and stained with propidium iodide (PI). The DNA contents were determined using the Aria FACS flow cytometry system and cell cycle distribution analysed with the MODFIT Program, n=3.

Table 5.1 Percentage of cell cycle distribution of direct DSB versus Broken Fork. [a]

	G1 (%)	S (%)	G2 (%)
Nocodazole	4.5±3.9	30.6±6.2	64.7±7.3
UNT-TA	61.4±2.5	30.4±2.3	8.1±1.1
UNT+TA	62.4±6.3	30.9±8.5	6.6±2.2
Mock-TA	62.8±6.1	30.8±8.5	6.2±2.6
Mock+TA	68.0±4.9	25.4±4.4	6.5±0.9
I-SceI-TA	65.5±5.4	28.3±7.0	6.1±2.0
I-SceI+TA	68.8±3.4	23.4±5.5	7.7±2.1
FLp-TA	66.0±6.5	26.3±7.5	7.6±1.5
FLP+TA	68.7±3.5	23.5±4.5	7.6±1.2

[a] Data represented as mean ± Standard deviation for three independent experiments. UNT, un-transfected. Mock, pdsRed-GR.

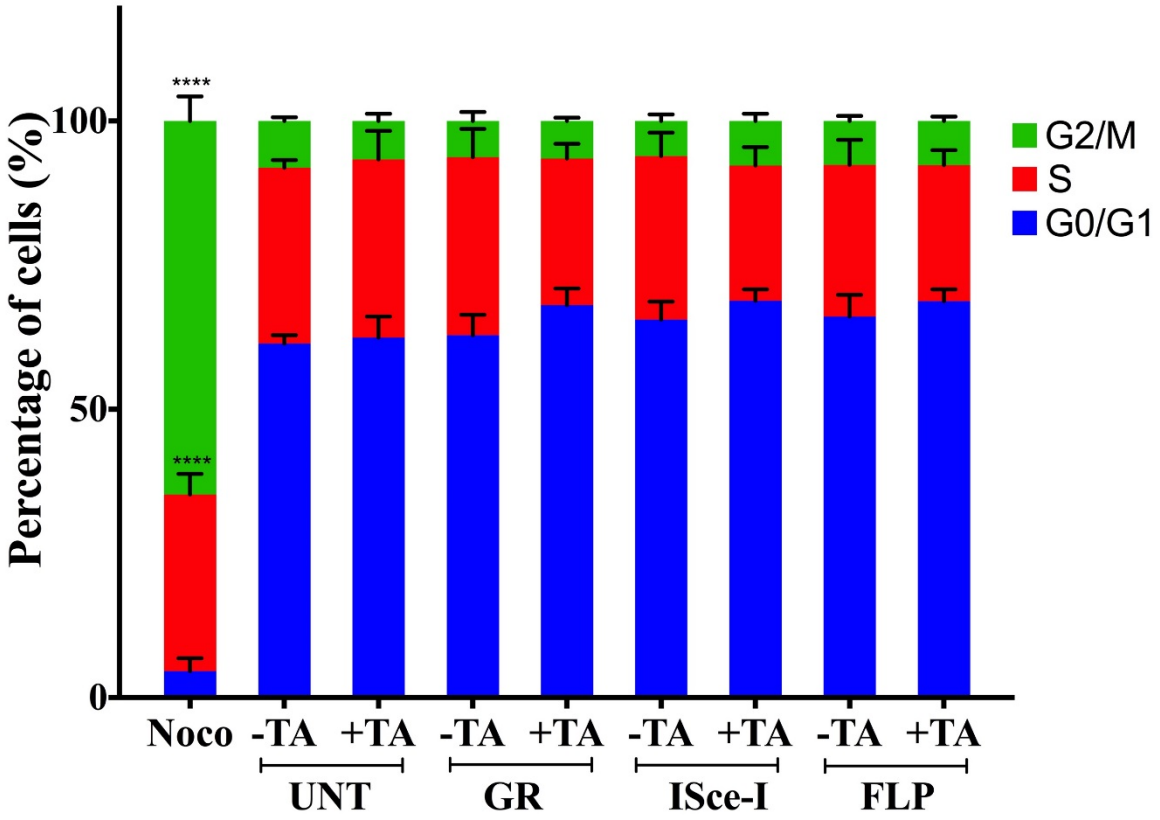

Figure 5.4 Analysis of cell cycle distribution under direct DSB versus Broken Fork. HEK293-FRT cells transiently transfected with pdsRed-GR, pdsRed-I-SceI-GR or pdsRed-FLPH305L-GR in the presence or absence of TA for 48 hr. Cells were collected by centrifugation and stained with propidium iodide (PI). Data was plotted on a bar chart G0/G1 (blue bars), S (red bars) and G2/M (green bars), mean and S.D for three independent experiments. The asterisks indicate a significant difference relative to the corresponding un-treated controls (****P<0.0001).

5.2.1.2 Assessing the cytotoxicity of the inducible broken RF vs. direct DSB

As the inducible DSB and RS did not induce an alteration in cell cycle progression, it was of interest to investigate the effect of the generated DNA damage on cell proliferation. Determining changes in cell proliferation following the induction of a BF or DSB would allow direct assessment of which was the most cytotoxic. The premixed WST-1 (Water-soluble Tetrazolium salts) cell proliferation reagent, in particular (2-methoxy-4-nitrophenyl)-3-(4-nitrophenyl)-5-(2,4-disulfophenyl)-2H-tetrazolium was used.

The WST-1 assay offers several advantages, including the convenience of adding the reagent directly to the cell culture for a simple colourimetric measurement of cell proliferation, yielding higher accuracy and sensitivity when measuring the viability of the cell in a 96-well format. The absorbance values (OD) are dependent on several parameters; such as the length of the incubation time, and the number of viable cells seeded. When considering all previous parameters, preliminary optimization experiments using the WST-1 reagent were carried out to identify the best cell number to plate in a 96-well plate, and to determine the optimal incubation time following the addition of the cell proliferation reagent. This was achieved by seeding a different number of cells in the 96-well plate and incubating them for five days before repeatedly measuring absorbance at different time points. Figure 5.5 shows the identification of the appropriate cell density and incubation time. According to the manufacturer's instructions, the absorbance values ranging between (0.5-1.8) were considered as appropriate measures. Thereby, it was revealed that 10,000 cells/well is an optimal cell seeding density for any incubation time period of WST-1 reagent. Indeed, no marked difference was identified between the readings after 30 minutes or one hour. It was observed that a longer incubation time of between two and four hours causes colour to deepen, thus increasing the absorbance readings above 1.8, which is too high, resulting in inaccurate readings.

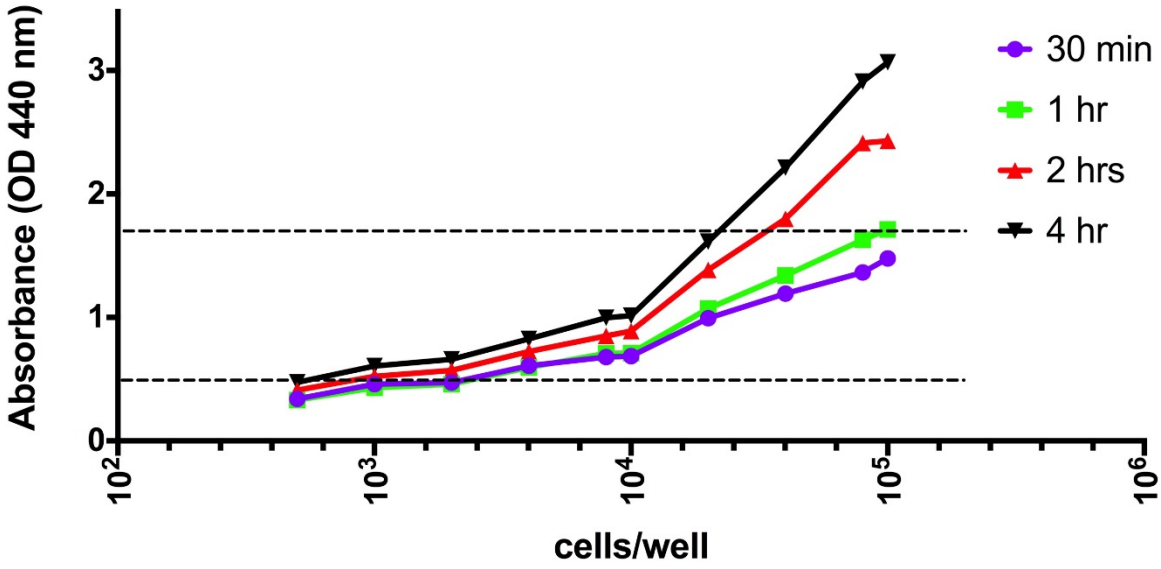

Figure 5.5 Determination of optimal cell seeding density and incubation time period of WST-1 proliferation reagent in HEK293 cells. HEK293-FRT cells were seeded in different densities in 96-well plates and allowed to grow in corresponding culture media for 5 days. Serial sample measurements of absorbance (0.5, 1, 2, 3, and 4 h) were determined against a blank control background after the addition of WST-1 reagent, using plate reader at 440 nm wavelength.

To determine changes in cell proliferation following the induction of a BF or DSB, HEK293-FRT and U2OS-FRT, cells were transiently transfected with dsRed-GR, pdsRed-I-SceI-GR or pdsRed-FLP-GR over a 48-hour period. As transfection efficiency varied according to the plasmid used, transfection was followed by FACS to isolate transfected cells expressing the RFP (Figure 5.6). An equal number of transfected cells (10,000 cells/well) were reseeded in flat 96-well plates and allowed to adhere for 48 hours.

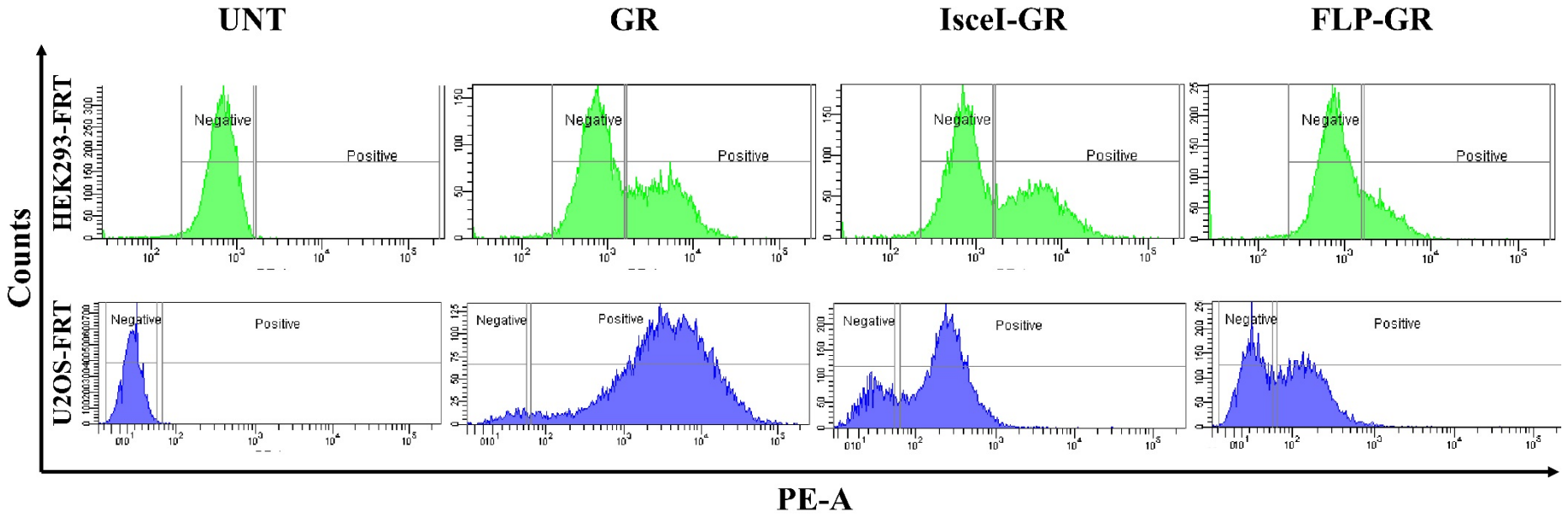

Figure 5.6 Transfection efficiency followed by FACS sorting. (A) HEK293-FRT-ANCH34 (cl.9), **(B)** U2OS-FRT-ANCH34 (cl.1.1).

GR, I-SceI and FLP were relocalized to the nucleus by adding TA for 48 hours to generate direct DSB or BF, respectively. WST-1 was employed to test viable cells, and cell viability was quantified by measuring absorbance after one hour of incubation at λ=440 nm (figure 5.7).

The cell viability for the induced direct DSB versus BF for HEK293-FRT cells is shown in Figure 5.7.A. It was observed that cells transfected with DNA damage-inducible plasmids (dsRed-I-SceI-GR and dsRed-FLP-GR), followed by 48 hours treatment with TA induced a decrease in cell viability to 76.6% and 71.1% for I-SceI- and FLP- cells respectively, compared to an un-transfected control sample.

A slight reduction in cell viability was also noticed in GR empty vector transfected cells, suggesting that HEK293-FRT cells are sensitive to TA or its induction of GR movement into the nucleus. The reduction in cell viability for I-SceI-transfected cells after adding the TA was not significant. However, FLP-transfected cells showed a significant reduction of cell viability after inducing the RS by adding TA (P-value=0.0026). The results show that cells with BFs displayed a significant reduction in cell viability, and that BFs may be more cytotoxic compared to direct DSB in HEK293 cells.

Figure 5.7.B shows the relative cell viability data for direct DSB versus BF in U2OS-FRT cells. TA induced loss of viability in all samples, but overall, there was no evidence that induced DNA damage had a statistically significant effect on cell viability. Nonetheless, a slight reduction in viability of I-SceI-transfected cells upon TA addition (62.9%) was noted in comparison to un-transfected, GR- only and FLP- transfected cells. This indicates that se-DSB are not cytotoxic in U2OS cells but DSB are slightly cytotoxic.

The differences between the observation in HEK293 and U2OS cells may be due to their different genetic backgrounds and suggest different cancers are differentially sensitive to different types of DNA damage (Further details in Section 5.3).

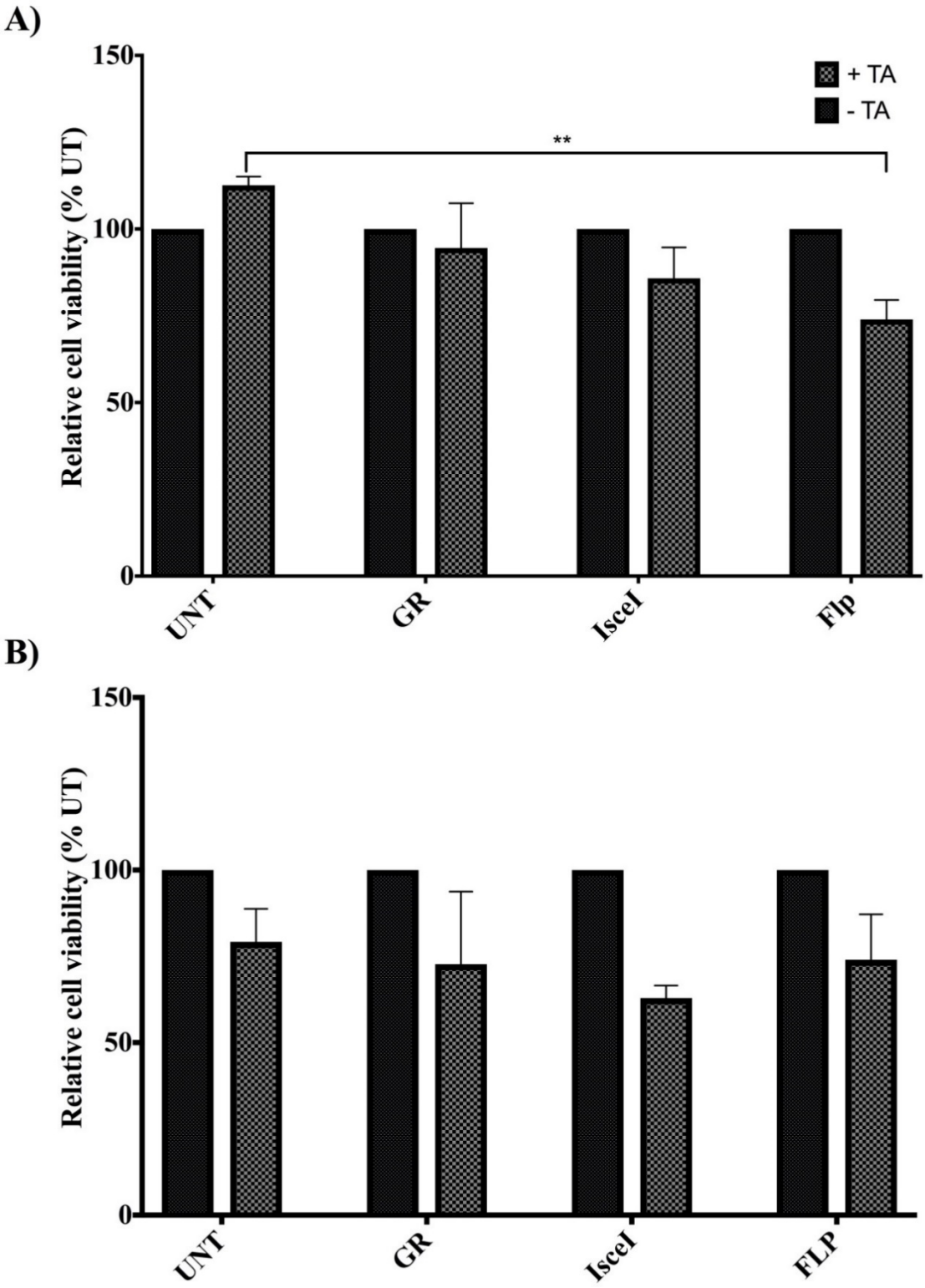

Figure 5.7 Quantification of cell viability for direct DBS versus Broken fork. The WST-1 assay on un-transfected HEK293-FRT cells (UNT), or cells transiently transfected for 48 hours with dsRed-GR, dsRed-I-SceI-GR or dsRed-FLPh305L-GR. Analysis of relative cell viability to corresponding –TA samples. **(A)** HEK293-FRT cell line (cl.9). The data shown represents the mean ± SD, as calculated in seven independent experiments. **(B)** U2OS-FRT. The data shown represents the mean ± SD, as calculated in three independent experiments. The asterisks indicate a significant difference relative to the corresponding un-transfected +TA control P-value=0.0026.

5.2.1.3 Determination the effect of broken RFs vs. direct DSBs on colony forming ability

To assess the cytotoxicity of BFs and DSBs using an alternative assay, colony formation ability (CFA) was analysed to quantify cell survival. HEK293-FRT and U2OS-FRT cells were transiently transfected using the dsRed-I-SceI-GR or dsRed-FLPH305L-GR constructs for 48 hours. Un-transfected cells and cells transfected with the mock pdsRed-GR acted as suitable excellent negative controls. The optimal cell number to seed in each well of the 6-well plate and the requisite incubation time for cells to attach was optimized.

CFA was analysed, as described in Section 2.5.8. Briefly, an equal number (3000 cells/well) of FACS-sorted cells were plated in triplicate wells in a 6-well plate for 48 hours. Quantification was performed following DSB or RS induction by adding TA for 48 hours prior to continuously incubation in a new fresh medium for 10–14 days. Visible colonies comprising at least 50 cells/colony were counted using a macro I created in ImageJ (Figure 2.1).

Figure 5.8 shows the CFA of HEK293-FRT cells after transfection with GR, I-SceI and FLP. Overall, there was a reduction in the percentage in the plating efficiency (PE) of the transfected cells relative to un-transfected cells. A slight reduction in PE and cell survival was observed in cells transfected with mock GR plasmid (16%) relative to the un-transfected cells (20%), indicating that cells are sensitive to the transfection reagent itself and that the intake of plasmids might be slightly toxic to cell proliferation. The percentage of the PE of the un-transfected cells decreased by 2% after the addition of TA, while it increased in GR control cells from 16% to 18%. Due to the transfection toxicity, cells transfected with GR empty vector were used as a negative control, since these cells were considered to constitute a more accurate control than the un-transfected cells as assesses not specific effects of GR movement, although all samples were handled in parallel in the subsequent experiments.

In the absence of TA, the percentage of PE was reduced in FRT-I-SceI (12.6 %) and FRT-Flp (8.6 %) cells compared to GR mock cells (16%), suggesting that inducible DNA damage reduces HEK293 cells' proliferation capacity. However, the reduction in viability observed in I-SceI- or FLP- transfected cells in the absence of TA may be due to the slight leakiness of the system, as discussed previously in Chapter 4, meaning DSBs and BFs are generated even without TA.

Even though the CFA of the FLP- transfected cells that generate BF was significantly reduced following treatment with TA (P-value=0.0416). However, no significant reduction was observed in I-SceI-transfected cells preior- or post-TA addition. These results correspond with the cell viability data, and indicate that the induction of BF is more cytotoxic to cells than to the direct-DSB.

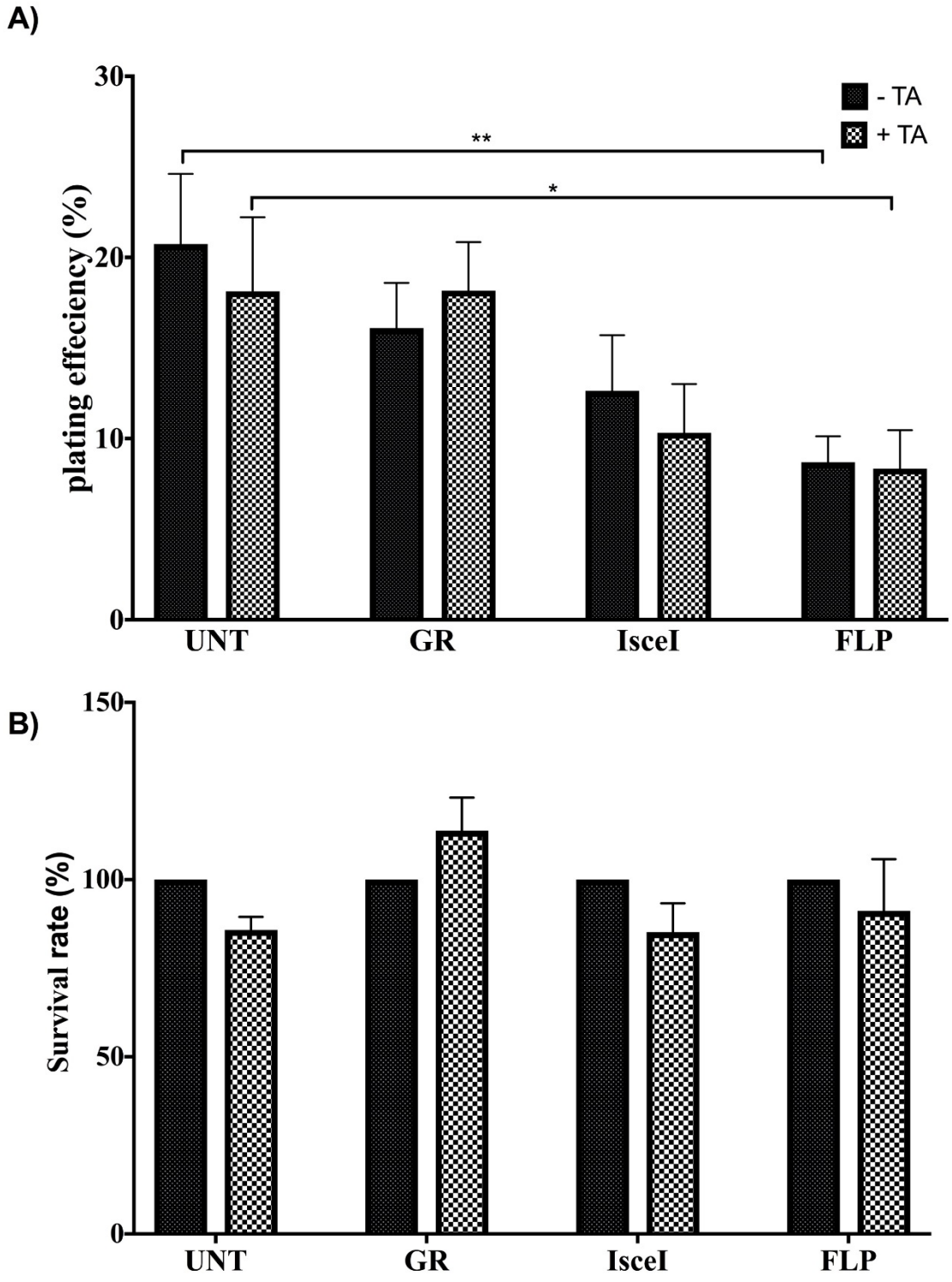

Figure 5.8 Colony formation ability following the induction of direct DSB or broken fork in HEK293-FRT. Cells transiently transfected with pdsRed-GR, pdsRed-I-SceI-GR and pdsRed-FLP-GR in the absence or presence of 100nM TA for 48 hours relative to untransfected cells. **(A)** Analysis of the plating efficiency for FRT-I-SceI and FRT-FLP cells, before and after TA addition. **(B)** Analysis of the survival rate of TA-treated cells. Data shows the mean ± SD of seven independent experiments normalized to corresponding no TA samples. The asterisks indicate a significant difference relative to the corresponding un-transfected control (**P<0.01, and *P<0.05).

Figure 5.9 represents the CFA of the induced direct-DSB or BF in U2OS-FRT cells. A slight reduction (1%) in PE was observed in cells transfected with mock GR plasmid (9 %) compared to the un-transfected cells (10.5 %) in the absence of TA. This compatible with the results obtained using HEK293-FRT cells and confirming that transfection reagent slightly increases the toxicity of the cells. Similar to the HEK293-FRT cells, there was a reduction in the percentage of the PE of I-SceI- or FLP- transfected cells relative to un-transfected cells, though not statistically significant. In the absence of TA, the percentage of PE was remarkably lower in I-SceI (5.3%) and FlP (4.7%) cells in comparison to GR mock cells.

However, post 48-hour exposure to TA revealed that the PE of I-SceI and FLP cells was suppressed to 2.5% and 2.9% respectively (Figure 5.9). This shows that induced DSB and BF are cytotoxic for the cells relative to GR-mock transfected cells. However, the induction of direct-DSB was more cytotoxic to U2OS-FRT cells than to the BF.

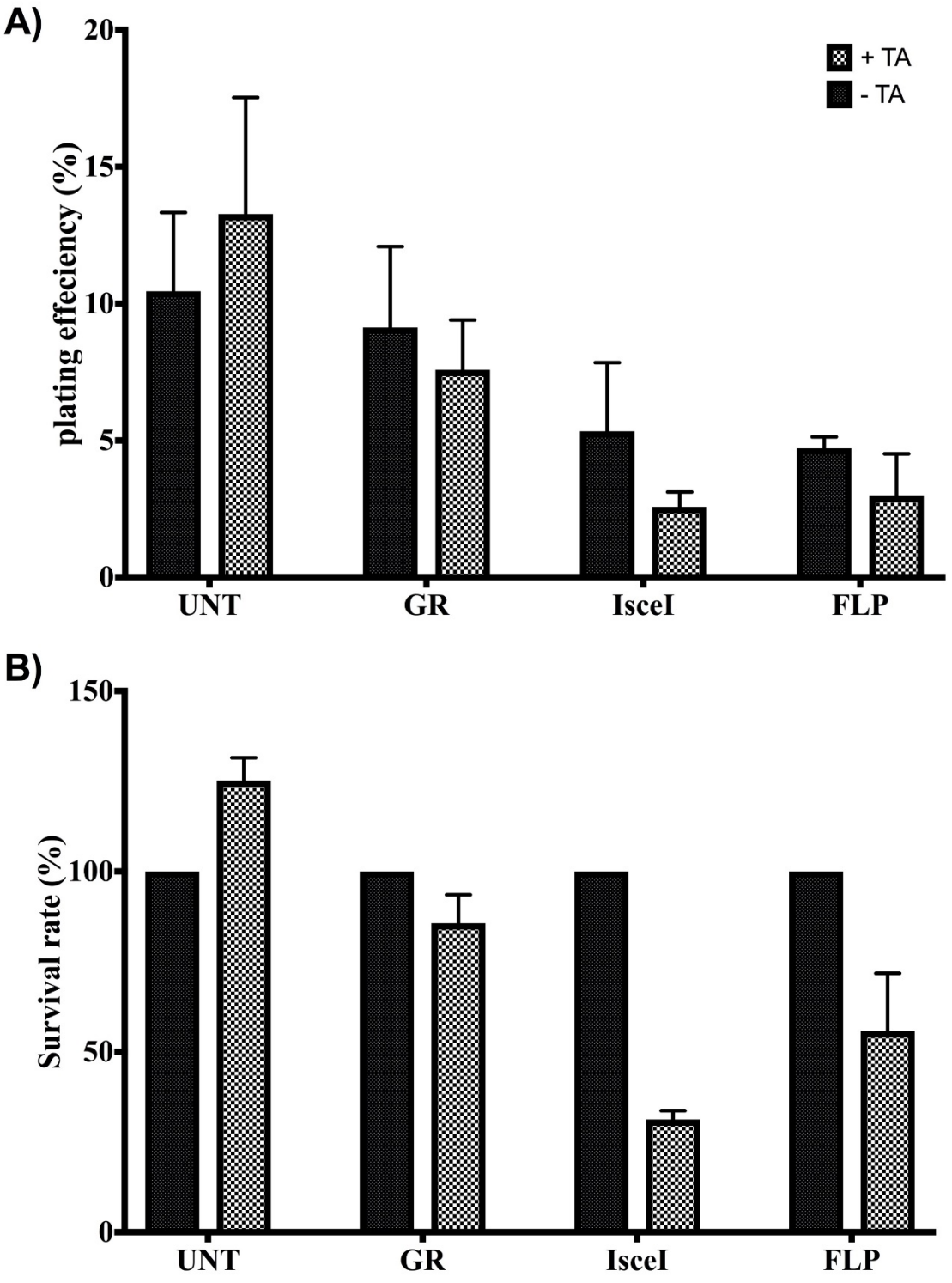

Figure 5.9 Colony formation ability following the induction of a direct DSB or broken fork in U2OS-FRT. Cells transiently transfected with pdsRed-GR, pdsRed-I-SceI-GR and pdsRed-FLP-GR in the absence or presence of 100 nM TA for 48 hours relative to untransfected cells. **(A)** Analysis of the plating efficiency for FRT-I-SceI and FRT-FLP cells, before and after TA addition. **(B)** Analysis of the survival rate and of TA-treated cells. Data shows the mean ± SD of three independent experiments normalized to corresponding no TA samples.

5.2.2 Assessing the genotoxicity of FLP-induced RS relative to direct DSB

DSBs leading to indel mutations (for example base substitutions, short heterogeneous insertions and deletions of a few nucleotides) is generally associated with replication errors, impairment of BER, mismatch repair (MMR) and/or NHEJ repair mechanisms (Zhang et al., 2009). A heteroduplex nuclease cleavage detection assay is commonly used assay to detect Indel mutations induced by CRISPR cas9-mediated DSBs (Ran et al., 2013).

To confirm and detect the heteroduplex formed by a mismatch of specifically introduced DSB or se-DSB of genomic DNA, surveyor nuclease assay was adapted. The GeneArt® Genomic Cleavage Detection Kit was used, and HEK293-FRT-ANCH3-4 cells were transiently transfected with constructs expressing either GR, I-SceI or FLP for 48 hours. The transfected cells were FACS-sorted, and the pooled cells were used for two different approaches. The first approach was referred to as 'early time detection'. The cells were seeded in a 96-well plate, and TA was added for 48 hours before cells were collected. At least 50,000 cells were collected immediately after incubation. The second approach, however, was referred to as 'late time detection'. The sorted cells were seeded into a 96-well plate and stimulated with TA for 48 hours. The cells were then expanded into a 6-well plate and cultured in TA-free media for a week before being collected for analysis.

PCR reactions were initially performed to amplify the locus around the site-specific DSB or BF prior to mismatch detection. The gDNA was extracted from the collected population of cells using a cell lysis buffer. An optimal amplification was achieved by using a manually designed pair of primers that flanked either the FRT or I-SceI sites. Figure 5.10 shows the schematic of the PCR primers that were designed to ensure optimal amplification and subsequent efficient cleavage detection. The primers were 20 bp in length and had a GC content of 60%. The primers were designed to yield total amplicon lengths of 547 bp (FRT) and 639 bp (I-SceI). To allow clear visualisation of two distinct cleaved bands, the potential cleavage site (i.e. where FRT and I-SceI sites are) was not in the centre of the amplicon. It was expected that the I-SceI amplicon would reveal 362 and 277 bp fragments and the FRT amplicon would reveal 483 and 114 bp bands. Candidate primers were tested using the NCBI Primer-BLAST in order to avoid nonspecific amplification.

To increase the annealing specificity of the selected primers, a gradient PCR was conducted to determine the optimal melting temperature for each pair of primers (data not shown). The temperature for primers flanking the I-SceI site (IsceI-FP and IsceI-RP) was 65°C, and the temperature for the FRT primers (406-FP and FRT-RP2) was 61°C.

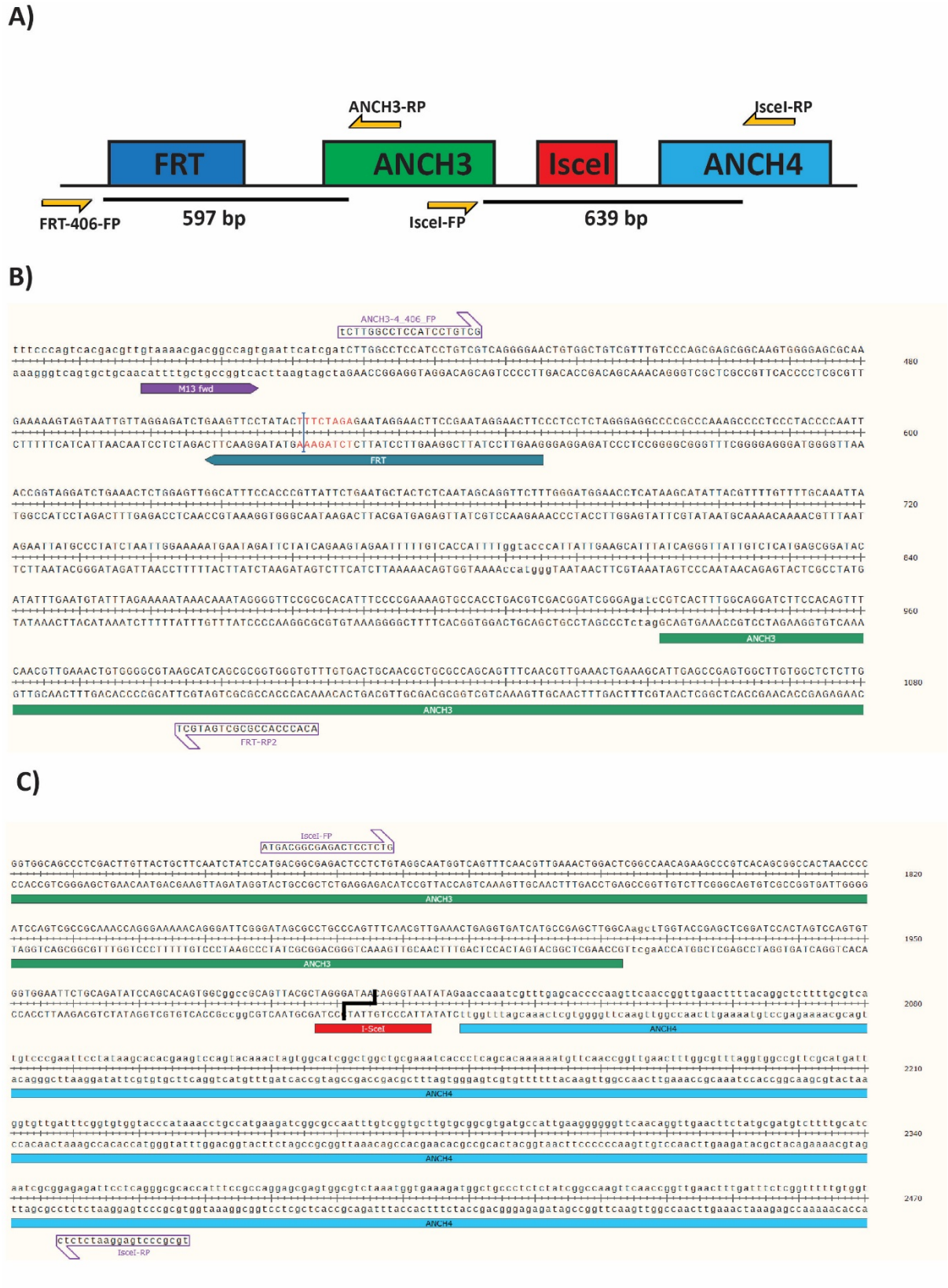

Figure 5.10 Schematic of the designed PCR primers used for cleavage detection. (A) FRT-406_FP and ANCH3-RP were used to amplify the FRT site. IsceI-FP and IsceI-RP were used to amplify the I-SceI site. **(B)** The annotation of the FRT primers; the cut site within the FRT sequence is highlighted in red**. (C)** The annotation of the I-SceI amplicon and the location of IsceI primers; the black line shows the cut site within the I-SceI sequence.

Single PCR products with the expected size was successfully produced. The IsceI primers generated a band of 639 bp and the FRT generated an amplicon of 597 bp (Figures 5.11. A and B). To obtain accurate cleavage detection, 100 ng of the amplified PCR product from both early and late detection times was used in the cleavage assay following purification using magnetic beads. The PCR product was denatured and randomly re-annealed in order to generate heterogeneous DNA duplexes containing mismatches. To identify genomic insertions, deletions or mismatched DNA created by the cellular repair mechanisms at the point of the mutation, the annealed heteroduplex DNA was subsequently digested by a mismatch specific endonuclease.

Figures 5.11.A shows the resultant bands for the early detection time by gel electrophoresis. The location of the mutation was inferred by observing fragments after cleavage. It was observed that the I-SceI cell line had two distinct band (277 bp and 362 bp) bands when using the IsceI-primers, demonstrating there were mismatches within the PCR products and strongly indicating mutations were present that might arise from misrepair of I-SceI-induced DSB. Cleavage fragments were detected even in the absence of TA (though not as much as in the presence of TA), suggesting DSB were induced even when system was OFF, confirming some leakiness as suspected from previous validation work (Chapter 4). As expected, no bands observed in GR control or FLP transfected cells. Digestion of the positive control template and primers produced two cleavage products that were 225 and 291 bp in size, confirming the endonuclease activity was present. As shown in Figure 5.11.B, no cleaved bands were detectable in the FLPH305L cell lines when using FRT primers, indicating mutations were not present. A similar result was observed for late detection samples (Figure 5.12). Collectively, these results suggest that Indel mutations were induced by I-SceI expression (DSB) but not FLP.

To determine the relative proportion of cleaved DNA for the I-SceI cell line, gel analysis software was used to quantify the density contained in each band. The cleavage efficiency was calculated by using the following equation: Cleavage Efficiency = 1 – [(1–fraction cleaved) $^{1/2}$] × 100%, where the fraction Cleaved = sum of cleaved band intensities/(sum of the cleaved and parental band intensities). Overall, it was estimated that the cleavage efficiency for the early detection time was 3% higher than the late detection time point.

In was revealed that in the early detection time the cleavage efficiency was 15 % and 17 % in the absence and presence of TA, respictevly. Whereas, in the late detection time point the efficency was 11.6 % and 13.7 % in the absence and presence of TA, respectively.

To confirm mutations were generated in these I-SceI samples, the amplicons were Sanger-sequenced, as mutations would expect to lead to complex peak patterns at I-SceI site. Small additional peaks were possibly present around the breakage site in the I-SceI samples compared to the untransfected cells sequence. However, it was difficult to assess if these were real differences as the addition peak was very small. This probably due to the low cleavage percentage from the mismatch assay, where 90% of the signal was wild type, while less 10% was repaired with errors (Figure 5.13).

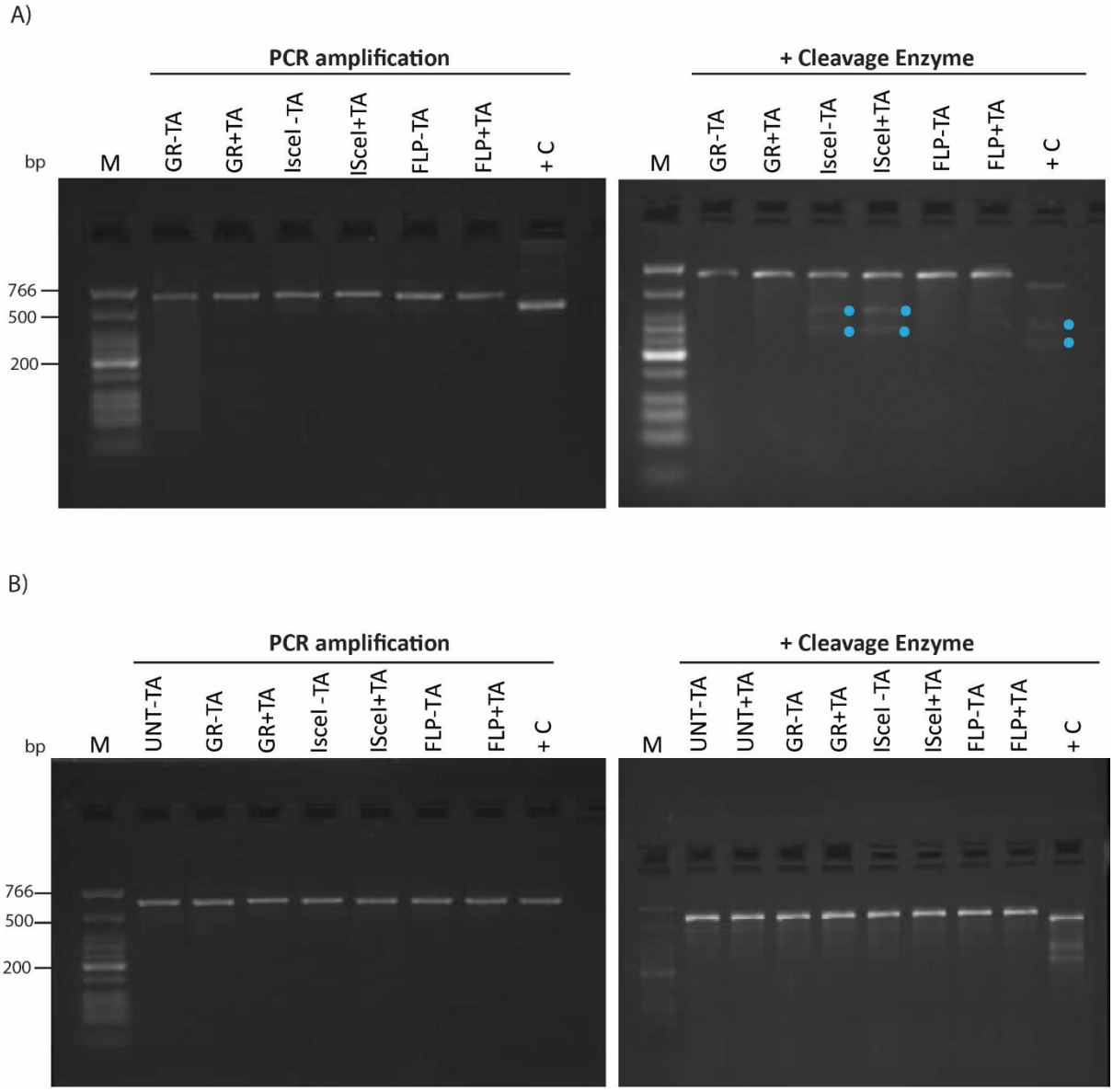

Figure 5.11 Genomic Cleavage Detection Assay for the early detection time. HEK293-FRT cells were transfected with I-SceI or FLP using a FUGEN transfection reagent. A negative control sample for cleavage was also prepared by transfecting the cells with a GR mock plasmid. Sorted cells were treated with or without TA for 48 hours to mediate the generation of DSB or BF. **(A)** A gel image of PCR amplification using a set of primers flanking the I-SceI site. After re-annealing, samples were treated with a cleavage enzyme and run on a 2.5% agarose gel. **(B)** A gel image of PCR amplification using a set of primers flanking the FRT site. After re-annealing, samples were treated with and without a detection enzyme and run on a 2.5% agarose gel. +C, positive control template and primers provided with the kit were used alongside the samples. Blue dots represent the cleaved fragment.

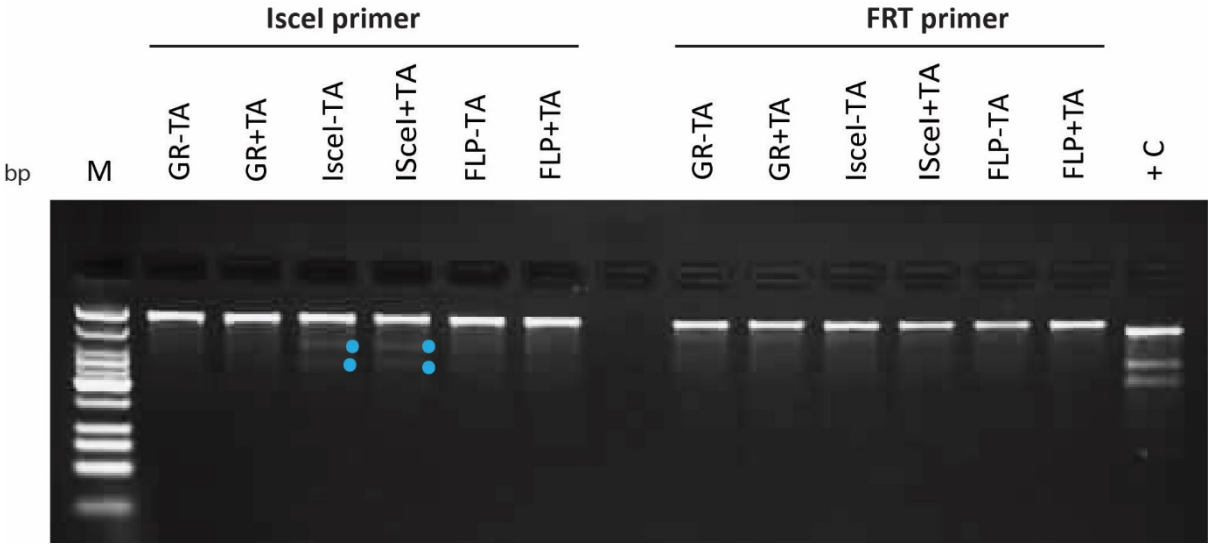

Figure 5.12 Genomic Cleavage Detection Assay for the late detection time. HEK293-FRT cells were transfected with I-SceI or FLP using a FUGEN transfection reagent. A negative control sample for cleavage was also prepared by transfecting it with a GR control. Sorted cells were treated with or without TA for 48 hours to mediate the generation of DSB or BF. Cells were cultured in TA-free media for one week. PCR amplification was conducted using a set of primers flanking either the I-SceI or FRT sites. After re-annealing, the samples were treated with cleavage enzyme and run on a 2.5% agarose gel. The +C, positive control template and primers provided with the kit were used in parallel to the samples. Blue dots represent the cleaved fragment.

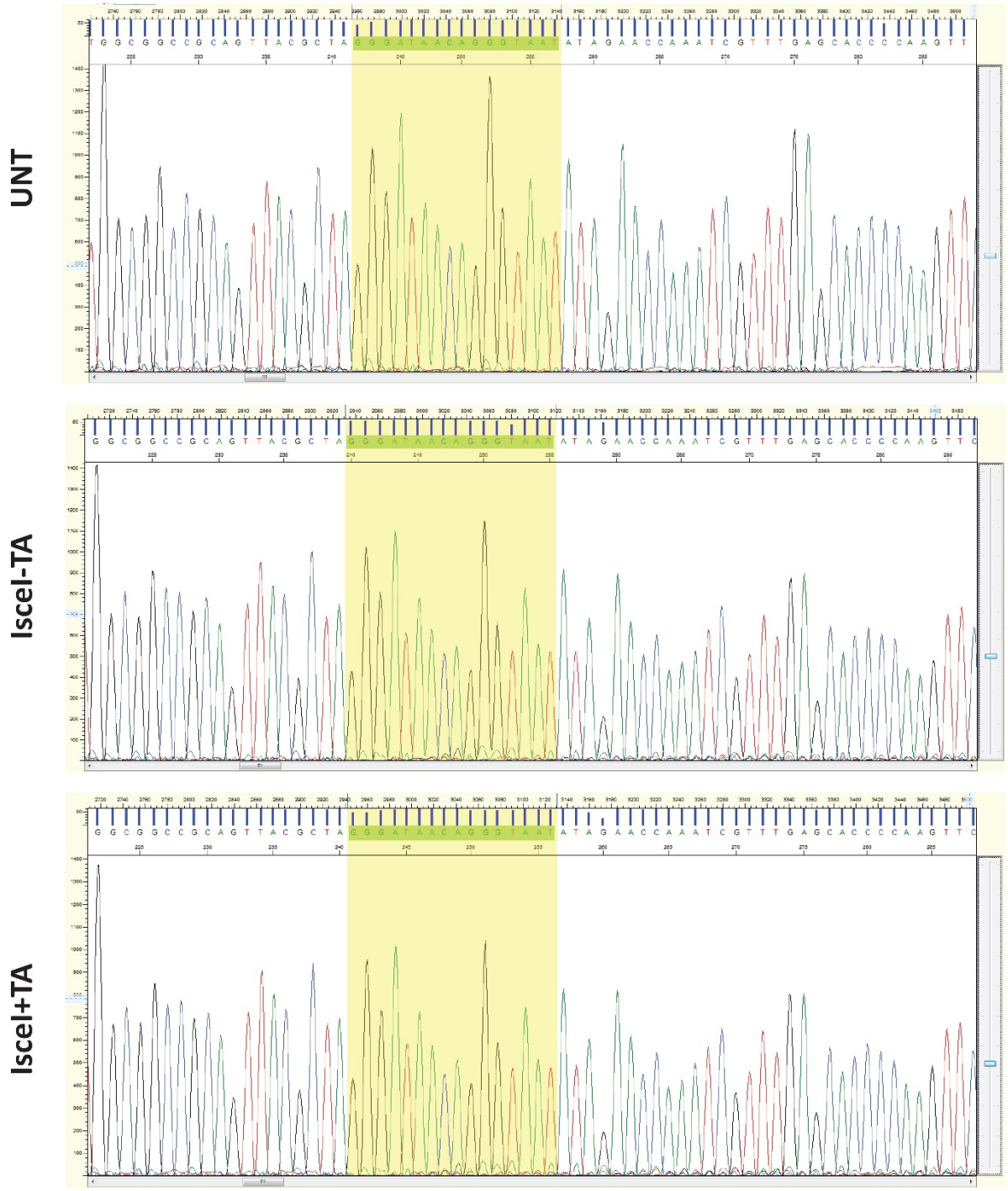

Figure 5.13 Detection of the mutations induced by I-SceI. An Electropherogram and Sequencing alignment of HEK293-FRT cells transfected with I-SceI in the absence or presence of TA.

5.3 Discussion

The majority of earlier studies characterized the phenotypic effect of direct DSBs on the cells of various organisms (Lemmens and Tijsterman, 2011). This was demonstrated using experimental external genotoxic agents or endonuclease agent to generate single DSB induction (Weinstock et al., 2008). These studies linked DSBs to GIN, the loss of cell viability and a predisposition to cancer. Moreover, they focused on understanding how cells respond to DSBs, providing a clearer understanding of how DNA DSBs are repaired, and the importance of DDR factors and their roles in different cellular events. The events surrounding the normal and aberrant processing of se-DSBs and their implications in cancer are very poorly defined due to the inability to know or precisely control where the forks break during genome replication.

This Chapter has demonstrated the phenotypic differences between BF generated by inducing the FRT-FLP system for the first time, and comparing it with direct-DSB generated by the expression of I-SceI endonuclease in stable FRT-HEK293 cells. The development of a FRT-FLP cell system was the first step towards directly studying diverse RS-associated processes in mammalian cells. As detailed in Chapter 3, this system allows for the regulation of the induction of DSBs or broken DNA RFs at specific genomic loci, with the addition of TA. However, the FRT-FLP system, while relying on a DSB, forms different damage to that created by the I-SceI endonuclease; it is cut so the DSB is replication-dependent and becomes one-sided owing to polymerase run off. This enabled analysis of the effects of these lesions on cell viability and genome stability. It is important to distinguish the consequences of structurally different DSBs generated by I-SceI induction that exposes two free DNA ends and replication-dependent se-DSBs generated by FLP induction.

Overall, there was no evidence that inducible DNA damage (either a DSB or BF) had a statistically significant effect on altering the cell cycle profile. This may indicate that the different generated RS-associated cell lines may not inhibit cell proliferation. Nevertheless, the colony formation results correspond with the cell viability data, and indicate that the induction of BF induced by FLP is more toxic to cells than to the direct-DSB induced by I-SceI. These phenotypic observations support the hypothesis of this study by suggesting that among the different damage types, generated BF insult is more toxic than the DNA DSB, and thus must be considered a deleterious threat to GIN.

A reduction in cell viability was found in the transfected cells compared to the un-transfected cells, suggesting that cells are sensitive to the transfection reagent itself and that the intake of plasmids might be slightly toxic to cell proliferation. Following the induction of a BFs or DSB systems, a significant reduction in cell viability was observed in FLP (cells harbouring BF), when compared to I-SceI (direct-DSB), thereby indicating greater cytotoxicity in HEK293-FRT. Despite the significant cytotoxicity of FLPH305L recombinase on HEK293-FRT cells, a slight reduction was observed in U2OS-FRT cells. The fact that growth differences were found indicates that FLp and I-SceI bind to the FRT and I-SceI sites respectively.

Furthermore, there was a significant reduction in the colony formation level of the generated DNA damage analysed by CFA, confirming that BFs are more cytotoxic than DSBs. The findings from the colony formation rate agree with the cell viability assay and both reveal a significant reduction in the proliferation of FRT-FlP cells in comparison with FRT-I-SceI cells. The fact that growth differences were observed in I-SceI- and FLP- transfected cells compared to FRT-GR cells in the absence of TA suggests that the system is slightly leaky, as previously speculated in Chapter 4, possibly indicating that the I-SceI endonuclease and Flp recombinase generated DSB and BF, respectively, in some cells even without TA. Despite the slight reduction in FRT-I-SceI and FRT-FLP cells before the addition of TA (system off), reduction was more pronounced post TA addition, indicating that Flp and I-SceI bind to FRT and I-SceI sites respectively. However, a comparison of the number of survival cells of direct-DSB (FRT-I-SceI cells) showed the difference was not significant in the presence or absence of TA (DSB-ON vs. DSB-Off). However, the CFA of the FRT-FLP cells that generate BF was significantly reduced post treatment with TA. In addition, these results suggest that after TA addition, FLp recombinase or IsceI endonuclease localizes from the cytoplasm to the nucleus, subsequently binding to the integrated FRT or I-SceI sites within the genome, generating a BF or a direct DSB respectively. This induced DNA damage was therefore expected to activate the DDR.

Collectively, the data suggests that a single se-DSB or direct- DSB are not sufficient to induce cell cycle arrest. Thus, contrasts with the effects on yeast (Sandell and Zakian, 1993; Nielsen et al., 2009). However, both lesions induce loss of cell viability. Whether a se-DSB or direct -DSB is the most cytotoxic may vary between different cell lines. This is likely due to genetic background differences, such as specific mutations/ DDR defects in specific cancer cell lines.

DSBs were confirmed to induce mutation as expected, surprisingly se-DSB did not induce detectable mutations, suggesting BFs are more readily repaired accurately relative to direct -DSB. Mutation occurred in the I-SceI break site, revealing two bands with the expected size, but not the FRT site. The PCR result using the I-SceI primers suggests that the cut was not followed by large insertions or deletions, but rather smaller mutation types since the amplicons reveal the same product size as control sampels. It was difficult to determine precisely the type of mutation due to the low cleavage percentage generated from DSB (10% of the cell population). These small mutations are likely generated due to the use of NHEJ repair (Vouillot et al., 2015). The NHEJ process is error-prone, often resulting in the introduction of mutations at the joining site (McVey and Lee, 2008; Shibata and Jeggo, 2014).

Paradoxically, the induced se-DSB did not appear to generate mutations, at least to a detectable level by the cleavage assay. The inability to detect mutations via cleavage assay for cells transfected with FLP can be explained by the fact that BF repair via a HR repair mechanism readily occurs, as previously hypothesised. Research has indicated that HR plays a crucial role in repairing and restarting se-DSBs that arise during aberrant DNA RF progression, including following collision with an SSB during the S-phase (Strumberg et al., 2000). Such se-DSBs can be repaired and synthesis restarted via a mechanism known as the break-induced replication mechanism (BIR) pathway of HR, and HR proteins may be required to facilitate correct pairing (Kraus et al., 2001; Michel et al., 2001). It is generally considered as error-free because HR requires sequence homology and uses the sister chromatid sequence to allow RF restart (Michel et al., 2001). The cellular responses to CPT-induced se-DSBs have been investigated in a range of model organisms, from yeast to humans; these studies have revealed the importance of HR in the repair of se-DSBs generated by Top1-mediated DNA damage (Arnaudeau et al., 2001; Pichierri et al., 2001). Even though the se-DSB can be preferentially repaired through the HR pathway, leading to the re-establishment of the DNA replication fork, the precise molecular mechanisms for the HR repair of se-DSB still remain largely unknown (Helleday, 2003).

In conclusion, the initial data in this Chapter provide evidence and suggests that se-DSB either lead to cell death or are repaired without error. The understanding of such RS-associated events (both normal and aberrant responses) is significant in revealing the genetic mechanisms of tumour initiation and progression.

Chapter 6: Identifying factors that influence genome stability and cell growth during DNA replication stress

6.1 Introduction

In response to aberrant RFs and DSBs, cells activate the DDR (Jossen and Bermejo, 2013). As discussed in Chapter 1 (Section 1.8), DDR mechanisms play a significant role in GIN, and numerous other aspects of cancer (Negrini et al., 2010; Hanahan and Weinberg, 2011). GIN arises as the result of defective DDR and ineffective processing of aberrant RFs (Gorgoulis et al., 2005). DDR is typically triggered when the MRN complex identifies DSBs (Carson et al., 2003; Lamarche et al., 2010). The MRN complex must engage with the DSB to activate the central protein kinases (Uziel et al., 2003). PIKK is a large family, containing ATM, ATR, and DNA-PKcs, which are the key regulators of the many downstream DDR processes (Shiloh, 2003; Jackson and Bartek, 2009; Ciccia and Elledge, 2010).

An important property of the DDR is its ability to effect DSB repair via two mechanisms: HDR and NHEJ (Aguliera and Gonzales, 2008; Helleday et al., 2007). Briefly, HDR is initiated through an Exo1-mediated and other endonucleases processing and resectioning of dsDNA ends to generate 3' ssDNA overhangs, which permits the strand invasion of homologous duplex DNA (Helleday et al., 2007; Sartori et al., 2007). Several studies have demonstrated how either defects in the DDR mechanism, or the deregulation of proteins such as ATM and MRE11, contribute to the progression of tumours from pre-malignant to malignant (Ottini et al., 2004; Bartkova et al., 2008; Kandoth et al., 2013).

Conversely, NHEJ ligates the dsDNA ends, being regulated by the DNA end-binding KU heterodimer, which can involve the prior processing of ends to remove chemically modified bases, or to reveal microhomology (Lieber, 2008). This process recruits and activates the DNA-PKcs, creating a DNA-PK complex (Van Heemst et al., 2004; Meek et al., 2008) (Several aspects of this topic were discussed in depth in Section 1.7).

As discussed previously (Section 1.10), ATM signalling acts as a major tumour-suppressor in cancer cells, and is considered to be a potentially exciting target for the promotion of cell death in response to radio- and chemo-therapies (Shrivastav et al., 2008). Many ATM inhibitors have been developed (Table 1.3) to sensitize cancer cells as part of combination treatments, namely when using both radio- and chemo- therapies (Powell et al., 1995; Price and Youmell, 1996; Rainey et al., 2008; Hickson et al., 2004; Golding et al., 2012; Batey et al., 2013). In their research, Hickson et al. (2004) identified a selective and specific ATM kinase inhibitor, (2-morpholin-4-yl-6-thianthren-1-yl-pyran-4-one), identified as KU-55933.

As with ATM, ATR has been a key target of proposed new cancer therapies. Table 1.3 shows that several ATR inhibitors have been developed (Powell et al., 1995; Nishida et al., 2009; Peasland et al., 2011; Maira et al., 2008; Foote et al., 2013). Among these ATR inhibitors, a potent cellular signalling inhibitor, NU6027, has also been discovered (Peasland et al., 2011). Reportedly, the NU6027 inhibitor, which was originally developed as a CDK2 inhibitor, represents important anticancer therapy developments that increase chemosensitization, thereby inhibiting the growth of human breast cancer cells, supporting treatment with various DNA damaging chemotherapeutic agents.

In addition to the above, DNA-PK inhibitors have been identified, such as NU7441, LY294002 and CC-115 (Vlahos et al., 1994; Zhao et al., 2006; Postel-Vinay et al., 2012; Veuger et al., 2003). However, these are not specific to DNA-Pkcs and are known to inhibit different PIKK proteins. Recently, another variant, NU7026 (2-(morpholin-4-yl)-benzo[h]chomen-4-one) has been identified as a novel DNA-PK inhibitor (Veuger et al., 2003).

Moreover, mirin (Z-5-(4-hydroxybenzylidene)-2-imino-1,3-thiazolidin-4-one) was developed to inhibit the MRN complex by disrupting and blocking the nuclease activity of Mre11 (Garner et al., 2009). Recently, a specific RAD51 small molecule inhibitor, B02, was developed to inhibit strand exchange in the HR repair pathway (Huang and Mazin, 2014).

This study hypothesised that the DDR is prone to defects during RS, with misrepair of broken DNA replication forks being a universal cause of the mutations that promote tumour initiation and evolution. The aim of this chapter was to discover fundamental similarities and differences between the molecular mechanisms used to repair BFs to permit a comparison with direct DSB. Various DDR defects were induced using inhibitors, namelyATRi (NU6027), ATMi (KU55933), Mre11i (Mirin), Rad51i (Rad51- B02) and DNA-PKcsi (NU7026) (Table 1.3).

The data presented in Chapter 5 suggests that cells with BFs (se-DSB) display a significant reduction in cell viability when compared to a direct DSB in HEK293 cells, suggesting they are more cytotoxic. The induced DNA damage was therefore expected to activate the DDR. To examine the roles of the different facets of the DDR in response to BFs (se-DSB) in comparison with direct DSBs, the viability of cells was assessed following acute Flp1 induction and DDR inhibition by measuring cellular metabolic activity using the WST-1 assay and CFA.

This should significantly advance understanding of how BFs are processed and repaired by the DDR, and the mechanism by which errors occur that lead to mutagenesis. Understanding these processes will illuminate RS responses, supporting the development of improved preventative and therapeutic strategies. Following this, initial survivor clones were selected to detect mutation frequency and PCR followed by sequencing was used to investigate the type of the mutations.

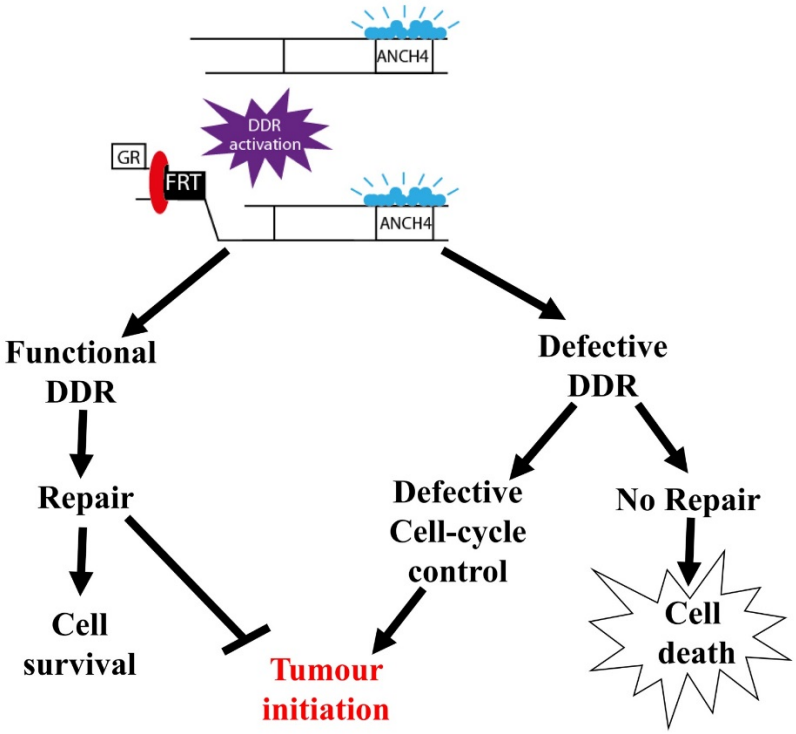

Figure 6.1 DNA damage response to the induced broken replication fork. Upon FLP induction, SSB will occur at the FRT site and during replication the replication fork will collides with the SSB generating a broken replication fork (se-DSB). (**left panel**): the generated broken fork (se-DSB) caused by FRT-FLP system, may repaired by functional DNA damage response leading to cell survival, genome stability and tumour suppression. (**Right panel**): if not repaired by a defective DNA damage response can induce defective cell-cycle control and potentially lead to cell death or tumour initiation.

6.2 Results

6.2.1 Analysing the effects of DNA damage response inhibitors on cell growth

Many DDR proteins are essential for cell viability and genome instability, and total inhibition will therefore be lethal or induce significant amounts of cell death. Hence, it was not possible to use high doses of the inhibitors. To determine the optimal dose for use in cell viability experiments, which was decided to be high enough to induce notable inhibition but with at least 50% of cells surviving the doses, the cytotoxicity (IC50) of the DDR inhibitors listed in Table 1.3 was assessed using the WST-1 assay. IC50 is defined as the concentration of an inhibitor that causes a 50% reduction in cell proliferation, and refers to the cytotoxicity of inhibitors (Figure 6.2).

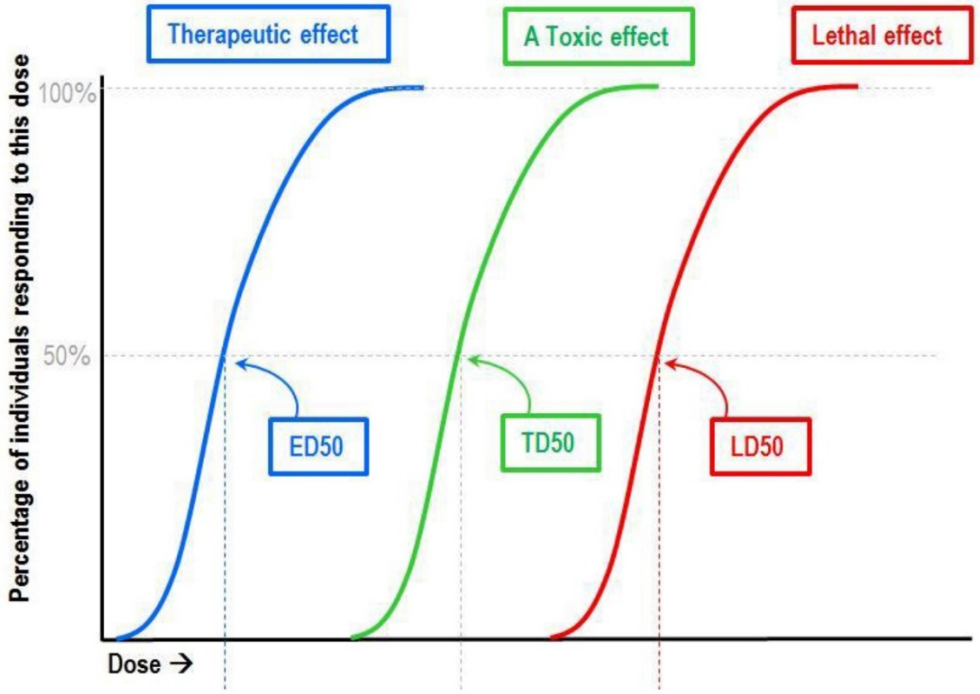

Figure 6.2 The concept of inhibitor concentration (IC50). IC50 determine the maximal concentration that cause 50% reduction in cell growth. (ED50) is the therapeutic dose that cause 50% reduction of any biological activity. (TD50) is the concentration that cause 50% toxic effect. (LD50) is the concentration that cause 50% cell death.

HEK293-FRT or U2OS-FRT cells were seeded in 96-well flat-bottom microtiter plates at a density of 10×10^3 cells/well. Following their attachment, the cells were exposed to various DDR inhibitor concentrations over periods of 24 and 48 hours. A negative control group with zero adjustment was also set. The reaction was terminated by adding the cell proliferation WST-1 solution to conclude the incubation period.

Relative cell growth was determined based on the manufacturer's instructions, and as described in Section 2.5.7. The incubation continued for one hour according to the incubation optimization result (Figure 5.5).

Figure 6.3 shows the growth inhibiting effect of the different DDRi inhibitors in HEK239-FRT cells after 24 and 48 hours incubation. A gradual decrease in cell viability was identified in HEK293-FRT cells in response to increasing concentrations of ATRi (Figure 6.3.A), ATMi (Figure 6.3.B), Rad51i (Figure 6.3.C), and MRE11i (Figure 6.3.D), when compared to untreated control cells (cells cultured in media with DMSO). Bigger increases in loss of viability were induced with 48 hours treatments relative to 24 hours. However, no marked differences were identified when using DNA-Pks between 24-hours and 48-hours (Figure 6.3.E). Overall, all DDR inhibitors decreased the viability of cells in a dose- and time-dependent manner.

The inhibitory rate effect of DDR inhibitors on HEK293-FRT cells was calculated, and the IC50 values for the selected DDR inhibitors over a 48-hour period are summarized in Table 6.1. The optimal concentration was determined by half maximal inhibitory concentration. This concentration of the selected DDR inhibitors was used as the fixed working concentration for each compound, and 48 hours was used as the incubation time for the subsequent experiments described in the next section.

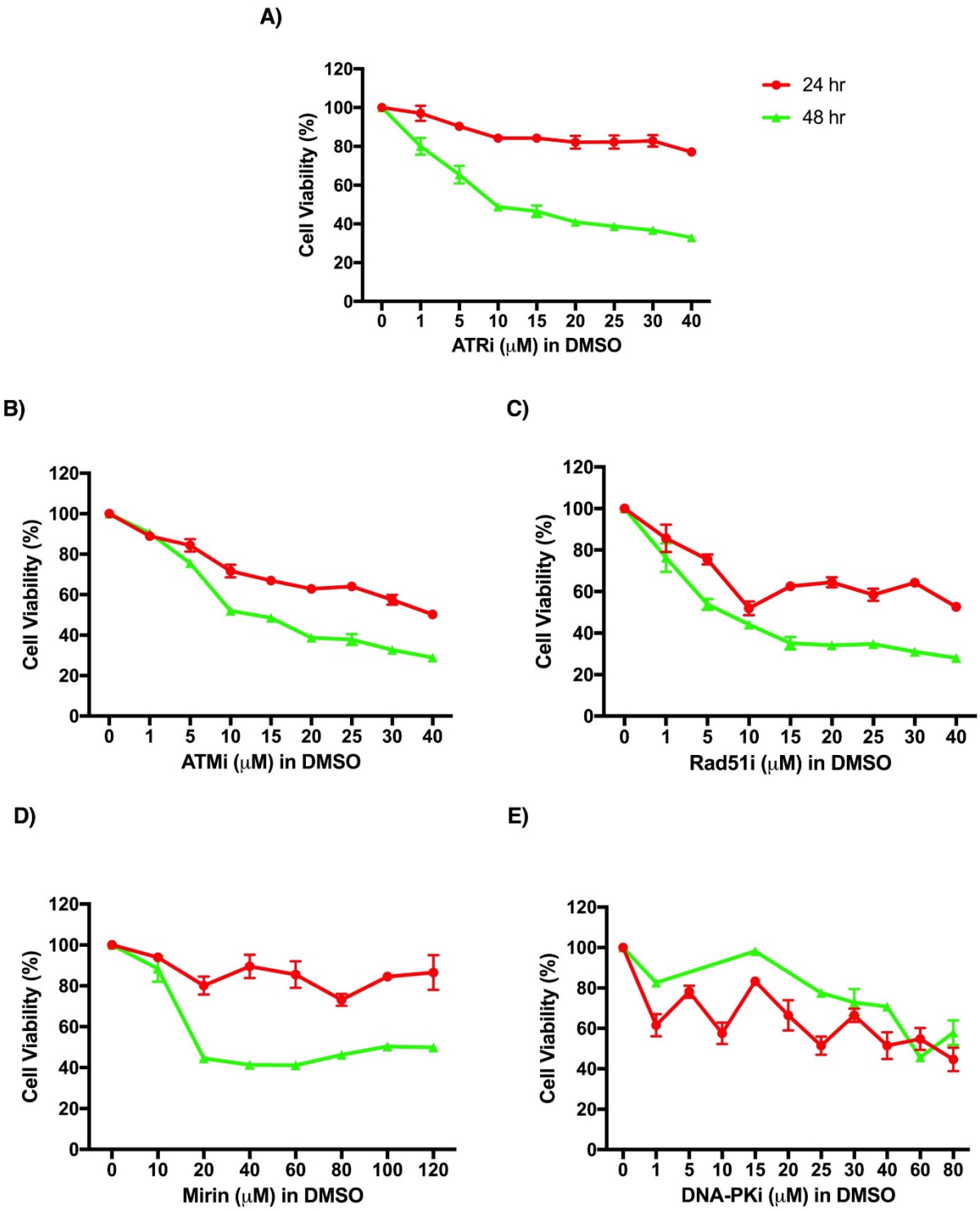

Figure 6.3 Growth inhibitory effect of DDRi inhibitors on HEK239-FRT cells. WST-1 assay measurement of the cytotoxicity of HEK293-FRT cells treated with gradually increasing concentrations of 1, 5, 10, 15, 20, 20, 25, 30, 40, 60 and 80 μM **(A)** ATRi (NU6027). **(B)** ATMi (KU55933). **(C)** Rad51i (Rad51-B02). **(D)** MRE11i (Mirin). **(E)** DNA-Pksi (NU7026), for 24 and 48 hours. Measurements of absorbance at λ=440 nm. Data shows means ± SD of two independent experiments. vs. the control group.

Similarly, U2OS-FRT were seeded and exposed to gradual increases in DDRi concentrations, as described above, although at a single time point (48 hours). Figure 6.4. shows the growth inhibitory effect of the different DDRi inhibitors in U2OS-FRT cells. The inhibitory cytotoxicity observed in the U2OS-FRT cells differed from the results obtained for the HEK293-FRT cells, suggesting that the cytotoxicity effect is cell type-dependent.

A gradual reduction in cell viability was identified in response to increased concentrations of ATRi (Figure 6.4.A), ATMi (Figure 6.4.B), and MRE11i (Figure 6.4.D), when compared to untreated control cells (media with DMSO). Interestingly and unexpectedly, an increase in cell growth was observed using Rad51i (Figure 6.4.C) and DNA-Pksi (Figure 6.4.E) after a 48-hour incubation period. The reason (s) for this effect induced by HR and NHEJ defects remains unclear.

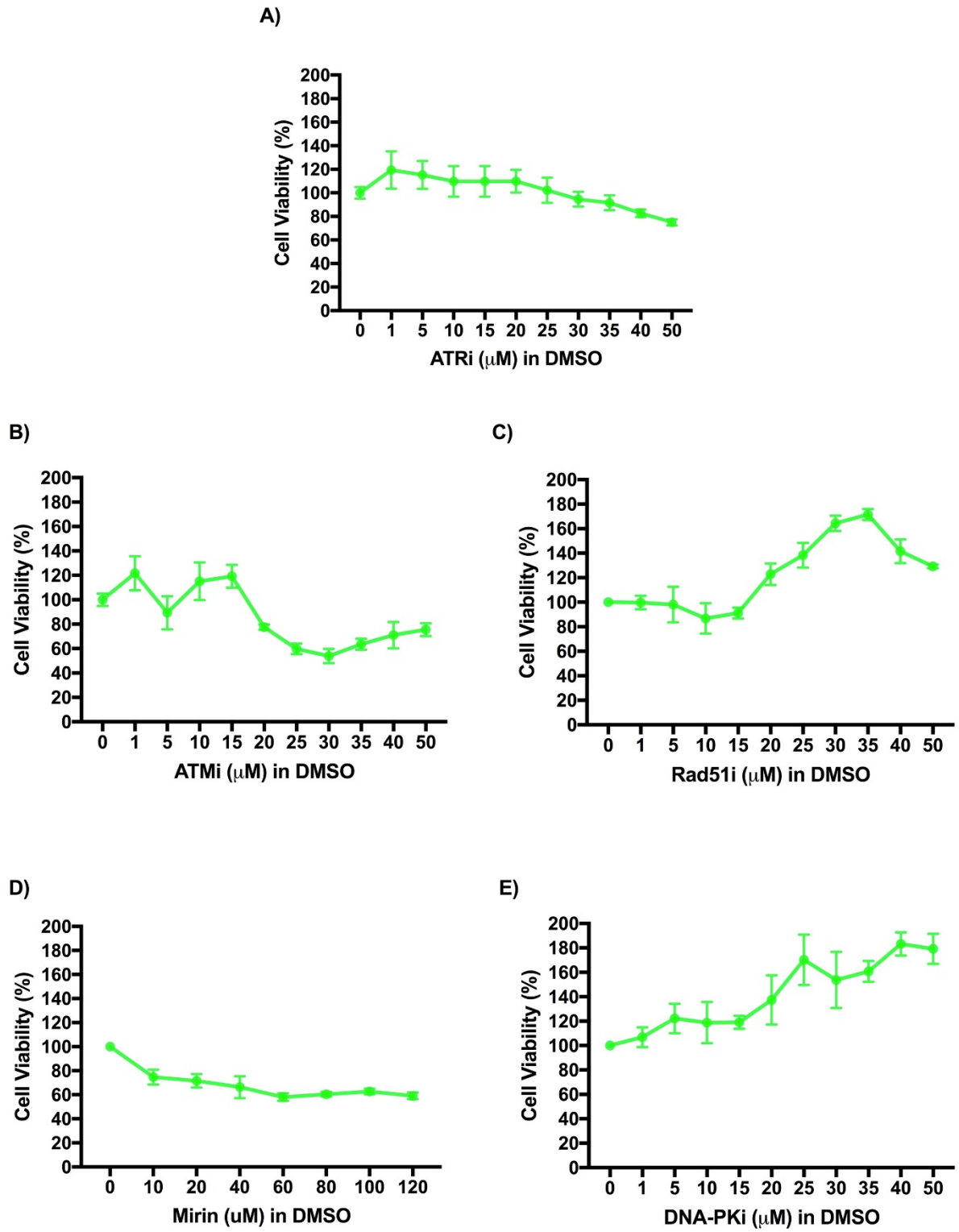

Figure 6.4 Growth inhibitory effect of DDRi inhibitors on U2OS-FRT cells. WST-1 assay measurement of the cytotoxicity of HEK293-FRT cells treated with gradually increasing concentrations of 1, 5, 10, 15, 20, 20, 25, 30, 40, 60 and 80 μM **(A)** ATRi (NU6027). **(B)** ATMi (KU55933). **(C)** Rad51i (Rad51-B02). **(D)** MRE11i (Mirin). **(E)** DNA-Pksi (NU7026), for 48 hours. Measurements of absorbance at λ=440 nm. Data shows means ± SD of two independent experiments. vs. the control group.

Table 6.1 The optimal concentration for DDR inhibition activity after 48 hours.

Inhibitor	IC50
ATRi	10 μM
ATMi	15 μM
Rad51i	10 μM
MRE11i	15 μM
DNA-PKsi	30 μM

6.2.2 Examination of effects of DDR inhibitors on CPT-induced H2AX phosphorylation

To investigate the effects of the selected concentrations of the DDR inhibitors on cell cycle phase distribution and DDR signalling during DNA damage, flow cytometric analysis was performed pre- and post-treatment with CPT. Briefly, and as mentioned in Section 1.11, CPT is a well-known topoisomerase I inhibitor that leads to DSBs and prevents DNA from unwinding to induce torsional stress (Hsiang et al., 1989). CPT was used to induce DNA damage, mimicking the damage induced by the prepared FRT-FlP system (Wang et al., 2002; Pommier, 2006), which facilitated the assessment of which DDRi might cause a phenotype following the induction of the FlP-FRT system. 25 μM of CPT was added to cell cultures to induce RS, as described in Section 2.5.6. CPT-treated cells were incubated for one, three or 24 hours to optimize the incubation time. Figure 6.5 shows that a complete synchronizing of CPT-treated cells in S-phase was observed following a 24-hour incubation period, demonstrating RS was induced.

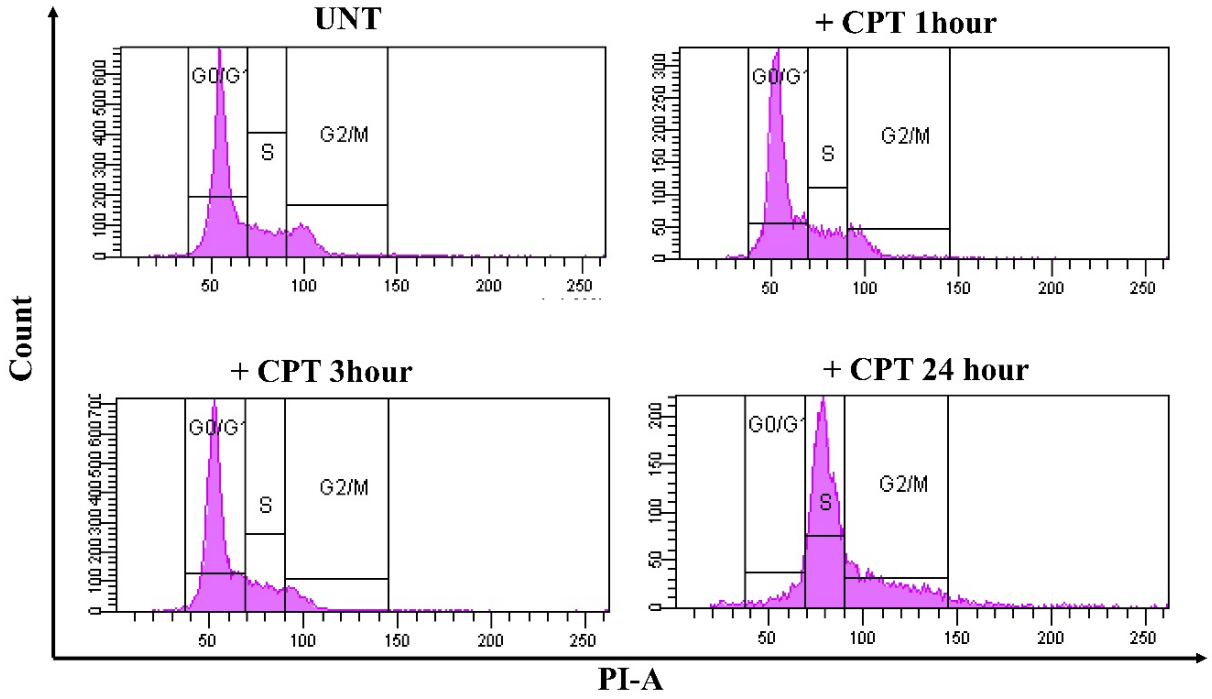

Figure 6.5 Optimization for the CPT DNA damaging agent incubation time. HEK293-FRT cells treated with 25 µM CPT to induce RS and incubated for one, three and twenty-four hours to optimize the incubation time.

To establish whether the activity of the DDR factors required for DDR signalling were inhibited at the doses used, immunocytochemical detection of histone H2AX phosphorylation at ser-139 as a marker of DSBs was undertaken. The cytometric detection of the H2AX phosphorylation approach (Bonner et al., 2008) was used to test of whether H2AX phosphorylation signal was less when MRE11, ATM, ATR and possibly DNA-PKcs were inhibited, as all promote this chromatin modification. Detection was achieved using a monoclonal γH2AX antibody as a marker, followed by indirect immunofluorescence using a secondary antibody tagged with fluorescein isothiocyanate labelling (FITC).

After the introduction of DSBs, phosphorylation of a special form of the nucleosome core histone 2A (H2A) family (H2AX) at sites flanking the breakage in chromatin proved to be an early indicator of DDR activation. Traditionally, the detection of gamma-H2AX (γH2AX) has been studied using immunofluorescence (IF) microscopy or western immunoblot analysis. However, the immunocytochemical technique offers some advantages over western blot, as it is considered more sensitive and the quantification of the phosphorylated protein is more accurate with a small number of cells.

In addition, this allows for the possibility of a simple and rapid monitor of γH2AX, thus revealing the measurement of the number of DSBs and DDR signalling in a large number of cells when compared with IF or other alternative techniques that require fixed cells.

Briefly, the HEK-FRT cells were treated with chosen inhibitor concentrations for one hour, and then exposed to CPT, which induced DNA damage that preferentially led to the formation of DSBs in actively replicating cells. A total of 25 μM CPT was added to the cells for two hours in the presence or absence of DDR inhibitors. The cells were processed and fixed in 70% ethanol, enabling the plasma membrane permeablization of the antibody. Further permeablization was achieved by blocking the cells in a solution containing the detergent Triton X-100. Sample analysis was performed as described in the material and methods in Chapter 2.5.10. The cell cycle distribution and the intensity of the stained nuclei cellular green (FITC) and red (PI) fluorescence were analysed with flow cytometry.

To assess the effect of the CPT on cells, the untreated cells were sorted along the scatterplot distributions of all the subpopulations of cells in the G0/G1, S, G2/M phases of the cell cycle, according to their DNA content. These were distinguished and gated as P11 and the level of DSBs by H2AX phosphorylation was measured (Figure 6.6). A post-acquisition analysis was conducted as the basis for further quantifications with all treated samples.

Generally, no increase in the H2AX level was observed in all the DDR inhibitor-treated cells compared with untreated cells, suggesting the levels of inhibition were not enough to increase notable DNA damage within 2 hours. However, a sharp increase was observed in CPT-DNA damage treated cells. Nonetheless, there were no apparent decreases in the H2AX phosphorylation percentage for cells treated with DDRi in combination with CPT, when compared to cells treated with CPT alone.

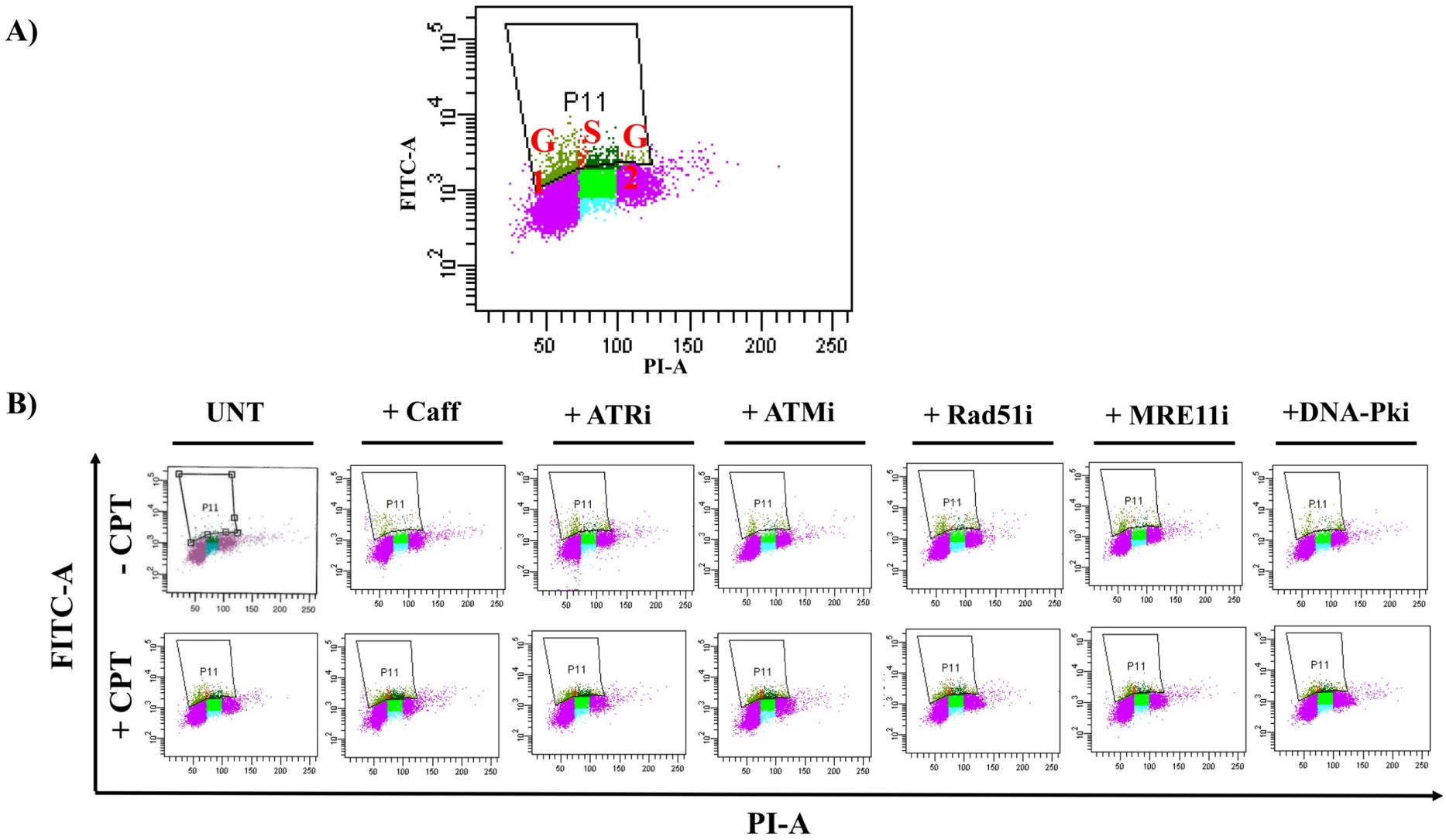

Figure 6.6 Cytometric Detection of Histone H2AX phosphorylation in relation to cell cycle stage. Representative flow cytometry plots of H2AX and DNA content (PI stain) in FRT-HEK293 cells treated with 25 μM CPT in the presence or absence of different DDR inhibitors used in their optimum inhibitory concentrations. P11 is the gated cell population for the three subpopulations G1, intra-S, and G2/M phases of the cell cycle. CPT= Camptothecin.

To quantify the DNA damage affecting the cells in a particular phase of the cycle, the values for γH2AX were gated in an alternative way to separate the G_1, S, and G_2/M subpopulation cells. The percentage of H2AX phosphorylation was re-gated as P10 for the subpopulation in the S-phase and the H2AX signal was recovered (Figure 6.7). As the results shown in Figure 6.8 demonstrate, in the non-treated cells, only a low level of H2AX phosphorylation was observed (23.9%). This represents intrinsic H2AX phosphorylation, which is primarily associated with DNA replication. However, this percentage of γH2AX signal intensity clearly increased to 41.3% after treating cells with CPT within S-phase cells (Figure 6.8.A). In contrast, treating the cells with the DDR inhibitors alone did not substantially increase the percentage of the H2AX phosphorylation signal in S-phase compared to the intrinsic H2AX phosphorylation of the un-treated negative control cells.

There was a considerable difference between the intensity of untreated and CPT-treated samples. The signal for the CPT-treated cells increased approximately 2-fold relative to the untreated cells (Figure 6.8.B), indicating that CPT-induced DNA damage increases H2AX phosphorylation as expected. Collectively, these results confirm that the overall proportion of cells exhibiting DDR did not significantly change after CPT treatment.

Collectively, these results indicate that inhibiting the DDR proteins alone does not increase H2AX phosphorylation. Data also indicates that the inhibitors at the chosen concentration though enough to induce a 50% loss of cell viability, is not enough to inhibit MRE11-, ATM-, ATR-mediated H2AX phosphorylation, or that any effects of inhibiting one factor can be compensated for by athers fot the phosphorylation of H2AX.

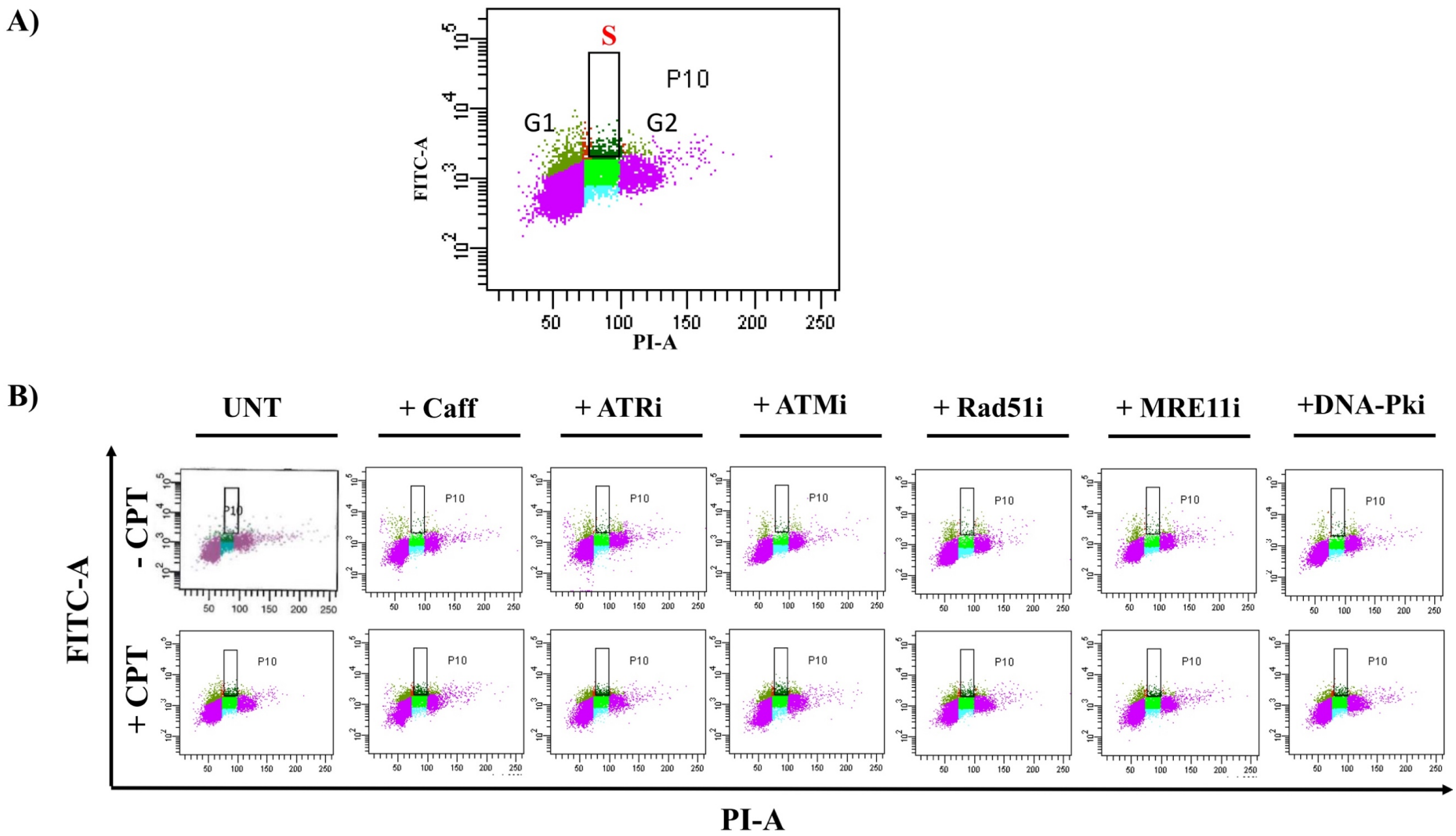

Figure 6.7 Cytometric Detection of Histone H2AX phosphorylation in relation to S-phase. Representative flow cytometry plots of H2AX and DNA content (PI stain) in FRT-HEK293 cells treated with 25 µM CPT in the presence or absence of different DDR inhibitors used in their optimum inhibitory concentrations. P10 is the gated cell population for the three subpopulations G1, intra-S, and G2/M phases of the cell cycle. CPT= Camptothecin.

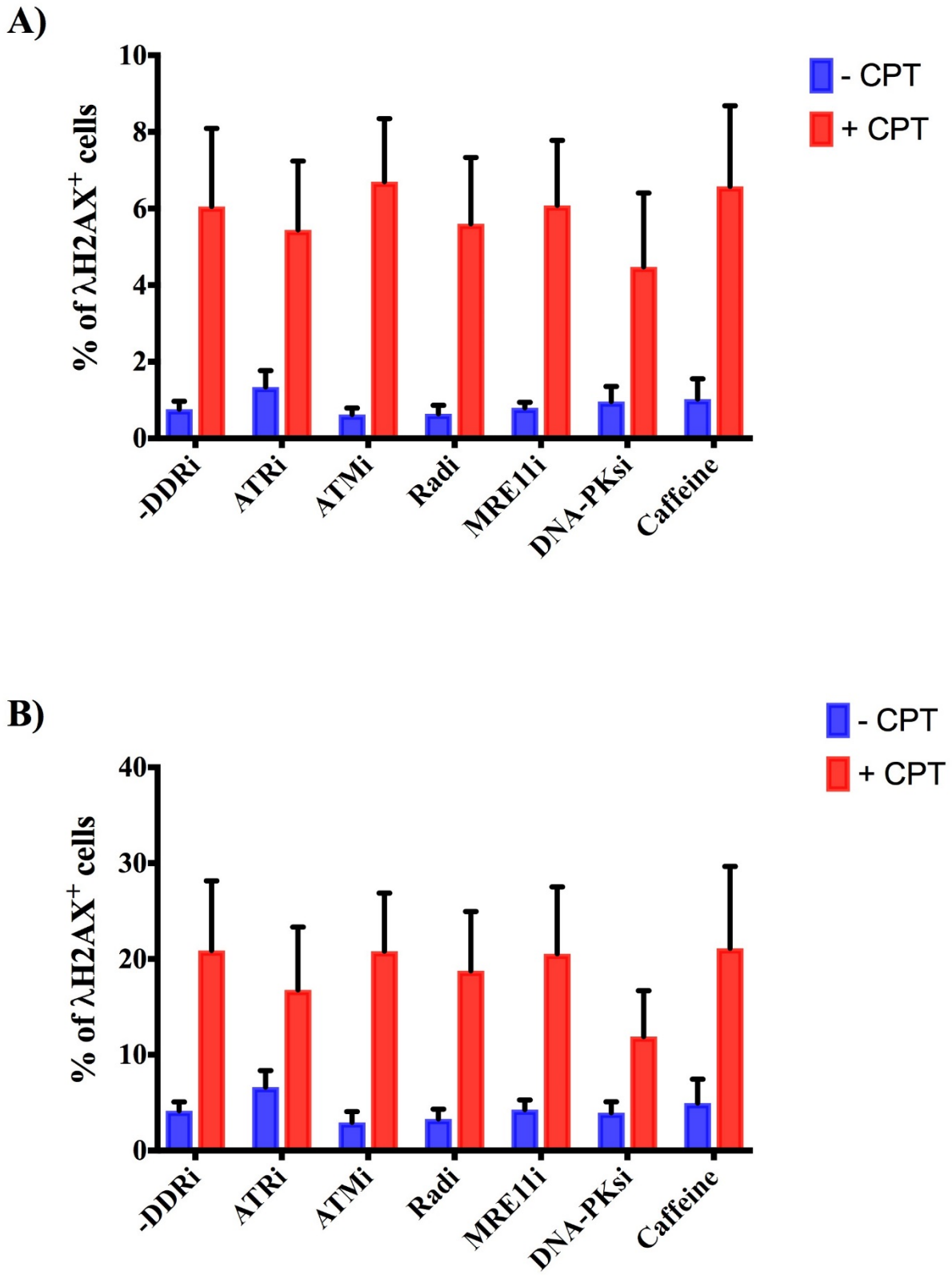

Figure 6.8 Quantification of H2AX phosphorylation in response to DDR inhibitors. HEK293-FRT cells treated with 25 μM CPT in the presence or absence of the different DDR inhibitors used in their optimum inhibitory concentrations. **(A)** A percentage of gH2AX positive cells analysed for the S-phase subpopulation gated as P10 of the cell cycle. **(B)** Percentage of gH2AX positive cells analysed for all the subpopulations of cells in the G0/G1, S, G2/M phases gated as P11 of the cell cycle. Data represented as mean ± Standard deviation for three independent experiments.

6.2.3 Determination of DNA damage response signalling requirments in the response to FLP-induced broken forks

As discussed previously (Section 1.6), ATM is a crucial component of the DDR signalling pathway, and plays an important role as a signal transducer in response to DNA damage, particularly in the case of DSBs (Savitsky et al., 1995).

ATR is activated and recruited to stalled RFs with accumulated ssDNA (Lukas et al., 2004; Cimprich and Cortez, 2008). These intra-S phase and G2/M cell cycle checkpoints allow for efficient DSB resolution and RF restart (Bakkenist and Kastan, 2003). Despite the broad understanding of ATM and ATR functions and signalling, the precise mechanisms that trigger DDR signalling under conditions of RS remain unclear.

To uncover signalling pathways that specifically affect BF cytotoxicity when defective, the FRT-FLP system was used to induce a BF or DSB. HEK293-FRT or U2OS-FRT cells were either un-transfected or transiently transfected with either pdsRed-GR, pdsRed-I-SceI-GR or pDsRed-FLPH305L-GR, and seeded and subjected to 10 μM ATR inhibitor or 15 μM ATM inhibitor for a period of two hours. Post incubation, the cells were treated with an inhibitor for a further 48 hours in the presence or absence of TA to induce the DNA damage.

6.2.3.1 Investigating the role of DDR signalling in maintaining cell viability during RS

Figure 6.9 shows the cytotoxicity of ATR and ATM deficiency on the viability of GR-, I-SceI- and FLP- transfected HEK293-FRT and U2OS-FRT cells. Overall, a clear difference emerged between un-transfected and transfected HEK293-FRT and U2OS-FRT cells. The relative cell viability data for HEK293-FRT cells showed that transfection with the different expression plasmids induced a decrease in cell viability compared with un-transfected cells. Therefore, cells transfected with empty plasmid pdsRed-GR were considered as better negative control cells than untransfected cells.

As shown in Figure 6.9.A, an unexpected increase in cell viability occurred in un-transfected HEK293 cells treated with ATR and ATM inhibitors both in the presence or absence of TA. The reason for this is unclear, as these concentrations were expected to induce 50% loss in cell viability (Figure 6.3).

In contrast, the GR-, I-SceI- and FLP- transfected cells resulted in a reduction in cell viability after treatment with 10 μM ATRi alone relative to DDRi-untreated cells. The data obtained for DDRi treatments is presented alongside the DDRi untreated data presented in Chapter 5 (note the –DDRi and +DDRi data was collected together over several independent repeat experiments).

TA reduced the viability of all transfected cells. However, no appreciable differences in cell viability were observed in ATR-defective I-SceI cells (63.5%) or ATR-defective FLP cells (61%) in comparison to FRT-GR (65%) in the presence of TA (Figure 6.9.A). Similar to ATR, ATMi-treated transfected HEK293-FRT cells showed around a 30% reduction in cell viability when compared to DDRi-untreated cells. However, no significant difference was evident between ATR-defective GR controls and ATR-defective I-SceI- or ATR-defective FLP-transfected cells.

In the U2OS-FRT cells, it was similarly observed that no notable differences were detectable between GR, I-SceI or FLP in ATRi- and ATMi-treated sampels with or without TA treatments (Figure 6.9.B).

In summary, addition of the ATR and ATM inhibitors at the concentrations used did not induce loss of viability in I-SceI or FLP expressing cells relative to GR only. The basis of the reduced cell viability induced by ATRi and ATMi in cells transfected with any constructs is unclear, but indicates ATM and ATR are required to maintain cell viability during the stress induced by transfection of plasmids.

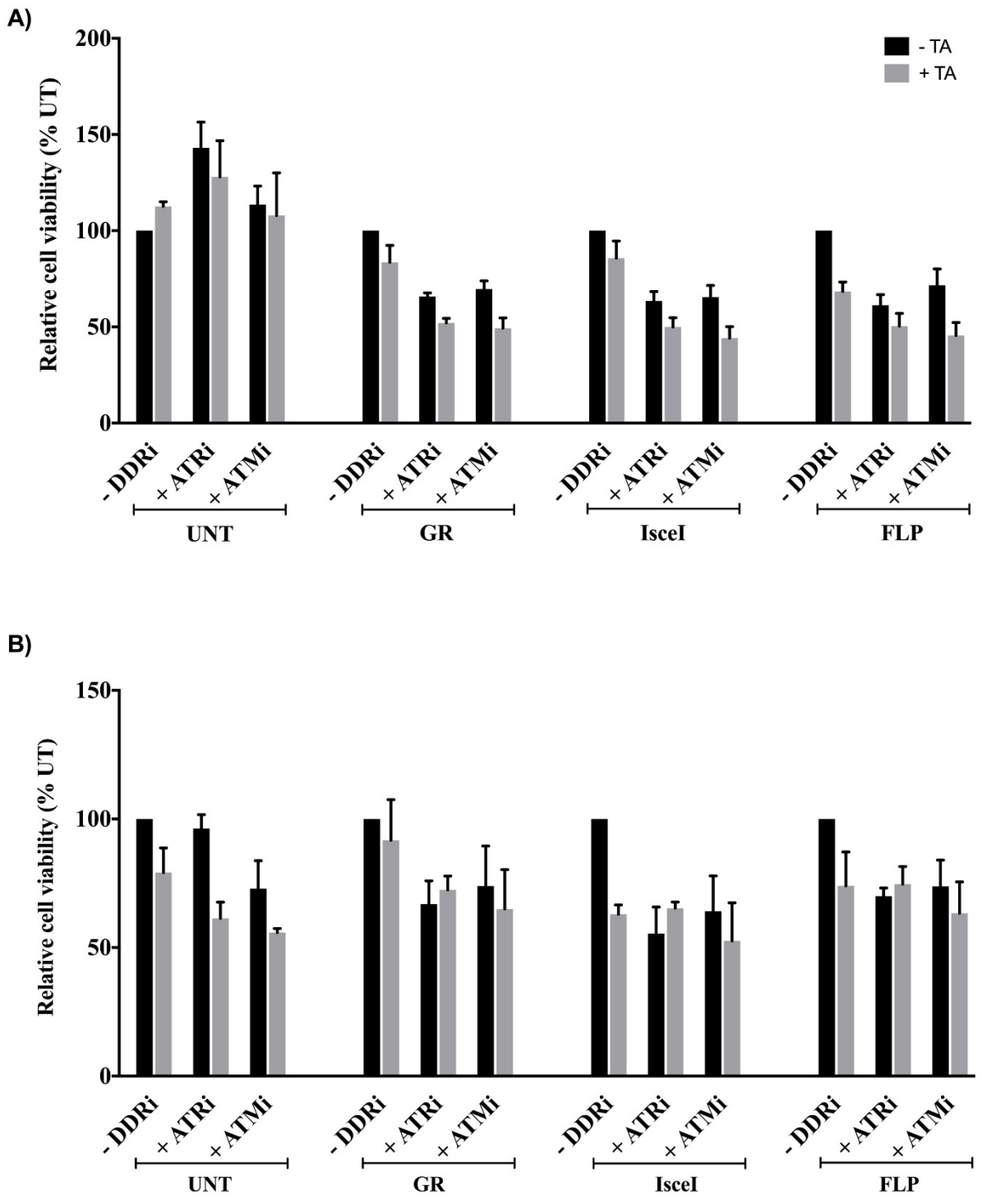

Figure 6.9 Cytotoxicity of ATR and ATM DDR deficiency on cell viability in GR, I-SceI and FLP-FRT cells. HEK293-FRT and U2OS-FRT cells were transfected with pdsRed-GR, pdsRed-I-SceI-GR or pdsRed-FLP-GR for 48 hours. Post FACS sorting cells were reseeded and exposed to 10 µM and 15 µM of ATRi and ATMi respectively, in the presence or absence of 10 nM TA. WST-1 assay was performed to determine cell viability **(A)** HEK293-FRT cells. Data represented as mean ± Standard deviation for seven independent experiments. **(B)** U2OS-FRT cells. Data represented as mean ± Standard deviation for three independent experiments. UNT, untransfected. – DDRi, DNA damage response inhibitor untreated.

6.2.3.2 Investigation of the role of DDR signalling in colony formation ability during RS

To further investigate the long-term effect of ATR or ATM inhibitors on viability of cells harbouring different DNA damage types, the CFA assay was performed as described in Section 2.5.8. Cells were transfected for 48 hours with either pdsRed-I-SceI-GR or pdsRed-FLp-GR. Un-transfected cells and cells transfected with mock pdsRed-GR served as controls. Cell sorting was used to collect all transfected (red) cells, which were then seeded by plating 3,000 of the FACS sorted cells and allowing them to adhere for 48 hours, before treatment with ATR and ATM inhibitors at optimized concentrations (Table 6.1) for two hours. The cells were treated with these DDR inhibitors for further 48 hours in the presence or absence of TA, before fresh media was added to permit single-cell colonies.

Figure 6.10, shows the effects of ATR and ATM inhibitors on the PE of GR-, I-SceI- and FLP-transfected HEK293-FRT. Overall, the PE for HEK293-FRT showed a clear difference in cell viability between transfected and un-transfected cells (similarly to the WST-1 result). An expected reduction in PE occurred in both untransfected and transfected cell defective in ATR and ATM in absence of TA in comparison to DDRi-untreated cells. This reduction was more remarkable after TA was added. Since the GR system is leaky, it was deduced that it may be more reliable to compare +TA values rather than the different between –TA and +TA for each sample.

Figure 6.10.A, shows a quantification of the PE rate for all cell lines defective in ATR in the presence or absence of TA. No significant difference was observed in ATRi-defective I-SceI cells (3.6%) in comparison to ATR-defective GR (5.7%) in the presence of TA. However, a significant reduction in PE rate was only found in ATR-defective FLP cells (3.4%) in comparison to ATR-defective GR cells (P-value = 0.0362). Thus, may indicate ATR is required to maintain colony formation ability after the induction BF in HEK293-FRT cells.

Similarly, the reduction was more apparent and significant in ATM-defective FLP-transfected cells (1%) in comparison to ATM-defective -GR (2.6%) in the presence of TA with P-value = 0.0299 (Figure 6.10.B). The reduction in cell viability in ATM-defective FLP cells in the absence of TA might be because the system was leaky, with RS occurring even when the system should be OFF. However, no significant different was evidence between ATM-defective I-SceI cells (1.7%) relative to GR control cells. Hence, similar to ATR, ATM appear to be required to promote CFA in the presence of a DSB or BF, with a BF inducing a greater loss of viability during ATM deficiency relative to a DSB.

In order to evaluate the effect of ATR and ATM inhibitors alone on transfection-induced cytotoxicity, survival fraction was measured (Section 2.5.8). It was observed that inhibiting ATR reduced CFA in both GR-transfected and un-transfected cells (2.7-fold). ATR deficiency also reduced the survival rate both I-SceI- and FLP-transfected cells to 2- and 1.7-fold relative to DDRi-untreated cells (Figure 6.11).

Similarly, ATM inhibitor treatment remarkably reduced cell proliferation in all samples. ATM deficiency also caused a reduction in the survival rate for both I-SceI- (4-fold) and FLP-transfected cells (4.7-fold) relative to DDRi-untreated cells.

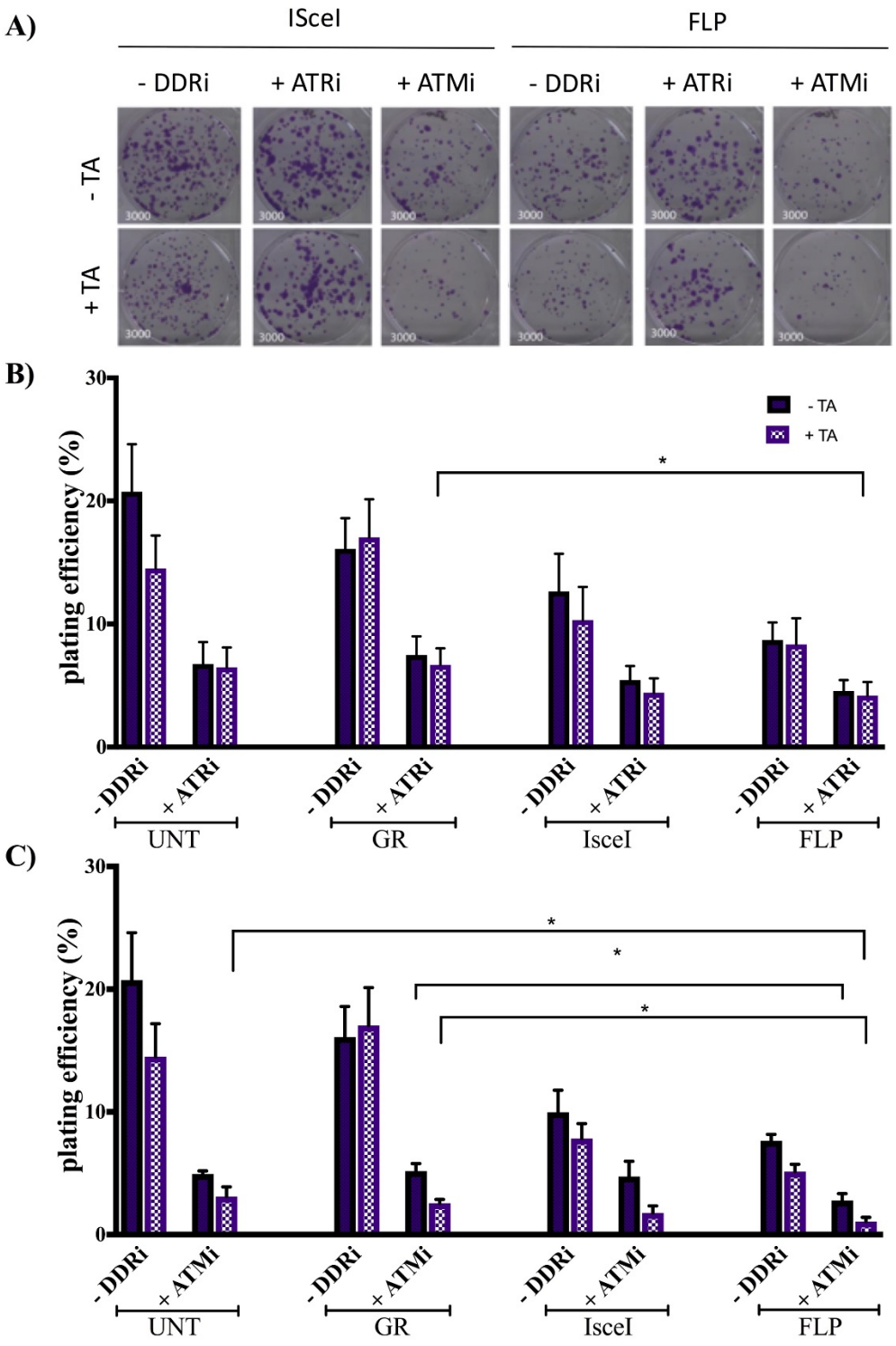

Figure 6.10 Colony Formation ability of the induced RS impaired by inhibiting DDR signalling factors in HEK293-FRT cells. HEK293-FRT cells transfected with pdsRed-GR, pdsRed-I-SceI-GR and pdsRed-FLP-GR exposed to DDR signalling inhibitors; 10 µM (ATRi) and 15 µM (ATMi) in the absence or presence of 100 nM TA. **(A)** Digital representative images of the effect of the induced DSB and DNA damage response on CFA on FRT-I-SceI and FRT-FLP cells exposed to ATRi or ATMi in the presence or absence of TA. **(B)** Analysis of plating efficiency of ATR deficient cells before and after TA addition. **(C)** Analysis of plating efficiency of ATM deficient cells before and after TA addition. Data represented as mean ± Standard deviation for seven independent experiments. UNT, untransfected. – DDRi, DNA damage response inhibitor untreated.

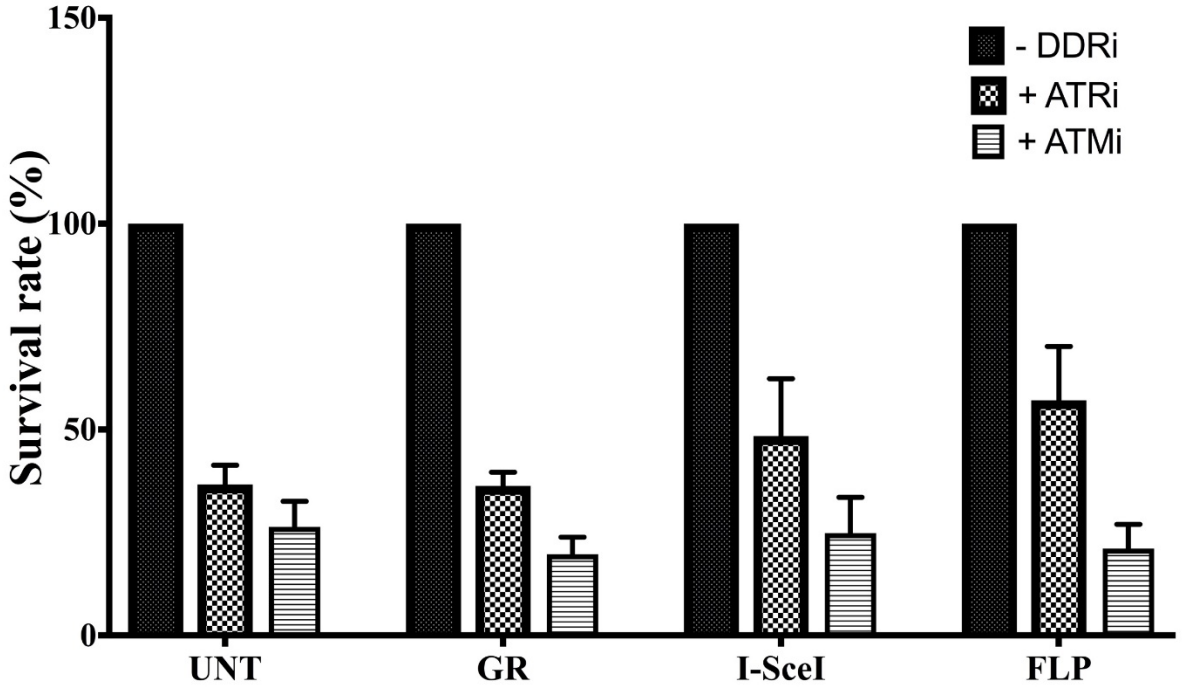

Figure 6.11 Survival rate and the fold difference of the induced RS impaired by inhibiting DDR signalling factors in HEK293-FRT cells.

These experiments were repeated in U2OS-FRT cells to assess reproducibility and cell line specificity (Figure 6.12). Generally, inhibiting ATR resulted in a decrease in cell survival of more than 50% for both the un-transfected cells and transfected cells. A significant reduction in PE rate was also noted in all transfected cells treated with ATR inhibitor combined with TA relative to the corresponding un-transfected cells (similar to HEK293-FRT cells).

A significant difference was observed in ATRi-defective I-SceI cells (0.4%) in comparison to ATR-defective GR (1.6%) in the presence of TA (P-value = 0.0157). A significant reduction in PE rate was also found in ATR-defective FLP cells (0.4%) in comparison to ATR-defective GR cells (P-value = 0.0112) (Figure 6.12.A).

Similar results were obtained following treatments with ATM inhibitor (Figure 6.12.B). Critically a remarkable drop was also found with ATMi-deficient I-SceI- and FLP- transfected cells relative to ATMi-deficient GR transfected cells with a P-value = 0.0058 and P-value = 0.0159, respectively.

Figure 6.13, shows a quantification of the survival fraction for all cell lines defective in ATR and ATM inhibitors in the presence of TA. It was observed that ATR deficiency reduced the survival rate both I-SceI- and FLP-transfected cells to 5- and 3.2-fold relative to DDRi-untreated cells. Similarly, ATM inhibitor treatment remarkably reduced cell proliferation in all samples. ATM deficiency also caused a reduction in the survival rate for both I-SceI- (14-fold) and FLP-transfected cells (8.3-fold) relative to DDRi-untreated cells.

In conclusion, ATR and ATM promote colony forming ability in the presence of a single direct DSB or se-DSB in both HEK293-FRT and U2OS-FRT cells.

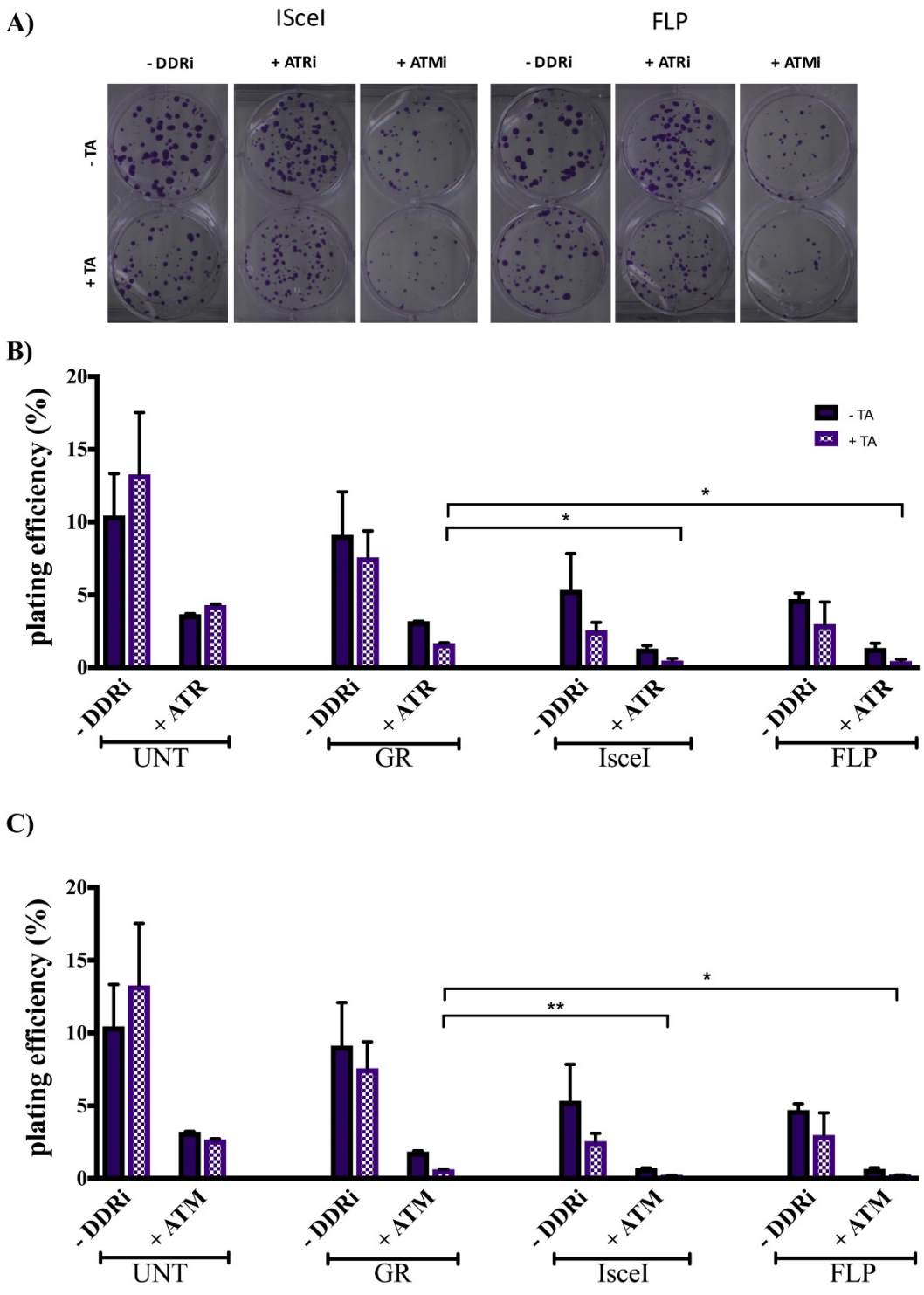

Figure 6.12 Colony Formation ability of the induced RS impaired by inhibiting DDR signalling factors in U2OS-FRT cells. U2OS-FRT cells transfected with pdsRed-GR, pdsRed-I-SceI-GR and pdsRed-FLP-GR exposed to DDR signalling inhibitors; 10 µM (ATRi) and 15 µM (ATMi) in the absence or presence of 100 nM TA. **(A)** Digital representative images of the effect of the induced DSB and DNA damage response on CFA on FRT-I-SceI and FRT-FLP cells exposed to ATRi or ATMi in the presence or absence of TA. **(B)** Analysis of plating efficiency of ATR dificent cells before and after TA addition. **(C)** Analysis of plating efficiency of ATM dificent cells before and after TA addition. Data represented as mean ± Standard deviation for three independent experiments. UNT, untransfected. – DDRi, DNA damage response inhibitor untreated.

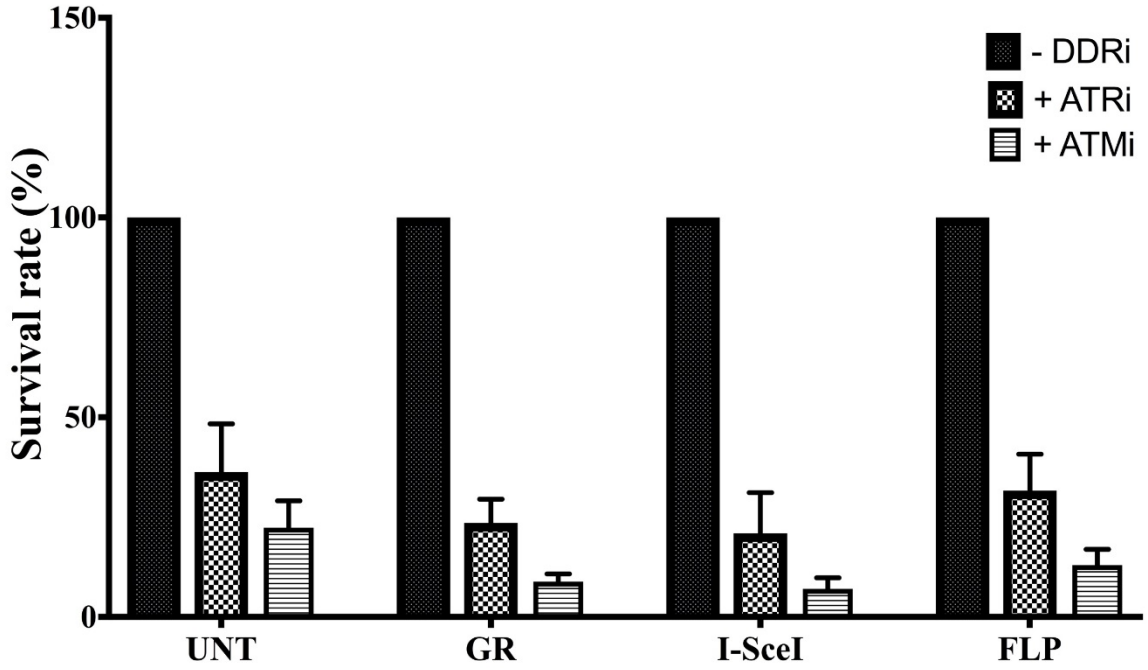

Figure 6.13 Survival rate and the fold difference of the induced RS impaired by inhibiting DDR signalling factors in U2OS-FRT cells.

6.2.4 Determination of the role of homologous recombination repair in the response to FLP-induced broken fork

The similarities and differences between the mechanisms by which de- and se-DSBs are repaired remain unknown. To establish whether the repair of a BF generated by the FRT-FLP systems relies on HR repair proteins, the major DSB components: Rad51 and MRE11 were inhibited.

RAD51 is a key HDR protein that promotes homology and DNA strand exchange between homologous DNA molecules (Baumann et al., 1996). Both HEK293-FRT and U2OS-FRT cells were transfected, and FACS was performed as described previously. Cells were subjected to 10 μM and 15 μM of Rad51 and MRE11 inhibitors respectively.

6.2.4.1 Investigation of the role of homologous recombination repair in maintaing cell viability during RS

Overall, the observations and results of the WST-1 assay following MRE11 and Rad51 inhibition uses very similar to ATR and ATM inhibition (Figure 6.9).

There was an unexpected increase in cell viability for the un-transfected cells deficient in both Rad51 and MRE11 compared to DDRi-untreated cells in the presence or absence of TA. This indicated the fact that the inhibitors did not induce a 50% reduction in viability as expected at this dose. In contrast, the GR-, I-SceI- and FLP- transfected cells resulted in a reduction in cell viability after treatment with Rad51i or MRE11i alone, in comparison to DDRi untreated cells.

Figure 6.14 shows the cytotoxicity of Rad51 and MRE deficiency on the viability of GR-, I-SceI- and FLP-transfected HEK293-FRT and U2OS-FRT cells. Overall, transfection induced a sensitivity to MRE11i and Rad51i independently of construct, and MRE11 and Rad51 inhibitors did not confer a greater loss of viability in I-SceI or FLP relative to GR-transfected cells.

As shown in Figure 6.14.A, no notable differences in cell viability were observed in Rad51-defective I-SceI cells (54.1%) or Rad51-defective FLP cells (48.5%) in comparison to Rad51-defective -GR (54.4%) in the presence of TA. Similarly, no appreciable reduction in cell viability was observed in MRE11-defective I-SceI cells (71.3%) or MRE11-defective FLP cells (61.4%) in comparison to MRE11-defective -GR (67.5%) in the presence of TA.

In the U2OS-FRT cells, it was similarly observed that no notable differences were detectable between GR, I-SceI or FLP in MRE11i- and Rad51i-treated sampels with or without TA treatments (Figure 6.14.B).

In summary, addition of the Rad51 and MRE11 inhibitors at the concentrations used did not induce 50% loss of viability as expected. Eventhough there was a reduced cell viability induced by Rad51i and MRE11i in cells transfected with any constructs, a very slight reduction was observed in I-SceI or FLP expressing cells relative to GR only. The basis of the is unclear, but indicates Rad51 and MRE11 are required to maintain cell viability during the stress induced.

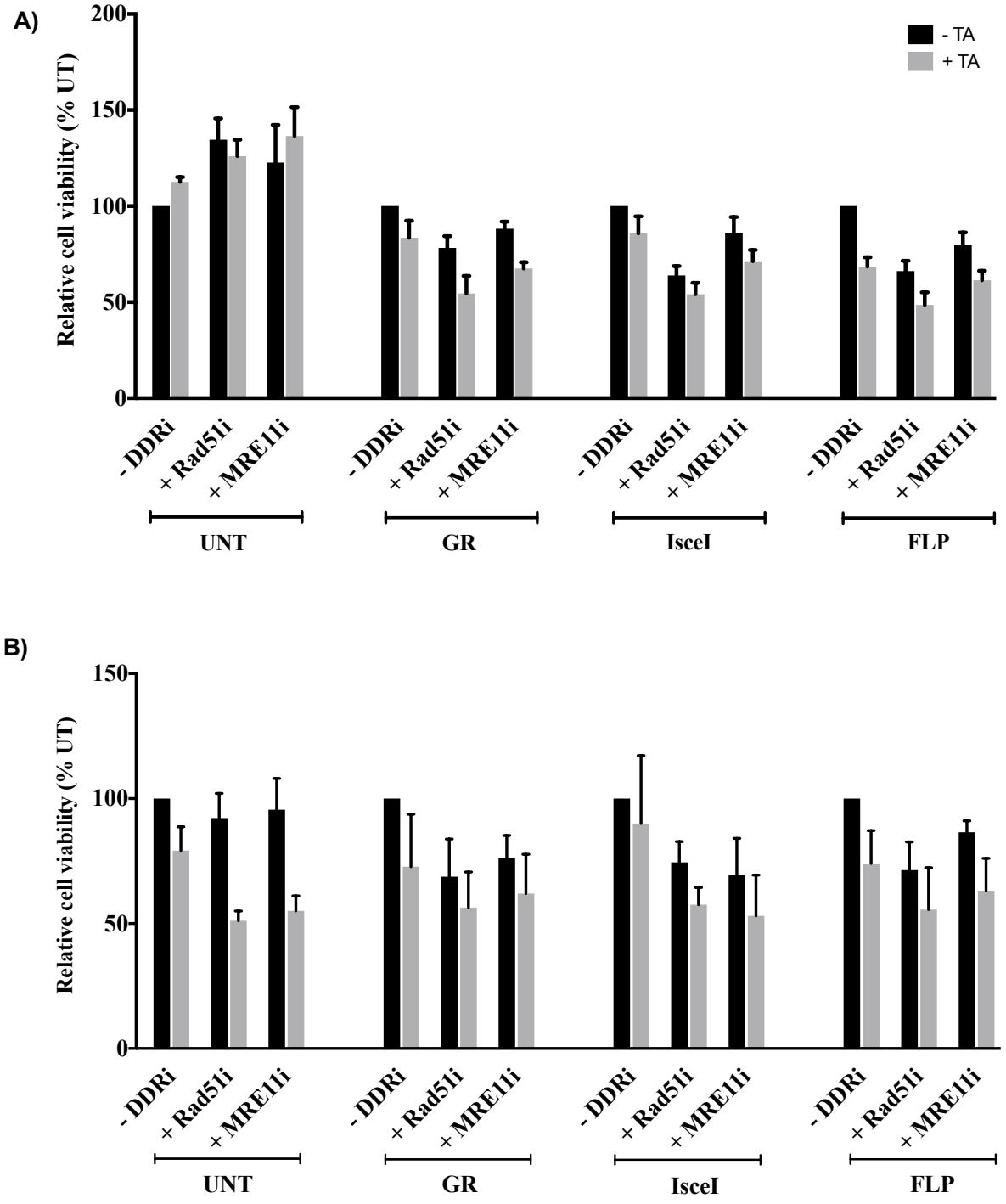

Figure 6.14 Cytotoxicity of Rad51 and MRE11 inhibitors on cell viability of GR, I-SceI and FLP-FRT expressing cells. FRT cells were transfected with pdsRed-GR, pdsRed-I-SceI-GR or pdsRed-FLP-GR. Cells were exposed to 10 μM and 15 μM of Rad51i and MRE11i respectively, in the presence or absence of 10 nM TA. **(A)** HEK293-FRT cells. Data represented as mean ± Standard deviation for seven independent experiments. **(B)** U2OS-FRT cells. Data represented as mean ± Standard deviation for three independent experiments. UNT, untransfected. – DDRi, DNA damage response inhibitor untreated.

6.2.4.2 Investigation of the role of HR repair in colony forming ability during RS

To further investigate the long-term effect of Rad51 or MRE11 inhibitors on viability of cells harbouring different DNA damage types, the CFA assay was performed as described in Section 2.5.8.

Figure 6.15, shows the effects of Rad51 and MRE11 inhibitors on the PE of GR-, I-SceI- and FLP-transfected HEK293-FRT. Overall, an expected reduction in PE occurred in untransfected and transfected cell defective in Rad51 and MRE11 in absence of TA in comparison to DDRi-untreated cells. This reduction was even more remarkable after TA was added.

Figure 6.15.A, shows a quantification of the PE rate for all cell lines defective in Rad51 in the presence or absence of TA. No significant difference in PE was observed in Rad51-defective I-SceI cells (2.2%) or Rad51-defective FLP cells (1.9%) in comparison to Rad51-defective -GR (3.7%) in the presence of TA. Thus, may indicate Rad51 is not required to maintain CFA after the induction BF in HEK293-FRT cells. However, this reduction was more apparent and significant in MRE11-defective FLP-transfected cells (3%) in comparison to MRE11-defective -GR (4.7%) in the presence of TA with P-value = 0.0402 (Figure 6.15.B). No significant different was evidence between MRE11-defective I-SceI cells (4%) relative to GR control cells (Figure 6.15.B).

In order to evaluate the role of Rad51 and MRE11 inhibitors alone on transfection-induced cytotoxicity, survival fraction was measured for DDRi-treated cells relative to DDRi-untreated cells (Section 2.5.8). A similar reduction was found in the Rad51-defective untransfected and transfected cells relative to Rad51i-untreated cells. the Rad51i-defeciency decreased the GR-transfected cells 5-fold relative to Rad51i-untreated cells, while the reduction in I-SceI- and FLP-transfected cells was 4.5- and 4.3-folds relative to Rad51i-untreated cells. Similarly, MRE11 inhibitor treatment remarkably reduced cell proliferation in all samples. It was observed that MRE11 deficiency reduced the survival rate both I-SceI- and FLP-transfected cells to 2.2- and 2.7-fold relative to DDRi-untreated cells (Figure 6.16).

Overall, the pattern of effects of Rad51 and MRE11 inhibition in GR-, I-SceI- and FLP-expressing HEK293-FRT cells is the same as ATR and ATM inhibition. Which is that the inhibitors cause a larger decrease in CFA of I-SceI- and FLP cells relative to GR only, with FLP being the least viable. Moreover, often these differences were significant, hence, indicating Rad51 and MRE11 required for BF as well as DSBs.

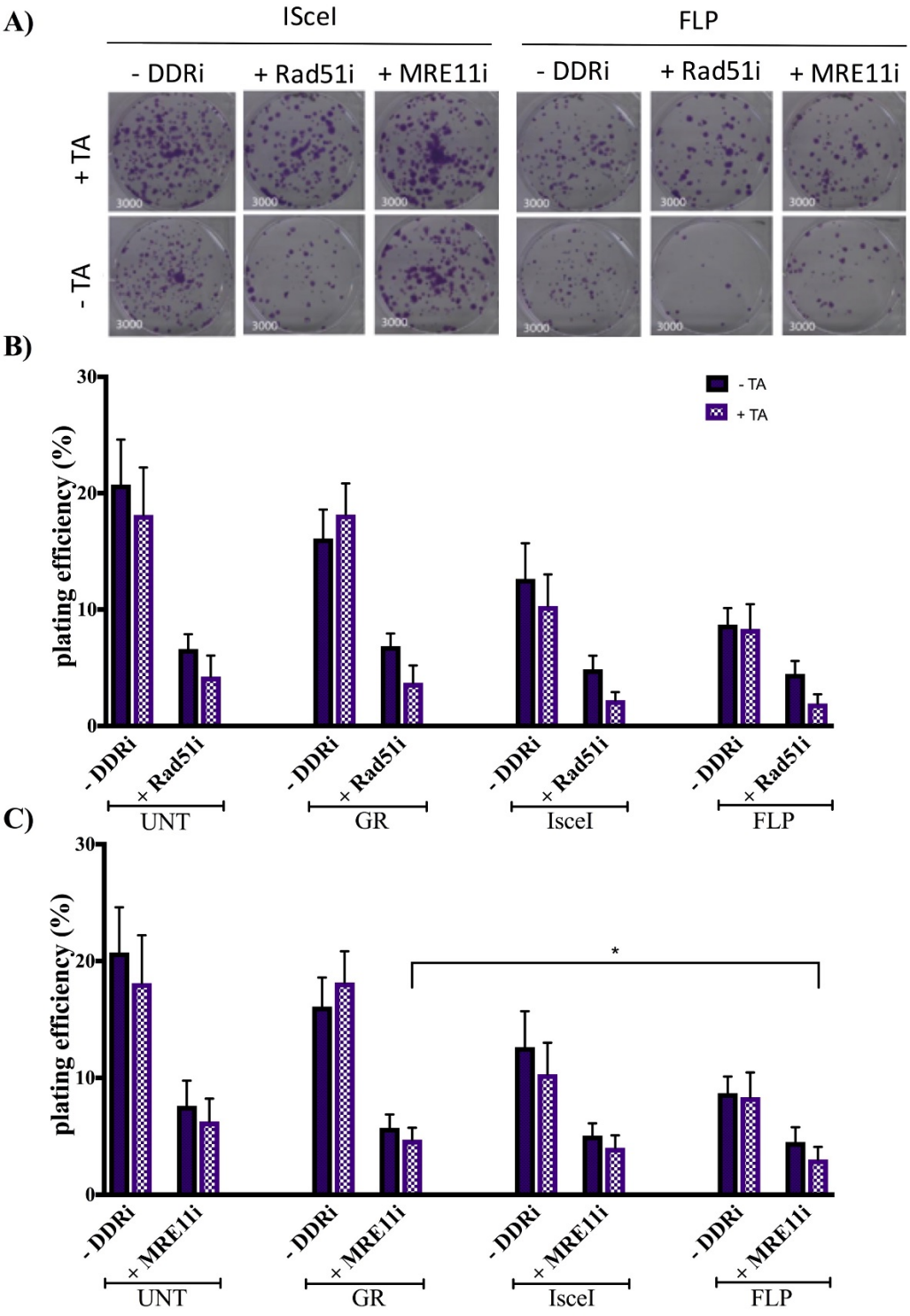

Figure 6.15 Colony Formation ability of the induced DNA damage impaired by inhibiting HR repair factors in HEK293-FRT cells. HEK293-FRT cells transfected with pdsRed-GR, pdsRed-I-SceI-GR and pdsRed-FLP-GR exposed to HR repair inhibitors; 10 µM (Rad51i) and 15 µM (MRE11i) in the absence or presence of 100 nM TA. **(A)** Digital representative images of the effect of the induced DSB and DNA damage response on CFA on FRT-I-SceI and FRT-FLP cells exposed to Rad51i or MRE11i in the presence or absence of TA. **(B)** Analysis of plating efficiency of Rad51 deficient cells before and after TA addition. **(C)** Analysis of plating efficiency of MRE11 deficient cells before and after TA addition. Data represented as mean ± Standard deviation for seven independent experiments. UNT, untransfected. – DDRi, DNA damage response inhibitor untreated.

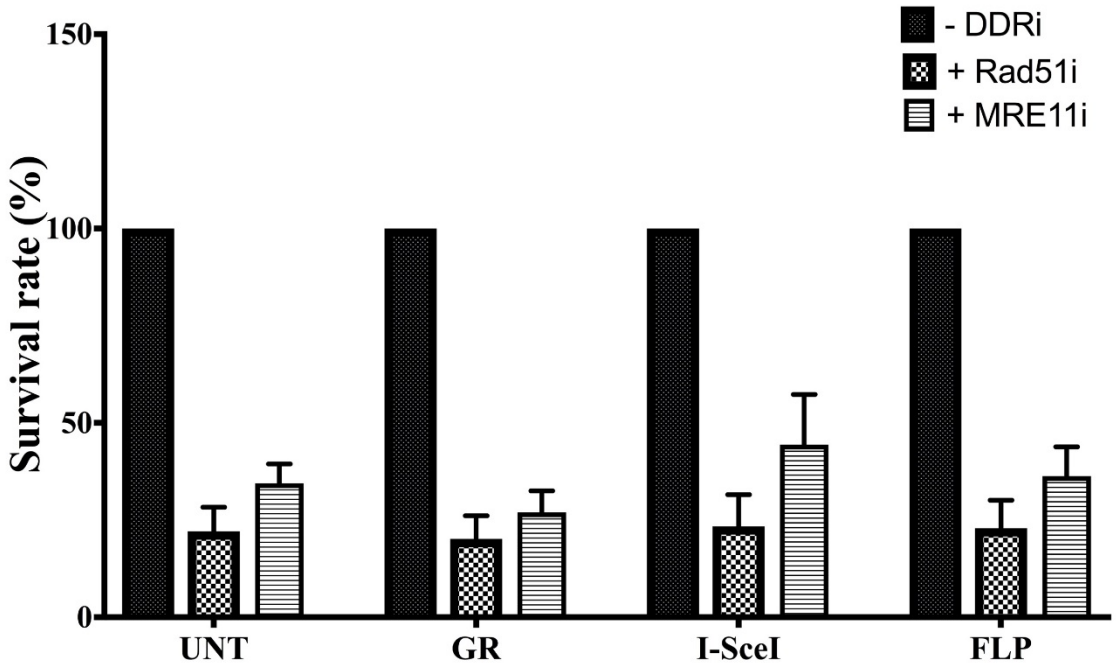

Figure 6.16 Survival rate and the fold difference of the induced RS impaired by inhibiting homologous recombination repair factors in HEK293-FRT cells.

In the U2OS-FRT cells, inhibiting Rad51 and MRE11 resulted in a decrease in cell survival of more than 50% for both the un-transfected cells and transfected cells. A significant reduction in PE was also noted in all transfected cells treated with Rad51 inhibitor combined with TA relative to the corresponding GR-transfected cells. A significant difference was observed in Rad51-defective I-SceI cells (0.18%) in comparison to Rad51-defective GR (0.64%) in the presence of TA (P-value = 0.0265). A significant reduction in PE rate was also found in Rad51-defective FLP cells (0.5%) in comparison to Rad51-defective GR cells (P-value = 0.0199). (Figure 6.17.A). Similar results were obtained following treatments with MRE11 inhibitor (Figure 6.17.B). Critically a remarkable drop was also found with MRE11-deficient I-SceI- (0.9%) and FLP- transfected cells (0.5%) relative to MRE11-deficient GR transfected cells (1.7%) with a P-value = 0.0110 and P-value = 0.0169 respectively.

Figure 6.18, shows a quantification of the survival fraction for all cell lines defective in Rad51 and MRE11 inhibitors in the presence of TA. It was observed that Rad51 deficiency reduced the survival rate both I-SceI- and FLP-transfected cells to 12- and 7.6-fold relative to DDRi-untreated cells.

Similarly, MRE11 inhibitor treatment remarkably reduced cell proliferation in all samples. MRE11 deficiency also caused a reduction in the survival rate for both I-SceI- (2.7-fold) and FLP-transfected cells (1.6-fold) relative to DDRi-untreated cells.

In summary, it was observed that no notable differences were detectable between GR, I-SceI or FLP in MRE11i- and Rad51i-treated sampels with TA treatments. Eventhough there was a reduced cell viability induced by Rad51i and MRE11i in cells transfected with any constructs, a very slight reduction was observed in I-SceI or FLP expressing cells relative to GR only. The basis of this is unclear, but indicates Rad51 and MRE11 are required to maintain cell viability during the stress induced.

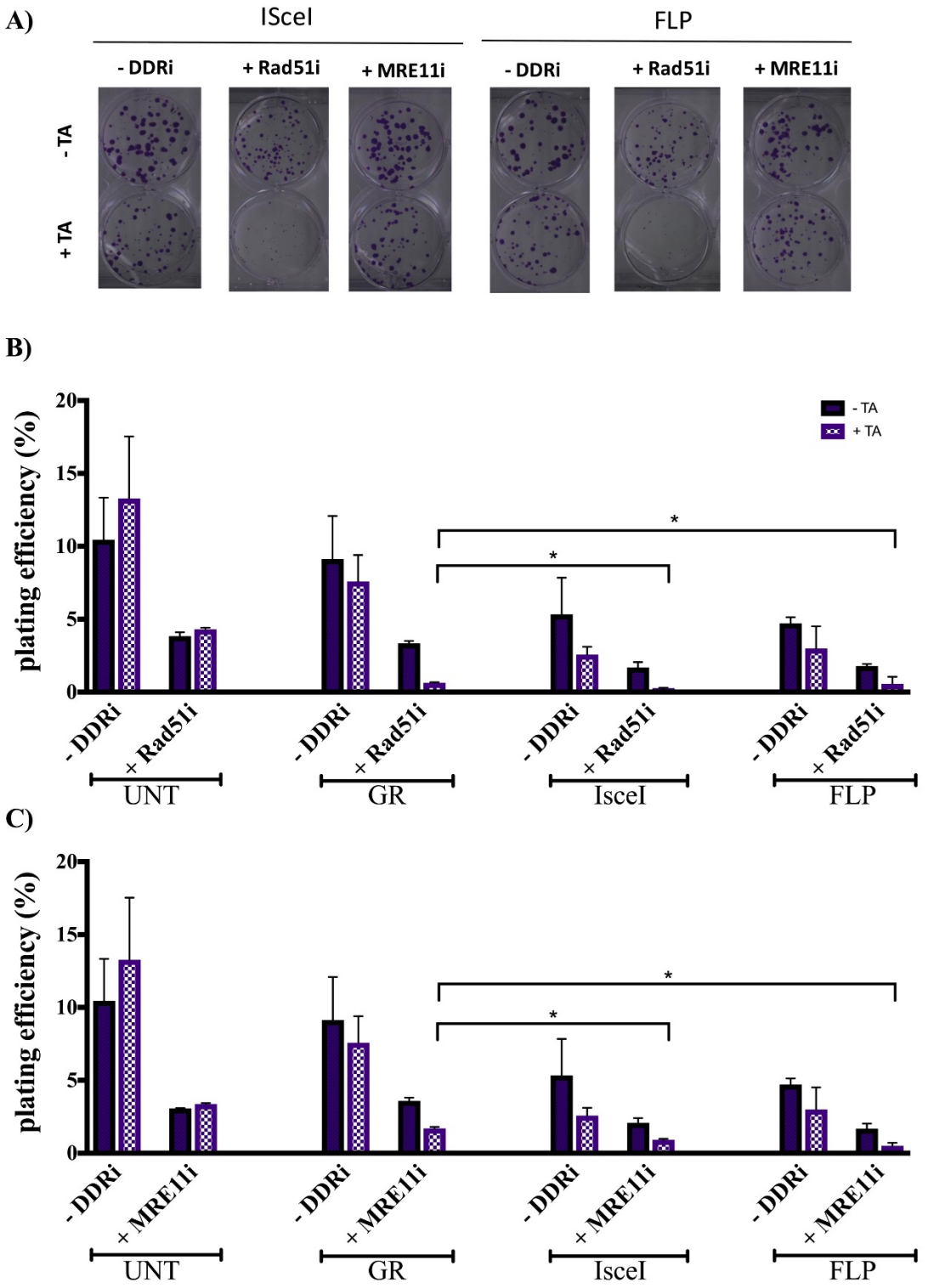

Figure 6.17 Colony Formation ability of the induced RS impaired by inhibiting HR repair factors in U2OS-FRT cells. U2OS-FRT cells transfected with pdsRed-GR, pdsRed-I-SceI-GR and pdsRed-FLP-GR exposed to HR repair inhibitors; 10 μM (Rad51i) and 15 μM (MRE11i) in the absence or presence of 100 nM TA. **(A)** Digital representative images of the effect of the induced DSB and DNA damage response on CFA on FRT-I-SceI and FRT-FLP cells exposed to Rad51i or MRE11i in the presence or absence of TA. **(B)** Analysis of plating efficiency of Rad51 deficient cells before and after TA addition. **(C)** Analysis of plating efficiency of MRE11 deficient cells before and after TA addition. Data represented as mean ± Standard deviation for three independent experiments. UNT, untransfected. – DDRi, DNA damage response inhibitor untreated.

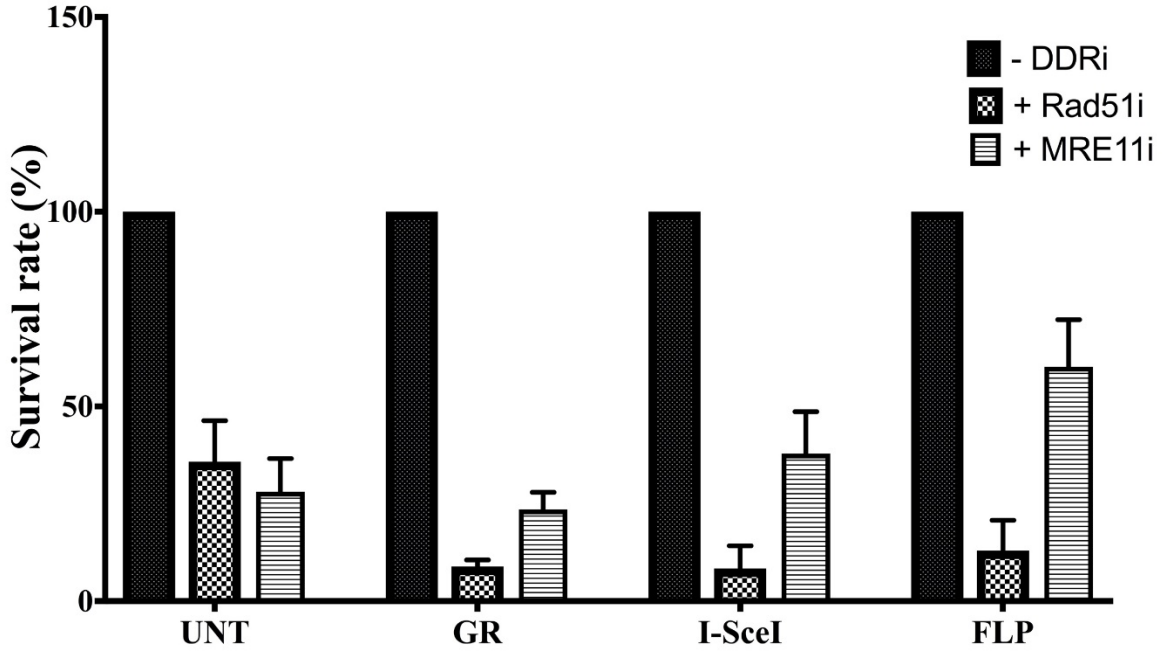

Figure 6.18 Survival rate and the fold difference of the induced RS impaired by inhibiting homologous recombination repair factors in U2OS-FRT cells.

6.2.5 Determination of the requirement of non-homologous end joining repair in response to FLP-induced broken fork

In NHEJ, the DNA-PK complex undergoes auto-phosphorylation (Ding et al., 2003); promoting the recruitment of several NHEJ repair proteins to the DSB (Lieber, 2010). It was hypothesized that the repair of stalled forks does not require NHEJ. To investigate whether the BF repair depends on NHEJ repair, both HEK293-FRT and U2OS-FRT cells were transfected and FACS performed as described previously. A total of 30 μM of DNA-PK inhibitor was added to cells in the presence or absence of TA.

6.2.5.1 Investigation of the role of non-homologues end joining repair in maintain cell viability

Figure 6.19 shows the cytotoxicity of DNA-PKs deficiency on the viability of GR-, I-SceI- and FLP-transfected HEK293-FRT and U2OS-FRT cells. Overall, in HEK293-FRT cells, as seen with other DDRi, there was an increase in cell viability for the un-transfected cells defective in DNA-PK in the presence or absence of TA compared to DDRi-untreated cells. Whereas, the GR-, I-SceI- and FLP- transfected cells resulted in a reduction in cell viability after treatment with DNA-PKi alone, in comparison to DDRi untreated cells.

A very slight increase in cell viability were evidence in DNA-PK-defective I-SceI (50.5%) or DNA-PK-defective FLP-transfected cells (56.1%) in comparison to DNA-PK-defective GR-transfected cells (46.6%) in the presence of TA (Figure 6.19.A).

In the U2OS-FRT cells, it was similarly observed that no notable differences were detectable between GR, I-SceI or FLP in MRE11i- and DNA-PKcsi-treated sampels with or without TA treatments (Figure 6.19.B). Overall, the results were very similar to other DDRi, which was no differences between I-SceI and FLP cells relative to GR-only cells.

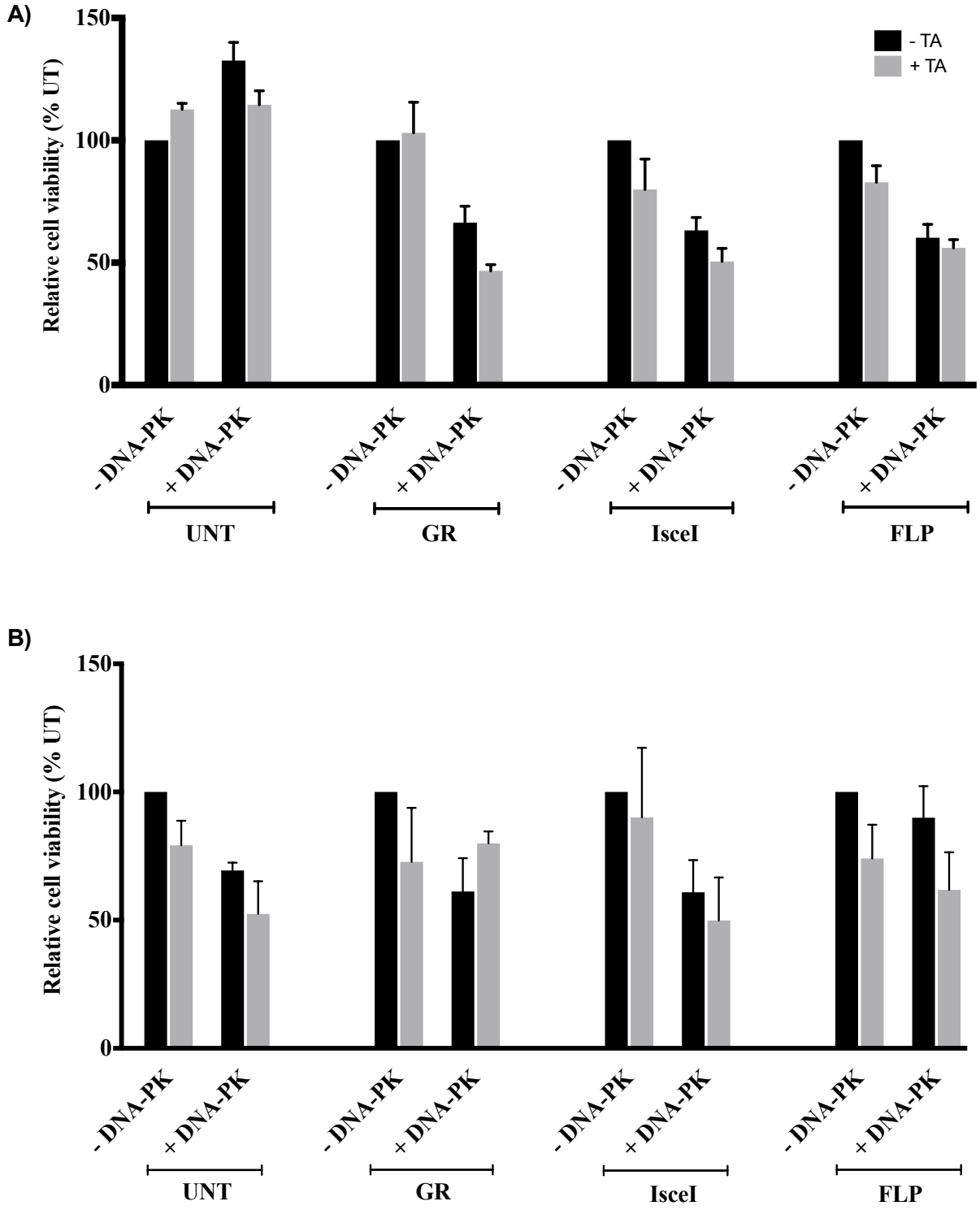

Figure 6.19 Cytotoxicity of DNA-PK NHEJ repair deficiency on cell viability of GR, I-SceI and FLP-FRT cells. FRT cells were transfected with pdsRed-GR, pdsRed-I-SceI-GR or pdsRed-FLP-GR. Cells were exposed to 30 of DNA-PKi, in the presence or absence of 10 nM TA**. (A)** HEK293-FRT cells. Data represented as mean ± Standard deviation for four independent experiments. **(B)** U2OS-FRT cells. Data represented as mean ± Standard deviation for three independent experiments. UNT, un-transfected. – DDRi, DNA damage response inhibitor untreated.

6.2.5.2 Investigation of the role of NHEJ repair in colony forming ability during RS

Though the DNA-PKcsi WST-1 assay result was inconclusive, given that phenotypes with other DDRi were observed by CFA, we similarly measured colony growth following DNA-PKcs inhibition.

Figure 6.20 shows the CFA for HEK293-FRT cells. Overall, both un-transfected and transfected cells showed a reduction of more than 50% in colony formation post-exposure to DNA-PK inhibitor in the absence of TA. No significant reduction in the PE was found in DNA-PK-deficient I-SceI- (3.0%) or FLP- transfected cells (2.6%) compared to DNA-PK-deficient GR-transfected cells (4.7%) in the presence of TA. Nonetheless, the pattern is similar to other DDRi, which is FLP and I-SceI had lower viability than GR only transfected cells. But, perhaps this indicates that DNA-PK is not essential to repair the induced DNA damage in HEK293-FRT cells. This was predicted for BF, though not direct DSB.

It was observed that DNA-PK deficiency reduced the survival rate both I-SceI- and FLP-transfected cells in a smiliar change fold relative to DDRi-untreated cells (Figure 6.21).

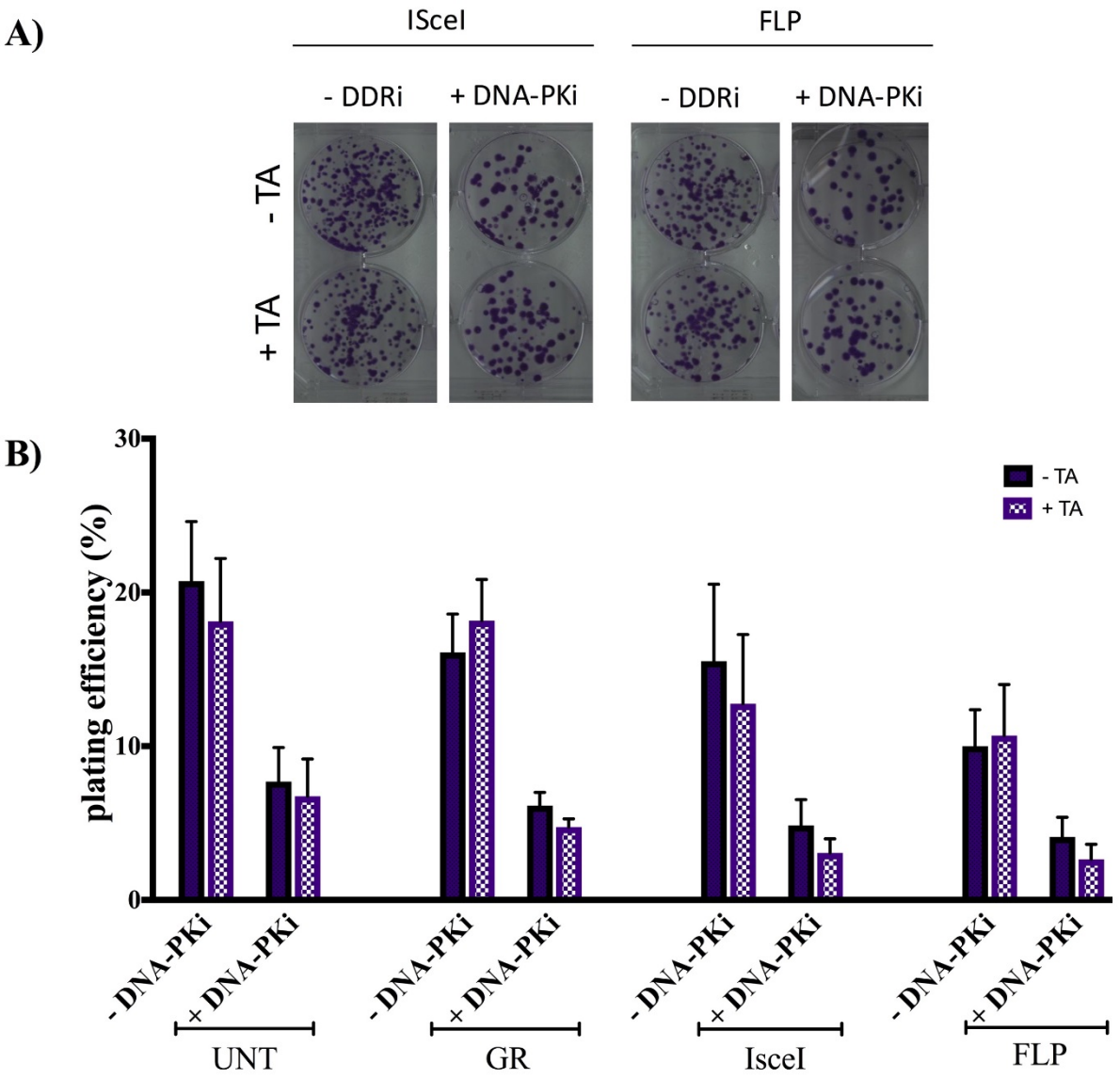

Figure 6.20 Colony Formation ability of the induced RS impaired by inhibiting NHEJ repair factor in HEK293-FRT cells. HEK293-FRT cells transfected with pdsRed-GR, pdsRed-I-SceI-GR and pdsRed-FLP-GR exposed to NHEJ repair inhibitor; 30 μM (DNA-PKi) in the absence or presence of 100 nM TA. **(A)** Digital representative images of the effect of the induced DSB and DNA damage response on CFA on FRT-I-SceI and FRT-FLP cells exposed to DNA-PKi in the presence or absence of TA. **(B)** Analysis of plating efficiency of FRT-I-SceI and FRT-FLP cells before and after TA addition. Data represented as mean ± Standard deviation for three independent experiments. UNT, untransfected. – DDRi, DNA damage response inhibitor untreated.

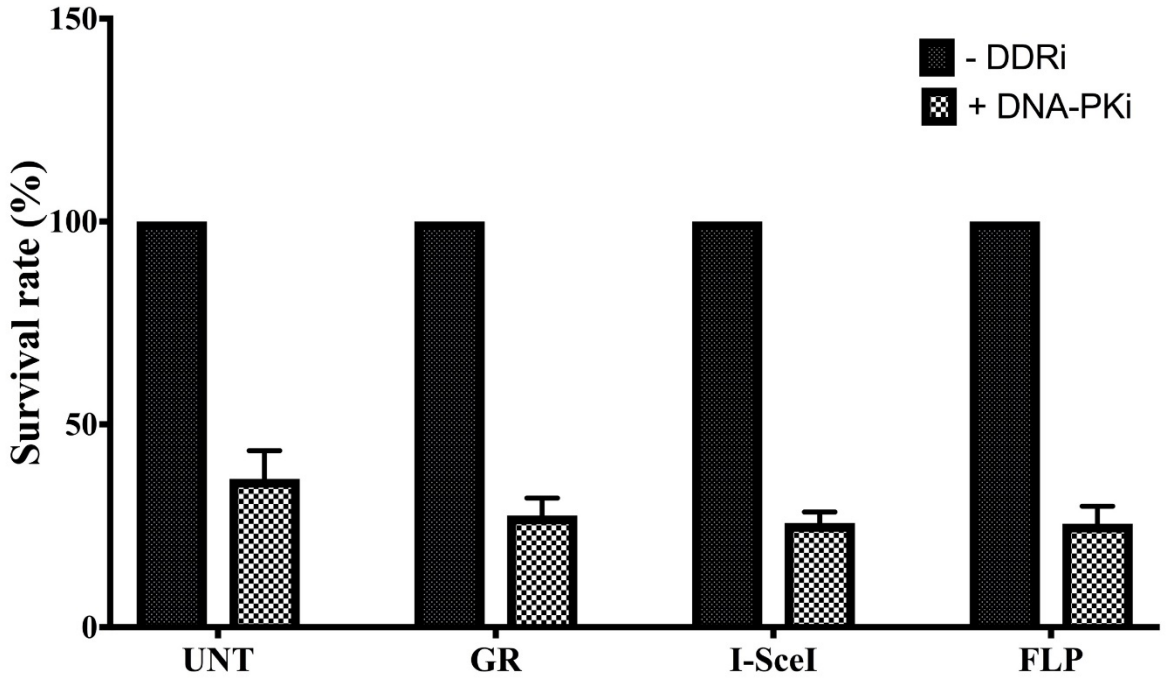

Figure 6.21 Survival rate and the fold difference of the induced RS impaired by inhibiting non-homologous end joining repair factors in HEK293-FRT cells.

Figure 6.22 shows the CFA in U2OS cells. Overall, the results are very similar to other DDRi significant different between FLP or I-SceI and GR in +TA conditions. A significant difference was observed in DNA-PK-defective I-SceI cells (0.5%) in comparison to DNA-PK-defective GR (1.9%) in the presence of TA (P-value = 0.0207). A significant reduction in PE rate was also found in DNA-PK-defective FLP cells (0.5%) in comparison to DNA-PK-defective GR cells (P-value = 0.0423). It was observed that DNA-PK deficiency reduced the survival rate both I-SceI- and FLP-transfected cells to 4.5- and 5.2-fold relative to DDRi-untreated cells (Figure 6.23).

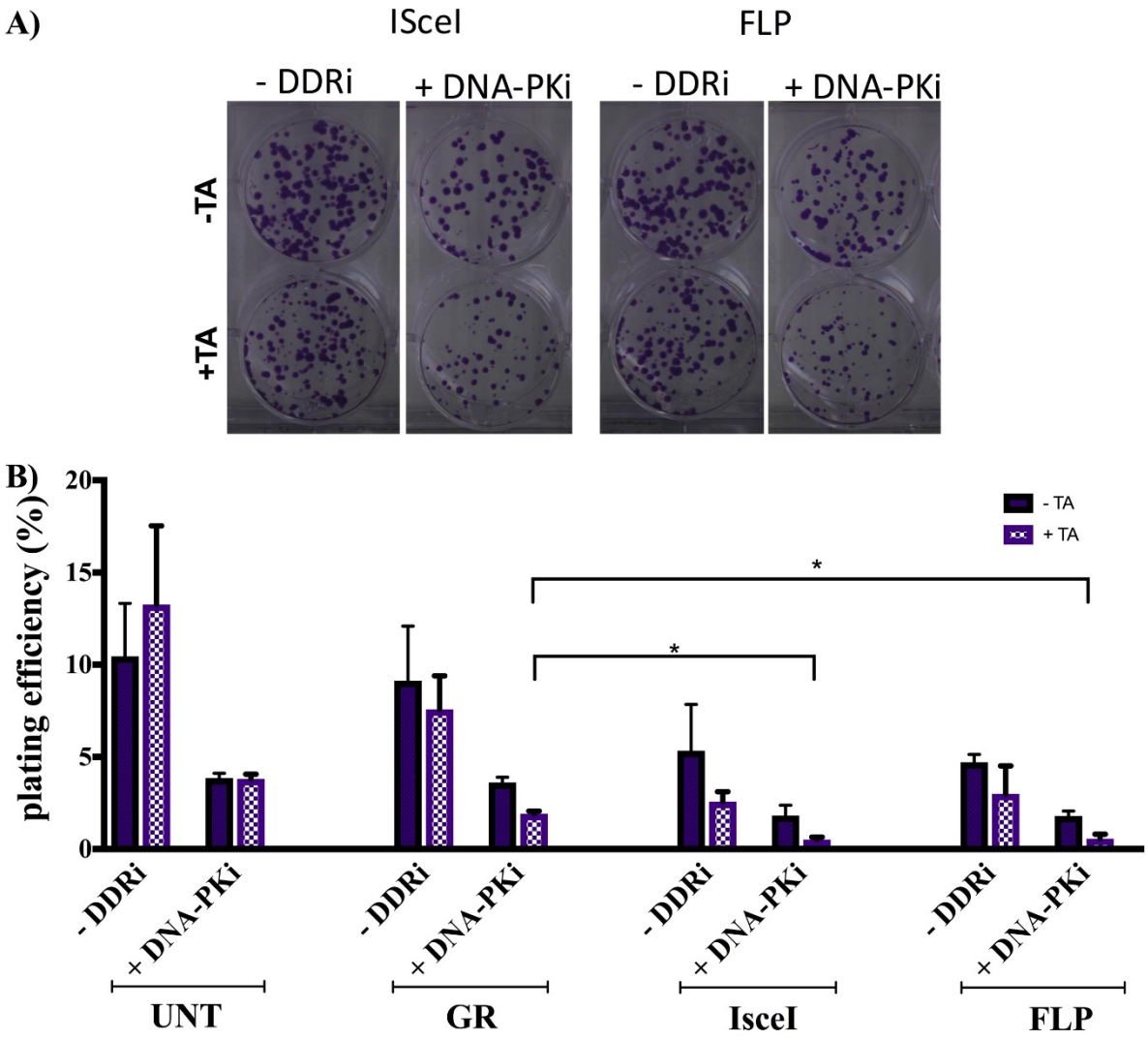

Figure 6.22 Colony Formation ability of the induced RS impaired by inhibiting NHEJ repair factor in U2OS-FRT cells. U2OS-FRT cells transfected with pdsRed-GR, pdsRed-I-SceI-GR and pdsRed-FLP-GR exposed to NHEJ repair inhibitor; 30 μM (DNA-PKi) in the absence or presence of 100 nM TA. **(A)** Digital representative images of the effect of the induced DSB and DNA damage response on CFA on FRT-I-SceI and FRT-FLP cells exposed to DNA-PKi in the presence or absence of TA. **(B)** Analysis of plating efficiency of FRT-I-SceI and FRT-FLP cells before and after TA addition. Data represented as mean ± Standard deviation for three independent experiments. UNT, untransfected. – DDRi, DNA damage response inhibitor untreated.

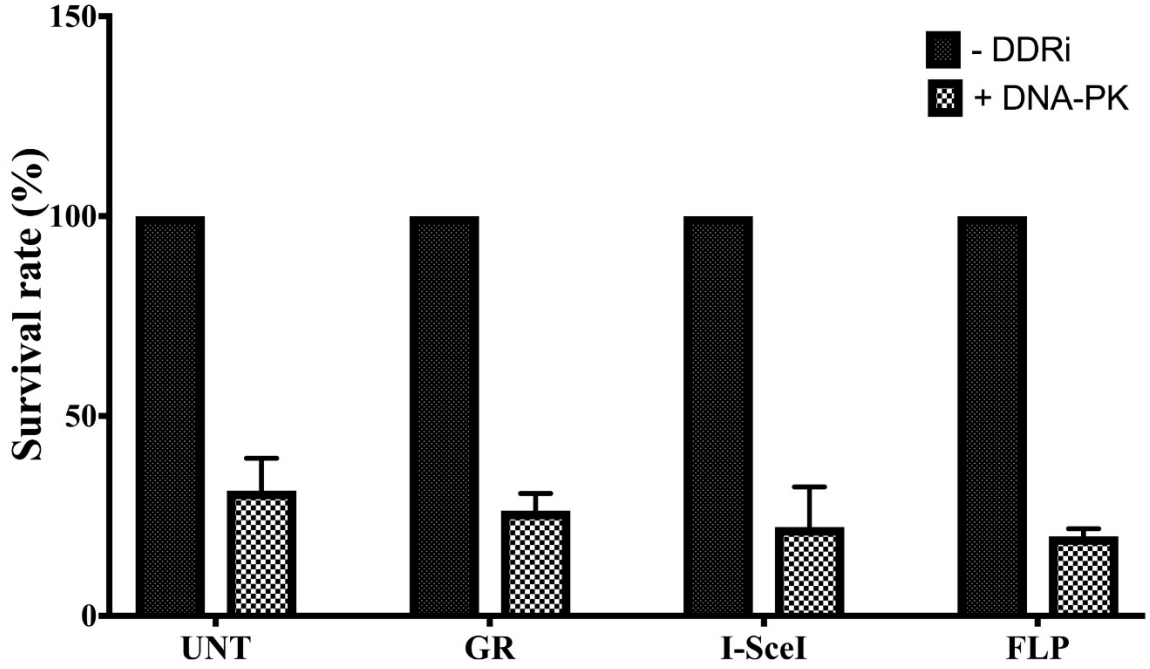

Figure 6.23 Survival rate and the fold difference of the induced RS impaired by inhibiting non-homologous end joining repair factors in U2OS-FRT cells.

6.2.6 Identifying the mutation associated with persistent fork breakage

It was possible that adapted Surveyor assay was not sensitive enough to detect mutations in FLP cultures (Section 5.2.2). Hence, if single cell clone analysis by PCR followed by sequencing was performed to characterise mutations can be directly caused by fork breakage in combination with different DDR defects, and if so what type of mutations. By performing serial dilution, HEK293-FRT-ANCH3-4 transfected cells with pdsRed-FLPH305L-GR were sorted and plated as a single cell in a 96-well plate. The cells were treated with 10 μM Rad51 and 15 μM MRE11 inhibitors for 48 hours in the presence or absence of TA. After incubation, the cells were cultured in normal media for seven days. A total of 12 transfected single-cell survivor colonies isolated after se-DSB induction for each type of DDR deficiency were randomly selected and expanded into a 6-well plate. Cell pellets were collected from each cell line for phenol:chloroform DNA extraction (Section 2.3.2).

Possible mutations that were detected by performing PCR amplification from extracted genomic DNA. PCR primers used were annealed outside the cleavage region (FRT) using ANCH3-4_406_FP and ANCH3_RP to produce a 1408 bp PCR product.

The PCR amplicon was purified and Sanger sequenced to detect mutation frequency and type in the region surrounding the FRT site after the induction a se-DSB in the survivor clones. As shown, all the selected clones had the same amplicon size, indicating that no large scale mutations (deletions/insertions) occurred within the region of interest. Moreover, no mutations were detected upon the alignment of the sequence of the selected clones with the parental cell line (Figure 6.24 and 6.25.A). This was unexpected, given that MRE11 and Rad51 are critical factors in DSB-response and HR repair.

To determine if a longer induction of RS +/- DDR defects was required to induce mutations; FLP transfected cells were treated with TA and MRE11 for the whole colony forming time period before being isolated and collected. However, no band shifs or mutations were observed in the clones (Figure 6.25.B).

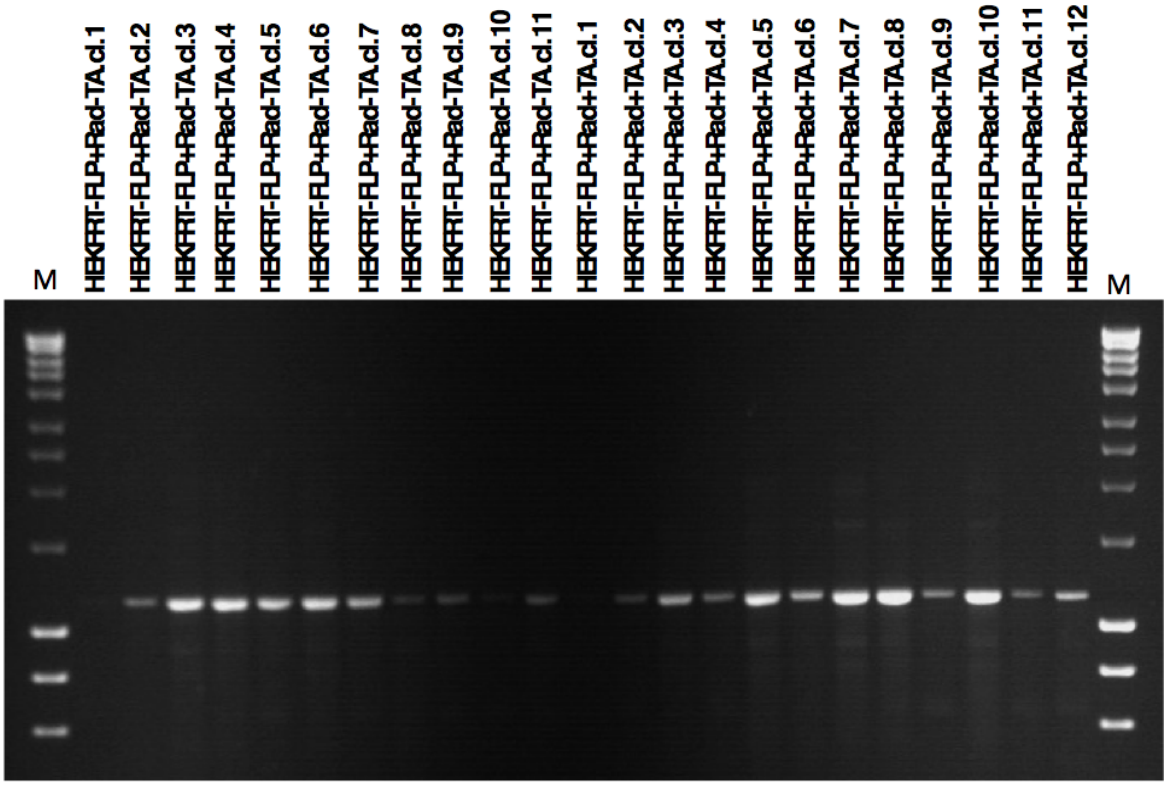

Figure 6.24 Genotyping of individual Rad51i survivor clones after se-DSB induction. HEK293-FRT cells were transfected with dsRed-FLPH305L-GR. The red cells were sorted and re-plated as a single cell using serial dilution. The cells were treated with Rad51i in the presence or absence of TA for 48 hours. The single clones were expanded and DNA was extracted. PCR was performed using FRT-406-FP and ANCH3_RP.

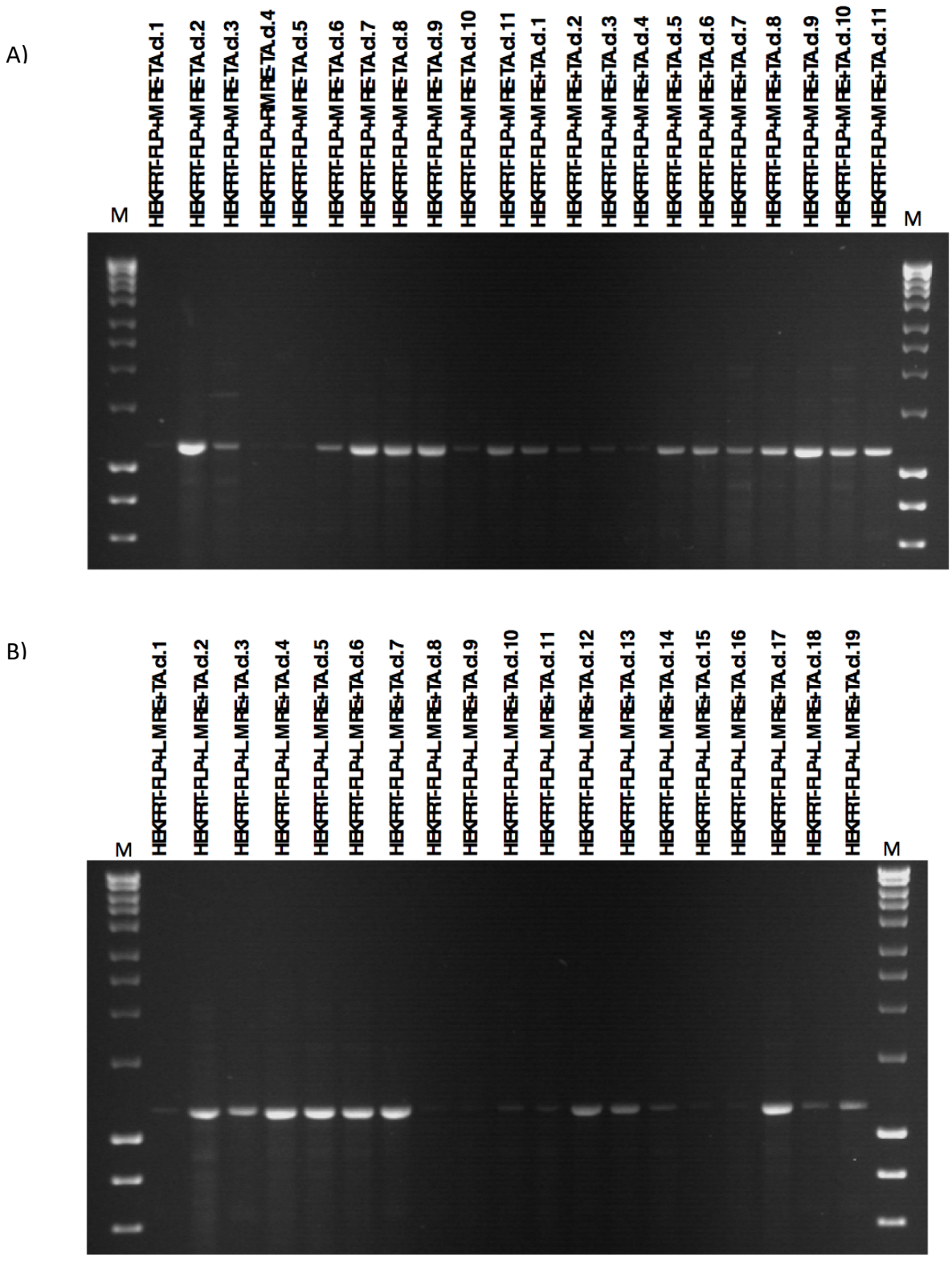

Figure 6.25 Genotyping of individual MRE11i survivor clones after se-DSB induction. HEK293-FRT cells were transfected with dsRed-FLPH305L-GR. The red cells were sorted and re-plated as a single cell using serial dilution. **A)** The cells were treated with 15 µM MRE11i in the presence of TA for 48 hours. **B)** The cells were treated with 15 µM MRE11i in the presence of TA for 10 days. The single clones were expanded and DNA was extracted. The single clones were expanded and DNA was extracted. PCR was performed using FRT-406-FP and ANCH3_RP.

6.3 Discussion

The objective of this chapter was to discover the fundamental similarities and differences by which BFs are processed and repaired comparison to direct DSBs (se-DSBs vs direct DSBs). It was expected that the repair of this type of damage (se-DSB) would be processed differently and have requirements other than repair in the case of a conventional DSB (two-sided DSB). Therefore, in this chapter it was tested whether the repair of BF generated by the FRT-Flp system requires the same DDR proteins as those needed for DSBs generated by I-SceI. To achieve this, and to examine the consequences of a defective DDR response, several synthetic DDR inhibitors were used. These were ATRi, ATMi, Mre11i (Mirin), Rad51i (Rad51-B02) and DNA-PKcsi (NU7026). All of these factors have been demonstrated as playing a critical role in repair, checkpoints, and the overall improvement of cell survival.

Unfortunately, our analyses were somewhat limited due to many DDR factors being essential. Hence, the doses recommended to fully inhibit the facors could not be used for the WST-1 and CFA assays. Ultimately, doses that induce only 50% cell death were chosen for use as these concentrations though clearly sufficient to have an effect, still permitted enough cell survival to assess how expressing FLP or I-SceI altered cell viability in the contest of at least partial DDR factor deficiency. Nonetheless, the subsequent analysis of CPT-induced gH2AX signal revealed little effect using the chosen concentrations, suggesting the factors retained significant activity, though this experiment needs to be repeated. This implies that the chosen doses may not inhibit activity enough to significantly effect any potential roles in DSB resolution. Further analysis of the effects of these doses on the factors is therefore required to fully comprehend the WST-1 and CFA data presented within this Chapter.

Overall, no notable effects of DDRi on FLP or I-SceI cells relative to GR only by WST-1. But by colony forming ability assay a pattern that all DDRi decreased viability in FLP or I-SceI relative to GR only was seen. This indicates they all have a role. Moreoveer DDRi was in general more cytotoxic in FLP than I-SceI. The reason for differences observed between WST-1 and CFA outcome might be due to the fact that these assays measures different aspects of cell biology.

The WST-1 measures the metabolism of cells whereas, the CFA measures the ability to form colonies from single cell. This highlights importance of assessing cell phenotypes and treatment effects using various assays.

However, the leakiness of the system makes it hard to measure differences between switching ON or OFF the system, and thus was hard to confirm the phenotypes are due to direct DSB and se-DSB and not some non-specific effect of I-SceI and FLP constructs, particularly as it is yet to be confirmed that FLP-DNA adducts (SSBs) are generated and lead to BFs in our cell lines. As it could be just that FLP is more toxic than I-SceI, which is more toxic than GR. though surveyor assay showed direct DSB occure with I-SceI (Chapter 5).

In this study, the importance of the key DDR mediators, ATM, and ATR was tested. The role of ATM in Flp-induced BF was investigated by inhibiting ATM alone using (KU-55933). The results in cells defective in ATM revealed an anti-proliferation effect in both transfected and un-transfected cells. This suggests its importance in cell viability and proliferation. ATM signalling is thought to suppress cancer through the induction of cell-cycle arrest by activating G1/S checkpoints to prevent cells from protecting the damaged DNA from entering the S-phase (Lukas et al., 2004). Unexpectedly, there was a pronounced trend (not significant) in the reduction of cell viability for the FRT-I-SceI and FRT-Flp cells treated with ATMi in the absence of TA. This was perhaps due to the leakiness of the system as mentioned before. However, this reduction was statistically significant post TA addition for both FRT-I-SceI and FRT-Flp in HEK293-FRT and U2OS-FRT cell lines. This highlights the importance of ATM in cell proliferation for cells harbouring DSB and BF. It has previously been observed that inhibition of ATM significantly increases radio-sensitization, reducing the chemo-resistance of cancer cells treated with DNA DSB-inducing chemotherapeutic agents, such as TopI and TopII poisons, for example CPT and etoposide, respectively (Khalil et al., 2012). Recently, it has been suggested that ATM signalling activation is also stimulated when an RF encounters a DNA lesion in the S-phase; this subsequently results in fork collapse/breakage and potential DSB formation (Yajima et al., 2009; Sirbu et al., 2011).

In addition, the role of ATR in the generated BF was identified using an NU6027 inhibitor. In this study, clear differences in growth and cell proliferation of cells lacking ATR compared to untreated were clearly observed, given that ATR is essential for replicating cells. The CFA for I-SceI- and FLP- transfected cells lacking ATR appeared to slightly decrease in the presence of TA compared to in the absence of TA. Nonetheless, there was a significant reduction in the colony formation rate of ATR-deficient FLP transfected HEK293-FRT cells compared to GR mock cells, while the ATR-deficient I-SceI cells did not show any significant reduction.

This may demonstrates the importance of ATR in fork stabilization and cell viability. However, a similarity in lesser cell viability for I-SceI- and FLP- transfected U2OS-FRT cells in response to the ATR defect was clearly evident. Furthermore, the DNA damage generated will require ATR to stabilize the resected ss-DNA along the HR repair pathway, which in turn is thought to be activated by ATR. ATR was found to have a key role in activating intra-S and G2/M cell cycle checkpoints, thereby preventing cells with DNA damage from entering mitosis (Kastan and Bartek, 2004; Cuadrado et al., 2006). Similarly, it was found that NU6027 causes attenuated G2/M arrest following CPT treatment in MCF7 cells (Peasland et al., 2011). Moreover, ATR has been found to stabilize stalled RFs and to be capable of restarting repair by signalling HR repair in response to DNA damage (Wang et al., 2004). The DDR, when activated at stalled RFs resulting from excess ssDNA, is principally associated with ATR kinase rather than ATM (Shiotani and Zou, 2009).

In addition, it has been reported that collapsed RFs and DSBs induced by UV in ATR-deficient cells have reduced ATM signalling. Thus, in certain instances, under RS, it is probable that ATM signalling is not only stimulated by DSBs, but also represents a specific response to ATR activation. However, the ATM and ATR signalling of the DNA damage responses are linked. As with DSBs, there is a clear switch between the two kinases. The ATM-dependent extensive resection of the 5′ strand exposes single-stranded DNA, inducing the activation of ATR (Shiotani and Zou, 2009; Weber and Ryan, 2015).

In order to investigate whether the generated BF relies on HR repair, the effect of MRE11i, and Rad51i on FLP-induced BF was examined. To achieve this, it was beneficial to exploit the well-known, I-SceI site specific endonuclease, which generates a DSB (Weinstock et al., 2008). It serves as a control when comparing the genetic requirements that allow cells to cope with an induced BF compared to DSB. The initial step of HR requires resection of the 5’ end to expose ssDNA, which is regulated by the MRN complex and CtIP (Sartori et al., 2007; Takeda et al., 2007; Stracker and Petrini, 2011). This ssDNA is coated with replication protein A (RPA) followed by either Rad51-dependent by loading of Rad51, the protein responsible for strand invasion (O’Driscoll and Jeggo, 2006; San Filippo et al., 2008) or Rad51-independent pathways (Davis and Symington, 2004). The latter pathway is known as microhomology-mediated BIR (MMBIR) (Zhang et al., 2009), and requires certain replication factors, such as DNA helicase, Cdc45, MCM, and GINS (Szostak et al., 1983).

The results suggest that defects effecting HR factors, Rad51 and MRE11 inhibitors significantly reduce cell survival in both the I-SceI-FRT and FLP/FRT cells. The cell viability of FRT-FLP cells closely resembles that of FRT-I-SceI cells. The reduction that occurred was statistically significant in TA-treated FRT-I-SceI and FRT-Flp cells compared to FRT-GR control cells. The results indicate that the HR factors Rad51 and MRE11 are needed to cope with the induced damage. Similarly, a role for HR in the repair of CPT-mediated se-DSBs has previously been suggested (Arnaudeau et al., 2001; Hinz et al., 2003). Effecting MRN prevents the activation of ATM, limiting the ability to repair DNA DSBs (Shibata et al., 2014). Mirin further abolished the radiation-induced G2/M checkpoint and HDR repair in vitro (Dupre et al., 2008).

In terms of repair mechanisms, one HDR sub-pathway is thought to have the function of repairing S phase DSBs. This explains why RAD51 overexpression occurs in a variety of cancer cells, suggesting it is essential in enabling cancer cells to tolerate higher RS levels. Nitiss and Wang demonstrated that HR-deficient cells are more sensitive to CPT (Nitiss and Wang, 1988).

Rather unexpectedly of the effects of NU7026 (DNA-PK) inhibitor on cell viability and CFA were found to be similar to ATM, ATR, MRE11 and Rad51 inhibition. Willmore et al. (2004) found NU7026 triggers significant inhibition in the growth of K562 leukaemia cells in response to six different TopII genotoxic poisons. In contrast, NU7026 did not potentiate CPT. Our finding that DNA-PKi had an effect in FLP1 cells is therefore unexpected and requires further investigation. Though as already mentioned, Ku can bind DSB ends in S-phase and can interfere with regulate HR-mediated repair during S-phase. Taken together, the results suggest the BFs are repaired by HR and not NHEJ.
Collectively, these findings demonstrate that BFs are processed in a variety of ways based on a range of requirements that overlap with direct DSB. From this perspective, under chronic RS conditions, and particularly in the absence of DNA repair pathways or non-functional checkpoint responses, aberrant RFs might result in altered cell viability and DNA alterations, that lead to mutations.

From the PCR reaction, it was found that most of the selected single survivor clonal cells with chronic BF resulted in complete PCR amplicon within the breakage site, suggesting that the breakage was more likely followed by an accurate repair mechanism. Single clonal cells were used to investigate the respective roles of HR in the repair of the induced se-DSBs.

However, the findings with RAD51 and MRE11 defictive clonal cells indicate that these survivor cells, though defective for the initial HR repair factors, reveal an accurate repair of the break site. These results imply that the factor may not be essential for RF re-establishment, suggesting that an efficient alternative pathway may work to repair the induced BF. This result, however, is compatible with recent evidence indicating that although multiple redundant pathways are involved in the initial repair processing of se-DSB generated by CPT, all the pathways eventually rely on HR to complete repair (Pourquier et al., 2001). Alternatively, it may be that more clones need to be isolated to detect the relatively rare events.

NHEJ is a fundamental mechanism required to rejoin two DSB ends, although it was previously thought that end joining is not available as a mechanism to repair se-DSBs, owing to the lack of another DNA end to be ligated to. However, a recent protein purification study demonstrated that Ku associates with the free double-stranded DNA ends in the replication sites shortly after treating human cells with CPT (Ribeyre et al., 2016). Moreover, in yeast, Ku was also found to accumulate around the DSB site, shielding DNA ends from exonucleases and suppressing DNA end resection and HR (Mimitou and Symington, 2010; Foster et al., 2011; Sun et al., 2012).

Understanding these processes will shed light on RS responses and aid the development of better preventative and therapeutic strategies.

Chapter 7: Characterization of the role for classical non-homologous end joining during replication stress

7.1 Introduction

The faithful transmission and propagation of intact genetic information from one cell to its offspring are prerequisites to maintaining genome integrity. As discussed in Section 1.6, one role of the DDR when mitigating RS is DSB repair. DSB occurs through a HDR-mediated pathway or through c-NHEJ or a-NHEJ (Rothkamm et al., 2003). Previous studies suggest that c-NHEJ factors promote mutagenicity when misused during S-phase, and that cells suppress NHEJ and preferentially use HR mechanisms (Adamo et al. 2010; Patel et al., 2011; Pace et al., 2010; Bunting et al., 2012). However, in contrast to previous observations, Steven Foster (head of this laboratory) previously detected an unexpected role of KU and LIG4 in preventing metaphase chromosomal aberration following the induction of DNA damage in the preceding S phase (Foster, unpublished). Genome integrity in metaphase spreads of WT mouse embryonic fibroblasts (MEFs) (NHEJ proficient) and *Ku86*$^{-/-}$ MEFs (NHEJ deficient) cells was compared after treating cells with phleomycin, a chemotherapeutic agent that generates both ds-DSBs and SSBs (Chen and Stubbe, 2005). The SSBs generated might then induce secondary DNA damage, as SSBs can create se-DSBs following collision with replication forks (similar to the developed Flp-FRT system and CPT treatment). This DSB-inducing genotoxic drug was used alongside caffeine, which inhibits ATM/ATR checkpoint signalling (Powell et al., 1995) (Table 1.3), which was done to block checkpoint activation, potentially allowing cells with DNA damage and instability to pass into metaphase for detection when they would otherwise remain in S-phase due to intra S-phase checkpoint and be missed from the analysis (Figure 7.1).

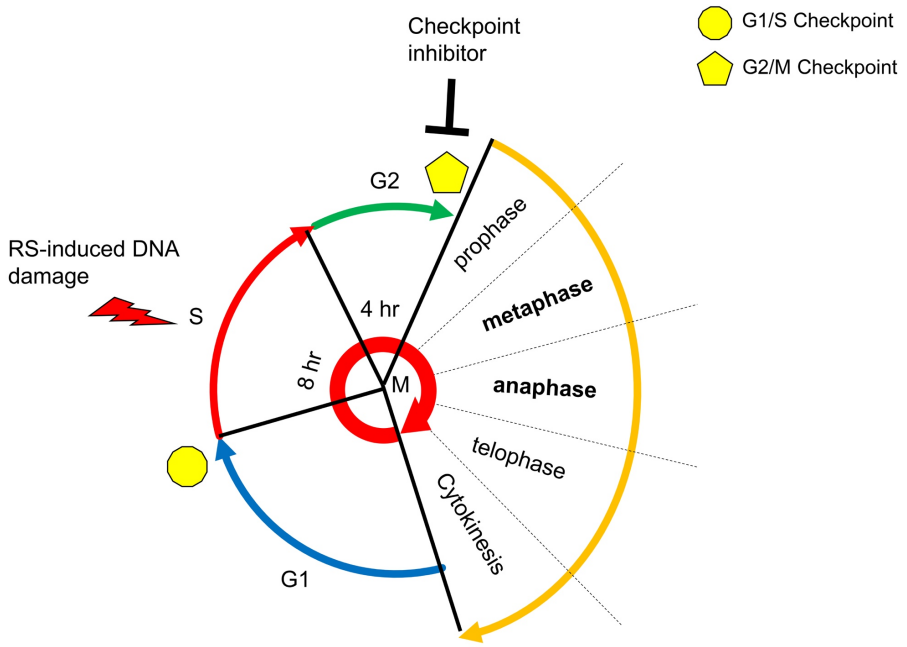

Figure 7.1 Schematic representation of the cell cycle phases and the progression into mitosis and cytokinesis. Cells are exposed to RS-induced DNA damage during S-phase. Treated cells are incubated for 8 hours and then collected for metaphase spreads, or incubated for 12 hours and fixed for anaphase bridge and micronuclei assays. G1, growth phase 1. S, synthesis phase. G2, growth phase 2. M, mitosis. The M-phase consist of subphathways: prophase, metaphase, anaphase, telophase and cytokinesis.

Observations showed that a deficiency of NHEJ factors, KU86 or DNA Ligase 4 (LIG4), can trigger a significant increase in phleomycin-induced chromosomal aberrations in metaphase spreads collected 8 hours after phleomycin treatment (i.e. cells that were in metaphase when collected were in S-phase during phleomycin treatment) (Foster and Petrini, unpublished; Figure 7.2). These aberrant metaphase chromosomal exchanges/fusions following phleomycin treatment included unusual multiple chromosomes exchanges/fusions. However, the higher aberrant levels were only found with c-NHEJ-deficient cells that were pre-treated with caffeine, suggesting that this phenotype was missed previously as c-NHEJ-deficient cells harbouring high levels of DNA damage do not progress to metaphase and are missed from the analysis. Overall, the data indicated that c-NHEJ is necessary to maintain genomic integrity rather than promoting genomic instability during RS. Given these results, it has been hypothesized that NHEJ has a role in repairing direct DSBs during S-phase, which phleomycin generates, but it was not envisaged that NHEJ repairs phleomycin-induced se-DSBs (Figure 1.6).

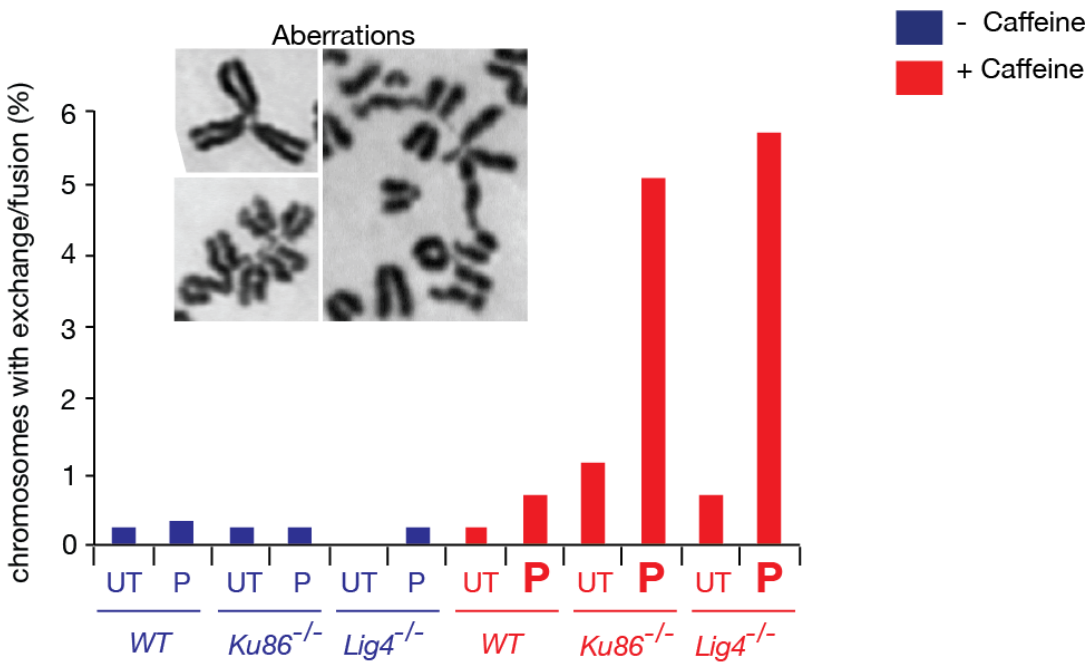

Figure 7.2 Effect of non-homologous end joining during DNA replication stress. Analysis of genome instability in the metaphase spreads of WT-MEF (NHEJ-proficient), Lig4$^{-/-}$ MEF and *Ku86*$^{-/-}$ MEF (NHEJ-deficient) cells were compared 8 h post treatment of the cells with phleomycin in the presence or absence of caffeine.

This chapter aims to identify and characterise the unexpected role of c-NHEJ during S-phase; specifically, its action in mitigating CIN and maintaining genome stability in response to RS, as suggested by the previous experiment. Genome integrity in metaphase spreads is compared to NHEJ-proficient and deficient MEFs post induction of se-DSBs and ds-DSBs during S-phase using various chemotherapeutic agents. It was also of interest to determine whether NHEJ factors are required to regulate the repair of therapeutic-induced direct DSBs and/or se-DSBs during the S-phase to prevent genomic instability, while comparing caffeine-treated and caffeine-untreated cell lines. How direct DSBs that are generated in S-phase independently of replication are rarely considered in the literature. However, these direct DSBs will be induced by treatments such as IR, and will majorly disrupt DNA replication as the chromosome is no longer intact. Moreover, if they occur at sites that have not yet been replicated, there will be no sister chromatid available for HR and NHEJ may be the only or best option. The investigation will include analysing metaphase spreads, anaphase bridges, and micronuclei to determine changes in and the persistence of genomic instability. This will help decipher the mechanisms underlying the unanticipated role of c-NHEJ, as well as to establish the biological significance of NHEJ as a suppressor of oncogene-driven tumourigenesis, and its role in maintaining genome integrity.

7.2 Results

7.2.1 Identification of the basis of the requirement for non-homologous end joining during replication stress

Previously unpublished data obtained from the metaphase spreads experiments revealed that NHEJ deficiency causes a significant increase in phleomycin-induced chromosomal aberrations (Foster and Petrini, unpublished). These include translocations and multiple chromosome fusions, compared to WT cells. To confirm the previously observed role of c-NHEJ as a suppressor of CIN and GCRs, chromosomal instability in metaphase spreads of WT-MEFs and *Ku86*$^{-/-}$ MEFs cells was compared eight hours (the approximate time permitted for the cells to pass into metaphase from S-phase) after treatment with phleomycin. As discussed previously, phleomycin was selected to measure the general role of NHEJ in the repair of RS-induced DNA damage.

Metaphase spread slides were prepared from the MEFs of each genotype, as described in Section 2.5.11. Examples of representative metaphases are depicted in Figure 7.3, and approximately 50 metaphase spreads/conditions per experiment (all agent treatments were included in each experiment) were blind scored for chromosome aberrations, such as chromosomes with chromatid/chromosome breaks and chromosomes with exchanges, including two-arm exchanges, translocations and fusions (Savage, 1976).

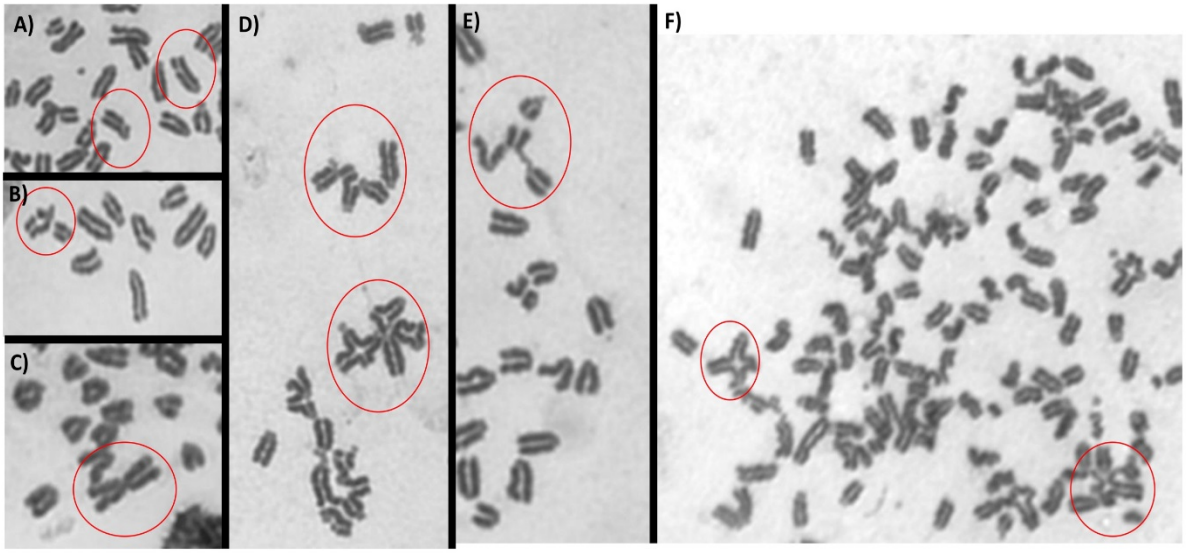

Figure 7.3 Representitive meta-phase spreads images of different DNA damage. Red circles represent the damaged chromosomes. **A) and B)** chromatid breakage. **C) . D), E) and F)** fusions/exchanges between three chromosomes.

The background total aberration levels for WT cells was 5.6%, and 10.5% for *Ku86*$^{-/-}$ cells (Figure 7.4). It was revealed that NHEJ deficiency increased phleomycin-induced chromosomal aberrations; these include chromosome breaks, chromatid breaks, and multiple chromosome fusions, compared with WT cells. Phleomycin alone did not increase total aberration in WT cells; however, it raised the abbreviation level by 7% in *Ku86*$^{-/-}$ cells (Figure 7.4.A). The initial experiment did not detect such an increase in phleomycin only Ku samples, but is concordant with the hypothesis that c-NHEJ acts to maintain viability during phleomycin-induced RS.

Treating cells with caffeine raised the total aberration in both cell lines to 9.2%, and 12.7% for WT and *Ku86*$^{-/-}$ cells respectively. The caffeine induced increase is expected as ATM and ATR defects will lead to RS response defects even with additional treatment with genotoxic agents.

There was a minimal 1% increase in WT cells in the total aberration level post phleomycin and caffeine treatment compared with caffeine treatment alone. However, a larger increase was found in *Ku86*$^{-/-}$ cells post phleomycin and caffeine treatment (15%), when compared with caffeine alone (17%). Though the increase in aberration levels in phleomycin and caffeine in Ku cells is not up to the 5-fold seen in Figure 7.2, the pattern is the same.

The increase in aberration in Ku conservted of both chromatid/ chromosome breaks and exchanges/ fusions gave the same numbers.

Together, the data from this study, together with the preliminary results, indicate that c-NHEJ acts to resolve DNA damage of replicating chromosome generated by phleomycin treatment. Therefore, the use of different chemotherapeutic drugs known to cause different specific types of replication stress-induced DSBs will test the role of NHEJ factors as a mechanism for repairing the damage these stresses induce. In addition, the aberrations observed suggest that c-NHEJ deficiency under increased RS might lead to subsequent severe mitotic defects that contribute to CIN and aneuploidy.

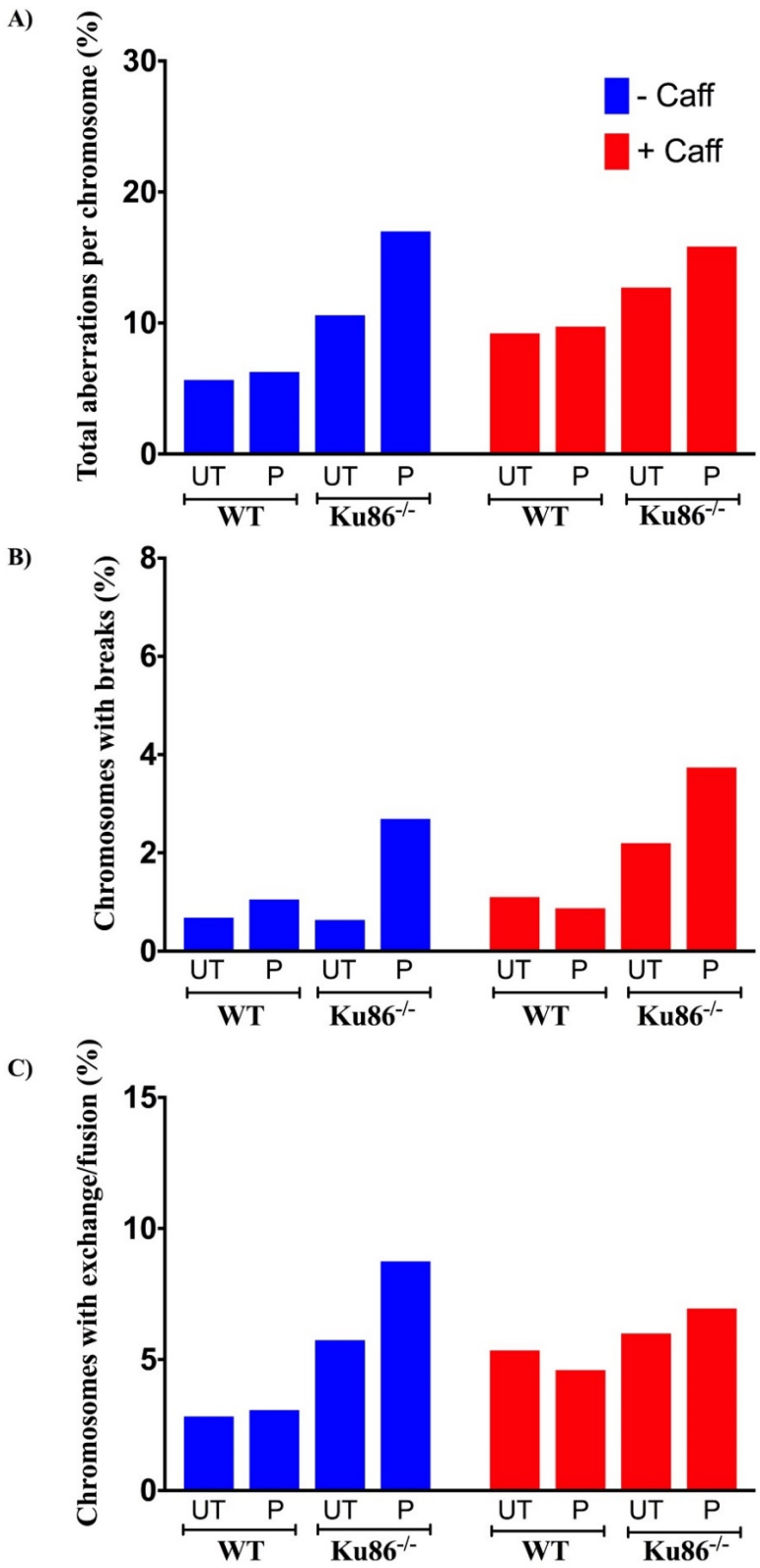

Figure 7.4 Effect of non-homologus end joining deficiency post phleomycin treatment. (A) Analysis of total chromosomal aberration. **(B)** Analysis of chromosomes with breaks, either chromosome or chromatid. **(C)** Analysis of chromosomes with exchange and fusions. In metaphase spreads of NHEJ proficient and NHEJ deficient cells treated for 8 hours with phleomycin, in the presence or absence of Caffeine. UT, untreated. P, phleomycin. Caff, Caffeine. Data represented as mean of 50 metaphase spreads/conditions for three independent experiments.

7.2.1.1 Requirement for c-NHEJ in response to se-DSBs

In this experiment, cells were treated with a chemotherapeutic agent, CPT, which causes SSBs and thus generates se-DSBs following collision with replication forks during replication, in both the absence or presence of a caffeine inhibitor.

It was observed that CPT alone increased total aberration levels in WT cells compared to untreated cells; it raised the aberration level from 5.6% to 17.4%. However, the percentage of total aberration also rose in *Ku86*$^{-/-}$ cells (21%) relative to the untreated cells (10.6%) (Figure 7.5.A). It was reveald that c-NHEJ defiecincy did not increase CPT-induced chromosomal aberration levels relative to WT, indicating that c-NHEJ deficiency promotes repair of se-DSB, which agrees with previous finding (Foster et al., 2012).

There was a large increase in the total aberration level post CPT and caffeine treatment compared with caffeine treatment alone in WT cells from 17.5% to 9.2% respectively. However, a smaller increase was found in *Ku86*$^{-/-}$ cells post CPT and caffeine treatment (16.8%), when compared with caffeine alone (12.7%).

CPT alone increased the chromosome break level in both WT and *Ku86*$^{-/-}$ cells compared to untreated cells. It was observed that CPT increased the number of chromatid breaks in WT cells to 4.5% relative to untreated cells (0.6%) (Figure 7.5.B). Similarly, it also rose in *Ku86*$^{-/-}$ cells (5.8%) relative to the untreated cells (0.6%). However, it was reveald that c-NHEJ defiecincy did not increase CPT-induced chromosomal breaks levels relative to WT. Although the percentage of chromosome breaks increased after treating the Ku$^{-/-}$ cells with the combined treatments (CPT and caffeine), this percentage was remarkably higher in WT cells (Figure 7.5.B).

Moreover, it was observed that CPT increases the percentage of chromosomes with exchanges/fusions in WT cells (5%) when compared to untreated cells (2.8%). This increase was much lower in CPT-treated *Ku86*$^{-/-}$ cells (6.6%) than untreated cells (5.7%). Although combining the treatments reduced the level of fused chromosomes in WT cells, the percentage rose remarkably in Ku-deficient cells (Figure 7.5.C).

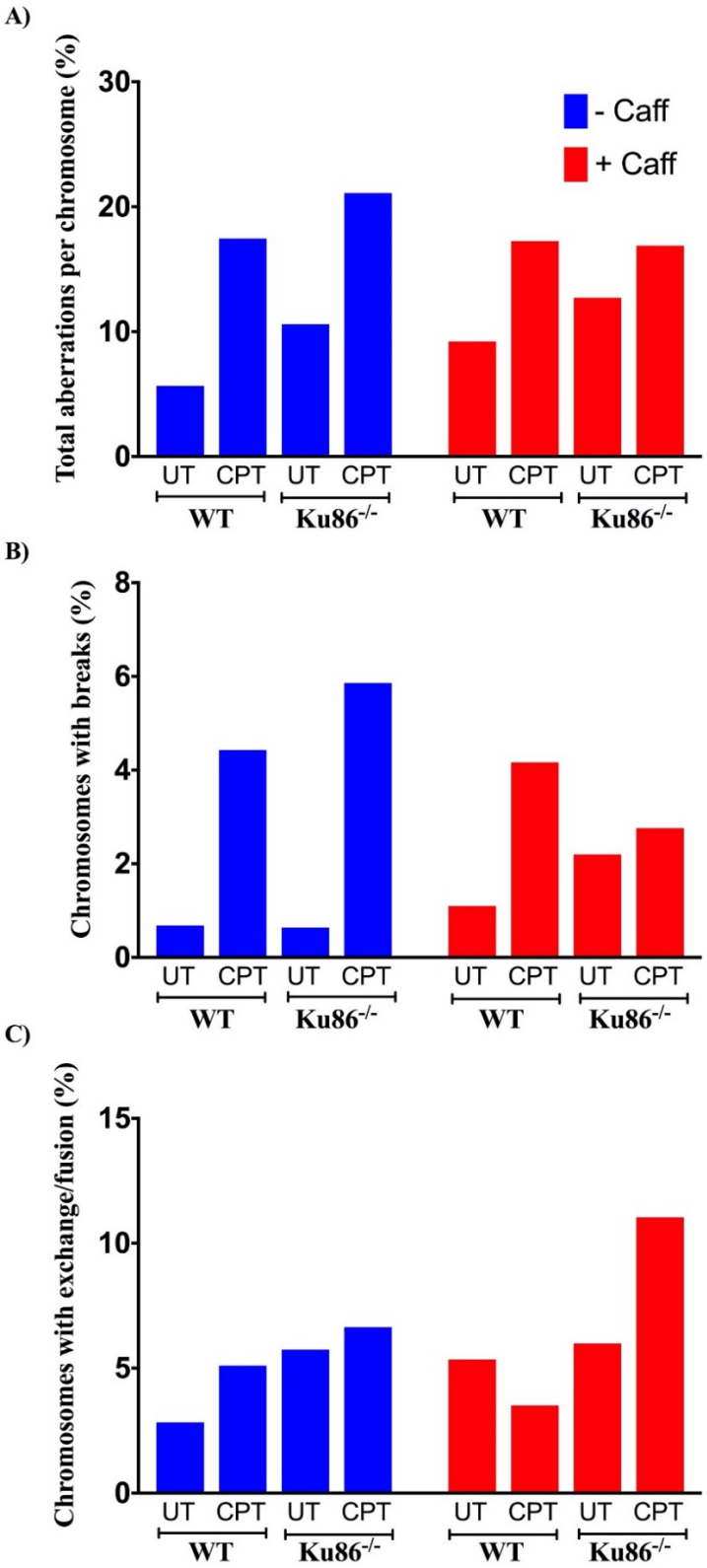

Figure 7.5 Effect of non-homologus end joining deficiency post Camptothecin treatment. (A) Analysis of total chromosomal aberration. **(B)** Analysis of chromosomes with breaks, either chromosome or chromatid. **(C)** Analysis of chromosomes with exchange and fusions. In metaphase spreads of NHEJ proficient and NHEJ deficient cells treated for 8 hours with camptothecin, in the presence or absence of Caffeine. UT, untreated. CPT, Camptothecin. Caff, Caffeine. Data represented as mean of 50 metaphase spreads/conditions for three independent experiments.

7.2.1.2 Requirement for c-NHEJ in response to direct DSB

To investigate the requirement for NHEJ in response to direct DSBs, cells were treated with etoposide, which generates chromosomal DSBs, in the presence or absence of caffeine.

There was an increase in the level of total chromosomal aberrations post etoposide-treated WT, and *Ku86*$^{-/-}$ cells compared to untreated cells. The total aberration level was 21.8% in etoposide treated WT cells compared to 5.6% in untreated cells. Even though there was an increase in the total abbreviations in etoposide *Ku86*$^{-/-}$ cells compared to untreated cells, this increase was 4% less than in WT.

In contrast, there was no increase in total aberration level in etoposide/caffeine treated WT cells compared with caffeine only-treated cells. As predicted, the increase in total aberrations was greater in NHEJ-deficient cells treated with etoposide and caffeine when compared to caffeine only cells (Figure 7.6.A).

Etoposide did not cause any chromosome breakage in WT cells. However, it was found to cause chromosome breaks in NHEJ-deficient cells. In addition, the percentage of chromosome breaks occurring was comparable in etoposide alone and etoposide combined with caffeine (Figure 7.6.B). As shown in Figure 7.6.C, the majority of the observed increase in total abbreviation was from the percentage of chromosomes with exchanges and/or fusions. It was found that the total fusion level increased to 10.8% in etoposide- and caffeine-treated *Ku86*$^{-/-}$ cells compared to cells treated with etoposide only (6.8%).

Hence, c-NHEJ deficiency combined with caffeine treatment increases aberration levels, but caffeine dose not have the same effect on etoposide treated WT cells.

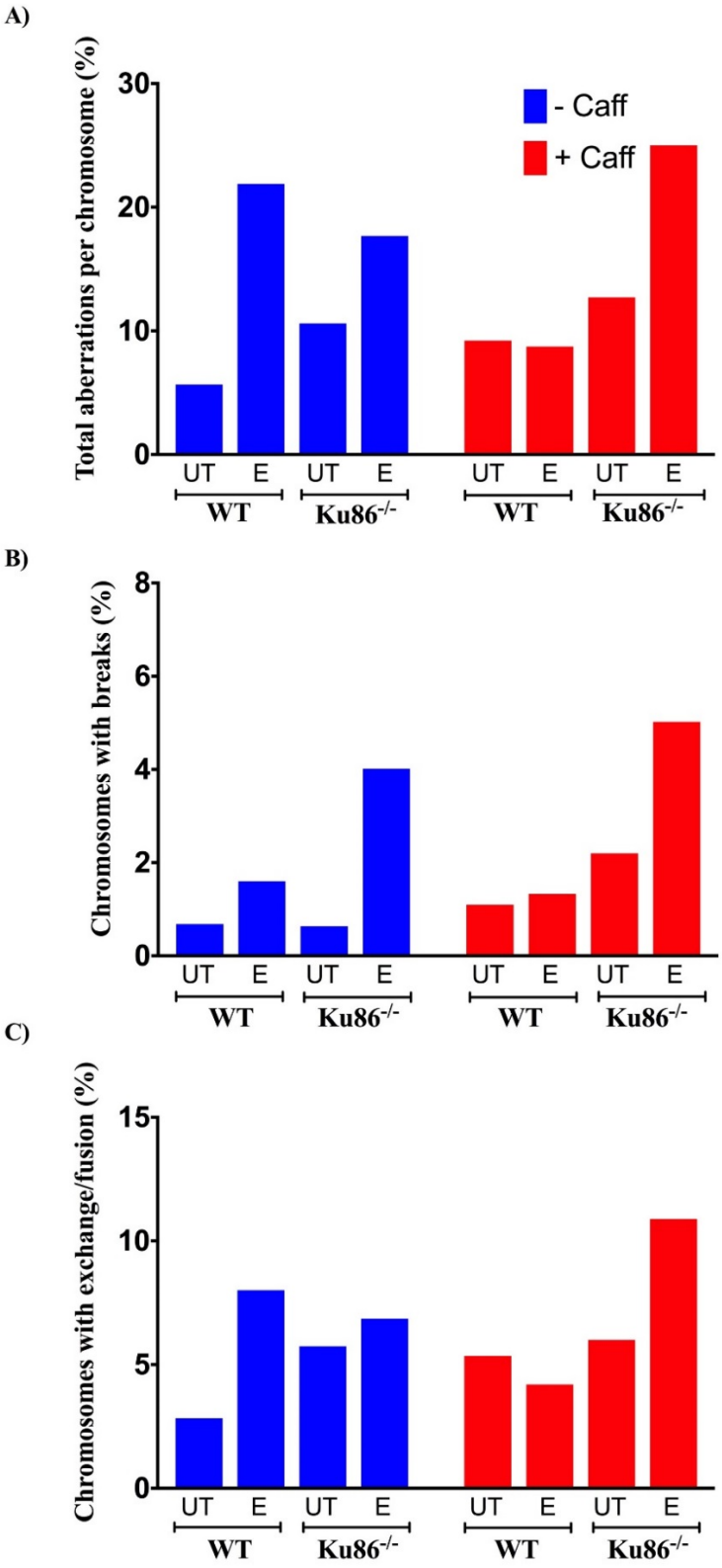

Figure 7.6 Effect of non-homologus end joining deficiency post Etoposide treatment. (A) Analysis of total chromosomal aberration. **(B)** Analysis of chromosomes with breaks, either chromosome or chromatid. **(C)** Analysis of chromosomes with exchange and fusions. In metaphase spreads of NHEJ proficient and NHEJ deficient cells treated for 8 hours with etoposide, in the presence or absence of Caffeine. UT, untreated. E, Etoposide. Caff, Caffeine. Data represented as mean of 50 metaphase spreads/conditions for three independent experiments.

7.2.2 Investigation of the impact of NHEJ deficiency on mitosis following replication stress

Anaphase experiments were performed to confirm the persistence of genome instability in NHEJ-deficient cells following RS, and to establish whether the aberrations presented at metaphase will cause defects at the anaphase stage of nuclear division, subsequently leading to anaphase bridges and micronuclei formation.

An anaphase bridges experiment was performed using WT and $Ku8^{-/-}$ MEFs cells, as explained in Section 2.5.12. The cells were treated with phleomycin only, caffeine only, or both phleomycin and caffeine. Levels of DAPI-stained anaphase bridges, lagging chromosomes and micronuclei were scored and quantified after 8 and 12 hours (approximate time permitted for the S-phase to transmit into anaphase).

Three independent anaphase experiments were performed to reduce sample-to-sample variability. However, when comparing untreated and phleomycin-treated cells, there was no notable difference in the number of anaphase bridges in the Ku86-deficient cells treated with phleomycin compared to the number of WT cells, whether caffeine was added or not (Figure 7.7). A similar lack of notable difference between WT and Ku cells in micronuclei levels was observed following phleomycin treatment in the presence or absence of caffeine (Figure 7.8). This finding is not consistent with the data from phleomycin metaphase experiments, which indicates that cells might resolve the aberrations between metaphase and anaphase.

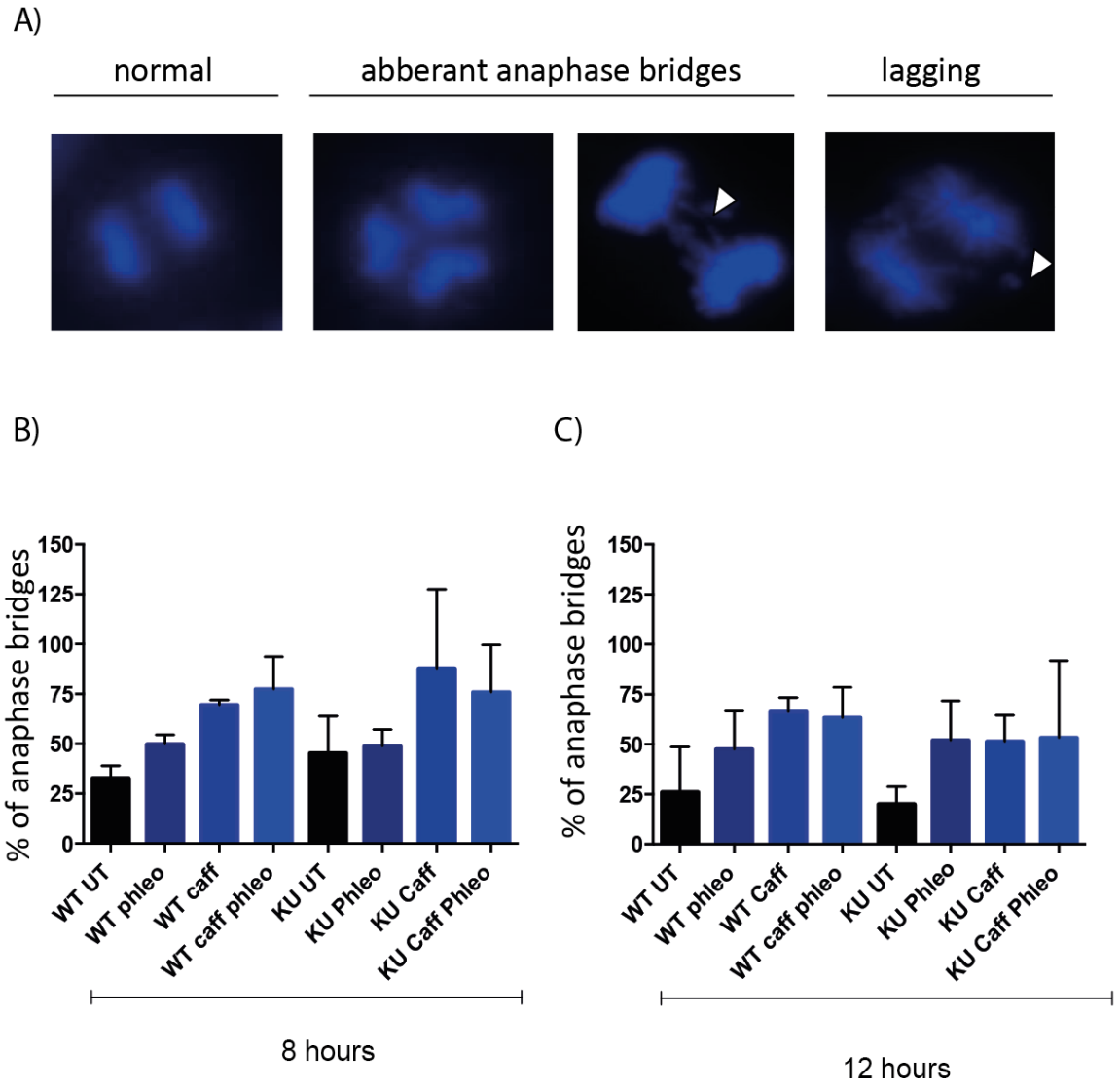

Figure 7.7 Effect of classical non-homologous end joining deficiency on mitosis following RS in previous S-phase. A) Representative images of the anaphase bridges of WT and *Ku*$^{-/-}$ MEFs cells treated with phleomycin only, caffeine only, and both phleomycin and caffeine. Images were taken with an Olympus cytological microscope. **B)** Analysis and quantification of the number of anaphase bridges and lagging chromosomes 8 h post treatment. **C)** Analysis and quantification of the number of anaphase bridges and lagging chromosomes after 12 h. UT- untreated, caff- caffeine, WT- wild type -MEFs (NHEJ proficient), KU- *Ku*$^{-/-}$ MEF (NHEJ-deficient) cells. Vertical bars represent the error bars. Results are means± S.D. n=3 independent experiments.

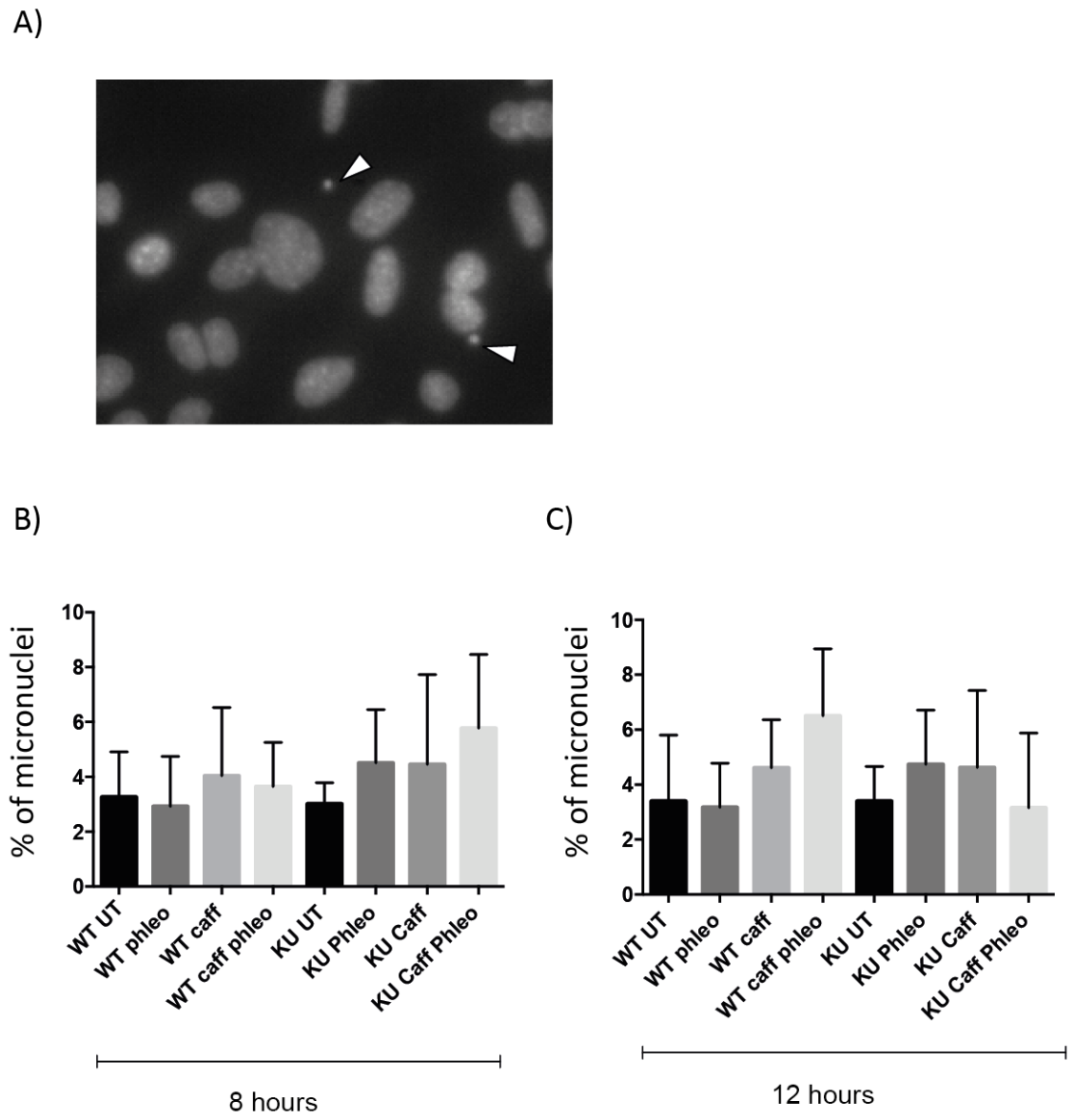

Figure 7.8 Effect of classical non-homologous end joining deficiecny on mitosis. A) Representative images of micronuclei. **B)** Analysis and quantification of the micronuclei of WT and *Ku*$^{-/-}$ MEFs cells treated with phleomycin only, caffeine only and both phleomycin and caffeine after 8 h. Images were taken with an Olympus cytological microscope. **C)** Analysis and quantification of the micronuclei of WT and *Ku*$^{-/-}$ MEFs cells treated with phleomycin only, caffeine only, and both phleomycin and caffeine after 12 h (permitted time for the S-phase to transition into the metaphase and anaphase respectively). Images were taken with an Olympus cytological microscope. Vertical bars represent the error bars. Results are means± S.D. n=3 independent experiments.

7.3 Discussion

The purpose of this chapter was to investigate the potentially unexpected role of c-NHEJ in maintaining genome stability during the S-phase in response to RS-induced DNA damage. It also aimed to determine whether c-NHEJ factors acts to resolve direct DSBs and/or se-DSBs on replicating chromosomes.

It was found that there is a trend in NHEJ-deficient cells towards increasing total chromosomal aberrations, including fusions and exchanges, compared to NHEJ-proficient cells following phleomycin treatment when combined with caffeine treatment. This result confirmed the observations from the preliminary experiment that c-NHEJ appears to maintain and promote genome integrity during the S-phase following the perturbation of DNA replication by oxidative DNA breaks. However, these results contradict previous research observations that suggest that mammalian NHEJ is mutagenic through S-phase resulting in GCR (Pace et al., 2010; Patel et al., 2010). This conflicting result might be due to the type of RS-induced DNA damage used. On the other hand, the dependence on caffeine to observe the increase in aberrations in phleomycin -treated cells could be due to checkpoint blocking, thus damaging the progress of the S-phase cells towards metaphase. Another explanation could be the inhibition of ATM/ATR (therefore inhibiting HR repair mechanisms and subsequently increasing GIN (Chanoux et al., 2009; Menezes et al., 2015). Giving this conflict and to further investigate the importance of NHEJ factor in maintaining genome stability during the S-phase, different RS-induced DNA damage drugs were used.

As predicted, there was a pronounced increase in the total level of chromosome aberrations found in NHEJ-deficient cells post etoposide treatment when combined with caffeine, which causes direct DSBs. This is similar to the phleomycin result, though it should be noted that etoposide increased aberrations in WT but not Ku cells. The majority of the etoposide-induced aberrations included chromosome and chromatid breaks.

Similarly, the anticancer drug CPT was used to detect whether c-NHEJ factors act to resolve se-DSBs. In contrast to the high aberrations level found in response to phleomycin or etoposide in Ku-deficient cells, it was found that CPT did not increase the level of total aberrations relative to Ku-deficient samples. Collectively, these findings suggest a role for NHEJ in repairing S-phase DSBs induced by phleomycin and possibly etoposide, but not se-DSB induced by CPT. This supports the theory of NHEJ being unable to repair se-DSBs induced by collapsed replication forks (Saleh-Gohari et al., 2005).

These results also indicate that NHEJ does not incorrectly ligate multiple se-DSBs together, since aberrations post se-DSB induction do not significantly increase Ku86 cells compared to WT cells, suggesting NHEJ is inhibited from attempting to repair this damage. In agreement with these findings, Adamo et al. (2010) used a cross-linking agent, which causes replication stress-induced DNA damage via replication fork stalling and collapse, resulting in the generation of se-DSBs. Therefore, NHEJ has been shown to maintain genome integrity in the S phase because it is required to suppress GIN.

As expected, the NHEJ repair mechanism has a role in repairing direct DSBs but not se-DSBs, as revealed from treating Ku-deficient cells with different RS-induced DNA damage treatments, as measured by the metaphase spreads of Ku-proficient and deficient cell lines subjected to different chemotherapeutic drugs. It was observed that NHEJ factors play a role in repairing therapy-induced direct DSBs by agents such as phleomycin and etoposide during the S phase to suppress genomic instability. This is because the NHEJ repair mechanism is dependent on ligating two broken (blunt) ends (Lieber, 2008). Data generated by CPT treatment shows that Ku86 does not contribute significantly to the repair of se-DSBs induced during the S-phase. This is probably due to the lack of a second broken DNA end in the induced se-DSB; the NHEJ thus preferentially repairs ds-DSBs but not se-DSBs during S-phase.

It remains possible however, that c-NHEJ does not act ducring S-phase but these direct DSB persist to G2/M. and then c-NHEJ repair the direct DSB. The fusions/exchanges observed when Ku is deficient may be caused by a-NHEJ acting, as a-NHEJ mediated misrepair of DSB ends is increases in frequency in the absence of c-NHEJ.

As the G2/M checkpoint regulates mitosis entry and could detect the unrepaired and persistent DNA damage (Bakkenist and Kastan, 2003), it is possible that the presence of an active checkpoint induces the highly-damaged cells with defective repairs to go into cell cycle arrest to try to repair the damage. This prevents them from proceeding to the G2-phase and subsequently reaching metaphase. For that reason, it was of interest to use checkpoint inhibitors in combination with these DSB-inducing genotoxic drugs to examine the total abbreviation found in metaphase spreads. This hypothesis can be checked by using more downstream target inhibitors, such as Chk1 and Chk2, rather than inhibiting ATM/ATR, which also have repair pathway functions.

It appeared that adding caffeine, which inhibits both ATM and ATR (Powell et al., 1995), prevents the senescence and apoptosis of cells in response to DNA damage (Chen and Kolodner, 1999). Interestingly, it was shown that adding caffeine alone increased the abbreviation level in both proficient and deficient cells compared to untreated cells. This is expected as ATM and ATR maintain genome stability and cell cycle checkpoint deficiency, particularly that which affects S phase cells, which has been found to be highly correlated with chromosomal instability (Myung et al., 2001; Myung and Kolodner, 2002). Alternatively, caffeine alone may increased aberration levels in c-NHEJ-deficient cells due to c-NHEJ having a wide-ranging genome maintenance role during the S phase when other DDR pathways are defective. An analysis of the phleomycin and caffeine-treated cells therefore showed that there was a significant increase in chromosome aberrations post-induction of DSBs when NHEJ is inhibited; therefore, NHEJ factors contribute significantly to the repair of DNA damage induced by replication stress. This is concordant with the hypothesis of highly damaged cells being arrested in the cell-cycle due to the DNA damage checkpoint, as caffeine treatment inhibits the DDR from activating the checkpoint and causes an increase in the number of aberrant chromosomes progressing and reaching metaphase. This highlight the limitations of the role of NHEJ during the S-phase observed in previous studies (Adamo et al., 2010; Pace et al., 2010; Patel et al., 2010).

This indicates that this phenotype may have been missed previously, either because of checkpoint activation preventing S-phase cells with interesting damage reaching metaphase (as induced DNA damage could cause cell-cycle arrest and apoptosis before this stage), or due to the NHEJ role only being required for ATM/ATR-defective cells, as it is dependent on the type of RS induced (Sowd et al., 2013).

The increased level of chromosomes with exchanges/fusions in Ku-deficient cells compared to proficient cells after treatment with etoposide or phleomycin suggests the importance of c-NHEJ in repair. This might provide some indication that the increase in the fusion percentage is due to the use of a different repair mechanism that is more toxic and related to translocations. There are two possible aberrant repair mechanisms, unregulated HDR and a-NHEJ. As discussed previously in Section 1.7.1, a-NHEJ is a Ku-independent error-prone pathway, although its precise mechanism is poorly understood (Weinstock et al., 2007; McVey and Lee, 2008). It is possible that these aberrations observed in Ku-deficent samples are generated by a-NHEJ.

Recent studies have demonstrated that a-NHEJ is more deleterious and induces genome rearrangement, such as chromosomal deletions, insertions or translocation at the breakpoints (Mansour et al., 2010; Frit et al., 2014). This is supported by several studies, which found that the inactivation of Ku and LigVI increases GIN (Weinstock et al., 2007; Kasparek and Humphrey, 2011).

Although the repair of se-DSBs is not completely understood, it is thought to be distinct from NHEJ, which requires two DNA ends to ligate together. Rather, it has been proposed that fork restart mechanisms involving HR factors, end-resection, and strand invasion are to a large extent associated with it and possible models for se-DSB resolution (Michel et al., 2001). Notably, the results of this study show that chromosome abbreviation decreased in Ku-deficient cells post CPT treatments compared to WT cells. This perhaps indicates that these cells are dependent on the recombination mechanism, and that inhibiting Ku prevented HR and decreased the level of aberrations. Recently, it was reported that Ku binds to se-DSBs ends and inhibits the early step of processing DNA for the end resection step in the HR repair mechanism (Mimitou and Symington, 2010; Foster et a., 2011; Chanut et al., 2016).

Further investigation will use different inhibitors to induce simultaneous deficiencies in c-NHEJ combined with either HDR (MRE11) or a-NHEJ (LIGIII), and will assess the loss of these chromosomal exchanges with a view to elucidating the mechanisms underlying the unexpected role of NHEJ.

Chapter 8: General discussion and future directions

8.1 General discussion

This study has two independent but interlinked aims: first, to clarify the molecular mechanisms of broken DNA replication fork processing and mutagenesis in mammalian cells; second, to uncover the unexpected role of c-NHEJ in genome stability maintenance during the S-phase, in response to RS-induced DNA damage.

A number of prior DDR studies have investigated how cells respond to DNA damage and RS using various genotoxic agents (such as radiation) or therapies such as CPT (Cobb et al., 2005). Although genotoxic agents are effective tools for use when conducting specific analyses of RS-dependent effects, these agents cause genome-wide damage, thereby preventing precise control over fork breakages, precluding RS associated events from being studied directly. In addition, these technical issues have previously obscured understanding of the molecular mechanisms underlying mammalian DNA replication-associated se-DSB resolution or misrepair at the level of single cells. It has become clear that a significant portion of DNA damage arises as a consequence of DNA replication; thus, indicating that defective progression of RF can lead to chromosomal instability. Although earlier studies have identified an association between aberrant DNA replication and cancer, the lack of a mammalian–based methodical tool to identify or regulate where replication fork breaks occur means it is not possible to study RS with a sufficiently high enough resolution.

To address this problem and dissect diverse RS associated processes directly, such as repair pathways and checkpoints in mammalian cells *in vivo*, this study induced a single genomic insult. A novel FRT-FLP cellular system was designed and employed to generate broken DNA replication forks at specific genomic loci. The system used mutant Flp recombinase (FlpH305L), originally from *Saccharomyces cerevisiae* budding yeast, which, when localized to the nucleus, leads to se-DSB generation at Flp recognition target (FRT) loci as demonstrated by Nielson et al. (2009). The generated system mimics CPT-mediated DNA damage and RS. it permits monitoring of repair at single sites, giving this study an advantage over genome wide DNA damage studies.

To set up the system, various series of FRT integration constructs and FLPH305L recombinase and/or I-SceI endonuclease expression vectors were successfully generated. In addition, several HEK293-FRT and U2OS-FRT clonal cells were established by stably integrating the FRT sequence into the genome.

Although the PCR reactions followed by Sanger sequencing confirmed the integration, identifying the location and copy number integration of the FRT sequence in the generated stable clonal cell lines proved challenging. During the study, identification of a single FRT integration clone was attempted using both southern blot and FISH techniques; however, neither technique proved sufficiently accurate to detect the copy number. Though the ANCHOR foci experiments indicated only a single integration site. However, this limitation can be overcome by whole genome sequencing the generated cell lines, as, when compared to the parental cell line (no FRT), it is possible to detect the number of the integration and annotate the location accurately.

The development of an inducible FLP-FRT system at a targeted locus would allow the study of various aspects of broken forks at the damage site, making genetic, biochemical and microscopic analyses possible. One advantage of the system refers to the flexibility of inserting a single strand break, which means that the orientation of the FRT sequence can be modified for integration into either the leading or lagging strand. However, in this study the random integration of the FRT sequence hindered the determination of the orientation of the integrated sequence and, subsequently, prevent determination of whether the break will arise in the leading or lagging strand. To overcome this limitation, the FRT can be integrated very accurately at a specific locus of the genome, using the recently available CRISPR Cas9-mediated genome-editing technology (Ran et al., 2013). Ideally, the FRT should be inserted where active firing DNA replication is taking place (as discussed in the future work in Section 8.2. However, to date, the origin of DNA replication in mammalian cells has been newly identified in Hela cells (Dellino et al., 2013).

The designed FRT-FLP system combines multiple features, each with unique advantages. Despite the limitation of being unable to determine the copy number integration in the established cell lines, it was decided to move forward and validate the different features of the system. The results indicated a successful high transfection efficiency. This was monitored by visualizing the red fluorescent signal. Differences were observed between the expression level in cell lines, possibly due to the variability in the effectiveness constitutive human cytomegalovirus (CMV) promoter, which derives the RFP expression, across different cell types (Qin et al., 2010).

Further experiments were carried out to validate GR system efficiency. GR is a well-studied member of the nuclear hormone receptor superfamily (Rousseau et al., 1979), and unleganded GR is performs as cytoplasmic residue in the absence of glucocorticoids hormone (GCs), and only translocates to the nucleus in response to the GCs ligand binding, post-exposure to a steroid (Martinez et al., 2005). In the constructed plasmids, the GR receptor was located downstream of the FLPH305L; this allows FLP relocalization from the cytoplasm to the nucleus (Htun et al., 1996) when TA is added (Soutoglou et al., 2007) allowing the system to rapidly switch control, i.e. ON/OFF. Some minimal leaking of the RFP was found in the nucleus, even in a TA-free media using the GR tagging system, indicating a slight weak regulation to control the localization of expressed proteins upon transient transfection of the FRT cell with either the RFP-I-SceI-GR or the RFP-FLPH305L-GR expression plasmid. Furthermore, it was observed that localization occurred more slowly than reported elsewhere, taking hours rather than minutes. Ideally, the inactivation of the RS fused to the GR should be precisely assessed to provide a RS-OFF phenotype in the absence of TA, or in response to the induction of the RS-ON phenotype upon the addition of TA.

An attempt was made to overcome the limitations of the GR tagging system by combining the GR and AID systems to provide tighter control of Flp1 activity and reduce the possibility of background Flp1 binding. It has been reported that using the AID system will provide tight control of protein levels fused with the degron (Nishimura et al., 2009). However, due to time constraints and difficulties in transfecting the cells with this large AIDFLPH305L-GR construct at the project outset, the dsRed-FLPH305L-GR plasmid was used in subsequent experiments, while taking into consideration its limitations regarding the control localization of the protein and the induction of RS, in order to obtain a ‘phenotype ON’ system.

The FRT-FLP system possess an additional useful feature, the ANCHOR labelling system, where fluorescent-labelled ‘OR’ proteins that loosely bind, and oligomers to small DNA segments called ‘ANCH’ to create fluorescent foci. Despite the poor transfection efficiency observed from cells transfected with OR3-GFP and/or OR4-CFP, most of the transfected cells formed only single GFP and CFP foci. This indicates the binding of OR3-GFP and/or OR4-CFP to a single ANCH3 and/or ANCH4 sites respectively. However, in some transfected cells, the formed foci were observed to localize in the cytoplasm instead of the nucleus. This was possibly a result of the lack of an NLS sequence in the OR plasmids.

Interestingly, a single CFP focus but not GFP focus was found in some of the transfected cells following the addition of the TA. It was speculated that this is due to OR proteins only binding to the dsDNA, meaning the loss of focus indicates BF has occurred in a particular cell, and that the ANCH3 sequence has become ssDNA.

Overall, although the ANCHOR labelling system potentially serves as a powerful tool for analysing the position of the broken RF directly, it was deduced that the use of the ANCHOR labelling system needs to be better optimized to overcome the poor transfection rates and rarity of the foci localization event before the tool can be fully utilized (as discussed in the future work in Section 8.2).

The determination of the generation of SSB or DSB by alkaline and native gel using the labelled ANCH probe appears difficult. Se-DSB using FLPH305L has been demonstrated in yeast. Although the ANCH visualization system worked and shows a single focus, the H2AX signal should be employed to verify that the signal is attributed to a broken site.

The characterization of the phenotypic similarities and differences between the inducible replication-associated DNA damage (se-DSB) and direct DSB was evaluated here for the first time. This was accomplished by conducting several genomic instability assays that accompanied the Flp1-FRT system. While FLP-induces a DSB, the FRT-FLP system causes different damage to that created by the I-SceI endonuclease; it is a SSB that the DSB becomes one-sided upon replication, owing to polymerase run off. In contrast, direct DSBs can be formed at any phase of the cell cycle, whereas the se-DSB is replication-dependent associated DNA damage. There was no evidence of any statistically significant differences obtained between the se-DSB and direct DSB on the cell cycle phase profile when compared to cells transfected with an empty vector. This indicates that the cells are proliferating and the induced single insult did not halt the cell cycle progression. Even though both se-DSB and direct DSB are cytotoxic, the data strongly suggests that the generated se-DSB is more cytootoxic than the direct DSB generated by the I-SceI endonuclease. A significant reduction in the cellular viability level and colony formation rate of cells harbouring se-DSB were found when compared to cells with the direct DSB. The differences observed in the mutation detection might be due to the fact that a single DSB is geneotoxic while, se-DSB appears not to be genotoxic. The repair of this particular DNA replication associated damage was expected to proceed differently, suggesting other DDR requirements to cope with the damage and repair than conventional DSB.

The roles of the DDR factor in the se-DSB response were initially tested, beginning with a candidate approach, which involved studying the effects of the loss of various DDR factors, including in repair, checkpoints, senescence and apoptosis on broken fork processing. It was beneficial to exploit the well-known, I-SceI site specific endonuclease, which generates a DSB (Weinstock et al., 2008). It serves as a control when comparing the genetic requirements for cells to cope with induced BF as compared to DSB.

Cell viability and colony formation ability were measured and quantified in various single deficient cells following acute induction of FLP or I-SceI to uncover pathways that, when defective, specifically increase RS-associated cytotoxicity. Overall, a clear difference emerged between un-transfected and transfected HEK293-FRT and U2OS-FRT cells. Therefore, cells transfected with empty plasmid pdsRed-GR were considered better negative control cells. FLP more toxic than I-SceI, but both more toxic than GR only.

Generally, given the similarities obtained using the system employed in this study with the previous studies assaying CPT treated cells. it has been deduced that survival cells depend on the same genetic requirement as cells treated with CPT. The FRT-FLP system will allow detailed studies of how repair factors are orchestrated at the damage site and the fate of the replication fork at the damaged site as well as how the damage might activate cell cycle checkpoint response. Improperly repaired DNA damage is likely the basis of GIN. This positively indicates that the system can be used to study the effect of RF breakage on genome stability, indicating that defective replication may generate DSB responsible for GCR.

The molecular mechanisms analysis of se-DSB processing was accomplished by conducting various assays such as mutation analyses and sequencing. The sequencing results obtained by Sanger sequencing of the break site of various isolated survivor clones fork breakage generated by chronic FLP-induction did not reveal any point mutations (insertions/deletions), whereas point mutations, particularly a slight shift (insertion) were observed from the I-SceI-induced DNA damage sequence. The fact that there is no sequence alteration at the break point could indicate that HR repair mechanism has occurred. HR is guided by much larger starches of homology, encompassing 100 base pairs or more.

The span of homology sequence is associated with repair processing, suggesting that the mutation occurring by the FLP induction might be a few base pairs apart from the break region. Thus, further sequencing will be needed to identify the type and frequency of mutations arising from se-DSBs.

Therefore, Ion Torrent next-generation sequencing might be required to sequence larger regions around the break site due to more complex rearrangements arising. Additionally, in this respect, different assays can be used, such as FISH of metaphase spreads, to visually detect CNV and translocations using the ANCHOR system (as discussed in section 8.2). could induce higher defects in DDR preior to acutely switching system ON.

Collectively, the generation of the FRT-FLP system to induce broken DNA replication forks (se-DSBs) at specific genomic loci during DNA replication provides a significant tool to study the molecular mechanisms and biological aspects of se-DSB resolution in mammalian cells *in vivo*. The system, thus, has great potential for identifying factors engaged in the repair of se-DSB, and might reveal new potential targets for drug design that can be used in combination with Top1-targeting drugs. Hence, understanding the mechanisms will shed light on the RS response and will aid in the development of better therapeutic strategies.

The laboratory recently uncovered an unexpected role for c-NHEJ in genome stability maintenance during RS. c-NHEJ was shown to play a role in mitigating chromosomal aberrations in response to DNA damage that occurred in S-phase, as measured by metaphase spreads of Ku proficient and deficient MEFs cells post treatment in S-phase. There was a pronounced trend of increased chromosomal aberration. Furthermore, Ku deficient cells treated with different RS-induced DNA damage treatments revealed that the c-NHEJ repair mechanism has a role in repairing direct DSBs but not se-DSB. Collectively, it was deduced that c-NHEJ factor deficiency likely causes RS-associated mitotic defects that potentially contribute to CIN and GCR.

8.2 Future directions

The developed FRT-FLP system provide the first tool to directly study diverse RS-associated processes in mammalian cells. Using this system seems to allow pioneering studies and further assays, as discussed below, to be carried out to elucidate the molecular mechanisms that suppress tumourigenesis by restarting DNA replication forks, along with those that cause misrepair and drive cancer progression.

Although in this study the FRT was inserted randomly into the genome, in future cell line generation, this could have been controlled more effectively by inserting FRT close to an active replication origin using CRISPR-Cas9 genome editing technology.

The generation of the SSB can be manipulated once know more about replication origin locations in human cells, so that it is on either the leading or lagging strand, depending on the orientation of the inserted FRT sequence. In addition, the FRT sequence can be inserted at any loci of choice using any cell line.

If the transfection efficiency and nuclear localization of OR proteins can be improved, then the ANCHOR system could be an excellent tool for visualising the disappearance and appearance of the loosely bound OR3-GFP/OR4-CFP proteins at RFs and BF undergoing repair. In addition, the disappearance of the fluorescent GFP foci inserted immediately at the break site makes it possible to distinguish cells that that have incurred a BF from normally replicating cells. Employing this feature in future experiments will serve to distinguish between cells that have undergone replication at the FLP-DNA adduct site following TA-induced FLP nuclear localization from those that have not. The induced se-DSB upon FLP localization can be confirmed by observing the phosphorylation of γH2AX and its accumulation at the FRT site using live-cell fluorescent confocal microscopy.

Accurate measurement of the kinetics of induction, and resolution of broken forks (se-DSB), will be monitored over time. This can be achieved by monitoring changes in OR-foci after switching on to monitor repair kinetics at site. However, due to cell-to-cell variability at the time of break induction and repair, disappearance of the GFP signal from the ANCH3 site must be studied in single cells to illustrate the relative speed at which focus is lost and regained. Due to the possibility that GFP disappearance occurred at the earliest point following TA induction, the CFP and GFP can be tracked three dimensionally in live cell imaging by acquiring up to 24 hours over the time frame to monitor focus intensity and changes to the overlapping degree of individual cells. Additionally, intrusive weak binding and oligomerization of OR proteins means there is no disruption of DNA replication and repair. Thus, this visualization feature provides the ability to accurately track repair kinetics of se-DSB induction and resolution, and of the replication completion by monitoring the appearance of two CFP foci.

Another potential future approach would be to monitor DDR proteins, which have a role in repairing aberrant RF. This could be achieved by tracking their recruitment to the damage site in replicating cells.

Moreover, genotoxicity analysis of the induction of mutations could be detected through analysis of more clones or cytogenetic analysis. For example, chromosome aberrations and micro nuclei can be used to estimate the frequency of the GCR structures.

The ANCHOR labelling can be utilized to test which mutation types are directly caused by fork breakage, this will be achieved by conducting FISH of metaphase spreads to detect CNV and translocations to detect insertion, deletions and other rearrangements. In addition, defects in various other candidate RS-response features could be induced, for example, by inhibitor or siRNA, to test for effects on the cytotoxicity and genotoxicity of FLP-induced BFs.

Appendix

Appendix I Strategy of cytometric detection of H2AX. At least 5,000–10,000 events were acquired in a linear side-scatter area (SSC) versus a linear forward-scatter area (FSC) axes. The major population of cells were gated to omit signals from degraded nuclei debris. Single cells were gated by isolating the cell doublets, and by plotting a linear pulse height (405-H) versus the pulse area (405-A) of the PI channel and setting a gate around single cells. The FITC and PI stain were excited with 488 nm and 405 nm excitation lasers respectively. The emitted light was detected via the filter/bandpass, using a 450/50 and 530/30 filter for FITC and PI respectively.

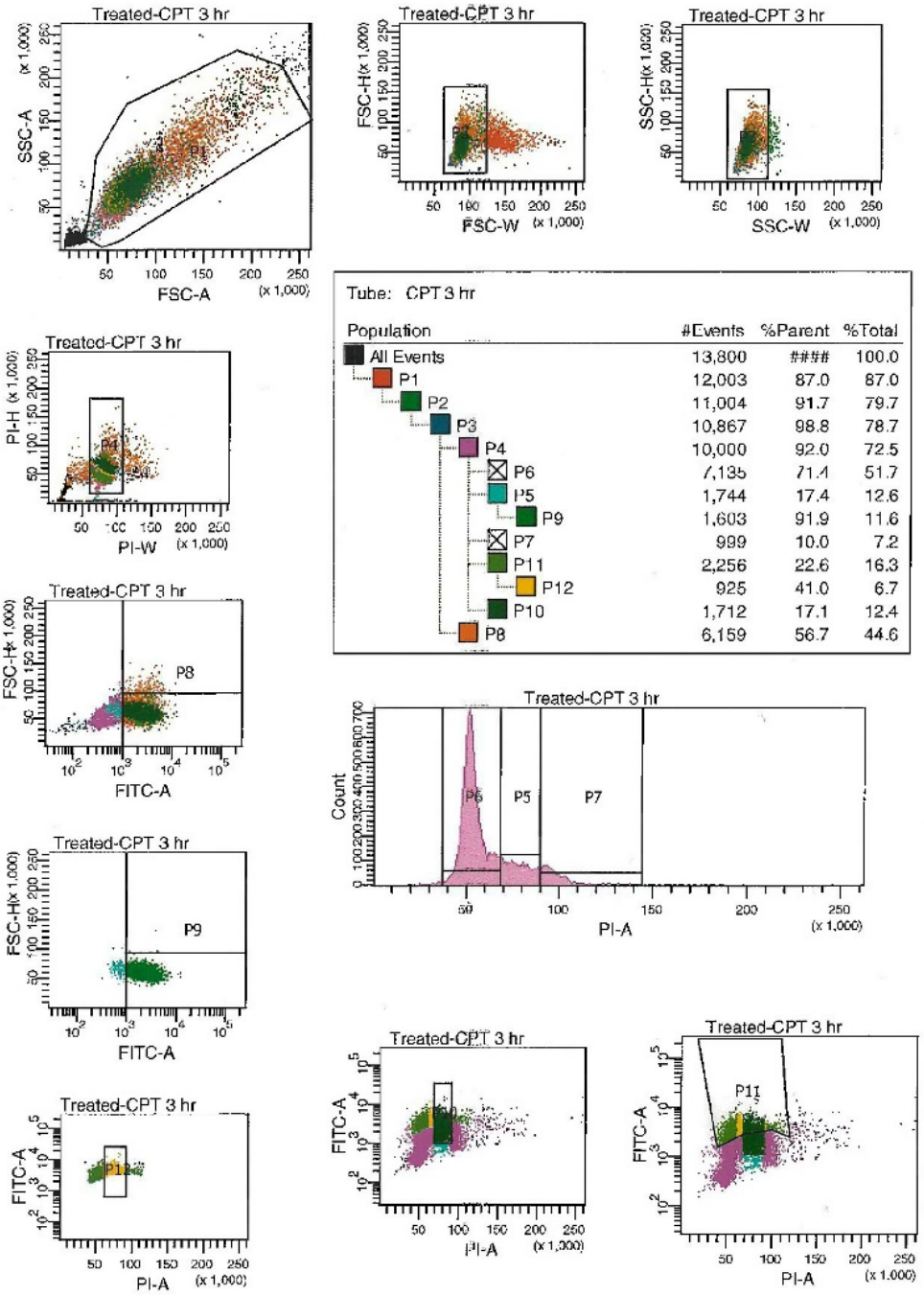

Appendix II Schematic partial map of the pYFP/LacO-I-SceI-CFP/tetR construct.

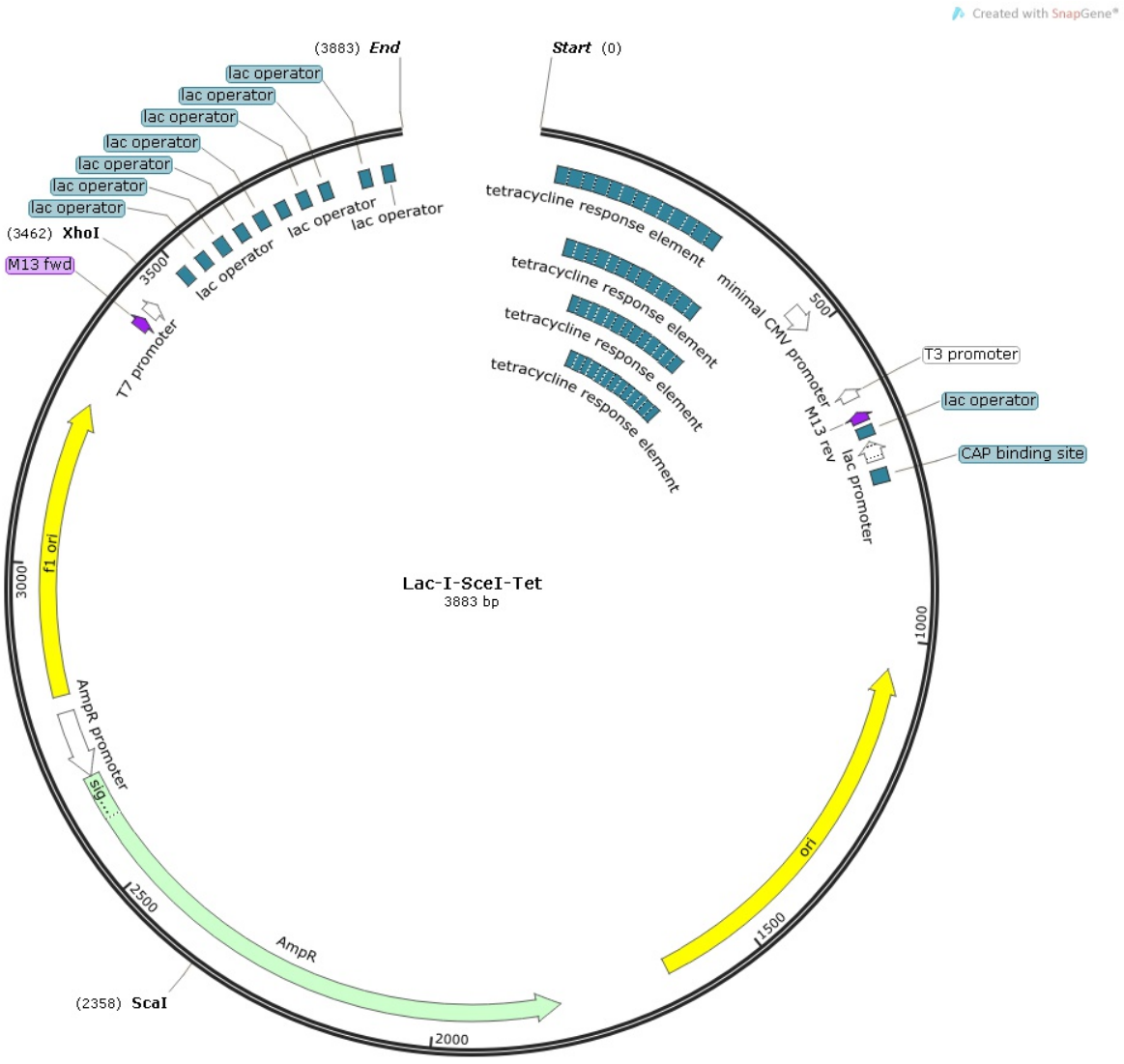

Appendix III Schematic map of the pUC19-H1-FRT-BglII-ANCH3-SacB-ANCH4-H2 construct. This was accomplished by insertion of a linker of 700 bp from pLEICS2 plasmid (PROTEX) between the ANCH3 and ANCH4 sites to allow the visualisation of the two foci in a good resolution

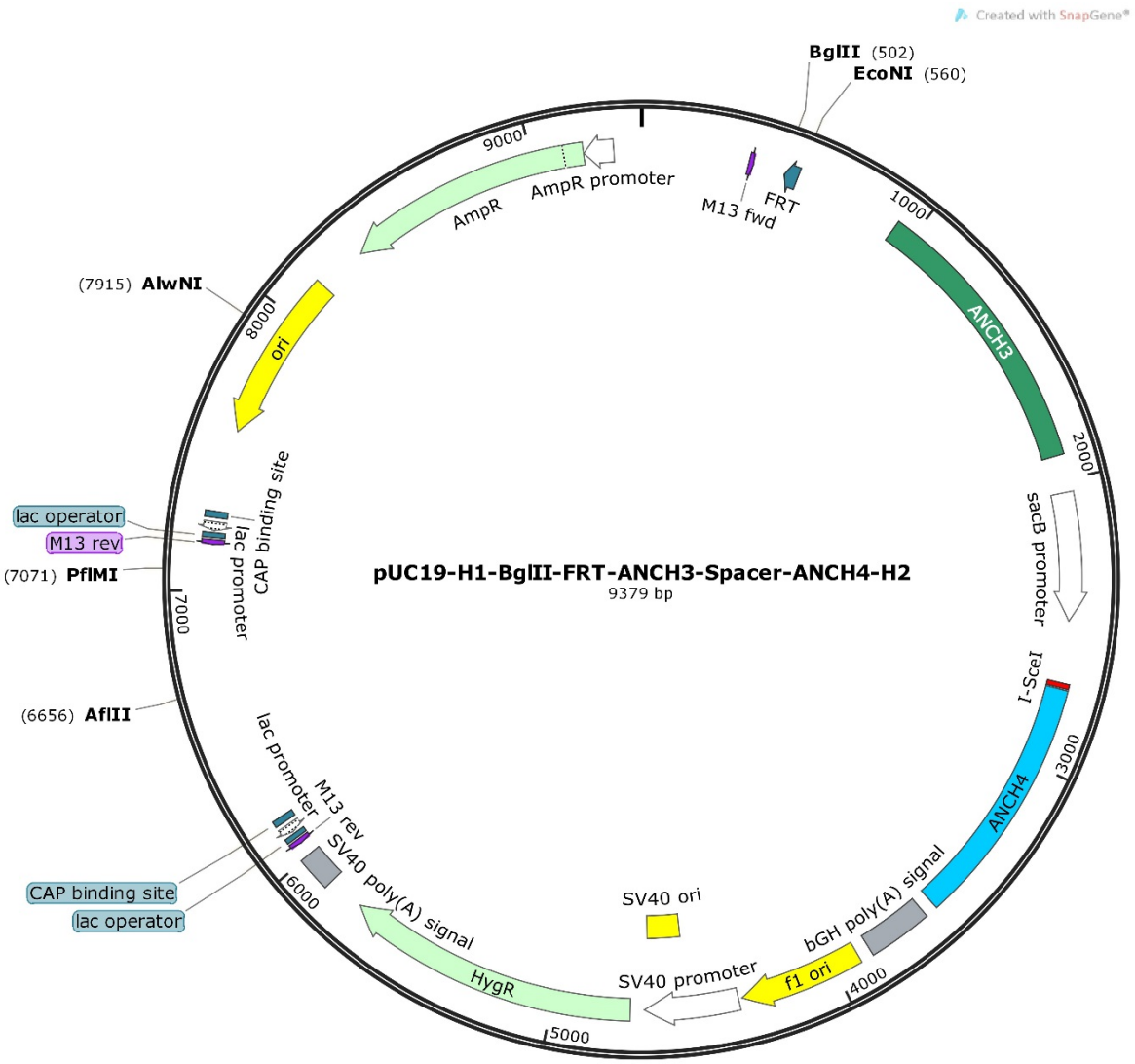

Appendix IV Schematic map of the pUC19-H2- ANCH3-I-SceI-ANCH4-H2 construct.

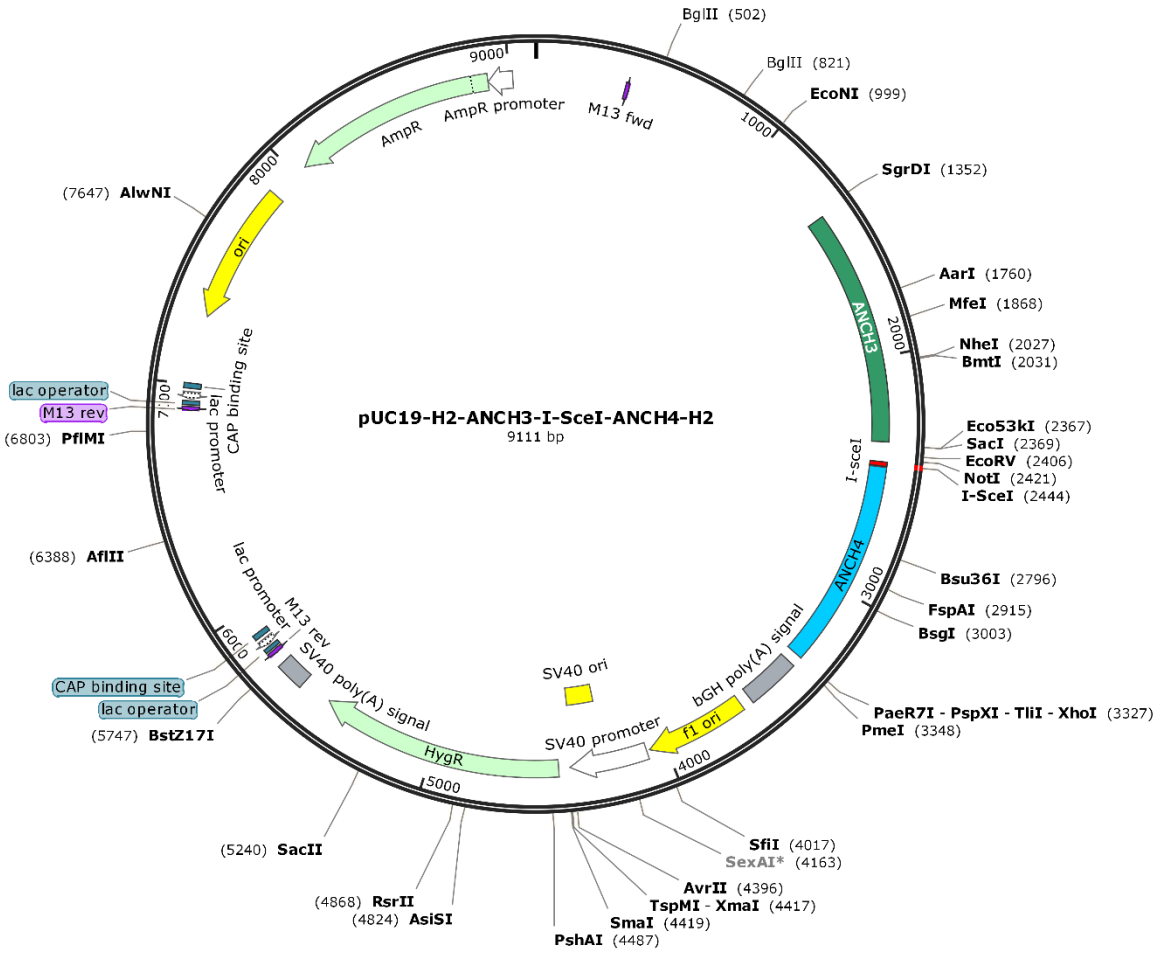

Appendix V Amino acid sequence of dsRed-FLPH305L-GR

*LLIVINYGVISS*PIYGVPRYITYGKWPAWLTAQRPPPIDVNNDVCSHSNANRDFPLTS
MGGVFTVNCPLGSTSSVSYAKYAPY*RQ*R*MARLALCPVHDLMGLSYLAVHLRISHRYY
HGDAVLAVHQWAWIAV*LTGISKSPPH*RQWEFVLAPKSTGLSKMS*QLRPIDANGR*AC
TVGGLYKQSWFSEPSDPLALPVATMDNTEDVIKEFMQFKVRMEGSVNGHYFEIEGEGEGK
PYEGTQTAKLQVTKGGPLPFAWDILSPQFQYGSKAYVKHPADIPDYMKLSFPEGFTWERS
MNFEDGGVVEVQQDSSLQDGTFIYKVKFKGVNFPADGPVMQKKTAGWEPSTEKLYPQDGV
LKGEISHALKLKDGGHYTCDFKTVYKAKKPVQLPGNHYVDSKLDITNHNEDYTVVEQYEH
AEARHSGSQSGLRSRAQPQFGILCKTPPKVLVRQFVERFERPSGEKIALCAAELTYLCWM
ITHNGTAIKRATFMSYNTIISNSLSFDIVNKSLQFKYKTQKATILEASLKKLIPAWEFTI
IPYYGQKHQSDITDIVSSLQLQFESSEEADKGNSHSKKMLKALLSEGESIWEITEKILNS
FEYTSRFTKTKTLYQFLFLATFINCGRFSDIKNVDPKSFKLVQNKYLGVIIQCLVTETKT
SVSRHIYFFSARGRIDPLVYLDEFLRNSEPVLKRVNRTGNSSSNKQEYQLLKDNLVRSYN
KALKKNAPYSIFAIKNGPKSLIGRHLMTSFLSMKGLTELTNVVGNWSDKRASAVARTTYT
HQITAIPDHYFALVSRYYAYDPISKEMIALKDETNPIEEWQHIEQLKGSAEGSIRYPAWN
GIISQEVLDYLSSYINRRICRRYRGYRKCLQAGMNLEARKTKKKIKGIQQATAGVSQDTS
ENPNKTIVPAALPQLTPTLVSLLEVIEPEVLYAGYDSSVPDSAWRIMTTLNMLGGRQVIA
AVKWAKAIPGFRNLHLDDQMTLLQYSWMFLMAFALGWRSYRQSSGNLLCFAPDLIINEQR
MSLPGMYDQCKHMLFVSSELQRLQVSYEEYLCMKTLLLLSSVPKEGLKSQELFDEIRMTY
IKELGKAIVKREGNSSQNWQRFYQLTKLLDSMHEVVENLLTYCFQTFLDKTMSIEFPEML
AEIITNQIPKYSNGNIKKLLFHQKWIHRI*IT

Appendix VI Co-expression of dsRed-FLP-GR, OR3 and OR4 in HEK293-FRT cells.

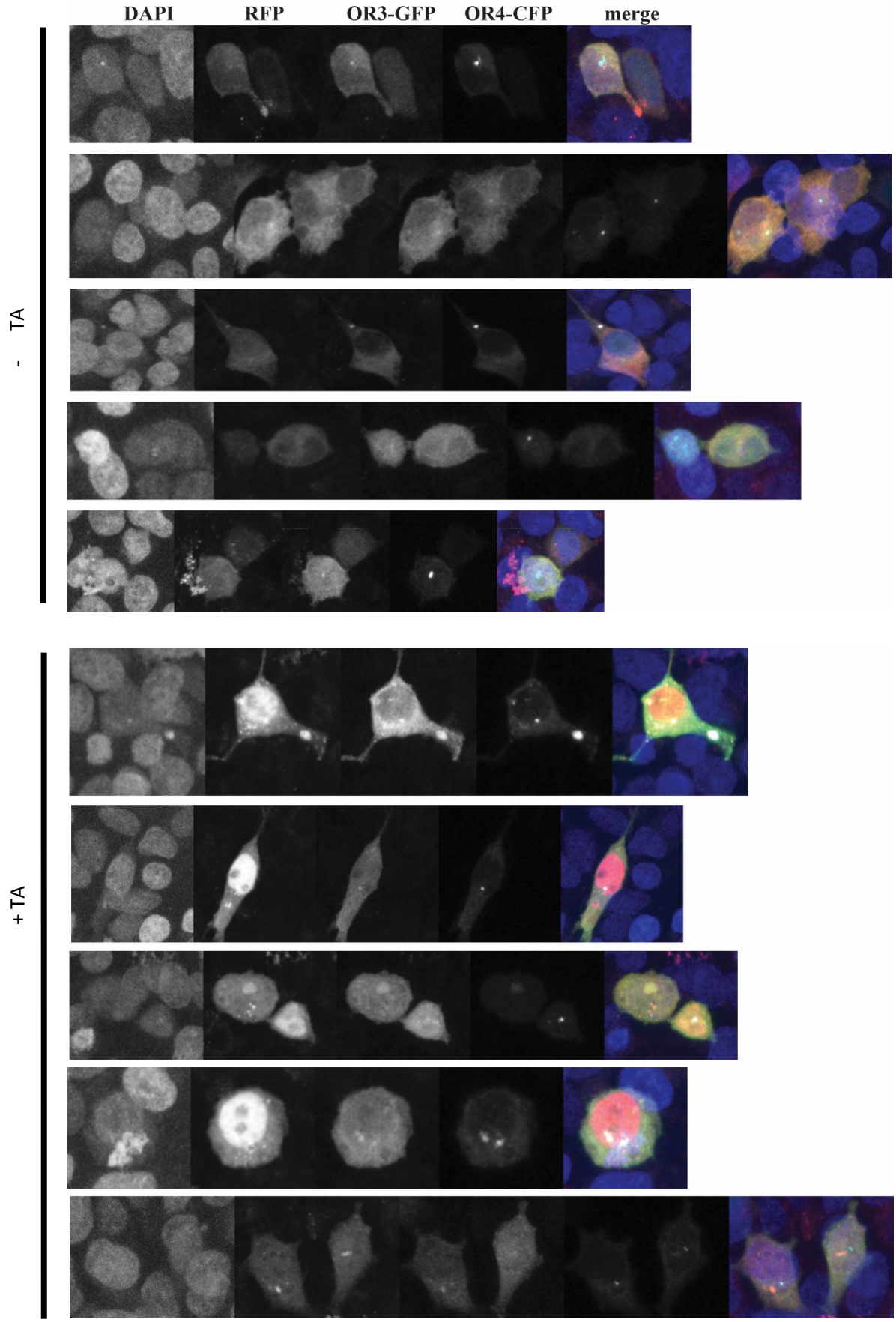

Appendix VII Co-expression of dsRed-FLP-GR, OR3 and OR4 in U2OS-FRT cells.

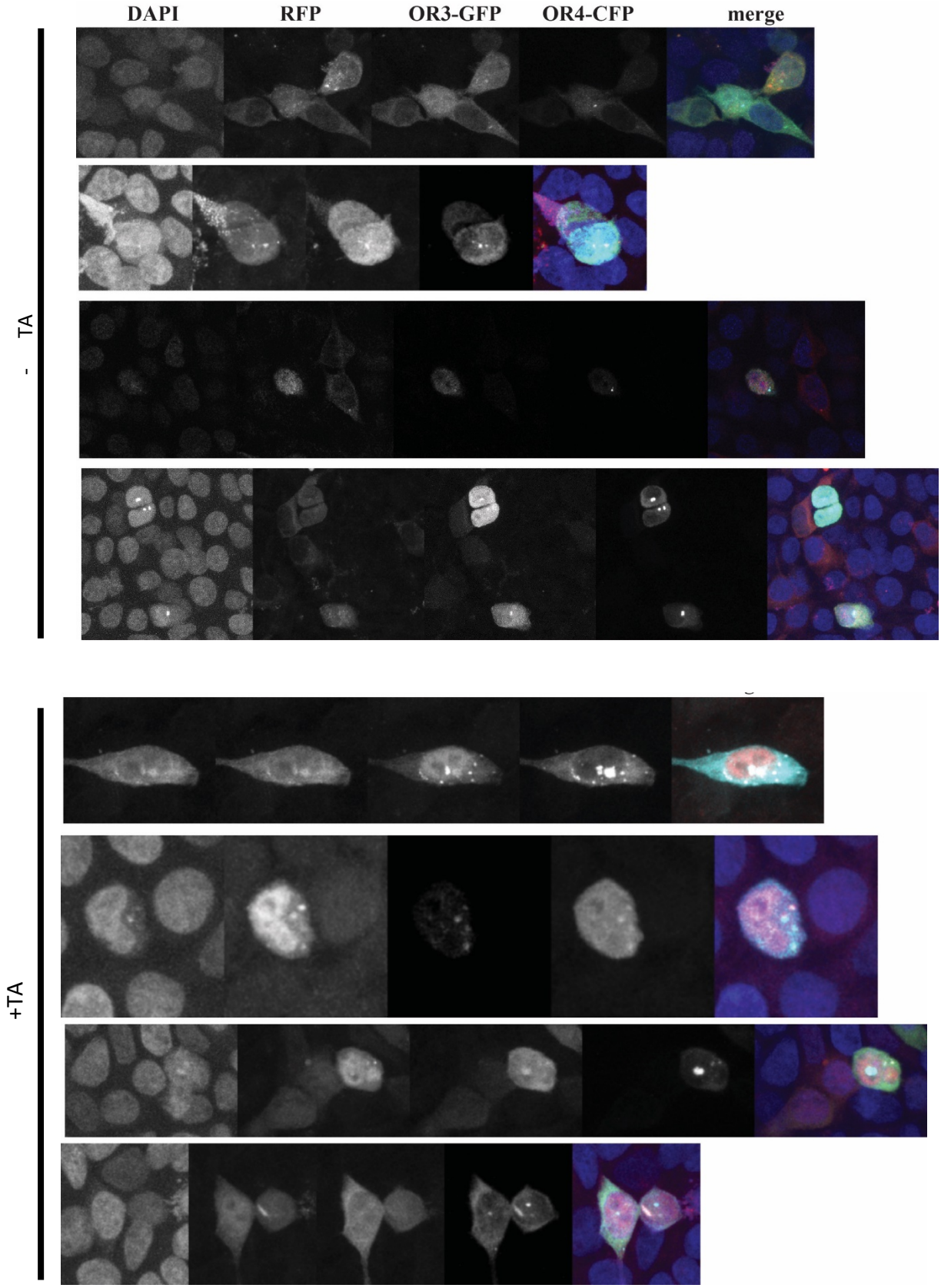

Appendix IIII Blastn results of the generated probes sequence aligned with the original plamids and human genome reference.

Query ID	Strand	Identity coverage	E-value	Identity %	Number of identites	Seq Ref
Probe 1	plus	100	0	100	567	BglII-FRT-ANCH3-ANCH4
Probe 1	minus	7	3.00E-05	80	32	BglII-FRT-ANCH3-ANCH4
Probe 1	plus	31	2.00E-83	100	174	chr11
Probe 1	plus	18	4.00E-43	100	100	chr11
Probe 2	plus	100	1.00E-170	100	324	BglII-FRT-ANCH3-ANCH4
Probe 2	minus	12	2.00E-05	80	32	BglII-FRT-ANCH3-ANCH4
Probe 2	plus	54	1.00E-83	100	174	chr11
Probe 2	plus	31	2.00E-43	100	100	chr11
Probe 3	plus	100	0	100	1143	BglII-FRT-ANCH3-ANCH4
Probe 3	plus	10	1.00E-58	100	119	BglII-FRT-ANCH3-ANCH4
Probe 3	minus	3	6.00E-05	80	32	BglII-FRT-ANCH3-ANCH4
Probe 3	plus	20	1.00E-115	100	234	chr11
Probe 3	plus	9	7.00E-43	100	100	chr11
Probe 3	minus	10	1.00E-57	100	117	dsRed_Flp1H305L_noATGorTAA_GR
Probe 4	plus	100	0	100	618	BglII-FRT-ANCH3-ANCH4
Probe 5	plus	100	0	100	525	BglII-FRT-ANCH3-ANCH4
Probe 6	plus	100	0	100	497	BglII-FRT-ANCH3-ANCH4

References

Abbas, T., Keaton, M.A. and Dutta, A. (2013) 'Genomic instability in cancer', *Cold Spring Harbor perspectives in biology,* 5(3), pp. a012914.

Abel, S. and Theologis, A. (1996) 'Early genes and auxin action', *Plant Physiology,* 111(1), pp. 9-17.

Adamo, A., Collis, S.J., Adelman, C.A., Silva, N., Horejsi, Z., Ward, J.D., Martinez-Perez, E., Boulton, S.J. and La Volpe, A. (2010) 'Preventing nonhomologous end joining suppresses DNA repair defects of Fanconi anemia', *Molecular cell,* 39(1), pp. 25-35.

Adams, K.E., Medhurst, A.L., Dart, D.A. and Lakin, N.D. (2006) 'Recruitment of ATR to sites of ionising radiation-induced DNA damage requires ATM and components of the MRN protein complex', *Oncogene,* 25(28), pp. 3894-3904.

Aguilera, A. and Garcia-Muse, T. (2013) 'Causes of genome instability', *Annual Review of Genetics,* 47, pp. 1-32.

Ahmed, A. and Podemski, L. (1998) 'Observations on template switching during DNA replication through long inverted repeats', *Gene,* 223(1-2), pp. 187-194.

Ahn, J.S., Osman, F. and Whitby, M.C. (2005) 'Replication fork blockage by RTS1 at an ectopic site promotes recombination in fission yeast', *The EMBO journal,* 24(11), pp. 2011-2023.

Ahnesorg, P., Smith, P. and Jackson, S.P. (2006) 'XLF interacts with the XRCC4-DNA ligase IV complex to promote DNA nonhomologous end-joining', *Cell,* 124(2), pp. 301-313.

Al-Allaf, F.A., Tolmachov, O.E., Zambetti, L.P., Tchetchelnitski, V. and Mehmet, H. (2013) 'Remarkable stability of an instability-prone lentiviral vector plasmid in Escherichia coli Stbl3', *3 Biotech,* 3(1), pp. 61-70.

Ali, S.H. and DeCaprio, J.A. (2001) 'Cellular transformation by SV40 large T antigen: interaction with host proteins', *Seminars in cancer biology,* 11(1), pp. 15-23.

Alqallaf, A.K., Alkoot, F.M. and Aldabbous, M.S. (2013) 'Discovering the Genetics of Autism', *Recent Advances in Autism Spectrum Disorders,* 1(10.5772/53797).

Andegeko, Y., Moyal, L., Mittelman, L., Tsarfaty, I., Shiloh, Y. and Rotman, G. (2001) 'Nuclear retention of ATM at sites of DNA double strand breaks', *The Journal of biological chemistry,* 276(41), pp. 38224-38230.

Araki, H. (2011) 'Initiation of chromosomal DNA replication in eukaryotic cells; contribution of yeast genetics to the elucidation', *Genes & genetic systems,* 86(3), pp. 141-149.

Arlt, M.F., Ozdemir, A.C., Birkeland, S.R., Wilson, T.E. and Glover, T.W. (2011) 'Hydroxyurea induces de novo copy number variants in human cells', *Proceedings of the National Academy of Sciences of the United States of America,* 108(42), pp. 17360-17365.

Armaghany, T., Wilson, J.D., Chu, Q. and Mills, G. (2012) 'Genetic alterations in colorectal cancer', *Gastrointestinal cancer research : GCR,* 5(1), pp. 19-27.

Arnaudeau, C., Lundin, C. and Helleday, T. (2001) 'DNA double-strand breaks associated with replication forks are predominantly repaired by homologous recombination involving an exchange mechanism in mammalian cells', *Journal of Molecular Biology,* 307(5), pp. 1235-1245.

Atkinson, J. and McGlynn, P. (2009) 'Replication fork reversal and the maintenance of genome stability', *Nucleic acids research,* 37(11), pp. 3475-3492.

Aylon, Y. and Kupiec, M. (2004) 'New insights into the mechanism of homologous recombination in yeast', *Mutation research,* 566(3), pp. 231-248.

Bakkenist, C.J. and Kastan, M.B. (2003) 'DNA damage activates ATM through intermolecular autophosphorylation and dimer dissociation', *Nature,* 421(6922), pp. 499-506.

Banaszynski, L.A., Chen, L.C., Maynard-Smith, L.A., Ooi, A.G. and Wandless, T.J. (2006) 'A rapid, reversible, and tunable method to regulate protein function in living cells using synthetic small molecules', *Cell,* 126(5), pp. 995-1004.

Banaszynski, L.A. and Wandless, T.J. (2006) 'Conditional control of protein function', *Chemistry & biology,* 13(1), pp. 11-21.

Bao, S., Lu, T., Wang, X., Zheng, H., Wang, L.E., Wei, Q., Hittelman, W.N. and Li, L. (2004) 'Disruption of the Rad9/Rad1/Hus1 (9-1-1) complex leads to checkpoint signaling and replication defects', *Oncogene,* 23(33), pp. 5586-5593.

Bartek, J. and Lukas, J. (2003) 'Chk1 and Chk2 kinases in checkpoint control and cancer', *Cancer cell,* 3(5), pp. 421-429.

Bartek, J., Lukas, J. and Bartkova, J. (2007) 'DNA damage response as an anti-cancer barrier: damage threshold and the concept of 'conditional haploinsufficiency'', *Cell cycle (Georgetown, Tex.),* 6(19), pp. 2344-2347.

Bartkova, J., Horejsi, Z., Koed, K., Kramer, A., Tort, F., Zieger, K., Guldberg, P., Sehested, M., Nesland, J.M., Lukas, C., Orntoft, T., Lukas, J. and Bartek, J.(2005) 'DNA damage response as a candidate anti-cancer barrier in early human tumorigenesis', *Nature,* 434(7035), pp. 864-870.

Bartkova, J., Tommiska, J., Oplustilova, L., Aaltonen, K., Tamminen, A., Heikkinen, T., Mistrik, M., Aittomaki, K., Blomqvist, C., Heikkila, P., Lukas, J., Nevanlinna, H. and Bartek, J. (2008) 'Aberrations of the MRE11-RAD50-NBS1 DNA damage sensor complex in human breast cancer: MRE11 as a candidate familial cancer-predisposing gene', *Molecular oncology,* 2(4), pp. 296-316.

Bartlett, D.W. and Davis, M.E. (2006) 'Insights into the kinetics of siRNA-mediated gene silencing from live-cell and live-animal bioluminescent imaging', *Nucleic acids research,* 34(1), pp. 322-333.

Bassing, C.H. and Alt, F.W. (2004) 'The cellular response to general and programmed DNA double strand breaks', *DNA repair,* 3(8-9), pp. 781-796.

Batey, M.A., Zhao, Y., Kyle, S., Richardson, C., Slade, A., Martin, N.M., Lau, A., Newell, D.R. and Curtin, N.J. (2013) 'Preclinical evaluation of a novel ATM inhibitor, KU59403, in vitro and in vivo in p53 functional and dysfunctional models of human cancer', *Molecular cancer therapeutics,* 12(6), pp. 959-967.

Baumann, P., Benson, F.E. and West, S.C. (1996) 'Human Rad51 protein promotes ATP-dependent homologous pairing and strand transfer reactions in vitro', *Cell,* 87(4), pp. 757-766.

Bell, S.P. and Dutta, A. (2002) 'DNA replication in eukaryotic cells', *Annual Review of Biochemistry,* 71, pp. 333-374.

Bell, S.P. and Stillman, B. (1992) 'ATP-dependent recognition of eukaryotic origins of DNA replication by a multiprotein complex', *Nature,* 357(6374), pp. 128-134.

Bellaiche, Y., Mogila, V. and Perrimon, N. (1999) 'I-SceI endonuclease, a new tool for studying DNA double-strand break repair mechanisms in Drosophila', *Genetics,* 152(3), pp. 1037-1044.

Bermejo, R., Lai, M.S. and Foiani, M. (2012) 'Preventing replication stress to maintain genome stability: resolving conflicts between replication and transcription', *Molecular cell,* 45(6), pp. 710-718.

Bevis, B.J. and Glick, B.S. (2002) 'Rapidly maturing variants of the Discosoma red fluorescent protein (DsRed)', *Nature biotechnology,* 20(1), pp. 83-87.

Bielinsky, A.K. and Gerbi, S.A. (2001) 'Where it all starts: eukaryotic origins of DNA replication', *Journal of cell science,* 114(Pt 4), pp. 643-651.

Bindra, R.S., Goglia, A.G., Jasin, M. and Powell, S.N. (2013) 'Development of an assay to measure mutagenic non-homologous end-joining repair activity in mammalian cells', *Nucleic acids research,* 41(11), pp. e115.

Blow, J.J. and Dutta, A. (2005) 'Preventing re-replication of chromosomal DNA', *Nature reviews.Molecular cell biology,* 6(6), pp. 476-486.

Bonger, K.M., Chen, L.C., Liu, C.W. and Wandless, T.J. (2011) 'Small-molecule displacement of a cryptic degron causes conditional protein degradation', *Nature chemical biology,* 7(8), pp. 531-537.

Bonner, W.M., Redon, C.E., Dickey, J.S., Nakamura, A.J., Sedelnikova, O.A., Solier, S. and Pommier, Y. (2008) 'GammaH2AX and cancer', *Nature reviews.Cancer,* 8(12), pp. 957-967.

Bothmer, A., Robbiani, D.F., Feldhahn, N., Gazumyan, A., Nussenzweig, A. and Nussenzweig, M.C. (2010) '53BP1 regulates DNA resection and the choice between classical and alternative end joining during class switch recombination', *The Journal of experimental medicine,* 207(4), pp. 855-865.

Branzei, D. and Foiani, M. (2010) 'Maintaining genome stability at the replication fork', *Nature reviews.Molecular cell biology,* 11(3), pp. 208-219.

Branzei, D. and Foiani, M. (2009) 'The checkpoint response to replication stress', *DNA repair,* 8(9), pp. 1038-1046.

Breier, A.M., Weier, H.U. and Cozzarelli, N.R. (2005) 'Independence of replisomes in Escherichia coli chromosomal replication', *Proceedings of the National Academy of Sciences of the United States of America,* 102(11), pp. 3942-3947.

Brown, E.J. and Baltimore, D. (2003) 'Essential and dispensable roles of ATR in cell cycle arrest and genome maintenance', *Genes & development,* 17(5), pp. 615-628.

Bryant, H.E., Schultz, N., Thomas, H.D., Parker, K.M., Flower, D., Lopez, E., Kyle, S., Meuth, M., Curtin, N.J. and Helleday, T. (2005) 'Specific killing of BRCA2-deficient tumours with inhibitors of poly(ADP-ribose) polymerase', *Nature,* 434(7035), pp. 913-917.

Bunting, S.F., Callen, E., Kozak, M.L., Kim, J.M., Wong, N., Lopez-Contreras, A.J., Ludwig, T., Baer, R., Faryabi, R.B., Malhowski, A., Chen, H.T., Fernandez-Capetillo, O., D'Andrea, A. and Nussenzweig, A. (2012) 'BRCA1 functions independently of homologous recombination in DNA interstrand crosslink repair', *Molecular cell,* 46(2), pp. 125-135.

Burgers, P.M. (2009) 'Polymerase dynamics at the eukaryotic DNA replication fork', *The Journal of biological chemistry,* 284(7), pp. 4041-4045.

Burma, S., Kurimasa, A., Xie, G., Taya, Y., Araki, R., Abe, M., Crissman, H.A., Ouyang, H., Li, G.C. and Chen, D.J. (1999) 'DNA-dependent protein kinase-independent activation of p53 in response to DNA damage', *The Journal of biological chemistry,* 274(24), pp. 17139-17143.

Burrell, R.A., McGranahan, N., Bartek, J. and Swanton, C. (2013) 'The causes and consequences of genetic heterogeneity in cancer evolution', *Nature,* 501(7467), pp. 338-345.

Byun, T.S., Pacek, M., Yee, M.C., Walter, J.C. and Cimprich, K.A. (2005) 'Functional uncoupling of MCM helicase and DNA polymerase activities activates the ATR-dependent checkpoint', *Genes & development,* 19(9), pp. 1040-1052.

Cadet, J. and Wagner, J.R. (2013) 'DNA base damage by reactive oxygen species, oxidizing agents, and UV radiation', *Cold Spring Harbor perspectives in biology,* 5(2), pp. 10.1101/cshperspect.a012559.

Calzada, A., Hodgson, B., Kanemaki, M., Bueno, A. and Labib, K. (2005) 'Molecular anatomy and regulation of a stable replisome at a paused eukaryotic DNA replication fork', *Genes & development,* 19(16), pp. 1905-1919.

Canman, C.E., Lim, D.S., Cimprich, K.A., Taya, Y., Tamai, K., Sakaguchi, K., Appella, E., Kastan, M.B. and Siliciano, J.D. (1998) 'Activation of the ATM kinase by ionizing radiation and phosphorylation of p53', *Science (New York, N.Y.),* 281(5383), pp. 1677-1679.

Carr, A.M., Paek, A.L. and Weinert, T. (2011) 'DNA replication: failures and inverted fusions', *Seminars in cell & developmental biology,* 22(8), pp. 866-874.

Carson, C.T., Schwartz, R.A., Stracker, T.H., Lilley, C.E., Lee, D.V. and Weitzman, M.D. (2003) 'The Mre11 complex is required for ATM activation and the G2/M checkpoint', *The EMBO journal,* 22(24), pp. 6610-6620.

Celeste, A., Fernandez-Capetillo, O., Kruhlak, M.J., Pilch, D.R., Staudt, D.W., Lee, A., Bonner, R.F., Bonner, W.M. and Nussenzweig, A. (2003) 'Histone H2AX phosphorylation is dispensable for the initial recognition of DNA breaks', *Nature cell biology,* 5(7), pp. 675-679.

Chanoux, R.A., Yin, B., Urtishak, K.A., Asare, A., Bassing, C.H. and Brown, E.J. (2009) 'ATR and H2AX cooperate in maintaining genome stability under replication stress', *The Journal of biological chemistry,* 284(9), pp. 5994-6003.

Chanut, P., Britton, S., Coates, J., Jackson, S.P. and Calsou, P. (2016) 'Coordinated nuclease activities counteract Ku at single-ended DNA double-strand breaks', *Nature communications,* 7, pp. 12889.

Charames, G.S. and Bapat, B. (2003) 'Genomic instability and cancer', *Current Molecular Medicine,* 3(7), pp. 589-596.

Chen, C. and Kolodner, R.D. (1999) 'Gross chromosomal rearrangements in Saccharomyces cerevisiae replication and recombination defective mutants', *Nature genetics,* 23(1), pp. 81-85.

Chen, J. and Stubbe, J. (2005) 'Bleomycins: towards better therapeutics', *Nature reviews.Cancer,* 5(2), pp. 102-112.

Chen, J.W., Lee, J. and Jayaram, M. (1992) 'DNA cleavage in trans by the active site tyrosine during Flp recombination: switching protein partners before exchanging strands', *Cell,* 69(4), pp. 647-658.

Cheng, C.H. and Kuchta, R.D. (1993) 'DNA polymerase epsilon: aphidicolin inhibition and the relationship between polymerase and exonuclease activity', *Biochemistry,* 32(33), pp. 8568-8574.

Chini, C.C. and Chen, J. (2004) 'Claspin, a regulator of Chk1 in DNA replication stress pathway', *DNA repair,* 3(8-9), pp. 1033-1037.

Chini, C.C. and Chen, J. (2003) 'Human claspin is required for replication checkpoint control', *The Journal of biological chemistry,* 278(32), pp. 30057-30062.

Ciccia, A. and Elledge, S.J. (2010) 'The DNA damage response: making it safe to play with knives', *Molecular cell,* 40(2), pp. 179-204.

Cimprich, K.A. and Cortez, D. (2008) 'ATR: an essential regulator of genome integrity', *Nature reviews.Molecular cell biology,* 9(8), pp. 616-627.

Cobb, J.A., Bjergbaek, L., Shimada, K., Frei, C. and Gasser, S.M. (2003) 'DNA polymerase stabilization at stalled replication forks requires Mec1 and the RecQ helicase Sgs1', *The EMBO journal,* 22(16), pp. 4325-4336.

Cobb, J.A., Schleker, T., Rojas, V., Bjergbaek, L., Tercero, J.A. and Gasser, S.M. (2005) 'Replisome instability, fork collapse, and gross chromosomal rearrangements arise synergistically from Mec1 kinase and RecQ helicase mutations', *Genes & development,* 19(24), pp. 3055-3069.

Colleaux, L., D'Auriol, L., Galibert, F. and Dujon, B. (1988) 'Recognition and cleavage site of the intron-encoded omega transposase', *Proceedings of the National Academy of Sciences of the United States of America,* 85(16), pp. 6022-6026.

Cortes-Ledesma, F. and Aguilera, A. (2006) 'Double-strand breaks arising by replication through a nick are repaired by cohesin-dependent sister-chromatid exchange', *EMBO reports,* 7(9), pp. 919-926.

Cortez, D., Guntuku, S., Qin, J. and Elledge, S.J. (2001) 'ATR and ATRIP: partners in checkpoint signaling', *Science (New York, N.Y.),* 294(5547), pp. 1713-1716.

Cotta-Ramusino, C., Fachinetti, D., Lucca, C., Doksani, Y., Lopes, M., Sogo, J. and Foiani, M. (2005) 'Exo1 processes stalled replication forks and counteracts fork reversal in checkpoint-defective cells', *Molecular cell,* 17(1), pp. 153-159.

Cuadrado, M., Martinez-Pastor, B. and Fernandez-Capetillo, O. (2006) '"ATR activation in response to ionizing radiation: still ATM territory"', *Cell division,* 1(1), pp. 7-1028-1-7.

Davis, A.P. and Symington, L.S. (2004) 'RAD51-dependent break-induced replication in yeast', *Molecular and cellular biology,* 24(6), pp. 2344-2351.

Deem, A., Keszthelyi, A., Blackgrove, T., Vayl, A., Coffey, B., Mathur, R., Chabes, A. and Malkova, A. (2011) 'Break-induced replication is highly inaccurate', *PLoS biology,* 9(2), pp. e1000594.

Dellino, G.I., Cittaro, D., Piccioni, R., Luzi, L., Banfi, S., Segalla, S., Cesaroni, M., Mendoza-Maldonado, R., Giacca, M. and Pelicci, P.G. (2013) 'Genome-wide mapping of human DNA-replication origins: levels of transcription at ORC1 sites regulate origin selection and replication timing', *Genome research,* 23(1), pp. 1-11.

Deriano, L. and Roth, D.B. (2013) 'Modernizing the nonhomologous end-joining repertoire: alternative and classical NHEJ share the stage', *Annual Review of Genetics,* 47, pp. 433-455.

Deshpande, A.M. and Newlon, C.S. (1996) 'DNA replication fork pause sites dependent on transcription', *Science (New York, N.Y.),* 272(5264), pp. 1030-1033.

Deweese, J.E. and Osheroff, N. (2009) 'The DNA cleavage reaction of topoisomerase II: wolf in sheep's clothing', *Nucleic acids research,* 37(3), pp. 738-748.

Dharmasiri, N., Dharmasiri, S. and Estelle, M. (2005) 'The F-box protein TIR1 is an auxin receptor', *Nature,* 435(7041), pp. 441-445.

Ding, Q., Reddy, Y.V., Wang, W., Woods, T., Douglas, P., Ramsden, D.A., Lees-Miller, S.P. and Meek, K. (2003) 'Autophosphorylation of the catalytic subunit of the DNA-dependent protein kinase is required for efficient end processing during DNA double-strand break repair', *Molecular and cellular biology,* 23(16), pp. 5836-5848.

DiTullio, R.A.,Jr, Mochan, T.A., Venere, M., Bartkova, J., Sehested, M., Bartek, J. and Halazonetis, T.D. (2002) '53BP1 functions in an ATM-dependent checkpoint pathway that is constitutively activated in human cancer', *Nature cell biology,* 4(12), pp. 998-1002.

Dohmen, R.J., Wu, P. and Varshavsky, A. (1994) 'Heat-inducible degron: a method for constructing temperature-sensitive mutants', *Science (New York, N.Y.),* 263(5151), pp. 1273-1276.

Doll, R. and Peto, R. (1981) 'The causes of cancer: quantitative estimates of avoidable risks of cancer in the United States today', *Journal of the National Cancer Institute,* 66(6), pp. 1191-1308.

Draviam, V.M., Xie, S. and Sorger, P.K. (2004) 'Chromosome segregation and genomic stability', *Current opinion in genetics & development,* 14(2), pp. 120-125.

Dubarry, N., Pasta, F. and Lane, D. (2006) 'ParABS systems of the four replicons of Burkholderia cenocepacia: new chromosome centromeres confer partition specificity', *Journal of Bacteriology,* 188(4), pp. 1489-1496.

Dujon, B. (1989) 'Group I introns as mobile genetic elements: facts and mechanistic speculations--a review', *Gene,* 82(1), pp. 91-114.

Echeverria, P.C., Mazaira, G., Erlejman, A., Gomez-Sanchez, C., Piwien Pilipuk, G. and Galigniana, M.D. (2009) 'Nuclear import of the glucocorticoid receptor-hsp90 complex through the nuclear pore complex is mediated by its interaction with Nup62 and importin beta', *Molecular and cellular biology,* 29(17), pp. 4788-4797.

Elbashir, S.M., Harborth, J., Lendeckel, W., Yalcin, A., Weber, K. and Tuschl, T. (2001) 'Duplexes of 21-nucleotide RNAs mediate RNA interference in cultured mammalian cells', *Nature,* 411(6836), pp. 494-498.

Elledge, S.J. (1996) 'Cell cycle checkpoints: preventing an identity crisis', *Science (New York, N.Y.),* 274(5293), pp. 1664-1672.

Ellison, V. and Stillman, B. (2001) 'Opening of the clamp: an intimate view of an ATP-driven biological machine', *Cell,* 106(6), pp. 655-660.

Fackenthal, J.D. and Olopade, O.I. (2007) 'Breast cancer risk associated with BRCA1 and BRCA2 in diverse populations', *Nature reviews.Cancer,* 7(12), pp. 937-948.

Falck, J., Petrini, J.H., Williams, B.R., Lukas, J. and Bartek, J. (2002) 'The DNA damage-dependent intra-S phase checkpoint is regulated by parallel pathways', *Nature genetics,* 30(3), pp. 290-294.

Farmer, H., McCabe, N., Lord, C.J., Tutt, A.N., Johnson, D.A., Richardson, T.B., Santarosa, M., Dillon, K.J., Hickson, I., Knights, C., Martin, N.M., Jackson, S.P., Smith, G.C. and Ashworth, A. (2005) 'Targeting the DNA repair defect in BRCA mutant cells as a therapeutic strategy', *Nature,* 434(7035), pp. 917-921.

Fattah, K.R., Ruis, B.L. and Hendrickson, E.A. (2008) 'Mutations to Ku reveal differences in human somatic cell lines', *DNA repair,* 7(5), pp. 762-774.

Ferguson, D.O. and Holloman, W.K. (1996) 'Recombinational repair of gaps in DNA is asymmetric in Ustilago maydis and can be explained by a migrating D-loop model', *Proceedings of the National Academy of Sciences of the United States of America,* 93(11), pp. 5419-5424.

Fokas, E., Prevo, R., Pollard, J.R., Reaper, P.M., Charlton, P.A., Cornelissen, B., Vallis, K.A., Hammond, E.M., Olcina, M.M., Gillies McKenna, W., Muschel, R.J. and Brunner, T.B. (2012) 'Targeting ATR in vivo using the novel inhibitor VE-822 results in selective sensitization of pancreatic tumors to radiation', *Cell death & disease,* 3, pp. e441.

Foote, K.M., Blades, K., Cronin, A., Fillery, S., Guichard, S.S., Hassall, L., Hickson, I., Jacq, X., Jewsbury, P.J., McGuire, T.M., Nissink, J.W., Odedra, R., Page, K., Perkins, P., Suleman, A., Tam, K., Thommes, P., Broadhurst, R. and Wood, C. (2013) 'Discovery of 4-{4-[(3R)-3-Methylmorpholin-4-yl]-6-[1-(methylsulfonyl)cyclopropyl]pyrimidin-2-y l}-1H-indole (AZ20): a potent and selective inhibitor of ATR protein kinase with monotherapy in vivo antitumor activity', *Journal of medicinal chemistry,* 56(5), pp. 2125-2138.

Forget, A.L. and Kowalczykowski, S.C. (2010) 'Single-molecule imaging brings Rad51 nucleoprotein filaments into focus', *Trends in cell biology,* 20(5), pp. 269-276.

Foster, S.S., Balestrini, A. and Petrini, J.H. (2011) 'Functional interplay of the Mre11 nuclease and Ku in the response to replication-associated DNA damage', *Molecular and cellular biology,* 31(21), pp. 4379-4389.

Foster, S.S., De, S., Johnson, L.K., Petrini, J.H. and Stracker, T.H. (2012) 'Cell cycle- and DNA repair pathway-specific effects of apoptosis on tumor suppression', *Proceedings of the National Academy of Sciences of the United States of America,* 109(25), pp. 9953-9958.

Friedel, A.M., Pike, B.L. and Gasser, S.M. (2009) 'ATR/Mec1: coordinating fork stability and repair', *Current opinion in cell biology,* 21(2), pp. 237-244.

Frit, P., Barboule, N., Yuan, Y., Gomez, D. and Calsou, P. (2014) 'Alternative end-joining pathway(s): bricolage at DNA breaks', *DNA repair,* 17, pp. 81-97.

Froelich-Ammon, S.J. and Osheroff, N. (1995) 'Topoisomerase poisons: harnessing the dark side of enzyme mechanism', *The Journal of biological chemistry,* 270(37), pp. 21429-21432.

Garner, K.M., Pletnev, A.A. and Eastman, A. (2009) 'Corrected structure of mirin, a small-molecule inhibitor of the Mre11-Rad50-Nbs1 complex', *Nature chemical biology,* 5(3), pp. 129-30; author reply 130.

Gasc, J.M. and Baulieu, E.E. (1986) 'Steroid hormone receptors: intracellular distribution', *Biology of the cell,* 56(1), pp. 1-6.

Gasser, S. and Raulet, D.H. (2006) 'Activation and self-tolerance of natural killer cells', *Immunological reviews,* 214, pp. 130-142.

Gellert, M., Hesse, J.E., Hiom, K., Melek, M., Modesti, M., Paull, T.T., Ramsden, D.A. and van Gent, D.C. (1999) 'V(D)J recombination: links to transposition and double-strand break repair', *Cold Spring Harbor symposia on quantitative biology,* 64, pp. 161-167.

Gelot, C., Magdalou, I. and Lopez, B.S. (2015) 'Replication stress in Mammalian cells and its consequences for mitosis', *Genes,* 6(2), pp. 267-298.

Gelot, C., Magdalou, I. and Lopez, B.S. (2015) 'Replication stress in Mammalian cells and its consequences for mitosis', *Genes,* 6(2), pp. 267-298.

Golding, S.E., Rosenberg, E., Valerie, N., Hussaini, I., Frigerio, M., Cockcroft, X.F., Chong, W.Y., Hummersone, M., Rigoreau, L., Menear, K.A., O'Connor, M.J., Povirk, L.F., van Meter, T. and Valerie, K. (2009) 'Improved ATM kinase inhibitor KU-60019 radiosensitizes glioma cells, compromises insulin, AKT and ERK prosurvival signaling, and inhibits migration and invasion', *Molecular cancer therapeutics,* 8(10), pp. 2894-2902.

Gorgoulis, V.G., Vassiliou, L.V., Karakaidos, P., Zacharatos, P., Kotsinas, A., Liloglou, T., Venere, M., Ditullio, R.A.,Jr, Kastrinakis, N.G., Levy, B., Kletsas, D., Yoneta, A., Herlyn, M., Kittas, C. and Halazonetis, T.D. (2005) 'Activation of the DNA damage checkpoint and genomic instability in human precancerous lesions', *Nature,* 434(7035), pp. 907-913.

Gossen, M. and Bujard, H. (1992) 'Tight control of gene expression in mammalian cells by tetracycline-responsive promoters', *Proceedings of the National Academy of Sciences of the United States of America,* 89(12), pp. 5547-5551.

Griffiths, D.J., Barbet, N.C., McCready, S., Lehmann, A.R. and Carr, A.M. (1995) 'Fission yeast rad17: a homologue of budding yeast RAD24 that shares regions of sequence similarity with DNA polymerase accessory proteins', *The EMBO journal,* 14(23), pp. 5812-5823.

Haber, J.E. (2000) 'Lucky breaks: analysis of recombination in Saccharomyces', *Mutation research,* 451(1-2), pp. 53-69.

Hache, R.J., Tse, R., Reich, T., Savory, J.G. and Lefebvre, Y.A. (1999) 'Nucleocytoplasmic trafficking of steroid-free glucocorticoid receptor', *The Journal of biological chemistry,* 274(3), pp. 1432-1439.

Halazonetis, T.D., Gorgoulis, V.G. and Bartek, J. (2008) 'An oncogene-induced DNA damage model for cancer development', *Science (New York, N.Y.),* 319(5868), pp. 1352-1355.

Han, L. and Yu, K. (2008) 'Altered kinetics of nonhomologous end joining and class switch recombination in ligase IV-deficient B cells', *The Journal of experimental medicine,* 205(12), pp. 2745-2753.

Hanahan, D. and Weinberg, R.A. (2011) 'Hallmarks of cancer: the next generation', *Cell,* 144(5), pp. 646-674.

Hanway, D., Chin, J.K., Xia, G., Oshiro, G., Winzeler, E.A. and Romesberg, F.E. (2002) 'Previously uncharacterized genes in the UV- and MMS-induced DNA damage response in yeast', *Proceedings of the National Academy of Sciences of the United States of America,* 99(16), pp. 10605-10610.

Harder, H.C. and Rosenberg, B. (1970) 'Inhibitory effects of anti-tumor platinum compounds on DNA, RNA and protein syntheses in mammalian cells in virtro', *International journal of cancer,* 6(2), pp. 207-216.

Harper, J.W. and Elledge, S.J. (2007) 'The DNA damage response: ten years after', *Molecular cell,* 28(5), pp. 739-745.

Harper, J.W., Elledge, S.J., Keyomarsi, K., Dynlacht, B., Tsai, L.H., Zhang, P., Dobrowolski, S., Bai, C., Connell-Crowley, L. and Swindell, E. (1995) 'Inhibition of cyclin-dependent kinases by p21', *Molecular biology of the cell,* 6(4), pp. 387-400.

Haruki, H., Nishikawa, J. and Laemmli, U.K. (2008) 'The anchor-away technique: rapid, conditional establishment of yeast mutant phenotypes', *Molecular cell,* 31(6), pp. 925-932.

Helleday, T. (2003) 'Pathways for mitotic homologous recombination in mammalian cells', *Mutation research,* 532(1-2), pp. 103-115.

Helleday, T., Lo, J., van Gent, D.C. and Engelward, B.P. (2007) 'DNA double-strand break repair: from mechanistic understanding to cancer treatment', *DNA repair,* 6(7), pp. 923-935.

Heller, R.C. and Marians, K.J. (2006) 'Replisome assembly and the direct restart of stalled replication forks', *Nature reviews.Molecular cell biology,* 7(12), pp. 932-943.

Helmrich, A., Ballarino, M., Nudler, E. and Tora, L. (2013) 'Transcription-replication encounters, consequences and genomic instability', *Nature structural & molecular biology,* 20(4), pp. 412-418.

Helt, C.E., Cliby, W.A., Keng, P.C., Bambara, R.A. and O'Reilly, M.A. (2005) 'Ataxia telangiectasia mutated (ATM) and ATM and Rad3-related protein exhibit selective target specificities in response to different forms of DNA damage', *The Journal of biological chemistry,* 280(2), pp. 1186-1192.

Helt, C.E., Wang, W., Keng, P.C. and Bambara, R.A. (2005) 'Evidence that DNA damage detection machinery participates in DNA repair', *Cell cycle (Georgetown, Tex.),* 4(4), pp. 529-532.

Hickson, I., Zhao, Y., Richardson, C.J., Green, S.J., Martin, N.M., Orr, A.I., Reaper, P.M., Jackson, S.P., Curtin, N.J. and Smith, G.C. (2004) 'Identification and characterization of a novel and specific inhibitor of the ataxia-telangiectasia mutated kinase ATM', *Cancer research,* 64(24), pp. 9152-9159.

Hills, S.A. and Diffley, J.F. (2014) 'DNA replication and oncogene-induced replicative stress', *Current biology : CB,* 24(10), pp. R435-44.

Hinz, J.M., Helleday, T. and Meuth, M. (2003) 'Reduced apoptotic response to camptothecin in CHO cells deficient in XRCC3', *Carcinogenesis,* 24(2), pp. 249-253.

Hoeijmakers, J.H. (2009) 'DNA damage, aging, and cancer', *The New England journal of medicine,* 361(15), pp. 1475-1485.

Hofmann, J.F. and Beach, D. (1994) 'cdt1 is an essential target of the Cdc10/Sct1 transcription factor: requirement for DNA replication and inhibition of mitosis', *The EMBO journal,* 13(2), pp. 425-434.

Holland, A.J., Fachinetti, D., Han, J.S. and Cleveland, D.W. (2012) 'Inducible, reversible system for the rapid and complete degradation of proteins in mammalian cells', *Proceedings of the National Academy of Sciences of the United States of America,* 109(49), pp. E3350-7.

Hsiang, Y.H., Lihou, M.G. and Liu, L.F. (1989) 'Arrest of replication forks by drug-stabilized topoisomerase I-DNA cleavable complexes as a mechanism of cell killing by camptothecin', *Cancer research,* 49(18), pp. 5077-5082.

Htun, H., Barsony, J., Renyi, I., Gould, D.L. and Hager, G.L. (1996) 'Visualization of glucocorticoid receptor translocation and intranuclear organization in living cells with a green fluorescent protein chimera', *Proceedings of the National Academy of Sciences of the United States of America,* 93(10), pp. 4845-4850.

Huang, F. and Mazin, A.V. (2014) 'A small molecule inhibitor of human RAD51 potentiates breast cancer cell killing by therapeutic agents in mouse xenografts', *PloS one,* 9(6), pp. e100993.

Iftode, C., Daniely, Y. and Borowiec, J.A. (1999) 'Replication protein A (RPA): the eukaryotic SSB', *Critical reviews in biochemistry and molecular biology,* 34(3), pp. 141-180.

Ira, G., Pellicioli, A., Balijja, A., Wang, X., Fiorani, S., Carotenuto, W., Liberi, G., Bressan, D., Wan, L., Hollingsworth, N.M., Haber, J.E. and Foiani, M. (2004) 'DNA end resection,

homologous recombination and DNA damage checkpoint activation require CDK1', *Nature,* 431(7011), pp. 1011-1017.

Iwamoto, M., Bjorklund, T., Lundberg, C., Kirik, D. and Wandless, T.J. (2010) 'A general chemical method to regulate protein stability in the mammalian central nervous system', *Chemistry & biology,* 17(9), pp. 981-988.

Jackson, S.P. and Bartek, J. (2009) 'The DNA-damage response in human biology and disease', *Nature,* 461(7267), pp. 1071-1078.

Jacome, A. and Fernandez-Capetillo, O. (2011) 'Lac operator repeats generate a traceable fragile site in mammalian cells', *EMBO reports,* 12(10), pp. 1032-1038.

Jasin, M. (1996) 'Genetic manipulation of genomes with rare-cutting endonucleases', *Trends in genetics : TIG,* 12(6), pp. 224-228.

Jazayeri, A., Falck, J., Lukas, C., Bartek, J., Smith, G.C., Lukas, J. and Jackson, S.P. (2006) 'ATM- and cell cycle-dependent regulation of ATR in response to DNA double-strand breaks', *Nature cell biology,* 8(1), pp. 37-45.

Jena, N.R. (2012) 'DNA damage by reactive species: Mechanisms, mutation and repair', *Journal of Biosciences,* 37(3), pp. 503-517.

Jeppesen, D.K., Bohr, V.A. and Stevnsner, T. (2011) 'DNA repair deficiency in neurodegeneration', *Progress in neurobiology,* 94(2), pp. 166-200.

Jin, J., Shirogane, T., Xu, L., Nalepa, G., Qin, J., Elledge, S.J. and Harper, J.W. (2003) 'SCFbeta-TRCP links Chk1 signaling to degradation of the Cdc25A protein phosphatase', *Genes & development,* 17(24), pp. 3062-3074.

Johnson, A. and O'Donnell, M. (2005) 'Cellular DNA replicases: components and dynamics at the replication fork', *Annual Review of Biochemistry,* 74, pp. 283-315.

Jones, J.R., Shelton, K.D. and Magnuson, M.A. (2005) 'Strategies for the use of site-specific recombinases in genome engineering', *Methods in Molecular Medicine,* 103, pp. 245-257.

Jossen, R. and Bermejo, R. (2013) 'The DNA damage checkpoint response to replication stress: A Game of Forks', *Frontiers in genetics,* 4, pp. 26.

Kandoth, C., McLellan, M.D., Vandin, F., Ye, K., Niu, B., Lu, C., Xie, M., Zhang, Q., McMichael, J.F., Wyczalkowski, M.A., Leiserson, M.D.M., Miller, C.A., Welch, J.S., Walter, M.J., Wendl, M.C., Ley, T.J., Wilson, R.K., Raphael, B.J. and Ding, L. (2013) 'Mutational landscape and significance across 12 major cancer types', *Nature,* 502(7471), pp. 333-339.

Karnitz, L.M., Flatten, K.S., Wagner, J.M., Loegering, D., Hackbarth, J.S., Arlander, S.J., Vroman, B.T., Thomas, M.B., Baek, Y.U., Hopkins, K.M., Lieberman, H.B., Chen, J., Cliby, W.A. and Kaufmann, S.H. (2005) 'Gemcitabine-induced activation of checkpoint signaling pathways that affect tumor cell survival', *Molecular pharmacology,* 68(6), pp. 1636-1644.

Kasparek, T.R. and Humphrey, T.C. (2011) 'DNA double-strand break repair pathways, chromosomal rearrangements and cancer', *Seminars in cell & developmental biology,* 22(8), pp. 886-897.

Kastan, M.B. and Bartek, J. (2004) 'Cell-cycle checkpoints and cancer', *Nature,* 432(7015), pp. 316-323.

Kastan, M.B. and Lim, D.S. (2000) 'The many substrates and functions of ATM', *Nature reviews.Molecular cell biology,* 1(3), pp. 179-186.

Kastan, M.B., Onyekwere, O., Sidransky, D., Vogelstein, B. and Craig, R.W. (1991) 'Participation of p53 protein in the cellular response to DNA damage', *Cancer research,* 51(23 Pt 1), pp. 6304-6311.

Kawabata, T., Luebben, S.W., Yamaguchi, S., Ilves, I., Matise, I., Buske, T., Botchan, M.R. and Shima, N. (2011) 'Stalled fork rescue via dormant replication origins in unchallenged S phase promotes proper chromosome segregation and tumor suppression', *Molecular cell,* 41(5), pp. 543-553.

Kawanishi, S. and Hiraku, Y. (2006) 'Oxidative and nitrative DNA damage as biomarker for carcinogenesis with special reference to inflammation', *Antioxidants & redox signaling,* 8(5-6), pp. 1047-1058.

Kawanishi, S., Hiraku, Y., Pinlaor, S. and Ma, N. (2006) 'Oxidative and nitrative DNA damage in animals and patients with inflammatory diseases in relation to inflammation-related carcinogenesis', *Biological chemistry,* 387(4), pp. 365-372.

Keith, C.T. and Schreiber, S.L. (1995) 'PIK-related kinases: DNA repair, recombination, and cell cycle checkpoints', *Science (New York, N.Y.),* 270(5233), pp. 50-51.

Khalil, H., Tummala, H., Chakarov, S., Zhelev, N. and Lane, D. (2012) 'Targeting ATM pathway for therapeutic intervention in cancer', *BioDiscovery,* 2012(10.7750), pp. 1-3.

Khanna, K.K. and Jackson, S.P. (2001) 'DNA double-strand breaks: signaling, repair and the cancer connection', *Nature genetics,* 27(3), pp. 247-254.

Khare, D., Ziegelin, G., Lanka, E. and Heinemann, U. (2004) 'Sequence-specific DNA binding determined by contacts outside the helix-turn-helix motif of the ParB homolog KorB', *Nature structural & molecular biology,* 11(7), pp. 656-663.

Kim, J.C. and Mirkin, S.M. (2013) 'The balancing act of DNA repeat expansions', *Current opinion in genetics & development,* 23(3), pp. 280-288.

Kinzler, K.W. and Vogelstein, B. (1997) 'Cancer-susceptibility genes. Gatekeepers and caretakers', *Nature,* 386(6627), pp. 761, 763.

Kitagawa, R., Bakkenist, C.J., McKinnon, P.J. and Kastan, M.B. (2004) 'Phosphorylation of SMC1 is a critical downstream event in the ATM-NBS1-BRCA1 pathway', *Genes & development,* 18(12), pp. 1423-1438.

Kobayashi, T. (2003) 'The replication fork barrier site forms a unique structure with Fob1p and inhibits the replication fork', *Molecular and cellular biology,* 23(24), pp. 9178-9188.

Kolb, A.F. (2002) 'Genome engineering using site-specific recombinases', *Cloning and stem cells,* 4(1), pp. 65-80.

Koster, D.A., Palle, K., Bot, E.S., Bjornsti, M.A. and Dekker, N.H. (2007) 'Antitumour drugs impede DNA uncoiling by topoisomerase I', *Nature,* 448(7150), pp. 213-217.

Kraus, E., Leung, W.Y. and Haber, J.E. (2001) 'Break-induced replication: a review and an example in budding yeast', *Proceedings of the National Academy of Sciences of the United States of America,* 98(15), pp. 8255-8262.

Kulkarni, A. and Wilson, D.M.,3rd (2008) 'The involvement of DNA-damage and -repair defects in neurological dysfunction', *American Journal of Human Genetics,* 82(3), pp. 539-566.

Labib, K. and De Piccoli, G. (2011) 'Surviving chromosome replication: the many roles of the S-phase checkpoint pathway', *Philosophical transactions of the Royal Society of London.Series B, Biological sciences,* 366(1584), pp. 3554-3561.

Labib, K. and Hodgson, B. (2007) 'Replication fork barriers: pausing for a break or stalling for time?', *EMBO reports,* 8(4), pp. 346-353.

Labib, K., Tercero, J.A. and Diffley, J.F. (2000) 'Uninterrupted MCM2-7 function required for DNA replication fork progression', *Science (New York, N.Y.),* 288(5471), pp. 1643-1647.

Lamarche, B.J., Orazio, N.I. and Weitzman, M.D. (2010) 'The MRN complex in double-strand break repair and telomere maintenance', *FEBS letters,* 584(17), pp. 3682-3695.

Lambert, S. and Carr, A.M. (2013) 'Impediments to replication fork movement: stabilisation, reactivation and genome instability', *Chromosoma,* 122(1-2), pp. 33-45.

Lambert, S., Watson, A., Sheedy, D.M., Martin, B. and Carr, A.M. (2005) 'Gross chromosomal rearrangements and elevated recombination at an inducible site-specific replication fork barrier', *Cell,* 121(5), pp. 689-702.

Lange, A., Mills, R.E., Lange, C.J., Stewart, M., Devine, S.E. and Corbett, A.H. (2007) 'Classical nuclear localization signals: definition, function, and interaction with importin alpha', *The Journal of biological chemistry,* 282(8), pp. 5101-5105.

Lassadi, I. and Bystricky, K. (2011) 'Tracking of single and multiple genomic loci in living yeast cells', *Methods in molecular biology (Clifton, N.J.),* 745, pp. 499-522.

Lee, J. and Jayaram, M. (1997) 'A tetramer of the Flp recombinase silences the trimers within it during resolution of a Holliday junction substrate', *Genes & development,* 11(18), pp. 2438-2447.

Lee, J., Jayaram, M. and Grainge, I. (1999) 'Wild-type Flp recombinase cleaves DNA in trans', *The EMBO journal,* 18(3), pp. 784-791.

Lee, J.A., Carvalho, C.M. and Lupski, J.R. (2007) 'A DNA replication mechanism for generating nonrecurrent rearrangements associated with genomic disorders', *Cell,* 131(7), pp. 1235-1247.

Lee, J.H. and Paull, T.T. (2004) 'Direct activation of the ATM protein kinase by the Mre11/Rad50/Nbs1 complex', *Science (New York, N.Y.),* 304(5667), pp. 93-96.

Lehmann, A.R., Niimi, A., Ogi, T., Brown, S., Sabbioneda, S., Wing, J.F., Kannouche, P.L. and Green, C.M. (2007) 'Translesion synthesis: Y-family polymerases and the polymerase switch', *DNA repair,* 6(7), pp. 891-899.

Leman, A.R. and Noguchi, E. (2013) 'The replication fork: understanding the eukaryotic replication machinery and the challenges to genome duplication', *Genes,* 4(1), pp. 1-32.

Lemmens, B.B. and Tijsterman, M. (2011) 'DNA double-strand break repair in Caenorhabditis elegans', *Chromosoma,* 120(1), pp. 1-21.

Lemoine, F.J., Degtyareva, N.P., Lobachev, K. and Petes, T.D. (2005) 'Chromosomal translocations in yeast induced by low levels of DNA polymerase a model for chromosome fragile sites', *Cell,* 120(5), pp. 587-598.

Lengauer, C., Kinzler, K.W. and Vogelstein, B. (1998) 'Genetic instabilities in human cancers', *Nature,* 396(6712), pp. 643-649.

Lieber, M.R. (2008) 'The mechanism of human nonhomologous DNA end joining', *The Journal of biological chemistry,* 283(1), pp. 1-5.

Lieber, M.R. and Wilson, T.E. (2010) 'SnapShot: Nonhomologous DNA end joining (NHEJ)', *Cell,* 142(3), pp. 496-496.e1.

Lim, D.S., Kim, S.T., Xu, B., Maser, R.S., Lin, J., Petrini, J.H. and Kastan, M.B. (2000) 'ATM phosphorylates p95/nbs1 in an S-phase checkpoint pathway', *Nature,* 404(6778), pp. 613-617.

Lin, S.Y., Li, K., Stewart, G.S. and Elledge, S.J. (2004) 'Human Claspin works with BRCA1 to both positively and negatively regulate cell proliferation', *Proceedings of the National Academy of Sciences of the United States of America,* 101(17), pp. 6484-6489.

Lindahl, T. (1993) 'Instability and decay of the primary structure of DNA', *Nature,* 362(6422), pp. 709-715.

Lindahl, T. and Barnes, D.E. (2000) 'Repair of endogenous DNA damage', *Cold Spring Harbor symposia on quantitative biology,* 65, pp. 127-133.

Lindahl, T. and Barnes, D.E. (1992) 'Mammalian DNA ligases', *Annual Review of Biochemistry,* 61, pp. 251-281.

Liu, P., Carvalho, C.M., Hastings, P.J. and Lupski, J.R. (2012) 'Mechanisms for recurrent and complex human genomic rearrangements', *Current opinion in genetics & development,* 22(3), pp. 211-220.

Liu, P., Erez, A., Nagamani, S.C., Dhar, S.U., Kolodziejska, K.E., Dharmadhikari, A.V., Cooper, M.L., Wiszniewska, J., Zhang, F., Withers, M.A., Bacino, C.A., Campos-Acevedo, L.D., Delgado, M.R., Freedenberg, D., Garnica, A., Grebe, T.A., Hernandez-Almaguer, D., Immken, L., Lalani, S.R., McLean, S.D., Northrup, H., Scaglia, F., Strathearn, L., Trapane, P., Kang, S.H., Patel, A., Cheung, S.W., Hastings, P.J., Stankiewicz, P., Lupski, J.R. and Bi, W. (2011) 'Chromosome catastrophes involve replication mechanisms generating complex genomic rearrangements', *Cell,* 146(6), pp. 889-903.

Liu, Q., Guntuku, S., Cui, X.S., Matsuoka, S., Cortez, D., Tamai, K., Luo, G., Carattini-Rivera, S., DeMayo, F., Bradley, A., Donehower, L.A. and Elledge, S.J.(2000) 'Chk1 is an essential kinase that is regulated by Atr and required for the G(2)/M DNA damage checkpoint', *Genes & development,* 14(12), pp. 1448-1459.

Llorente, B., Smith, C.E. and Symington, L.S. (2008) 'Break-induced replication: what is it and what is it for?', *Cell cycle (Georgetown, Tex.),* 7(7), pp. 859-864.

Lopes, M., Cotta-Ramusino, C., Pellicioli, A., Liberi, G., Plevani, P., Muzi-Falconi, M., Newlon, C.S. and Foiani, M. (2001) 'The DNA replication checkpoint response stabilizes stalled replication forks', *Nature,* 412(6846), pp. 557-561.

Lovejoy, C.A. and Cortez, D. (2009) 'Common mechanisms of PIKK regulation', *DNA repair,* 8(9), pp. 1004-1008.

Lukas, J., Lukas, C. and Bartek, J. (2004) 'Mammalian cell cycle checkpoints: signalling pathways and their organization in space and time', *DNA repair,* 3(8-9), pp. 997-1007.

Luo, J., Solimini, N.L. and Elledge, S.J. (2009) 'Principles of cancer therapy: oncogene and non-oncogene addiction', *Cell,* 136(5), pp. 823-837.

Maira, S.M., Stauffer, F., Brueggen, J., Furet, P., Schnell, C., Fritsch, C., Brachmann, S., Chene, P., De Pover, A., Schoemaker, K., Fabbro, D., Gabriel, D., Simonen, M., Murphy, L., Finan, P., Sellers, W. and Garcia-Echeverria, C. (2008) 'Identification and characterization of NVP-BEZ235, a new orally available dual phosphatidylinositol 3-kinase/mammalian target of rapamycin inhibitor with potent in vivo antitumor activity', *Molecular cancer therapeutics,* 7(7), pp. 1851-1863.

Malkova, A., Ivanov, E.L. and Haber, J.E. (1996) 'Double-strand break repair in the absence of RAD51 in yeast: a possible role for break-induced DNA replication', *Proceedings of the National Academy of Sciences of the United States of America,* 93(14), pp. 7131-7136.

Mansour, W.Y., Rhein, T. and Dahm-Daphi, J. (2010) 'The alternative end-joining pathway for repair of DNA double-strand breaks requires PARP1 but is not dependent upon microhomologies', *Nucleic acids research,* 38(18), pp. 6065-6077.

Martin, L.P., Hamilton, T.C. and Schilder, R.J. (2008) 'Platinum resistance: the role of DNA repair pathways', *Clinical cancer research : an official journal of the American Association for Cancer Research,* 14(5), pp. 1291-1295.

Martinez, E.D., Rayasam, G.V., Dull, A.B., Walker, D.A. and Hager, G.L. (2005) 'An estrogen receptor chimera senses ligands by nuclear translocation', *The Journal of steroid biochemistry and molecular biology,* 97(4), pp. 307-321.

Masai, H., Matsumoto, S., You, Z., Yoshizawa-Sugata, N. and Oda, M. (2010) 'Eukaryotic chromosome DNA replication: where, when, and how?', *Annual Review of Biochemistry,* 79, pp. 89-130.

Massague, J. (2004) 'G1 cell-cycle control and cancer', *Nature,* 432(7015), pp. 298-306.

Matsuoka, S., Rotman, G., Ogawa, A., Shiloh, Y., Tamai, K. and Elledge, S.J. (2000) 'Ataxia telangiectasia-mutated phosphorylates Chk2 in vivo and in vitro', *Proceedings of the National Academy of Sciences of the United States of America,* 97(19), pp. 10389-10394.

Matthews, L., Johnson, J., Berry, A., Trebble, P., Cookson, A., Spiller, D., Rivers, C., Norman, M., White, M. and Ray, D. (2011) 'Cell cycle phase regulates glucocorticoid receptor function', *PloS one,* 6(7), pp. e22289.

Maya, R., Balass, M., Kim, S.T., Shkedy, D., Leal, J.F., Shifman, O., Moas, M., Buschmann, T., Ronai, Z., Shiloh, Y., Kastan, M.B., Katzir, E. and Oren, M. (2001) 'ATM-dependent phosphorylation of Mdm2 on serine 395: role in p53 activation by DNA damage', *Genes & development,* 15(9), pp. 1067-1077.

McIlwraith, M.J., Vaisman, A., Liu, Y., Fanning, E., Woodgate, R. and West, S.C. (2005) 'Human DNA polymerase eta promotes DNA synthesis from strand invasion intermediates of homologous recombination', *Molecular cell,* 20(5), pp. 783-792.

McMurray, C.T. (2010) 'Mechanisms of trinucleotide repeat instability during human development', *Nature reviews.Genetics,* 11(11), pp. 786-799.

McMurray, M.A. and Gottschling, D.E. (2003) 'An age-induced switch to a hyper-recombinational state', *Science (New York, N.Y.),* 301(5641), pp. 1908-1911.

McVey, M. and Lee, S.E. (2008) 'MMEJ repair of double-strand breaks (director's cut): deleted sequences and alternative endings', *Trends in genetics : TIG,* 24(11), pp. 529-538.

Meek, K., Dang, V. and Lees-Miller, S.P. (2008) 'DNA-PK: the means to justify the ends?', *Advances in Immunology,* 99, pp. 33-58.

Mefford, H.C. and Eichler, E.E. (2009) 'Duplication hotspots, rare genomic disorders, and common disease', *Current opinion in genetics & development,* 19(3), pp. 196-204.

Menezes, D.L., Holt, J., Tang, Y., Feng, J., Barsanti, P., Pan, Y., Ghoddusi, M., Zhang, W., Thomas, G., Holash, J., Lees, E. and Taricani, L. (2015) 'A synthetic lethal screen reveals enhanced sensitivity to ATR inhibitor treatment in mantle cell lymphoma with ATM loss-of-function', *Molecular cancer research : MCR,* 13(1), pp. 120-129.

Michel, B., Flores, M.J., Viguera, E., Grompone, G., Seigneur, M. and Bidnenko, V. (2001) 'Rescue of arrested replication forks by homologous recombination', *Proceedings of the National Academy of Sciences of the United States of America,* 98(15), pp. 8181-8188.

Mimitou, E.P. and Symington, L.S. (2010) 'Ku prevents Exo1 and Sgs1-dependent resection of DNA ends in the absence of a functional MRX complex or Sae2', *The EMBO journal,* 29(19), pp. 3358-3369.

Mimitou, E.P. and Symington, L.S. (2008) 'Sae2, Exo1 and Sgs1 collaborate in DNA double-strand break processing', *Nature,* 455(7214), pp. 770-774.

Mirkin, E.V. and Mirkin, S.M. (2007) 'Replication fork stalling at natural impediments', *Microbiology and molecular biology reviews : MMBR,* 71(1), pp. 13-35.

Mochan, T.A., Venere, M., DiTullio, R.A.,Jr and Halazonetis, T.D. (2004) '53BP1, an activator of ATM in response to DNA damage', *DNA repair,* 3(8-9), pp. 945-952.

Moyer, S.E., Lewis, P.W. and Botchan, M.R. (2006) 'Isolation of the Cdc45/Mcm2-7/GINS (CMG) complex, a candidate for the eukaryotic DNA replication fork helicase', *Proceedings of the National Academy of Sciences of the United States of America,* 103(27), pp. 10236-10241.

Myers, J.S. and Cortez, D. (2006) 'Rapid activation of ATR by ionizing radiation requires ATM and Mre11', *The Journal of biological chemistry,* 281(14), pp. 9346-9350.

Myers, K., Gagou, M.E., Zuazua-Villar, P., Rodriguez, R. and Meuth, M. (2009) 'ATR and Chk1 suppress a caspase-3-dependent apoptotic response following DNA replication stress', *PLoS genetics,* 5(1), pp. e1000324.

Myung, K., Chen, C. and Kolodner, R.D. (2001) 'Multiple pathways cooperate in the suppression of genome instability in Saccharomyces cerevisiae', *Nature,* 411(6841), pp. 1073-1076.

Myung, K. and Kolodner, R.D. (2002) 'Suppression of genome instability by redundant S-phase checkpoint pathways in Saccharomyces cerevisiae', *Proceedings of the National Academy of Sciences of the United States of America,* 99(7), pp. 4500-4507.

Neale, M.J. and Keeney, S. (2006) 'Clarifying the mechanics of DNA strand exchange in meiotic recombination', *Nature,* 442(7099), pp. 153-158.

Negrini, S., Gorgoulis, V.G. and Halazonetis, T.D. (2010) 'Genomic instability--an evolving hallmark of cancer', *Nature reviews.Molecular cell biology,* 11(3), pp. 220-228.

Nick McElhinny, S.A., Snowden, C.M., McCarville, J. and Ramsden, D.A. (2000) 'Ku recruits the XRCC4-ligase IV complex to DNA ends', *Molecular and cellular biology,* 20(9), pp. 2996-3003.

Nielsen, I., Andersen, A.H. and Bjergbaek, L. (2012) 'Studying repair of a single protein-bound nick in vivo using the Flp-nick system', *Methods in molecular biology (Clifton, N.J.),* 920, pp. 393-415.

Nielsen, I., Bentsen, I.B., Lisby, M., Hansen, S., Mundbjerg, K., Andersen, A.H. and Bjergbaek, L. (2009) 'A Flp-nick system to study repair of a single protein-bound nick in vivo', *Nature methods,* 6(10), pp. 753-757.

Nimonkar, A.V., Ozsoy, A.Z., Genschel, J., Modrich, P. and Kowalczykowski, S.C. (2008) 'Human exonuclease 1 and BLM helicase interact to resect DNA and initiate DNA repair', *Proceedings of the National Academy of Sciences of the United States of America,* 105(44), pp. 16906-16911.

Nishida, H., Tatewaki, N., Nakajima, Y., Magara, T., Ko, K.M., Hamamori, Y. and Konishi, T. (2009) 'Inhibition of ATR protein kinase activity by schisandrin B in DNA damage response', *Nucleic acids research,* 37(17), pp. 5678-5689.

Nishimura, K., Fukagawa, T., Takisawa, H., Kakimoto, T. and Kanemaki, M. (2009) 'An auxin-based degron system for the rapid depletion of proteins in nonplant cells', *Nature methods,* 6(12), pp. 917-922.

Nishitani, H. and Lygerou, Z. (2002) 'Control of DNA replication licensing in a cell cycle', *Genes to cells : devoted to molecular & cellular mechanisms,* 7(6), pp. 523-534.

Nishitani, H., Lygerou, Z., Nishimoto, T. and Nurse, P. (2000) 'The Cdt1 protein is required to license DNA for replication in fission yeast', *Nature,* 404(6778), pp. 625-628.

Nitiss, J. and Wang, J.C. (1988) 'DNA topoisomerase-targeting antitumor drugs can be studied in yeast', *Proceedings of the National Academy of Sciences of the United States of America,* 85(20), pp. 7501-7505.

Nussenzweig, A. and Nussenzweig, M.C. (2010) 'Origin of chromosomal translocations in lymphoid cancer', *Cell,* 141(1), pp. 27-38.

O'Driscoll, M., Ruiz-Perez, V.L., Woods, C.G., Jeggo, P.A. and Goodship, J.A. (2003) 'A splicing mutation affecting expression of ataxia-telangiectasia and Rad3-related protein (ATR) results in Seckel syndrome', *Nature genetics,* 33(4), pp. 497-501.

Ogawa, H., Inouye, S., Tsuji, F.I., Yasuda, K. and Umesono, K. (1995) 'Localization, trafficking, and temperature-dependence of the Aequorea green fluorescent protein in cultured vertebrate cells', *Proceedings of the National Academy of Sciences of the United States of America,* 92(25), pp. 11899-11903.

Ottini, L., Falchetti, M., Saieva, C., De Marco, M., Masala, G., Zanna, I., Paglierani, M., Giannini, G., Gulino, A., Nesi, G., Mariani Costantini, R. and Palli, D.(2004) 'MRE11 expression is impaired in gastric cancer with microsatellite instability', *Carcinogenesis,* 25(12), pp. 2337-2343.

Pace, P., Mosedale, G., Hodskinson, M.R., Rosado, I.V., Sivasubramaniam, M. and Patel, K.J. (2010) 'Ku70 corrupts DNA repair in the absence of the Fanconi anemia pathway', *Science (New York, N.Y.),* 329(5988), pp. 219-223.

Pacek, M. and Walter, J.C. (2004) 'A requirement for MCM7 and Cdc45 in chromosome unwinding during eukaryotic DNA replication', *The EMBO journal,* 23(18), pp. 3667-3676.

Pages, V. and Fuchs, R.P. (2003) 'Uncoupling of leading- and lagging-strand DNA replication during lesion bypass in vivo', *Science (New York, N.Y.),* 300(5623), pp. 1300-1303.

Parsons, R.L., Prasad, P.V., Harshey, R.M. and Jayaram, M. (1988) 'Step-arrest mutants of FLP recombinase: implications for the catalytic mechanism of DNA recombination', *Molecular and cellular biology,* 8(8), pp. 3303-3310.

Patel, A.G., Sarkaria, J.N. and Kaufmann, S.H. (2011) 'Nonhomologous end joining drives poly(ADP-ribose) polymerase (PARP) inhibitor lethality in homologous recombination-deficient cells', *Proceedings of the National Academy of Sciences of the United States of America,* 108(8), pp. 3406-3411.

Peasland, A., Wang, L.Z., Rowling, E., Kyle, S., Chen, T., Hopkins, A., Cliby, W.A., Sarkaria, J., Beale, G., Edmondson, R.J. and Curtin, N.J. (2011) 'Identification and evaluation of a potent novel ATR inhibitor, NU6027, in breast and ovarian cancer cell lines', *British journal of cancer,* 105(3), pp. 372-381.

Petermann, E., Orta, M.L., Issaeva, N., Schultz, N. and Helleday, T. (2010) 'Hydroxyurea-stalled replication forks become progressively inactivated and require two different RAD51-mediated pathways for restart and repair', *Molecular cell,* 37(4), pp. 492-502.

Peto, J. (2001) 'Cancer epidemiology in the last century and the next decade', *Nature,* 411(6835), pp. 390-395.

Picard, D. (2000) 'Posttranslational regulation of proteins by fusions to steroid-binding domains', *Methods in enzymology,* 327, pp. 385-401.

Picard, D., Salser, S.J. and Yamamoto, K.R. (1988) 'A movable and regulable inactivation function within the steroid binding domain of the glucocorticoid receptor', *Cell,* 54(7), pp. 1073-1080.

Picard, D. and Yamamoto, K.R. (1987) 'Two signals mediate hormone-dependent nuclear localization of the glucocorticoid receptor', *The EMBO journal,* 6(11), pp. 3333-3340.

Pichierri, P., Franchitto, A., Mosesso, P. and Palitti, F. (2001) 'Werner's syndrome protein is required for correct recovery after replication arrest and DNA damage induced in S-phase of cell cycle', *Molecular biology of the cell,* 12(8), pp. 2412-2421.

Pomerantz, R.T. and O'Donnell, M. (2010) 'Direct restart of a replication fork stalled by a head-on RNA polymerase', *Journal of visualized experiments : JoVE,* (38). pii: 1919. doi(38), pp. 10.3791/1919.

Pommier, Y., Barcelo, J.M., Rao, V.A., Sordet, O., Jobson, A.G., Thibaut, L., Miao, Z.H., Seiler, J.A., Zhang, H., Marchand, C., Agama, K., Nitiss, J.L. and Redon, C.(2006) 'Repair of topoisomerase I-mediated DNA damage', *Progress in nucleic acid research and molecular biology,* 81, pp. 179-229.

Possoz, C., Filipe, S.R., Grainge, I. and Sherratt, D.J. (2006) 'Tracking of controlled Escherichia coli replication fork stalling and restart at repressor-bound DNA in vivo', *The EMBO journal,* 25(11), pp. 2596-2604.

Postel-Vinay, S., Vanhecke, E., Olaussen, K.A., Lord, C.J., Ashworth, A. and Soria, J.C. (2012) 'The potential of exploiting DNA-repair defects for optimizing lung cancer treatment', *Nature reviews.Clinical oncology,* 9(3), pp. 144-155.

Pourquier, P., Waltman, J.L., Urasaki, Y., Loktionova, N.A., Pegg, A.E., Nitiss, J.L. and Pommier, Y. (2001) 'Topoisomerase I-mediated cytotoxicity of N-methyl-N'-nitro-N-nitrosoguanidine: trapping of topoisomerase I by the O6-methylguanine', *Cancer research,* 61(1), pp. 53-58.

Powell, S.N., DeFrank, J.S., Connell, P., Eogan, M., Preffer, F., Dombkowski, D., Tang, W. and Friend, S. (1995) 'Differential sensitivity of p53(-) and p53(+) cells to caffeine-induced radiosensitization and override of G2 delay', *Cancer research,* 55(8), pp. 1643-1648.

Pratt, W.B. and Dittmar, K.D. (1998) 'Studies with Purified Chaperones Advance the Understanding of the Mechanism of Glucocorticoid Receptor-hsp90 Heterocomplex Assembly', *Trends in endocrinology and metabolism: TEM,* 9(6), pp. 244-252.

Price, B.D. and Youmell, M.B. (1996) 'The phosphatidylinositol 3-kinase inhibitor wortmannin sensitizes murine fibroblasts and human tumor cells to radiation and blocks induction of p53 following DNA damage', *Cancer research,* 56(2), pp. 246-250.

Pursell, Z.F., Isoz, I., Lundstrom, E.B., Johansson, E. and Kunkel, T.A. (2007) 'Yeast DNA polymerase epsilon participates in leading-strand DNA replication', *Science (New York, N.Y.),* 317(5834), pp. 127-130.

Putnam, C.D., Hayes, T.K. and Kolodner, R.D. (2010) 'Post-replication repair suppresses duplication-mediated genome instability', *PLoS genetics,* 6(5), pp. e1000933.

Putnam, C.D., Hayes, T.K. and Kolodner, R.D. (2009) 'Specific pathways prevent duplication-mediated genome rearrangements', *Nature,* 460(7258), pp. 984-989.

Qin, J.Y., Zhang, L., Clift, K.L., Hulur, I., Xiang, A.P., Ren, B.Z. and Lahn, B.T. (2010) 'Systematic comparison of constitutive promoters and the doxycycline-inducible promoter', *PloS one,* 5(5), pp. e10611.

Raghuraman, M.K., Winzeler, E.A., Collingwood, D., Hunt, S., Wodicka, L., Conway, A., Lockhart, D.J., Davis, R.W., Brewer, B.J. and Fangman, W.L. (2001) 'Replication dynamics of the yeast genome', *Science (New York, N.Y.),* 294(5540), pp. 115-121.

Ragland, R.L., Patel, S., Rivard, R.S., Smith, K., Peters, A.A., Bielinsky, A.K. and Brown, E.J. (2013) 'RNF4 and PLK1 are required for replication fork collapse in ATR-deficient cells', *Genes & development,* 27(20), pp. 2259-2273.

Rainey, M.D., Charlton, M.E., Stanton, R.V. and Kastan, M.B. (2008) 'Transient inhibition of ATM kinase is sufficient to enhance cellular sensitivity to ionizing radiation', *Cancer research,* 68(18), pp. 7466-7474.

Ran, F.A., Hsu, P.D., Wright, J., Agarwala, V., Scott, D.A. and Zhang, F. (2013) 'Genome engineering using the CRISPR-Cas9 system', *Nature protocols,* 8(11), pp. 2281-2308.

Ray Chaudhuri, A., Hashimoto, Y., Herrador, R., Neelsen, K.J., Fachinetti, D., Bermejo, R., Cocito, A., Costanzo, V. and Lopes, M. (2012) 'Topoisomerase I poisoning results in PARP-mediated replication fork reversal', *Nature structural & molecular biology,* 19(4), pp. 417-423.

Ribeyre, C., Zellweger, R., Chauvin, M., Bec, N., Larroque, C., Lopes, M. and Constantinou, A. (2016) 'Nascent DNA Proteomics Reveals a Chromatin Remodeler Required for Topoisomerase I Loading at Replication Forks', *Cell reports,* 15(2), pp. 300-309.

Riesterer, O., Matsumoto, F., Wang, L., Pickett, J., Molkentine, D., Giri, U., Milas, L. and Raju, U. (2011) 'A novel Chk inhibitor, XL-844, increases human cancer cell radiosensitivity through promotion of mitotic catastrophe', *Investigational new drugs,* 29(3), pp. 514-522.

Rogatsky, I., Trowbridge, J.M. and Garabedian, M.J. (1997) 'Glucocorticoid receptor-mediated cell cycle arrest is achieved through distinct cell-specific transcriptional regulatory mechanisms', *Molecular and cellular biology,* 17(6), pp. 3181-3193.

Rothkamm, K., Kruger, I., Thompson, L.H. and Lobrich, M. (2003) 'Pathways of DNA double-strand break repair during the mammalian cell cycle', *Molecular and cellular biology,* 23(16), pp. 5706-5715.

Rouse, J. and Jackson, S.P. (2002) 'Interfaces between the detection, signaling, and repair of DNA damage', *Science (New York, N.Y.),* 297(5581), pp. 547-551.

Rousseau, G.G. and Baxter, J.D. (1979) 'Glucocorticoid receptors', *Monographs on endocrinology,* 12, pp. 49-77.

Saad, H., Gallardo, F., Dalvai, M., Tanguy-le-Gac, N., Lane, D. and Bystricky, K. (2014) 'DNA dynamics during early double-strand break processing revealed by non-intrusive imaging of living cells', *PLoS genetics,* 10(3), pp. e1004187.

Sabatinos, S.A. (2010) '*Replication fork stalling and the fork protection complex*', *Nature education,* 9(40).

Sakofsky, C.J., Ayyar, S. and Malkova, A. (2012) 'Break-induced replication and genome stability', *Biomolecules,* 2(4), pp. 483-504.

Saleh-Gohari, N., Bryant, H.E., Schultz, N., Parker, K.M., Cassel, T.N. and Helleday, T. (2005) 'Spontaneous homologous recombination is induced by collapsed replication forks that are caused by endogenous DNA single-strand breaks', *Molecular and cellular biology,* 25(16), pp. 7158-7169.

San Filippo, J., Sung, P. and Klein, H. (2008) 'Mechanism of eukaryotic homologous recombination', *Annual Review of Biochemistry,* 77, pp. 229-257.

Sandell, L.L. and Zakian, V.A. (1993) 'Loss of a yeast telomere: arrest, recovery, and chromosome loss', *Cell,* 75(4), pp. 729-739.

Sartori, A.A., Lukas, C., Coates, J., Mistrik, M., Fu, S., Bartek, J., Baer, R., Lukas, J. and Jackson, S.P. (2007) 'Human CtIP promotes DNA end resection', *Nature,* 450(7169), pp. 509-514.

Sauer, B. and Henderson, N. (1988) 'Site-specific DNA recombination in mammalian cells by the Cre recombinase of bacteriophage P1', *Proceedings of the National Academy of Sciences of the United States of America,* 85(14), pp. 5166-5170.

Savage, J.R. (1976) 'Classification and relationships of induced chromosomal structual changes', *Journal of medical genetics,* 13(2), pp. 103-122.

Savitsky, K., Bar-Shira, A., Gilad, S., Rotman, G., Ziv, Y., Vanagaite, L., Tagle, D.A., Smith, S., Uziel, T., Sfez, S., Ashkenazi, M., Pecker, I., Frydman, M., Harnik, R., Patanjali, S.R., Simmons, A., Clines, G.A., Sartiel, A., Gatti, R.A., Chessa, L., Sanal, O., Lavin, M.F., Jaspers, N.G., Taylor, A.M., Arlett, C.F., Miki, T., Weissman, S.M., Lovett, M., Collins, F.S. and Shiloh, Y. (1995) 'A single ataxia telangiectasia gene with a product similar to PI-3 kinase', *Science (New York, N.Y.),* 268(5218), pp. 1749-1753.

Saxena, S. and Dutta, A. (2005) 'Geminin-Cdt1 balance is critical for genetic stability', *Mutation research,* 569(1-2), pp. 111-121.

Schaaf, M.J. and Cidlowski, J.A. (2003) 'Molecular determinants of glucocorticoid receptor mobility in living cells: the importance of ligand affinity', *Molecular and cellular biology,* 23(6), pp. 1922-1934.

Schmidt, B.J. and Bloom, F.R. (1999) 'Electromax STbL4 cells for stable maintenance of repeat sequences', *Focus,* 21(2), pp. 52-53.

Schneider, C.A., Rasband, W.S. and Eliceiri, K.W. (2012) 'NIH Image to ImageJ: 25 years of image analysis', *Nature methods,* 9(7), pp. 671-675.

Schumacher, B., Garinis, G.A. and Hoeijmakers, J.H. (2008) 'Age to survive: DNA damage and aging', *Trends in genetics : TIG,* 24(2), pp. 77-85.

Shechter, D., Costanzo, V. and Gautier, J. (2004) 'ATR and ATM regulate the timing of DNA replication origin firing', *Nature cell biology,* 6(7), pp. 648-655.

Shen, Z. (2011) 'Genomic instability and cancer: an introduction', *Journal of molecular cell biology,* 3(1), pp. 1-3.

Shibata, A. and Jeggo, P.A. (2014) 'DNA double-strand break repair in a cellular context', *Clinical oncology (Royal College of Radiologists (Great Britain)),* 26(5), pp. 243-249.

Shibata, A., Moiani, D., Arvai, A.S., Perry, J., Harding, S.M., Genois, M.M., Maity, R., van Rossum-Fikkert, S., Kertokalio, A., Romoli, F., Ismail, A., Ismalaj, E., Petricci, E., Neale, M.J., Bristow, R.G., Masson, J.Y., Wyman, C., Jeggo, P.A. and Tainer, J.A. (2014) 'DNA double-strand break repair pathway choice is directed by distinct MRE11 nuclease activities', *Molecular cell,* 53(1), pp. 7-18.

Shichiri, M., Hanson, K.D. and Sedivy, J.M. (1993) 'Effects of c-myc expression on proliferation, quiescence, and the G0 to G1 transition in nontransformed cells', *Cell growth & differentiation : the molecular biology journal of the American Association for Cancer Research,* 4(2), pp. 93-104.

Shiloh, Y. (2003) 'ATM and related protein kinases: safeguarding genome integrity', *Nature reviews.Cancer,* 3(3), pp. 155-168.

Shiloh, Y. and Kastan, M.B. (2001) 'ATM: genome stability, neuronal development, and cancer cross paths', *Advances in Cancer Research,* 83, pp. 209-254.

Shiotani, B. and Zou, L. (2009) 'Single-stranded DNA orchestrates an ATM-to-ATR switch at DNA breaks', *Molecular cell,* 33(5), pp. 547-558.

Shrivastav, M., De Haro, L.P. and Nickoloff, J.A. (2008) 'Regulation of DNA double-strand break repair pathway choice', *Cell research,* 18(1), pp. 134-147.

Sirbu, B.M. and Cortez, D. (2013) 'DNA damage response: three levels of DNA repair regulation', *Cold Spring Harbor perspectives in biology,* 5(8), pp. a012724.

Sirbu, B.M., Couch, F.B., Feigerle, J.T., Bhaskara, S., Hiebert, S.W. and Cortez, D. (2011) 'Analysis of protein dynamics at active, stalled, and collapsed replication forks', *Genes & development,* 25(12), pp. 1320-1327.

Smith, C.E., Llorente, B. and Symington, L.S. (2007) 'Template switching during break-induced replication', *Nature,* 447(7140), pp. 102-105.

Sofueva, S., Osman, F., Lorenz, A., Steinacher, R., Castagnetti, S., Ledesma, J. and Whitby, M.C. (2011) 'Ultrafine anaphase bridges, broken DNA and illegitimate recombination induced by a replication fork barrier', *Nucleic acids research,* 39(15), pp. 6568-6584.

Sogo, J.M., Lopes, M. and Foiani, M. (2002) 'Fork reversal and ssDNA accumulation at stalled replication forks owing to checkpoint defects', *Science (New York, N.Y.),* 297(5581), pp. 599-602.

Sonoda, E., Sasaki, M.S., Buerstedde, J.M., Bezzubova, O., Shinohara, A., Ogawa, H., Takata, M., Yamaguchi-Iwai, Y. and Takeda, S. (1998) 'Rad51-deficient vertebrate cells accumulate chromosomal breaks prior to cell death', *The EMBO journal,* 17(2), pp. 598-608.

Soulas-Sprauel, P., Rivera-Munoz, P., Malivert, L., Le Guyader, G., Abramowski, V., Revy, P. and de Villartay, J.P. (2007) 'V(D)J and immunoglobulin class switch recombinations: a paradigm to study the regulation of DNA end-joining', *Oncogene,* 26(56), pp. 7780-7791.

Soutoglou, E., Dorn, J.F., Sengupta, K., Jasin, M., Nussenzweig, A., Ried, T., Danuser, G. and Misteli, T. (2007) 'Positional stability of single double-strand breaks in mammalian cells', *Nature cell biology,* 9(6), pp. 675-682.

Sowd, G.A., Li, N.Y. and Fanning, E. (2013) 'ATM and ATR activities maintain replication fork integrity during SV40 chromatin replication', *PLoS pathogens,* 9(4), pp. e1003283.

Stevens, A., Ray, D.W., Zeggini, E., John, S., Richards, H.L., Griffiths, C.E. and Donn, R. (2004) 'Glucocorticoid sensitivity is determined by a specific glucocorticoid receptor haplotype', *The Journal of clinical endocrinology and metabolism,* 89(2), pp. 892-897.

Stracker, T.H. and Petrini, J.H. (2011) 'The MRE11 complex: starting from the ends', *Nature reviews.Molecular cell biology,* 12(2), pp. 90-103.

Straight, A.F., Belmont, A.S., Robinett, C.C. and Murray, A.W. (1996) 'GFP tagging of budding yeast chromosomes reveals that protein-protein interactions can mediate sister chromatid cohesion', *Current biology : CB,* 6(12), pp. 1599-1608.

Strumberg, D., Pilon, A.A., Smith, M., Hickey, R., Malkas, L. and Pommier, Y. (2000) 'Conversion of topoisomerase I cleavage complexes on the leading strand of ribosomal DNA into 5'-phosphorylated DNA double-strand breaks by replication runoff', *Molecular and cellular biology,* 20(11), pp. 3977-3987.

Sun, J., Lee, K.J., Davis, A.J. and Chen, D.J. (2012) 'Human Ku70/80 protein blocks exonuclease 1-mediated DNA resection in the presence of human Mre11 or Mre11/Rad50 protein complex', *The Journal of biological chemistry,* 287(7), pp. 4936-4945.

Sundararajan, R. and Freudenreich, C.H. (2011) 'Expanded CAG/CTG repeat DNA induces a checkpoint response that impacts cell proliferation in Saccharomyces cerevisiae', *PLoS genetics,* 7(3), pp. e1001339.

Symington, L.S. and Gautier, J. (2011) 'Double-strand break end resection and repair pathway choice', *Annual Review of Genetics,* 45, pp. 247-271.

Szostak, J.W., Orr-Weaver, T.L., Rothstein, R.J. and Stahl, F.W. (1983) 'The double-strand-break repair model for recombination', *Cell,* 33(1), pp. 25-35.

Takai, H., Naka, K., Okada, Y., Watanabe, M., Harada, N., Saito, S., Anderson, C.W., Appella, E., Nakanishi, M., Suzuki, H., Nagashima, K., Sawa, H., Ikeda, K. and Motoyama, N. (2002) 'Chk2-deficient mice exhibit radioresistance and defective p53-mediated transcription', *The EMBO journal,* 21(19), pp. 5195-5205.

Takeda, S., Nakamura, K., Taniguchi, Y. and Paull, T.T. (2007) 'Ctp1/CtIP and the MRN complex collaborate in the initial steps of homologous recombination', *Molecular cell,* 28(3), pp. 351-352.

Tercero, J.A. and Diffley, J.F. (2001) 'Regulation of DNA replication fork progression through damaged DNA by the Mec1/Rad53 checkpoint', *Nature,* 412(6846), pp. 553-557.

Tomasetti, C. and Vogelstein, B. (2015) 'Cancer etiology. Variation in cancer risk among tissues can be explained by the number of stem cell divisions', *Science (New York, N.Y.),* 347(6217), pp. 78-81.

Tsukamoto, T., Hashiguchi, N., Janicki, S.M., Tumbar, T., Belmont, A.S. and Spector, D.L. (2000) 'Visualization of gene activity in living cells', *Nature cell biology,* 2(12), pp. 871-878.

Uziel, T., Lerenthal, Y., Moyal, L., Andegeko, Y., Mittelman, L. and Shiloh, Y. (2003) 'Requirement of the MRN complex for ATM activation by DNA damage', *The EMBO journal,* 22(20), pp. 5612-5621.

van Heemst, D., Brugmans, L., Verkaik, N.S. and van Gent, D.C. (2004) 'End-joining of blunt DNA double-strand breaks in mammalian fibroblasts is precise and requires DNA-PK and XRCC4', *DNA repair,* 3(1), pp. 43-50.

Venclovas, C. and Thelen, M.P. (2000) 'Structure-based predictions of Rad1, Rad9, Hus1 and Rad17 participation in sliding clamp and clamp-loading complexes', *Nucleic acids research,* 28(13), pp. 2481-2493.

Veuger, S.J., Curtin, N.J., Richardson, C.J., Smith, G.C. and Durkacz, B.W. (2003) 'Radiosensitization and DNA repair inhibition by the combined use of novel inhibitors of DNA-dependent protein kinase and poly(ADP-ribose) polymerase-1', *Cancer research,* 63(18), pp. 6008-6015.

Vlahos, C.J., Matter, W.F., Hui, K.Y. and Brown, R.F. (1994) 'A specific inhibitor of phosphatidylinositol 3-kinase, 2-(4-morpholinyl)-8-phenyl-4H-1-benzopyran-4-one (LY294002)', *The Journal of biological chemistry,* 269(7), pp. 5241-5248.

Vogelstein, B. and Kinzler, K.W. (2004) 'Cancer genes and the pathways they control', *Nature medicine,* 10(8), pp. 789-799.

Vouillot, L., Thelie, A. and Pollet, N. (2015) 'Comparison of T7E1 and surveyor mismatch cleavage assays to detect mutations triggered by engineered nucleases', *G3 (Bethesda, Md.),* 5(3), pp. 407-415.

Waga, S. and Stillman, B. (1998) 'The DNA replication fork in eukaryotic cells', *Annual Review of Biochemistry,* 67, pp. 721-751.

Walker, J.R., Corpina, R.A. and Goldberg, J. (2001) 'Structure of the Ku heterodimer bound to DNA and its implications for double-strand break repair', *Nature,* 412(6847), pp. 607-614.

Walter, J. and Newport, J. (2000) 'Initiation of eukaryotic DNA replication: origin unwinding and sequential chromatin association of Cdc45, RPA, and DNA polymerase alpha', *Molecular cell,* 5(4), pp. 617-627.

Wang, B., Matsuoka, S., Carpenter, P.B. and Elledge, S.J. (2002) '53BP1, a mediator of the DNA damage checkpoint', *Science (New York, N.Y.),* 298(5597), pp. 1435-1438.

Wang, H., Wang, H., Powell, S.N., Iliakis, G. and Wang, Y. (2004) 'ATR affecting cell radiosensitivity is dependent on homologous recombination repair but independent of nonhomologous end joining', *Cancer research,* 64(19), pp. 7139-7143.

Wang, J.C. (2002) 'Cellular roles of DNA topoisomerases: a molecular perspective', *Nature reviews.Molecular cell biology,* 3(6), pp. 430-440.

Wang, X., Zou, L., Zheng, H., Wei, Q., Elledge, S.J. and Li, L. (2003) 'Genomic instability and endoreduplication triggered by RAD17 deletion', *Genes & development,* 17(8), pp. 965-970.

Ward, J.F. (1988) 'DNA damage produced by ionizing radiation in mammalian cells: identities, mechanisms of formation, and reparability', *Progress in nucleic acid research and molecular biology,* 35, pp. 95-125.

Weber, A.M. and Ryan, A.J. (2015) 'ATM and ATR as therapeutic targets in cancer', *Pharmacology & therapeutics,* 149, pp. 124-138.

Weinert, T., Kaochar, S., Jones, H., Paek, A. and Clark, A.J. (2009) 'The replication fork's five degrees of freedom, their failure and genome rearrangements', *Current opinion in cell biology,* 21(6), pp. 778-784.

Weinstock, D.M., Brunet, E. and Jasin, M. (2008) 'Induction of chromosomal translocations in mouse and human cells using site-specific endonucleases', *Journal of the National Cancer Institute.Monographs,* (39):20-4. doi(39), pp. 20-24.

Weinstock, D.M., Brunet, E. and Jasin, M. (2007) 'Formation of NHEJ-derived reciprocal chromosomal translocations does not require Ku70', *Nature cell biology,* 9(8), pp. 978-981.

Weterings, E. and van Gent, D.C. (2004) 'The mechanism of non-homologous end-joining: a synopsis of synapsis', *DNA repair,* 3(11), pp. 1425-1435.

Willmore, E., de Caux, S., Sunter, N.J., Tilby, M.J., Jackson, G.H., Austin, C.A. and Durkacz, B.W. (2004) 'A novel DNA-dependent protein kinase inhibitor, NU7026, potentiates the cytotoxicity of topoisomerase II poisons used in the treatment of leukemia', *Blood,* 103(12), pp. 4659-4665.

Wogan, G.N., Hecht, S.S., Felton, J.S., Conney, A.H. and Loeb, L.A. (2004) 'Environmental and chemical carcinogenesis', *Seminars in cancer biology,* 14(6), pp. 473-486.

Wold, M.S. (1997) 'Replication protein A: a heterotrimeric, single-stranded DNA-binding protein required for eukaryotic DNA metabolism', *Annual Review of Biochemistry,* 66, pp. 61-92.

Woods, D. and Turchi, J.J. (2013) 'Chemotherapy induced DNA damage response: convergence of drugs and pathways', *Cancer biology & therapy,* 14(5), pp. 379-389.

Wu, L., Liu, Y. and Kong, D. (2014) 'Mechanism of chromosomal DNA replication initiation and replication fork stabilization in eukaryotes', *Science China.Life sciences,* 57(5), pp. 482-487.

Xu, X., Qiao, W., Linke, S.P., Cao, L., Li, W.M., Furth, P.A., Harris, C.C. and Deng, C.X. (2001) 'Genetic interactions between tumor suppressors Brca1 and p53 in apoptosis, cell cycle and tumorigenesis', *Nature genetics,* 28(3), pp. 266-271.

Yao, N.Y. and O'Donnell, M. (2010) 'SnapShot: The replisome', *Cell,* 141(6), pp. 1088, 1088.e1.

Yatagai, F., Suzuki, M., Ishioka, N., Ohmori, H. and Honma, M. (2008) 'Repair of I-SceI induced DSB at a specific site of chromosome in human cells: influence of low-dose, low-dose-rate gamma-rays', *Radiation and environmental biophysics,* 47(4), pp. 439-444.

You, Z., Chahwan, C., Bailis, J., Hunter, T. and Russell, P. (2005) 'ATM activation and its recruitment to damaged DNA require binding to the C terminus of Nbs1', *Molecular and cellular biology,* 25(13), pp. 5363-5379.

Zegerman, P. and Diffley, J.F. (2010) 'Checkpoint-dependent inhibition of DNA replication initiation by Sld3 and Dbf4 phosphorylation', *Nature,* 467(7314), pp. 474-478.

Zeman, M.K. and Cimprich, K.A. (2014) 'Causes and consequences of replication stress', *Nature cell biology,* 16(1), pp. 2-9.

Zhang, F., Khajavi, M., Connolly, A.M., Towne, C.F., Batish, S.D. and Lupski, J.R. (2009) 'The DNA replication FoSTeS/MMBIR mechanism can generate genomic, genic and exonic complex rearrangements in humans', *Nature genetics,* 41(7), pp. 849-853.

Zhang, J. and Zhou, P. (2005) 'Ectopic targeting of substrates to the ubiquitin pathway', *Methods in enzymology,* 399, pp. 823-833.

Zhao, Y., Thomas, H.D., Batey, M.A., Cowell, I.G., Richardson, C.J., Griffin, R.J., Calvert, A.H., Newell, D.R., Smith, G.C. and Curtin, N.J. (2006) 'Preclinical evaluation of a potent novel DNA-dependent protein kinase inhibitor NU7441', *Cancer research,* 66(10), pp. 5354-5362.

Zhong, Q., Chen, C.F., Li, S., Chen, Y., Wang, C.C., Xiao, J., Chen, P.L., Sharp, Z.D. and Lee, W.H. (1999) 'Association of BRCA1 with the hRad50-hMre11-p95 complex and the DNA damage response', *Science (New York, N.Y.),* 285(5428), pp. 747-750.

Zhou, B.B. and Elledge, S.J. (2000) 'The DNA damage response: putting checkpoints in perspective', *Nature,* 408(6811), pp. 433-439.

Zhou, P. (2005) 'Targeted protein degradation', *Current opinion in chemical biology,* 9(1), pp. 51-55.

Zou, H. and Rothstein, R. (1997) 'Holliday junctions accumulate in replication mutants via a RecA homolog-independent mechanism', *Cell,* 90(1), pp. 87-96.

Zou, L. and Elledge, S.J. (2003) 'Sensing DNA damage through ATRIP recognition of RPA-ssDNA complexes', *Science (New York, N.Y.),* 300(5625), pp. 1542-1548.

Zou, L., Liu, D. and Elledge, S.J. (2003) 'Replication protein A-mediated recruitment and activation of Rad17 complexes', *Proceedings of the National Academy of Sciences of the United States of America,* 100(24), pp. 13827-13832.

Zou, L. and Stillman, B. (2000) 'Assembly of a complex containing Cdc45p, replication protein A, and Mcm2p at replication origins controlled by S-phase cyclin-dependent kinases and Cdc7p-Dbf4p kinase', *Molecular and cellular biology,* 20(9), pp. 3086-3096.